The Solvation of Aryl Trifluoromethyl Carbenes at Low-Temperatures

Dissertation

To obtain the degree of
Doctor of natural science (Dr. rer. nat.)

Linda Sofie Klute

from Hagen

Bochum 2020

RUHR UNIVERSITÄT BOCHUM

RUB

Für meine Familie.

This work was carried out from 2015 to 2020 at the Department of Organic Chemistry II of the Ruhr-Universität Bochum under the supervision of Prof. Dr. Wolfram Sander.

First Referee: Prof. Dr. W. Sander
Second Referee: Prof. Dr. P. B. Petersen
Day of submission:
Day of disputation:

Scientific Meetings

Graduate School Solvation Science Summer School, RUB, 05/2015 (Poster).

Chemistry and Physics at Low Temperatures (CPLT), 03.-08.07.2016, Biarritz, France (Poster).

Graduate School of Solvation Science Autumn Workshop, 05.10.2016, Technische Universität Dortmund (Poster).

International Symposium on Reactive Intermediates and Unusual Molecules (ISRIUM), 18.-22.06.2017, Sorrento, Italy (Poster).

Publications

"Matrix Isolation of Aryl Trifluoromethyl Cations." Linda Klute and Wolfram Sander -in preparation.

“What we observe is not nature itself, but nature exposed to our method of questioning.”

— Werner Heisenberg, Physics and Philosophy: The Revolution in Modern Science.

Table of Contents

Summary

The protonation of carbenes[1] and the addition of nucleophiles to carbocations are important reactions steps in organic chemistry.[2] Thus, a deeper knowledge about the involved reactive species and an understanding of the reaction mechanism is crucial. Recent experiments on the protonation of aryl carbenes by low density amorphous (LDA) water ice indicated a correlation of the calculated proton affinity (PA) of carbenes to the observability of the corresponding cations in LDA water ices.[3-5] In this work, those studies should be expanded by investigating α-trifluoromethyl carbenes and carbocations. Carbocations with a trifluoromethyl (CF_3) group directly attached to the cationic center are referred to as "destabilized", due to the electronegativity of CF_3 pulling electron density from the cationic core and could not be isolated in amorphous ices in previous experiments.[6, 7] Thus, to increase the stability and to enable a spectroscopic analysis of α-trifluoromethyl carbocations, the influence of counteracting, electron pushing groups was studied. Based on the calculated PA's, trifluoromethyl carbenes **1** and **20** with π donating *para*-methoxyphenyl and *para*-dimethylaminophenyl substitutions were selected. A promising stability of the corresponding cations **2** and **22** is reported as well.[8, 9] In contrast, according to its lower calculated PA, trifluoromethyl carbene **30** with an inductively electron withdrawing *meta*-methoxyphenyl group is not expected to form a stable cation in amorphous water ice. The highly reactive carbenes were generated via photolysis of the corresponding matrix isolated diazo precursors. Apart from an evaluation of the ground states of those carbenes, the complexation with H_2O and other Lewis acids in doped argon matrices and their reactivity in direct contact to H_2O, as in low density amorphous water ice, was investigated. The results of the spectroscopic investigations were supported by comparison to synthesized reference compounds and by DFT calculations.

Singlet carbene *p*-methoxyphenyl-1-(trifluoromethyl)carbene S-**1** was generated upon photolysis of diazo compound **6**. The carbene was photostable at 3 K (650 nm - 254 nm) and no photochemically or thermally induced rearrangement or interconversion to its triplet state was observed. Instead, the carbene was observed in its two different conformers, with its methoxy group pointing upwards (S-**1**u) and downwards (S-**1**u). The ratio between conformer S-**1**u and S-**1**d could be shifted via annealing or irradiation (Scheme 1). The complexation of S-**1** in an argon matrix doped with 1 % of H_2O resulted in the usual hydrogen-bonded complex S-**1**--H_2O. This complex was stable at 3 K and the OH insertion product **8** was generated upon 365 nm photolysis. In amorphous water ice, alcohol **8** and small amounts of cation **2** are directly formed upon photolysis of **6**. Cation **2** is only stable at temperatures up to ~40 K, and the OH insertion product **8** is formed at higher temperatures. The generation of **2** in low yield and its

relatively low thermal stability can be rationalized by the high pK_R^+ value of **2** (-20.8) [10] pointing to an increased reactivity towards nucleophiles. Moreover, the results do underline the correlation of the calculated PA to the observability of the cations in LDA water ice, and carbene **1** with a PA of -260 kcal mol^{-1} (B3LYP-D3/6-311+G(d,p)) marks a new limiting value to observe those highly reactive species via matrix isolation. Traces of S-**1**--H_2O were observed after irradiation of **6** as well and could be converted to **8** via UV photolysis. Additionally, the complexation of the singlet carbene **1** with the weaker Lewis acid ammonia and deuterated ammonia was studied via IR spectroscopy. As with H_2O dopant, S-**1** forms the hydrogen-bonded complexes S-**1**--HNH_2 and S-**1**--DND_2 at elevated temperatures in argon matrices doped with NH_3 and ND_3, respectively. In contrast to S-**1**--H_2O, the complex S-**1**--HNH_2 is only metastable and rearranges slowly to the NH_2 insertion product **8a** at 3 K. Deuterated complex S-**1**--DND_2 is instead stable under these conditions. This strong kinetic isotope effect hints at the involvement of quantum mechanical tunneling (QMT).

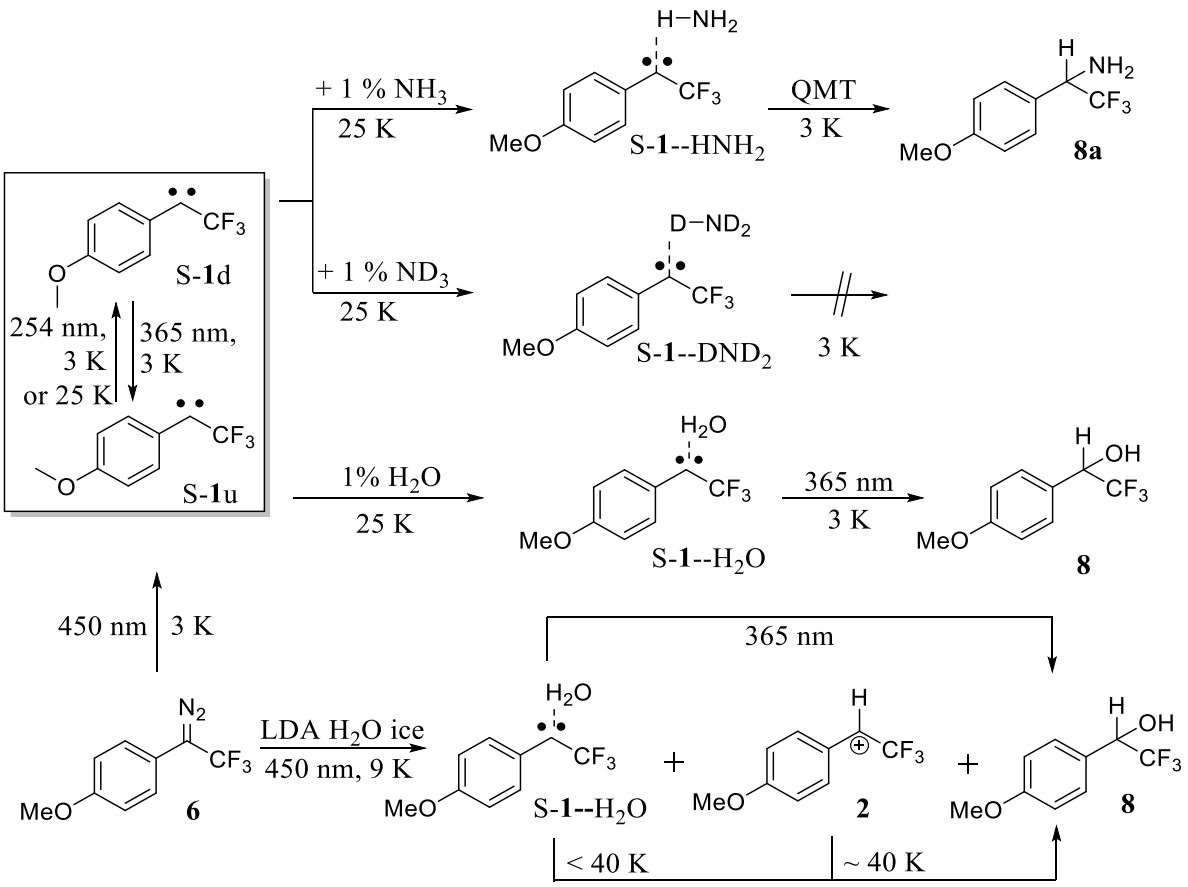

Scheme **1:** Generation and reaction of **1** with H_2O and ND_3.

In analogy to **6**, precursor **26** was matrix isolated and photolyzed to obtain carbene **20** in its singlet state (Scheme 2). S-**20** is stable at 3 K upon photolysis (650 nm - 254 nm), as well as by annealing. Interestingly, during annealing of S-**20** to 30 K in H_2O-doped argon matrices, the

color of the matrix turned blue, as an UV-vis absorption at around 600 nm approves. This indication for the formation of a new photoactive species was found for S-**20** in matrices doped with 1 % of D_2O and 1 % of MeOH as well. With the help of IR, UV-vis and EPR spectroscopy combined with DFT calculations, the blue colored species was assigned to cation **22**. Resonance stabilized α-trifluoromethyl cation **22** was, depending on the dopant, accompanied by hydrogen-bonded complex S-**20**--H_2O, S-**20**--D_2O or S-**20**--MeOH. These singlet complexes inserted into the OH of the dopants to form alcohol **28a** and d-**28a** upon UV and the methanol complex S-**20**--MeOH upon IR photolysis. In contrast, irradiation of **22** with IR light resulted in the not yet identified product **u3**. Based on those observations and on results from previous experiments,[11] it was assumed that the OH insertion took place at a different position. This may be rationalized with the ability of this molecule to delocalize the positive charge throughout the *p*-dimethylaminophenyl group possibly facilitated by the negatively charged CF_3 dipol. The photolysis of precursor **26** was also investigated in LDA water ice, but no color change of the matrix or an evidence for a cationic species was observed. Instead, upon irradiation, **28a** and **u3** were formed directly in high yields. This may be explained with a concurring reaction initiated by more water molecules in proximity to the carbene than in 1 % water doped matrices.

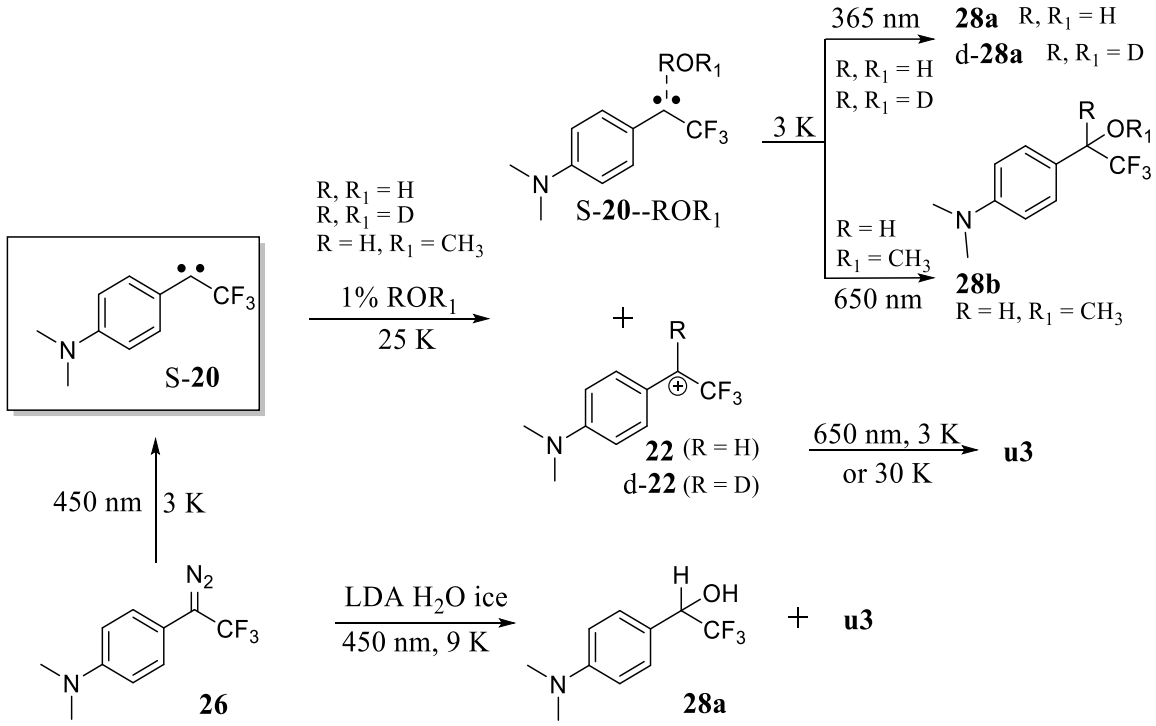

Scheme **2:** Generation and reaction of **20** with water and methanol.

The same methodology was used to study the triplet ground state *m*-methoxyphenyl-1-(trifluoromethyl)carbene **30**. The complexation in H_2O-doped matrices exhibited a chemistry also observed for other triplet carbenes with small singlet-triplet gaps: The interaction with

Lewis acids,[12, 13] resulted in an intersystem crossing from T-**30** to the corresponding thermodynamically stabilized singlet water complex S-**30**--H_2O, which is converted to alcohol **38** upon UV light irradiation. In LDA H_2O ice, this OH insertion product was formed directly upon photolysis of **36** and no cationic species was observed.

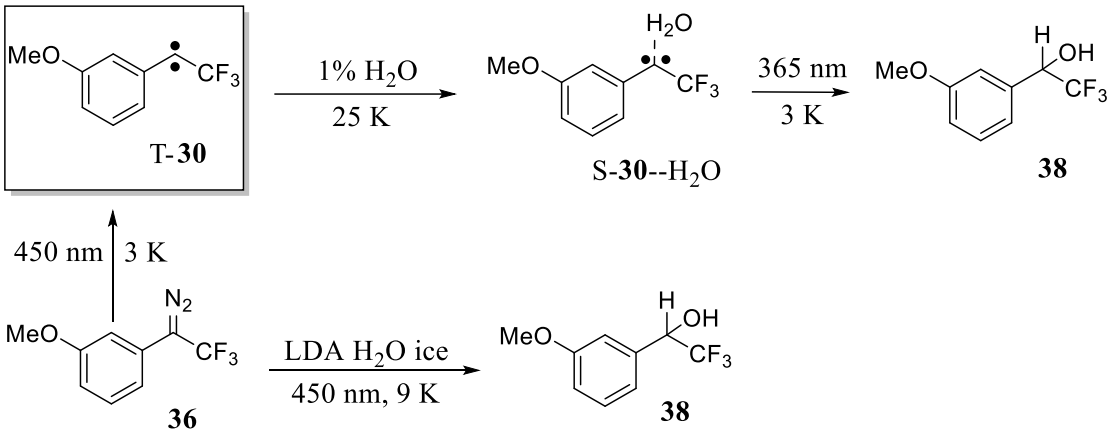

Scheme **3:** Generation and reaction of **30** with water.

Overall, experiments in this work demonstrate that the destabilizing pull effect of α-trifluoromethyl substituted cations can be overcome by introducing counteracting pushing groups such as *p*-methoxyphenyl or *p*-dimethylaminophenyl. The observability of the cations at cryogenic conditions correlates to the calculated PA of the corresponding carbene.

1. General Introduction

1.1. Matrix Isolation

The study of reactive intermediates has always been a challenge for scientists, since the timescale in which highly reactive molecules like carbenes, carbocations or radicals exist under ambient conditions ranges only from micro- to picoseconds (10^{-6} – 10^{-12} seconds).[14, 15] Two classical methods which enable the analysis of highly reactive compounds are laser flash photolysis (LFP) and matrix isolation technique. The LFP technique was developed in 1949 by M. Eigen, R. G. W. Norrish and G. Porter. In 1967 they got the Nobel Prize in Chemistry "*for their studies of extremely fast chemical reactions, effected by disturbing the equilibrium by means of very short pulses of energy*."[16-18] With LFP, the molecule is produced or exited by short-pulsed laser irradiation and subsequently studied within the time window of their existence by spectroscopic methods. In case of matrix isolation, the reactive species are produced under cryogenic conditions in an inert environment to elongate their lifetime and enabling their extensive study. This technique was invented and developed in the 1950 by G. C. Pimentel [19] and at the same time by I. Norman and G. Porter.[20] The low-temperatures of 3 to 40 K are provided by a closed-cycle helium cryostat connected to the cold window where the sample (guest) and the matrix material (host) are deposited.[21, 22] The reactive species can be photolytically or thermally generated out of a more stable precursor molecule e.g. diazo or diazirine for carbenes. The precursors must have a suitable vapor pressure at temperatures which will not lead to a decomposition. To obtain a good isolation of guest and to avoid intermolecular reactions, the sample must be deposited highly diluted in the host material on the cold window. Usual hosts are inert gases like noble gases and nitrogen, which provide a transparent matrix for spectroscopic reasons. To avoid co-deposition of impurities like oxygen from air, the experiments must be performed under a high vacuum (10^{-3} to 10^{-7} mbar) achieved by a turbo or diffusion pump connected to a rotary pump. Spectroscopic techniques like infrared, UV-vis and EPR in combination with quantum chemical calculations are used to characterize the generated compounds.

The main features of the matrix apparatus, which offers the possibility to isolate a molecule under cryogenic conditions and enables the subsequent photolysis as well as the IR and UV-vis spectroscopy, are (Picture **1**):

- The deposition unit, consisting of a sample connection and gas support -> enabling the co-deposition of the sample and an excess of the matrix gas onto the cold window.

- The cold window -> the sample holder on which the diluted sample is deposited. Materials are Cesium iodide for IR and sapphire for UV-vis spectroscopy. The connection to the cryostat and the vacuum system provides cryogenic conditions.
- The two opposing external windows -> enabling for IR and UV-vis spectroscopy. Usual materials are potassium bromide (KBr) for IR spectroscopy and sapphire for UV-vis spectroscopy.
- The quartz window -> transparency range from UV to the near IR light, enabling photolysis.

Picture **1:** Setup to deposit a volatile sample on the matrix window for IR and UV-vis spectroscopy (exemplarily).

Since rotational-vibrational coupling is excluded due to the low-temperatures and the rigidity of the host, the resulting IR spectra are simplified and they can be compared with theoretical spectra more easily.

The matrix setup enabling EPR spectroscopic studies differs in some parts, but the general conditions remain: a copper rod is usually used for the deposition of the guest-host mixture. This copper rod is connected to the cryostat and to the pump system and is shielded from the atmosphere by a transparent quartz glass, which also enables for photolysis. The magnets and the resonator are at the bottom part and the copper rod can be moved in for spectroscopy or moved out for photolysis.

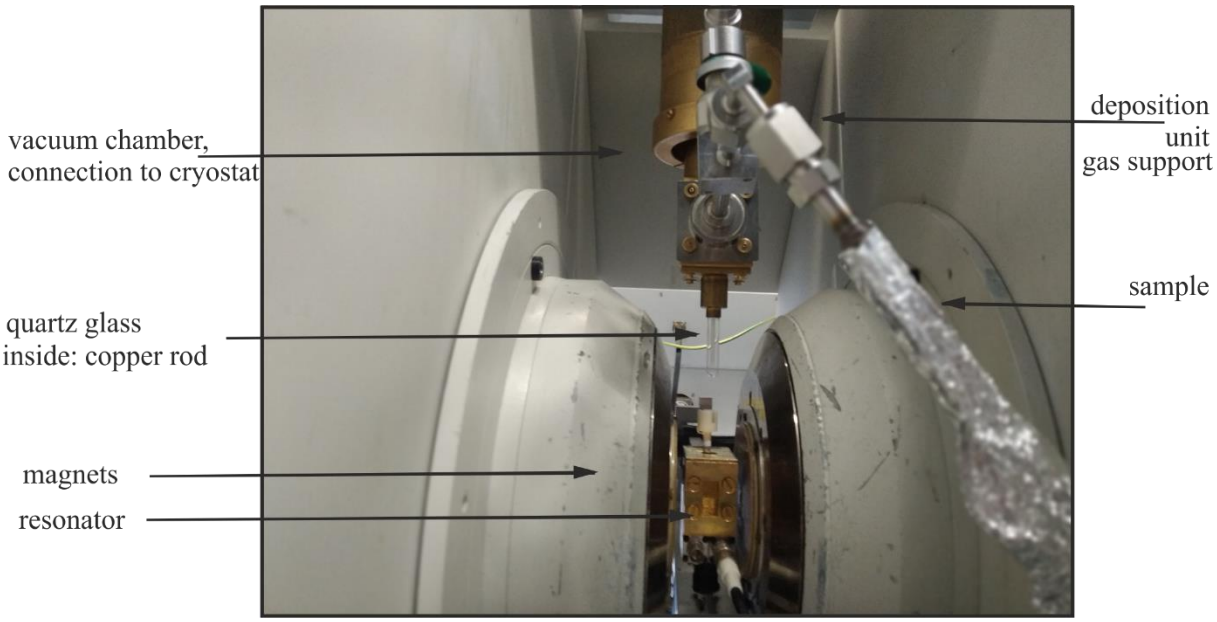

Picture 2: Matrix isolation experiment enabling for EPR spectroscopy (exemplarily).

Besides the isolation and spectroscopically characterization of reactive molecules, the matrix isolation technique found many applications. For example, to study bimolecular reactions, the host can be doped with small molecules like H_2O or O_2 and co-deposited with the guest onto the cold window. At elevated temperatures, about 20 – 30 K for argon matrices, the matrix loses rigidity and small molecules start to diffuse and can react with the isolated guest molecules. This annealing enables the study of weak interactions as hydrogen- or halogen-bonding[13, 23, 24] and van-der Waals complexes[25] as well as the formation of new products and intermediates. Depending on the studied compound and the reaction other host materials can be used, e.g. LDA water ice[26], ammonia or hydrogen.[27-29] Moreover, conformational studies[30] and quantum mechanical tunneling (QMT)[31] can be observed and investigated with this technique. With all those applications the matrix isolation technique assistances to shed a light on classical reaction mechanisms in organic chemistry. Additionally, the ultracold and high vacuum environment can be used to simulate the conditions in space and therefore is useful for the study of astrochemical processes.[32]

1.2. Carbenes

Carbenes are carbon containing compounds which are highly reactive. The history of carbenes nicely demonstrates their transient and short-lived nature: despite their fundamental role in organic chemistry as reaction intermediates and the early proposal of these species in the 1900th century,[33-37] it took years of research and synthetic innovations until the synthesis of a stable carbene succeeded 150 years later. Early attempts began in 1830 with Dumas` unsuccessful trial to dehydrate methanol in the expectation to get methylene. Whereas the spectroscopic characterization of carbenes, stabilized in frozen glasses or studied with ultrafast techniques like laser flash photolysis, delivered the proof of their existence in the 1960's,[38] the isolation of a carbene that is stable at ambient conditions was achieved in 1980 with Bertrands highly substituted (phosphino)(silyl)carbene **40**[39] followed in 1991 by Arduengos isolation of a N-heterocyclic carbene imidazole-2-ylidene **41**[40] (Chart 1).

40 **41**

Chart **1:** Examples of stable carbenes: **40** and **41** (Ad = adamantyl).

Carbenes are neutral molecules with six electrons in the valence shell, they can be generalized to the formula: RR`C**:**. The arrangement of the two non-bonding electrons in the σ and π orbitals defines their spin state and therefore their properties and reactivity (Scheme 4). Most carbenes obtain the closed-shell $^1A_1$-σ2π0 singlet state with two paired electrons of opposite spin occupying the σ orbital or the $^3B_1$-σ1π1 triplet state with two unpaired electrons with parallel spin distributed among the σ and π orbitals. The open-shell $^1B_1$-σ1π1 and the $^1A_1$-σ0π2 singlets states are usually high in energy and are rarely observed as a ground-state of carbenes[41] and mostly describe their excited states.[42]

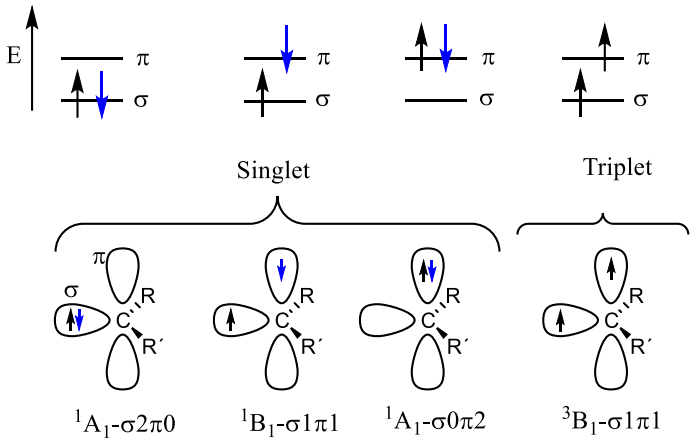

Scheme **4:** Electronic configuration of carbenes.[42-44]

The energy difference between the singlet and triplet state of a carbene is called singlet-triplet splitting (S-T gap or ΔE_{S-T}), and usually refers to the triplet and the closed-shell singlet state. The spin state of a carbene is influenced by electronic and steric effects of its substitution.[45, 46] By lowering the energy of the σ-molecular orbital (MO) or by raising the π orbital, the singlet state can be stabilized. Accordingly, a substitution with electron donating substituent stabilizes the singlet state by raising the energy of the π orbital. In other words, π donor (e.g. -OR, $-NR_2$) and σ acceptor groups (e.g. halogen atoms) are stabilizing the singlet state by raising the energy of the π orbital of the carbene, while the σ orbital remains basically unperturbed. The other way around stabilizes the triplet state. Another factor which influences the ΔE_{S-T} are steric effects. Very bulky substituents like adamantly favor of the triplet state by forcing a linear structure, which is favored by triplet carbenes due to their *sp* geometry. On the other hand, constraint rings (4 or 5 membered rings) are forcing the carbene to a singlet state.[47] The spin specific reactivity of carbenes can be observed e.g. in the reaction with alcohols. Triplet carbenes can be considered as diradicals and react usually with insertion into the C–H bond of the alcohol, whereas the basic singlet carbenes undergo OH insertion reactions.[48-50] Also small molecules like H_2, O_2, CO and HCl are found to react characteristically with carbenes depending on their ground state. Whilst triplet carbenes react at cryogenic temperatures directly with H_2 and O_2, most singlet carbenes instead react with HCl and CO.[45, 48]

The effects of substitution on the chemistry of a carbene was investigated in past years. Since in this work carbenes with a CF_3 group adjacent to the carbene center were studied, the effects of β-fluorination on carbenes are here of special interest.[51, 52] Whilst α-fluorination results in a thermodynamically stabilization of the singlet state by electron donation to the empty 2p orbital, a β-fluorination causes a kinetical stabilization by inhibiting 1,2-rearrangements. Carbenes, which are substituted with groups of opposing character (electron donating and electron withdrawing), so called push-pull carbenes, are found to be stabilized in their singlet state by preserving a kind of "electroneutrality of the carbene center".[53-55] As depicted in Scheme 5, the stabilization is a result of the donating group pulling electron density to the "empty" carbonic p orbital and a simultaneous delocalization of the carbenes lone pair to the accepting groups free orbital.

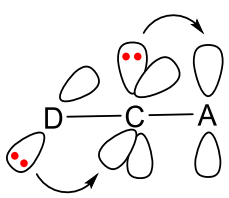

Scheme **5:** Stabilization of a singlet carbene by push-pull substitution. D = donor, A = acceptor.

For example, room temperature stable carbene **40** falls in the class of push-pull stabilized carbenes. The phosphino group acts as a π donor, whereas the silyl group function as a π attractor. The effect of the CF_3 substitution on the (push-pull) stability of carbenes was also studied by Moss with methoxytrifluoromethyl carbene **42**.[56, 57] **42** is observed to be highly reactive and electronically unselective towards alkenes. Relative to **43**, the trifluoromethyl substitution leads to a higher reactivity and no stabilization of the singlet carbene **42**. The authors state "*Despite the intuitively attractive possibility of push-pull stabilization by carbenic substituents of opposing properties, it is the 'pull' by CF_3 that appears to dominate the 'push' by MeO in the substituents' electronic tug of war*." [54] It was concluded that the destabilizing influence of the trifluoromethyl group and the additional pull inductive effect of the methoxy group are counteracting the stabilizing resonance effect of the methoxy group. Later Bertrand investigated another CF_3 containing push-pull carbene **44** with a phosphonyl group bearing a resonance and an inductive push effect and found a high thermodynamic stability for this push-pull carbene.[55]

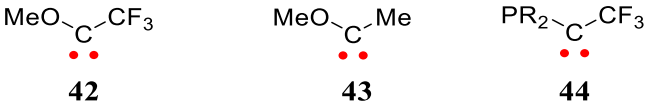

42 **43** **44**

Chart **2:** Carbenes **42**, **43** and **44**. R = c-Hex_2N.

1.3. Carbocations

Carbocations are carbon compounds with a positive charge located on one or more carbon atoms.[58-60] Classical carbocations are trivalent and are also referred to as carbenium ions, whereas the pentavalent compounds are named carbonium ions.[61] Usually, carbocations prefer a sp^2 hybridization with a planar geometry and an empty p orbital (Chart 3). As electron deficient species they can be classified as electrophiles and are generally extremely reactive towards nucleophiles. Like other transient species, carbocations are observed as reactive intermediates in many organic reactions and rearrangements.[62-64]

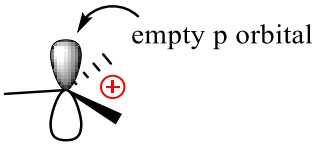

Chart **3:** Geometry of a carbocation.

Due to their empty p orbital, electron donating groups are stabilizing a cation by pushing electrons to the unoccupied orbital via hyperconjugation. Thus, in general primary cations are the least and tertiary the most stable by providing σ-bonds to the vacant orbital of the cation (Scheme 6). For this reason, the stability of such cations is increased whenever the charge can be distributed over a larger number of carbon atoms.

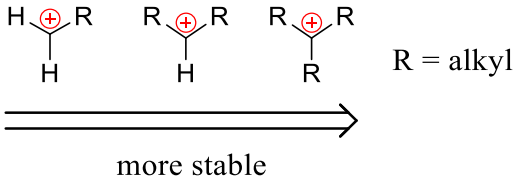

Scheme **6:** Stabilization of a cation by hyperconjugation of adjacent alkyl groups.

Some well-known and relative stable carbocations are: triphenylmethane **98**, malachite green **99** and crystal violet **100** (Chart 4). All those compounds are tertiary cations bearing aromatic ring systems. Among these three, the most stable species is **100**. This can be explained with two additional factors stabilizing a carbocation: π-electron donation to the empty p orbital of the cation and the enhanced ability to delocalize the positive charge e.g over one or more phenyl or dimethylaminophenyl moieties.

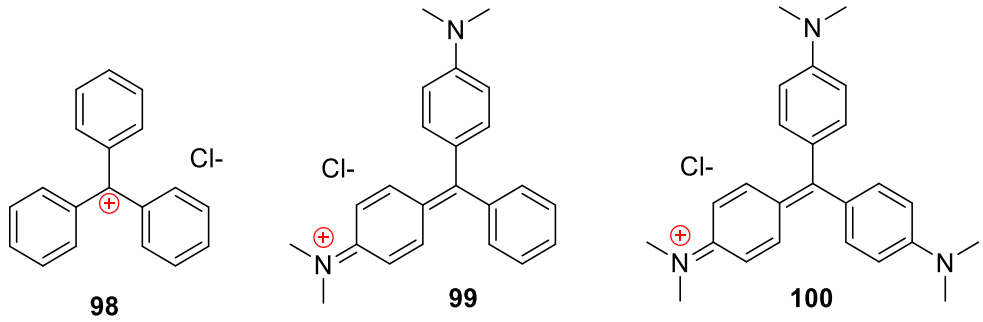

98 **99** **100**

Chart **4:** Structures of triphenylmethane **98**, malachite green **99** and crystal violet **100**.

Aromaticity also influences the stability of cations, thus, aromatic cations (Hückel (4n+2)π system) such as tropylium cation **102** are relatively stable, whereas antiaromatic cations (Hückel (4π system) e.g. cyclopenadienyl cation **103** are highly unstable.[65-68] To the previously mentioned factors, it should also be added the steric influence which can have a negative effect on the stability if the optimal sp^2 hybridization is affected e.g. **104**.

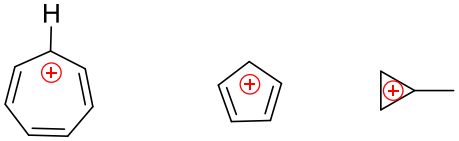

102 **103** **104**

Chart **5:** Aromatic cation **102**, antiaromatic cation **103** and sterically destabilized cation **104**.

Due to the focus of this work on trifluoromethyl containing cations, the effect of fluorine atoms on the cationic stability must be considered as well. The stability of fluorinated carbocations is determined by an interplay of destabilizing and stabilizing effects (Scheme 7). A positive charge at the carbon atom in α-position to the fluorine is stabilizing the compound by π donation from the lone electron pairs to the empty p orbital. At the same time, they are destabilized by a negative inductive effect from the electronegative fluorine atom. β-Carbocations instead, as e.g. α-trifluoromethyl cations, are less stable as they are only exposed to this inductive destabilization.[6, 7, 69]

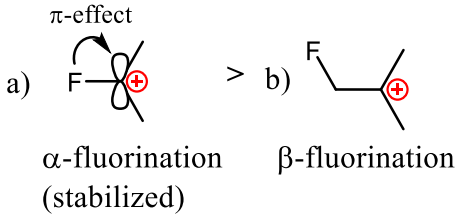

Scheme **7:** Stabilization/destabilization effects induced by a) α-fluorination and b) β-fluorination.

Apart from purely carbon and hydrogen possessing carbocations such as **99** and **102**, other well-known groups of organic cations are iminium and oxocarbenium cations with structures as shown in Scheme 8. The previously mentioned cations **99** and **100** are examples of iminium cations, where the positive charge is partially translocated to the heteroatom. Because of this, they can be depicted in at least two mesomeric structures. Iminium ions prefer a coplanar structure with a C–N bond lengths shorter than C-N single bond.

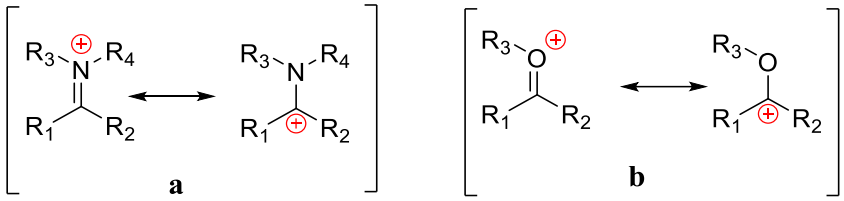

Scheme **8:** Resonance structures of a) iminium and b) oxocarbenium cations.

Most highly reactive carbocations could only be stabilized and thus spectroscopically analyzed in super acidic solvents.[62, 70] However, to study the reactivity of those species with e.g. solvents and/or nucleophiles, other techniques must be applied. One method is LFP where the carbocations are generated e.g. by heterolytic cleavage of a C–X bond of a halide precursor induced by a short laser pulse or by photolysis of diazo compounds.[2, 71, 72] The subsequent decay of the short-lived cations in a nucleophilic environment can be followed spectroscopically and the absolute rate constant can be obtained. Another way to synthesize highly reactive carbocations is by the protonation of carbenes.[73-75] Reactive secondary cations like the

benzhydryl **62** could be isolated previously in low density amorphous water ices at low-temperatures and studied spectroscopically.[3]

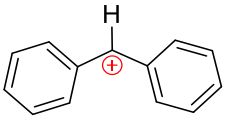

62

Chart **6:** Structures of benzhydryl **62** which could be isolated in LDA H_2O ice.

The substitution of carbocations often determine their color. For example are many very colorful cations found to bear larger delocalized systems with amino substitution as the widely known crystal violet **100** or bis[*p*-(dimethylamino)phenyl]methylium cation **101** studied by Mayr. The study including various *para*-substituted benzhydryl cations found that *p*-dimethylamino substituted benzhydryl cations showed a blue color, while alkoxy- and alkyl-substituted benzhydryl cations are yellow or red.[76] Malachite green **99** with two amino groups shows, as the name indicates, a green coloration, whereas **98** with no phenyl substitution is red. In general, auxochromic (electron donating) groups (-NMe_2, -NH_2, -OH or -OR) can influence the color through a mesomeric effect if attached to a conjugated π system. A combination of auxochromic groups with antiauxochromic groups (electron withdrawing) can enhance the color further. Thus, cationic species are used as dyes like the triarylmethane dyes (e.g. **98**) or the strongly absorbing cyanine dyes like **102** with the general form: $R_2N[CH=CH]nCH=N^+R_2$ ↔ $R_2N^+=CH[CH=CH]nNR_2$.[58]

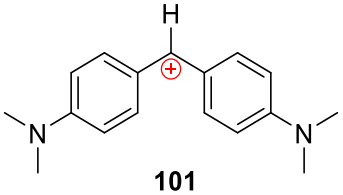

101

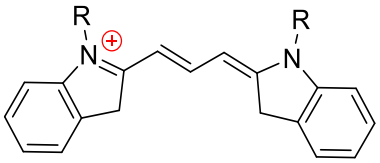

102

Chart **7:** Structures of the blue cation **101** observed by Mayr[76] and a green-yellow cyanine dye.

2. Aryl trifluoromethyl carbenes

2.1. Introduction

Aryl(trifluoromethyl)diazirines and the corresponding diazo compounds are widely used for photoaffinity labeling (PAL).[77-80] This involves the UV photolysis of those compounds to form highly reactive carbenes, which then insert into C–H, N–H and O–H bonds of biological receptors establishing a covalent crosslink to e.g. biomolecules. Therefore, those precursors are applied for probing the location and structure of binding sites of proteins in biochemistry, for drug targeting in medical science[81, 82] as well as for photochemical cross-linking of biomolecules to polymers in material science.[83, 84] Thus, the chemistry and the reactivity of aryl trifluoromethyl carbenes is of interest for these fields, as well as in basic research. In this work a closer look is given at the effect of substitution at the aryl moiety on the reactivity of those carbenes towards Lewis acids, especially H_2O. Aryl trifluoromethyl carbenes **1**, **20** and **30** were photolytically generated from their diazo precursors and characterized with matrix isolation spectroscopy (Scheme 9).

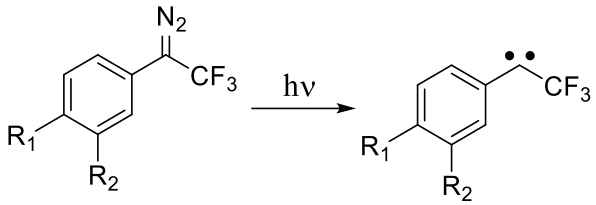

Scheme **9:** The precursors and carbenes studied in this work. **1**: R_1 = OMe, R_2 = H; **20**: R_1 = NMe_2, R_2 = H; **30**: R_1 = H, R_2 = OMe.

Previous experiments with carbenes **50**, **60**, **70** and **90** in annealed water-doped argon matrices showed the formation of hydrogen-bonded complexes out of their basic singlet states with H_2O and other Lewis acids.[5, 12, 13, 24, 28] It was observed that singlet ground state carbene **90** forms a strongly hydrogen-bonded complex with H_2O. Furthermore, it was found that triplet ground state carbenes with a small ΔE_{S-T} can switch their spin state, if the corresponding complexes are thermodynamically stabilized. However, for triplet ground state carbene **80** with a higher ΔE_{S-T} of 9.37 kcal mol^{-1} calculated at B3LYP-D3/6-311+G(d,p) level of theory (ΔE_{S-T} = 10.2 kcal mol^{-1} at B3LYP/Def2-TZVP), the spin switching could not be achieved by complexation with H_2O. Instead with the stronger Lewis acid ICF_3 the spin switching to the singlet state was observed by the formation of a halogen-bonded complex. This was rationalized by the larger singlet triplet energy separation of **80** compared to **60**, **70** and **50** as shown in Table **1**, which does not allow the stabilization of the singlet state by hydrogen-bonding. In this work the reactivity of singlet carbenes **1** and **20** and triplet carbene **30** (ΔE_{S-T} = 3.98 kcal mol^{-1} at B3LYP-

D3/6-311+G(d,p)) are studied in a similar way expecting a hydrogen-bonding interaction in annealed water-doped matrices. To illustrate the basic properties of singlet carbenes, the electrostatic potential (ESP) maps of some aryl and aryl trifluoromethyl carbenes were computed with B3LYP/Def2-TZVP as shown in Figure 1. The non-bonding electron pair located at the σ orbital of the carbenes is visualized as a red-colored area. This negatively charged region enhances the basicity of the molecule, facilitating the interaction with electron acceptor groups e.g. for hydrogen-bonding.

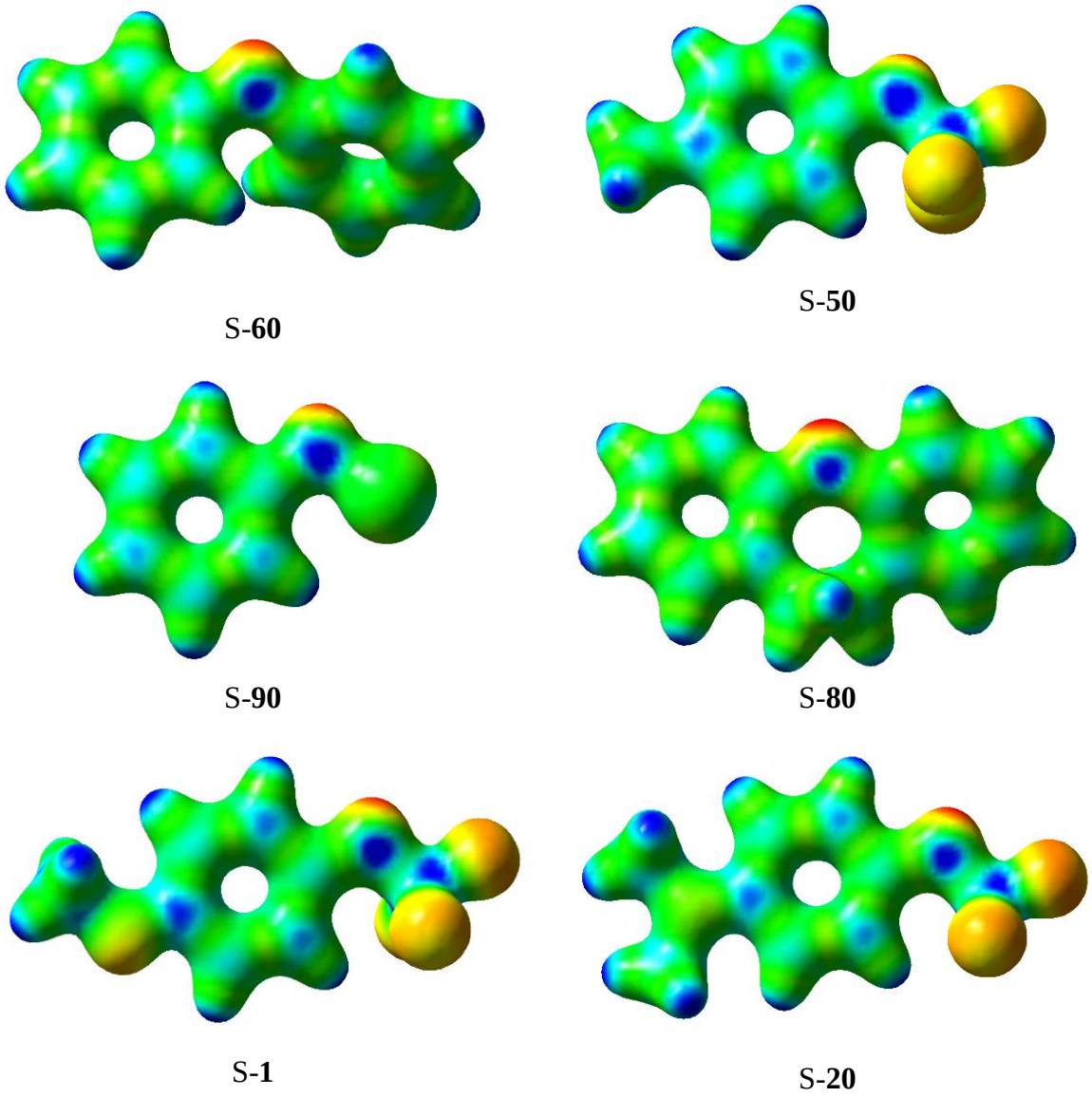

Figure **1:** Electrostatic potential maps of different carbenes in their singlet state (color range from red with -13 kcal mol^{-1} to blue with 318 kcal mol^{-1} on a density of 0.07 a_0^{-3}). Calculated at B3LYP/Def2-TZVP level of theory.

In contrast, in LDA water ice, in-situ protonation of carbenes has been observed, showing that this process is very efficient even at such low temperatures. For example, photolysis of diazo

precursor **66**, **76**, and **86** in amorphous water ice does not afford carbenes **60**,[3] **70**[4] and **80**[85], instead the corresponding cations **62**, **72** and **82** are directly detected (Scheme 10).

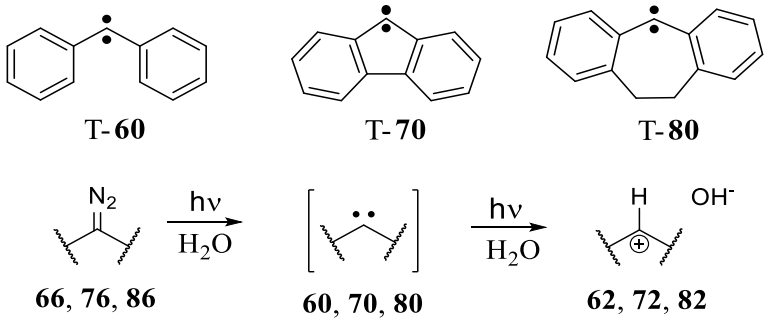

Scheme **10:** The protonation of carbenes observed for T-**60**, T-**70** and T-**80** in LDA water ice.

Contrarily, singlet chlorophenyl- **90** and fluorophenyl- **91** carbene in LDA water ice show the same product as in 1 % of H_2O. By irradiating precursor **96** (**95**), hydrogen-bonded complex S-**90**/**91**--H_2O is formed directly and subsequent irradiation results, depending on the wavelengths, in a back formation of the carbene and H_2O or the formation of benzaldehyde HCl/HF complex **94** (**93**) (Scheme 11). This was rationalized by the conversion of unstable insertion product **98** (**99**) via C–Cl (C–F) bond cleavage to a complex of benzaldehyde with chlorine (fluorine). For these carbenes no cationic species was observed.[5, 86]

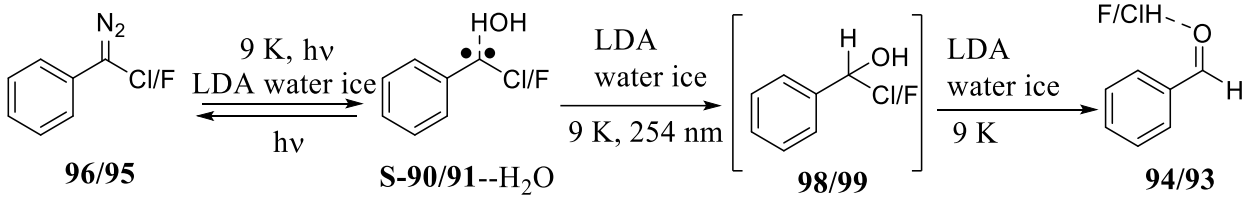

Scheme **11:** Photolysis of **96**/**95** in LDA water ice.

Also for the aryl trifluoromethyl carbene **50** and **11a** no cationic species could be detected in amorphous water ice matrices.[28] Irradiation of the precursor resulted directly in the OH insertion product, suggesting a direct/concerted reaction to the insertion product. This observation was explained by the lower proton affinity (PA) of **50** compared to **60**, **70** and **80**. The PA describes the energy change caused from protonation of the carbene and is therefore expected to give a hint on the stability of the corresponding cation.[75, 87] Following this correlation, it is interesting to examine a limiting PA value until which cations are experimentally observable in LDA water ices. Secondly it is tempting to study if there are other factors controlling the formation of cations like the ground state multiplicity of the carbene. Another factor is to study if also unfavored cations like inductively destabilized β-fluorinated cations are possible to generate in similarly conducted experiments. Thus, singlet carbene **1** with a PA of -260 kcal mol^{-1}

(B3LYP/6-311+G(d,p)) lying in between the PA of recently observed and not observed cations will be studied in this work as well as singlet carbene **20** with a PA similar to **60** (see Table 1).

Table **1:** Singlet-triplet gaps (ΔE_{S-T}) and proton affinities (PA) of selected carbenes.

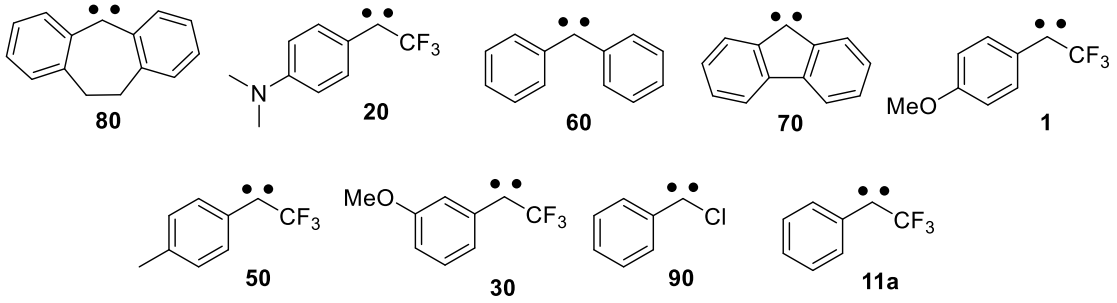

Carbene	ΔE_{S-T}	ground state	PA	cation observed*
80 [e]	9.37	Triplet	-281	yes
20 [a]	-4.33	Singlet	-272	?
60 [c]	5.58	Triplet	-272	yes
70 [d]	3.98	Triplet	-271	yes
1 [a]	-1.21	Singlet	-260	?
50 [b]	1.93	Triplet	-254	no
30 [a]	3.98	Triplet	-251	?
90 [f]	-5.64	Singlet	-250	no
11a [b]	3.58	Triplet	-247	no

Values calculated at B3LYP-D3/6-311+G(d,p) level of theory and in kcal mol^{-1}. PA referred to singlet-carbenes (PA = E_{ZPE}(cation) – E_{ZPE}(carbene)).* in LDA water ice after photolysis of precursor. a This work, b [28], c [3], d [4], e [85], f [5].

Besides the PA, the equilibrium constant pK_R^+ (– log K_R^+) is another value that determines the stability of a species and may, therefore, reflect to the stability of cations in LDA water ices (Scheme 12). This value describes the hydrolysis of the cation to the alcohol. A higher value means that the cation is more acidic, hence favoring the formation to the corresponding alcohol.

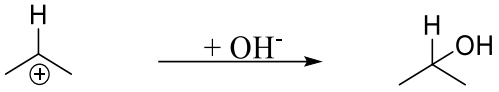

$$R^+ + H_2O \rightleftharpoons ROH + H^+$$

$$pK_R^+ = \log[R^+]/[ROH] + pH$$

Scheme **12:** The equilibrium constant pK_R^+ for the reaction from the cation to the alcohol.

Matrix isolation experiments suggest that cations with higher pK_R^+ values are more reactive upon annealing of the LDA water ice matrix (Scheme 13).[4, 85] While fluorenyl cation **72** with a

pK_R^+ of -15.9 decays at ~30 K,[4] benzhydryl cation **62** with a pK_R^+ of -11.7 decays at ~50 K [3] and dihydrodibenzotropylium cation **82** with a pK_R^+ of -8.0 needs ~100 K to react to the corresponding alcohol.[80] The aromatic tropylium cation **102** is even persistent in LDA water ices until 160 K, where the water ice starts subliming.[88] Thus, cation **2** is expected to be very reactive based on the determined pK_R^+ value of -20.8 (estimated from the equilibrium constant for ionization of the corresponding chloride), whereas cation **22** with a pK_R^+ value of -9.4 is estimated to be less reactive.[10]

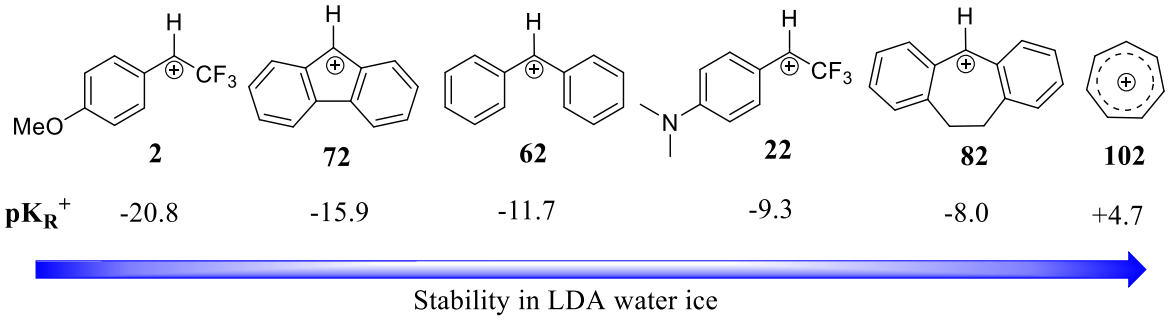

Scheme **13:** Relation of the pK_R^+ value to the thermal stability of cations in LDA water ices.[89, 10]

The electrostatic potential maps of the corresponding cations are calculated with B3LYP/Def2-TZVP and are shown in Figure 2. As mentioned above, cations **62** and **82** are stable in LDA water ices up to around 50 and 100 K, respectively. In contrast, cations **52** and **92** were not observed in analogously conducted experiments.[5, 28] Also the surfaces of the cations show slight differences in the color mapping, and hence the charge distribution. The electrostatic potential maps indicate that the rings in cations **52** and **92** are more deactivated (blue spots) than those in **62** and **82**. Hence, in **62** and **82** the cation moiety is more delocalized into the electron-rich ring, increasing the stability. Likewise, the ESP map of cation **22** shows a favorable delocalization that might indicate a similar stability as **62** or **82**. The surface of cation **2** instead shows less delocalization and is ambiguous to be stabilized in LDA water ice.

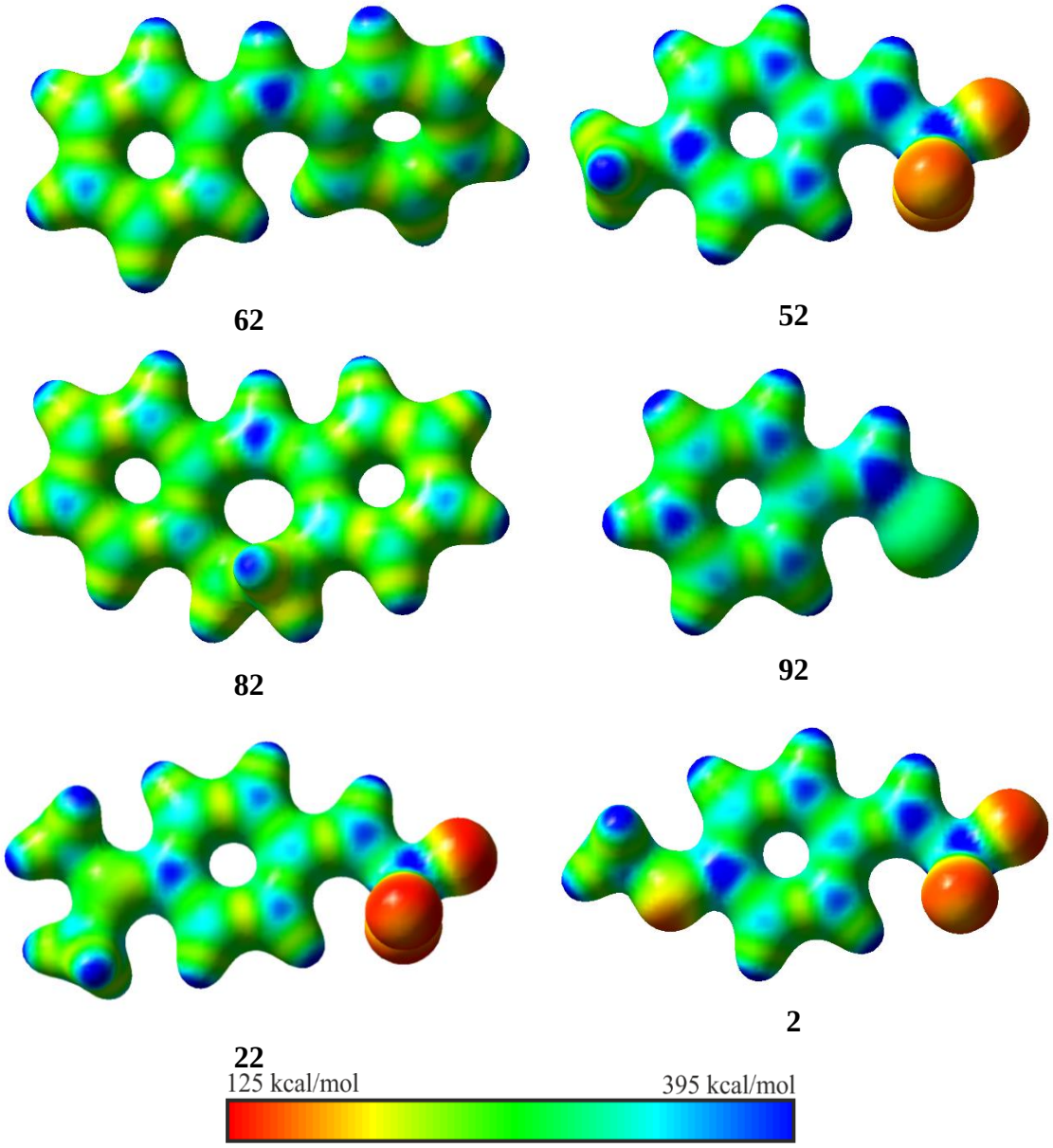

Figure **2:** Electrostatic potential maps of cations **62**, **52**, **82**, **92**, **22** and **2u** (color range from red with 125 kcal mol^{-1} to blue with 395 kcal mol^{-1} on a density of 0.07 a_0^{-3}). Calculated at B3LYP/Def2-TZVP level of theory.

2.2. Calculation methods for trifluoromethyl containing carbenes

With the help of quantum chemical calculations ground-state energies, geometrical structures and vibrational frequencies of molecules can be predicted. One popular method to perform those investigations is with the Density Functional Theory (DFT).[90] This method is in principle a less computationally intense compromise for energy estimations and IR spectral analysis than e.g. coupled cluster calculations. Since DFT is based on a couple of estimations, the results of those calculations have to be taken with vigilance and respect to each system. For example, for trifluoromethyl group containing molecules, it was observed that the intense C–F stretching vibrations usually in the region between 1200 and 1100 cm^{-1} are found to be calculated up to 50 cm^{-1} shifted to the right. Due to this poor harmonic frequency predictions of the B3LYP functional it was found necessary, in order to perform a reliable spectra analysis for molecules with fluorine containing groups, to use the M06-2x functional.[91] For this the optimized structures obtained with B3LYP/Def2-TZVP level of theory were used as an input for the calculations at M06-2x /Def2-TZVP level of theory. To probe the value of the calculation method for the used systems, precursor **6** and the corresponding carbene **1** were used as references for the IR analysis, because the IR spectrum of **1** is experimentally reported.[48] Therefore, the IR spectra of **6** (conformers u+d) were calculated using three different methods of theory (B3LYP/Def2-TZVP, B3LYP/6-31+G(d,p) and M06-2x/Def2-TZVP//B3LYP/Def2-TZVP) and compared to the IR spectrum of diazo compound **6** in an argon matrix at 3 K. In Figure 3 it is shown that the IR spectrum computed with M06-2x/Def2-TZVP//B3LYP/Def2-TZVP level of theory shows the best fitting to the IR spectrum at 3 K. The IR spectra calculated with B3LYP/Def2-TZVP, B3LYP/6-31+G(d,p) level of theory look nearly similar and are showing a poor congruency in C–F stretching region (1100 - 1200 cm^{-1}) with calculated red-shifted vibrations up to ~50 cm^{-1}. The IR spectrum generated at M06-2x/Def2-TZVP//B3LYP/Def2-TZVP level of theory shows an incongruency regarding the intensities of the asymmetrical stretching vibration of the methoxy-group which is calculated to 1325 cm^{-1} and more intense than the assigned experimental signal at 1293 cm^{-1}. But the calculated signal sums up both conformers **6**u and **6**d, and since the experimental signal is broadened it suggests a slight splitting of the responsible signals.

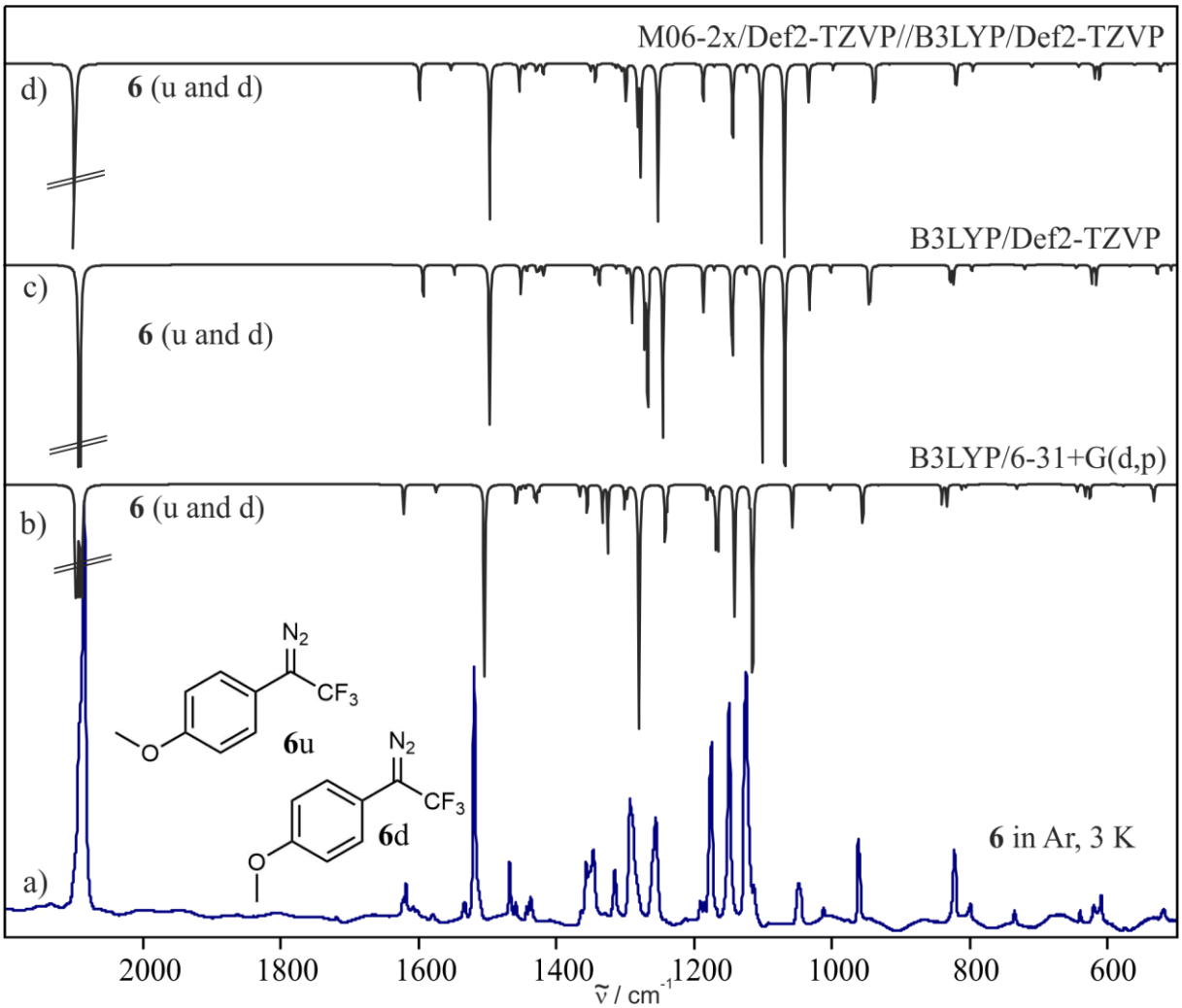

Figure **3:** Comparison of a) the experimental IR spectrum of precursor **6** in argon at 3 K, to the calculated spectra of **6** obtained with the b) M06-2x/Def2-TZVP//B3LYP/Def2-TZVP, c) B3LYP/Def2-TZVP d) B3LYP/6-31+G(d,p level of theory).

To further verify the fitting of the calculated IR spectra of carbene **1** to the experimentally obtained IR spectrum, three different methods are used: B3LYP/6-31+G(d, p), B3LYP/6-31+G(d,p) and M06-2x/Def2-TZVP//B3LYP/Def2-TZVP (Figure 4). The comparison shows especially in the region from 1300 to 1000 cm^{-1} a better agreement to the IR frequencies obtained with M06-2x/Def2-TZVP//B3LYP/Def2-TZVP. Particularly the C–C–C symmetrical stretching vibration assigned to the experimentally obtained IR medium intense signal at 1202 cm^{-1} is not matching to the spectra calculated at B3LYP/6-31+G(d,p) and B3LYP/Def2-TZVP level of theory. The same applies for the signal at 1078 cm^{-1} (C–F asymmetric stretching).

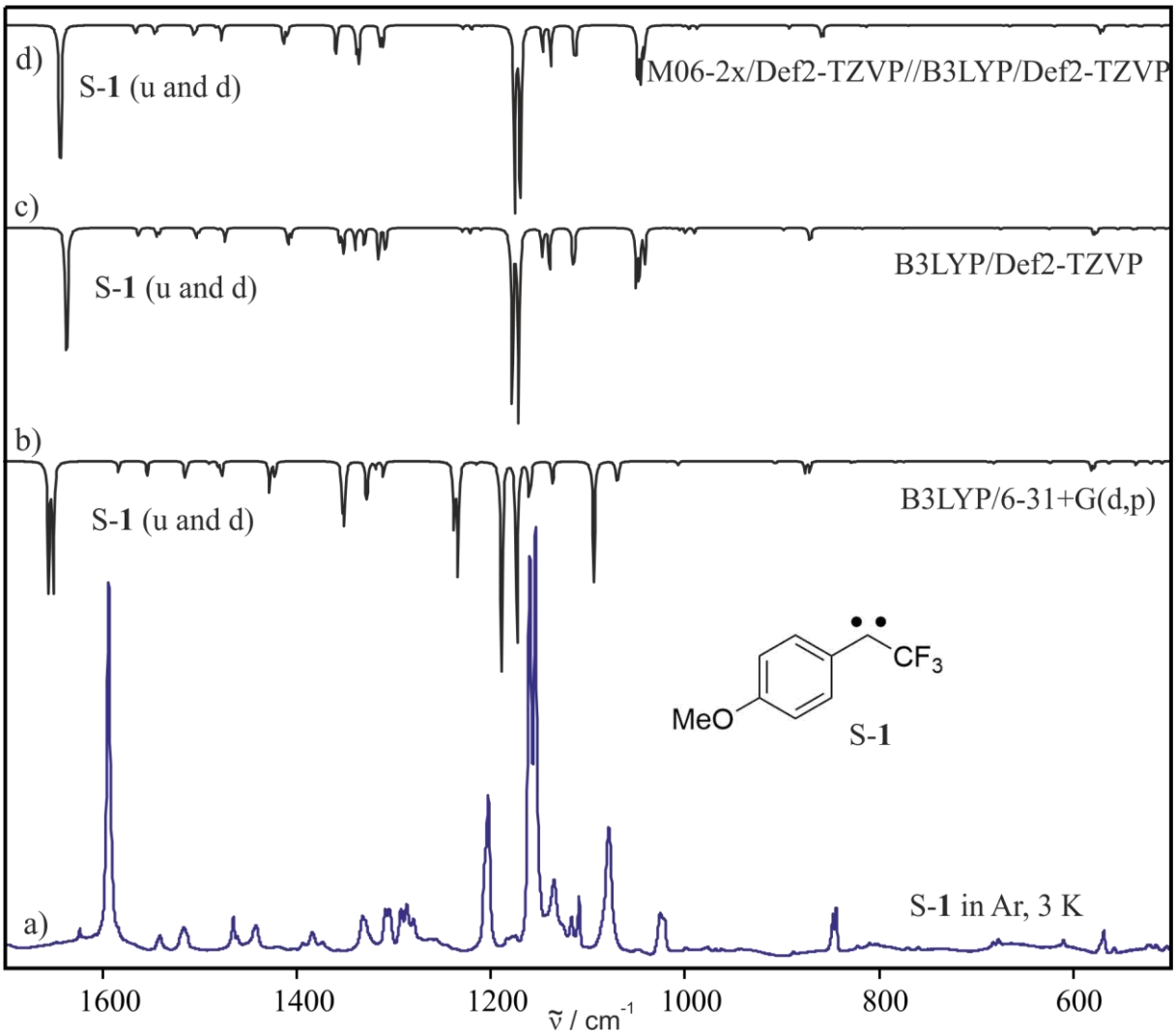

Figure **4:** Comparison of a) the experimental IR spectrum of carbene **1** in argon at 3 K) to the calculated spectra obtained with b) B3LYP/6-31+G(d,p), c) B3LYP/Def2-TZVP and d) M06-2x/Def2-TZVP//B3LYP/Def2-TZVP level of theory.

The comparison indicates that the IR spectra obtained with M06-2x/Def2-TZVP//B3LYP/Def2-TZVP level of theory give a better representation of the experimental spectra. Therefore, in this work, IR spectra were computed with M06-2x/Def2-TZVP//B3LYP/Def2-TZVP as described. Structure optimization and energy calculations were performed with B3LYP/Def2-TZVP level of theory.

2.3. *p*-Methoxyphenyl-1-(trifluoromethyl)carbene

2.3.1. Characterization in argon matrices

2.3.1.1. Introduction

Carbene **1** possess an electron-withdrawing trifluoromethyl (CF_3) unit and an aryl ring with an methoxy group (OMe) in *para* position. The *p*-methoxyphenyl group can be referred to as electron-donating by resonance, although the inductive effect of the negative oxygen atom counts against. Due to the counteracting effect of the CF_3 and *p*-OMe group, **1** can be referred to the group of push-pull substituted molecules.

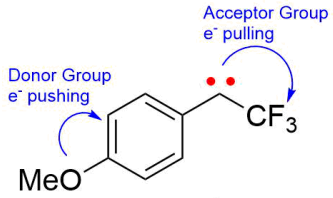

1

Carbene **1** was studied by Song and Sheridan in nitrogen matrices via IR, UV-vis and EPR spectroscopy. The spin specific reactivity of **1** was probed in H_2-, O_2-, and HCl-doped matrices supporting a singlet ground state.[48] The carbene did not react with O_2 and H_2, but inserted into H–CL forming adduct **18** (Scheme 14).

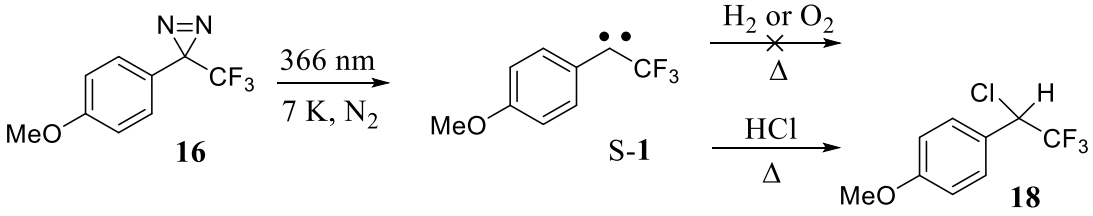

Scheme **14:** Generation and observed reactivity of S-**1** with O_2, H_2 and HCl at low-temperatures.[48]

2.3.1.2. Results and discussion

Before studying bimolecular reactions of carbene **1**, the photochemistry of precursor *p*-methoxyphenyl-1-trifluoromethyldiazomethane **6** and the thermal- and photostability of **1** must be studied in an inert environment. Therefore, *p*-methoxy-2,2,2-trifluoroacetophenone-*p*-tosylhydrazonide **5** was synthesized, converted via thermolysis to **6**, which was directly deposited with an excess of argon on a cesium iodide (CsI) window at 3 K. The obtained IR spectrum shows the strong, characteristic N=N stretching vibration of **6** at 2085 cm^{-1} (Figure 5). A closer look indicates that many signals are doublets, which most likely is due to the presence of two conformers **6**u and **6**d (Scheme 15). The IR spectrum of **6** was compared to the calculated spectra of the two conformers **6**u and **6**d (M06-2x/Def2-TZVP//B3LYP/Def2-TZVP) and shows a reasonable agreement. Due to difficulties to obtain reliable IR spectra of trifluoromethyl-containing molecules the IR frequencies were calculated using the M06-2x/Def2-TZVP//B3LYP/Def2-TZVP level of theory as explained in Chapter 2.2..

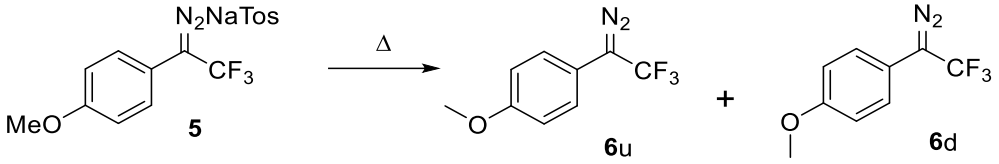

Scheme **15:** Generation of 6 by thermolysis of **5**.

2.3. p-Methoxyphenyl-1-(trifluoromethyl)carbene

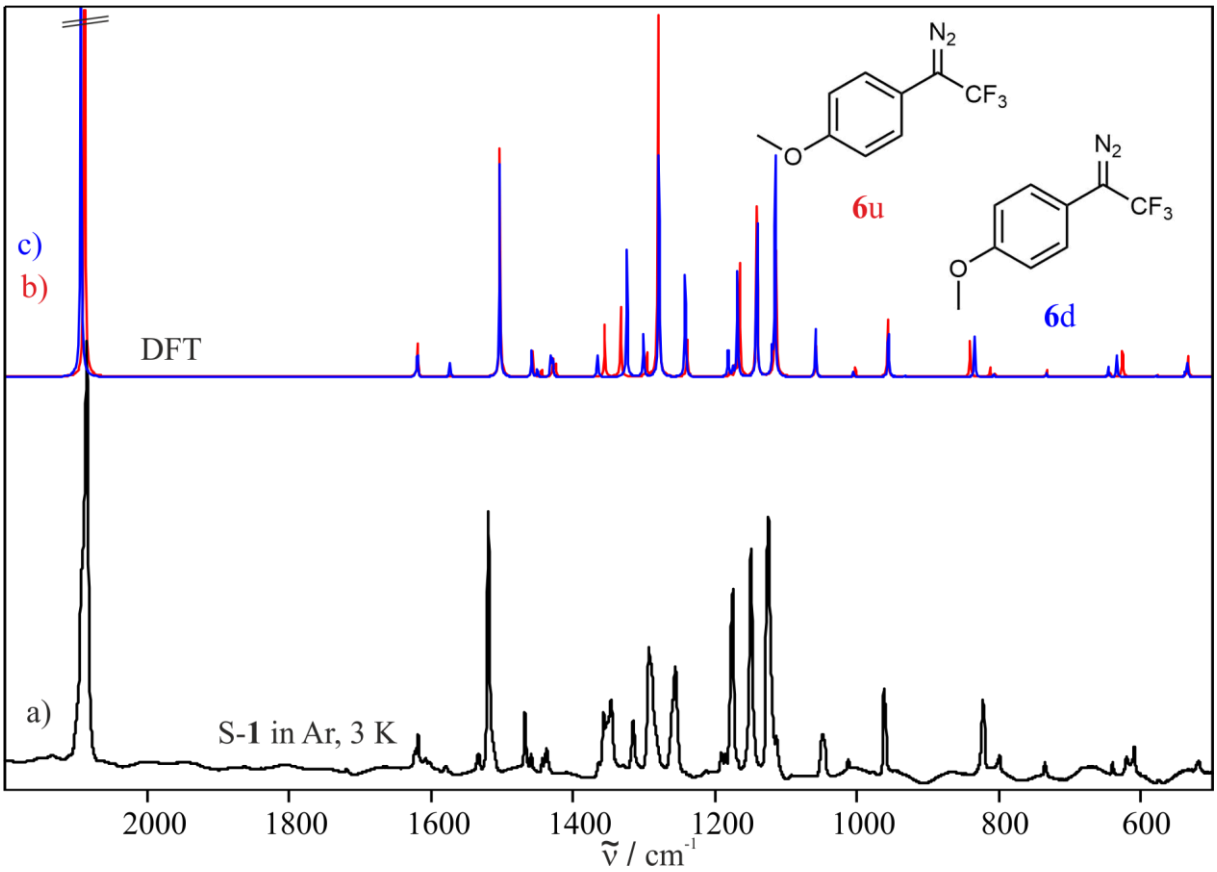

Figure **5:** a) IR spectrum obtained after deposition of precursor **6** in argon at 3 K. Calculated spectra of b) **6u** and c) **6d** (M06-2x/Def2-TZVP//B3LYP/Def2-TZVP).

Table **2:** Experimental and calculated vibrational frequencies of **6**.

Exp.[b]		Calc.[a]				Assignment [c]
		6u		**6**d		
$\tilde{\nu}$	$I_{rel.}$	$\tilde{\nu}$	$I_{rel.}$	$\tilde{\nu}$	$I_{rel.}$	
2960	3			3178.2	2	C-H str. (CH_3)
2943	2	3155.7	2			C-H str. (CH_3)
2918	1	3100.4	3	3108.5	3	C-H str. (CH_3)
2843	2	3035.4	5	3045.8	5	C-H str. (CH_3)
2085	100	2182.3	100	2189.4	100	N=N str.
1619	4	1685.9	5	1686.5	4	C=C Ring str.
1520	36	1562.0	33	1562.8	30	C=C Ring str.
1469	3	1513.3	4	1514.9	4	C-H bend. (CH_3)
1440	4	1405.7	8	1486.1	3	C-N str.
1358, 1347	14	1382.1	10	1373.0	18	C-C-C def. antisym.
1316	7	1343.3	4	1348.1	6	C-H bend.
1294	35	1326.0	53	1324.7	33	C-O str.
1256	27	1283.2	6	1285.7	15	C=C Ring str.
1176	30	1204.2	17	1207.1	15	C-F str.
1150	35	1179.0	25	1178.0	21	C-F str.
1125	62	1150.0	34	1151.2	33	C-F str.
1048	10	1090.9	5	1090.8	7	C-O str.
1013	1	1031.8	1	1033.9	1	C=C Ring def.
963, 960	11	983.1	8	981.4	7	C=C Ring def.
823	10	859.9	5	852.3	6	C-H bend. out of plane
799	2	830.2	1	829.6	0	C-H bend. out of plane
735	1	746.1	1	744.6	1	C-F bend.
640	1	651.8	1	653.0	1	C=C Ring def.
621	5			639.6	4	C=C Ring def.
609	6	632.6	4			C=C Ring def.
521	1	534.9	2	534.3	2	C-H bend. out of plane

[a] Calculated at M06-2x/Def2-TZVP//B3LYP/Def2-TZVP level of theory. [b] In argon at 3 K. [c] Tentative assignment.

To generate carbene **1**, precursor **6** was irradiated with a 450 nm light-emitting diode (LED) for 17 hours until the complete depletion of the precursor signals. The IR spectra obtained before and after photolysis can be found in Figure 6. The newly formed signals are matching the IR signals obtained by Song and Sheridan for singlet carbene **1** and to the calculated IR frequencies of S-**1** as well (Table 3).[48] The most intense bands of **1** can be found at 1594 cm^{-1} (C–C–C symmetric stretching) and at 1160, 1155 cm^{-1} (aryl C=C stretching). A careful analysis as shown in the fingerprint region of the IR spectrum indicates that some peaks are doublets. This points to the presence of two similar species which is likely due to the presence of the two conformers of **1** with the methoxy group pointing upwards S-**1**u and downwards S-**1**d regarding the CF_3 group. This agrees with calculations showing an energy difference of only 0.20 kcal mol^{-1}

between the two conformers S-**1**u and S-**1**d. The bistability of the singlet and triplet state of the carbene can be ruled out due to a similarly conducted EPR experiment which did not show any signal for a triplet species.[92, 93] With the help of calculated IR spectra of the two conformers S-**1**u and S-**1**d, the two species were assigned preliminarily to S-**1**u and S-**1**d. The very similar IR spectra of S-**1**u and S-**1**d can be explained with the similar dipole moments of the conformers. Nonetheless, the intensities of the doublet at 848 and 844 cm^{-1} (C–H bend. out of plane) was used for a rough estimation of the ratio of S-**1**u and S-**1**d. The conformers are produced after irradiation of **6** in a ratio of approximately 0.8:1 on side of the computationally most stable conformer S-**1**u. As the energy difference between the two conformers is with 0.20 kcal mol^{-1} nearly degenerate, the most stable conformer cannot be determined with the used calculations. The conformers and selected parameters of carbene **1** in its singlet and triplet state are depicted in Chart 8. B3LYP/Def2-TZVP calculations confirm the singlet ground state of carbene **1** by predicting a singlet-triplet energy gap (ΔE_{ST}) of -0.43 and -0.16 kcal mol^{-1} for the u- and d-conformers, respectively. Because the electronic correlation in the singlet state is not properly treated by exchange-correlation functionals as B3LYP,[94] the corrected ΔE_{ST} is typically overestimated by about 2.5 kcal mol^{-1}. Hence the corrected ΔE_{ST} should be about -3 kcal mol^{-1}.

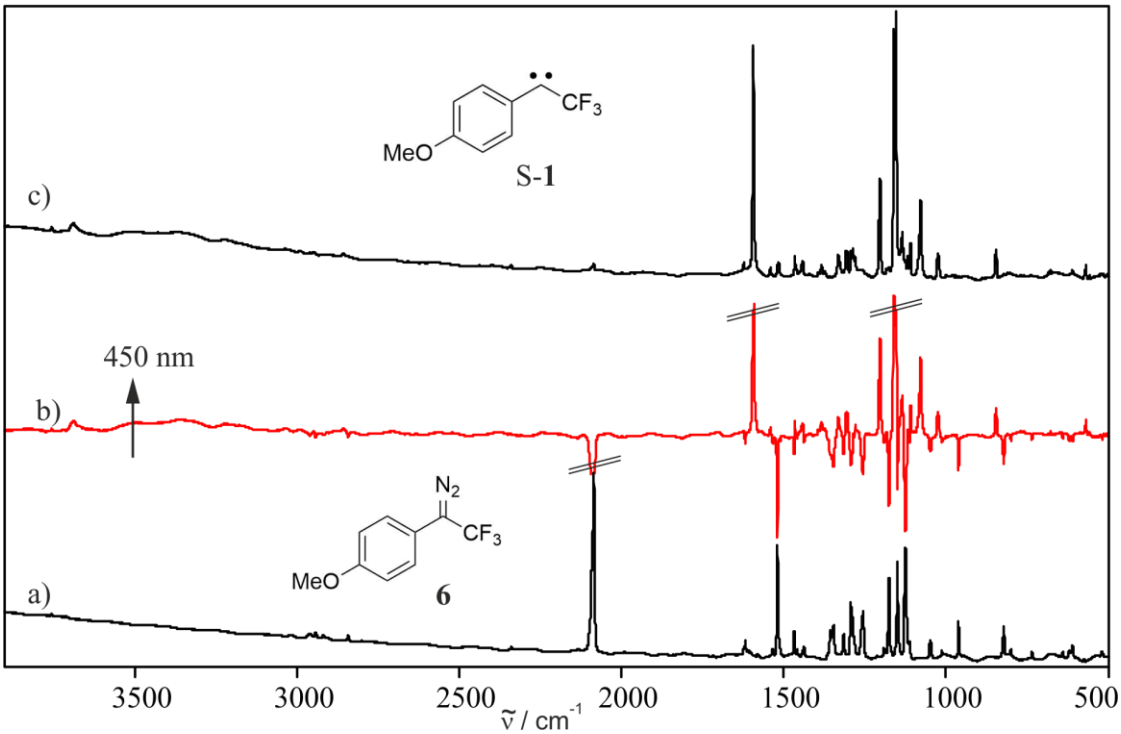

Figure **6:** a) IR spectrum obtained after deposition of **6** in argon at 3 K. b) IR difference obtained after 17 hours 450 nm irradiation. Bands pointing upwards increase in intensity. Bands pointing downwards decrease in intensity. c) The absolute IR spectrum of carbene **1**.

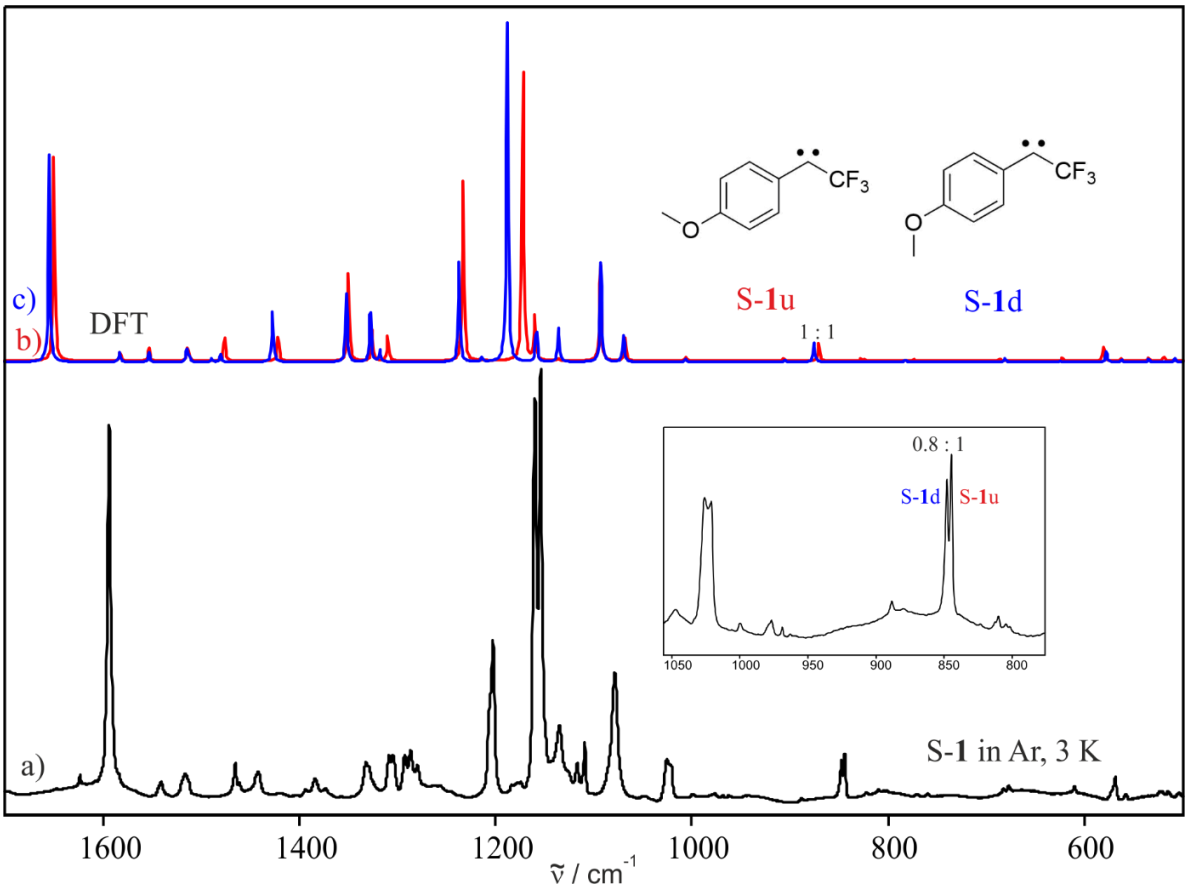

Figure **7:** Formation of carbene **1**. a) IR spectrum obtained after irradiation of **6** and calculated IR spectra of both conformers b) S-**1**u and c) S-**1**d (M06-2x/Def2-TZVP//B3LYP/Def2-TZVP).

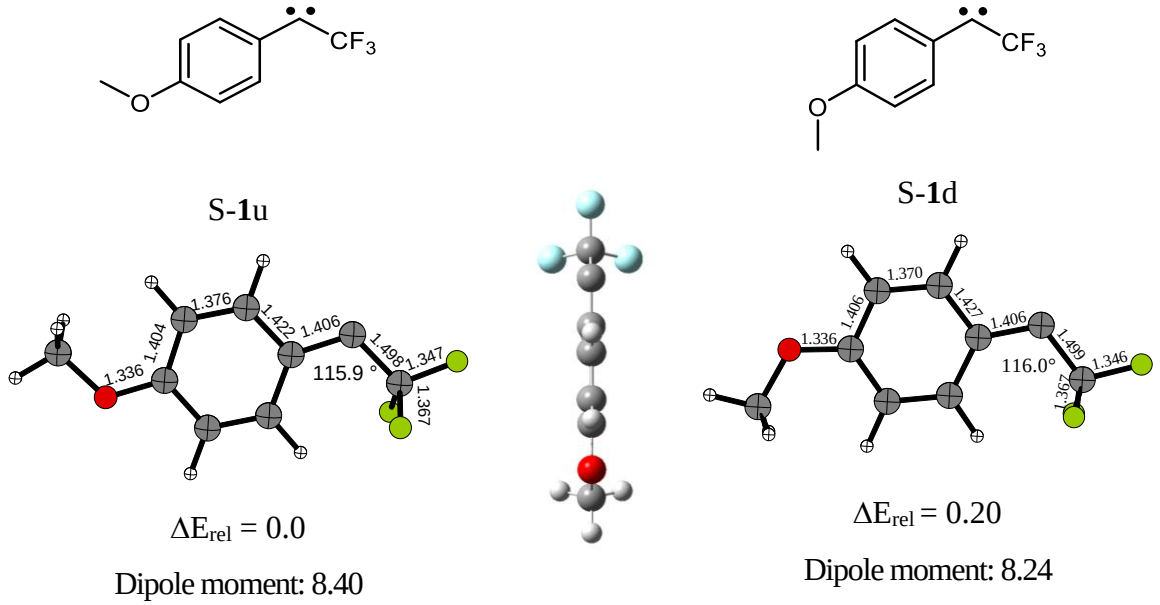

ΔE_{rel} = 0.0

Dipole moment: 8.40

ΔE_{rel} = 0.20

Dipole moment: 8.24

Chart **8:** Structures and selected parameters of the different conformers of **1** in the singlet state. ΔE_{rel} in kcal mol^{-1}. Bond lengths in Å. Energies, structures and dipole moments calculated with B3LYP/Def2-TZVP level of theory.

Table **3:** Experimental and calculated vibrational frequencies of S-**1**.

Exp.[b]		Calc.[a]				Assignment [c]
		S-**1**u		S-**1**d		
$\tilde{\nu}$	$I_{rel.}$	$\tilde{\nu}$	$I_{rel.}$	$\tilde{\nu}$	$I_{rel.}$	
2987	26	3194.0	1	3178.6	1	C-H str. (CH_3)
2946	13	3143.5	2	3137.8	1	C-H str. (CH_3)
2857	19	3069.9	4	3062.2	3	C-H str. (CH_3)
1594	60	1649.9	66	1654.8	60	C=C Ring str.
1542	2	1582.6	3	1583.2	3	C=C Ring str.
1515	5	1553.3	4	1553.2	3	C-H bend.
1466	4	1513.9	3	1514.4	4	C-H bend. (CH_3)
1442	5	1476.3	8	1480.2	2	C=C Ring def.
1384	9	1421.7	8	1427.1	14	C-C-C str. antisym.
1332	8	1349.9	28	1351.8	20	C=C Ring str.
1307	8	1325.7	11	1327.5	17	C-H bend.
1287	14	1309.8	8	1317.8	3	C-H bend.
1203	30	1233.2	59	1237.2	29	C-C-C str. sym.
1160, 1155	100	1172.3	100	1188.2	100	C-H bend.
1135	10			1158.5	10	C-F str.
1117	2	1160.2	15			C-F str.
1109	3			1135.7	11	C-H bend.
1079	31	1093.4	34	1092.7	31	C-F str.
1024	11	1068.1	7	1069.8	8	C-O str. (CH_3)
848, 844	7	870.8	6	875.6	6	C-H bend. out of plane
567	3	580.7	5	577.7	3	Ring def.

[a] Calculated at M06-2x/Def2-TZVP//B3LYP/Def2-TZVP level of theory. [b] In argon at 3 K. [c] Tentative assignment.

Interestingly, by secondary photolysis the ratio of S-**1**u and S-**1**d changes. It is found that irradiation of carbene **1** with a 365 nm LED causes the decrease of the bands of S-**1**d and the increase of the bands of the S-**1**u (Figure 8). The opposite happens if 254 nm light is used. The switching of the species by light is reversible. In contrast to our experiments, Song and Sheridan used 366 nm light to convert the diazirine precursor to carbene **1**.[48] Since this wavelength converts S-**1**d to S-**1**u, he may not have observed S-**1**d. The band at 1109 cm^{-1}, preliminarily assigned to S-**1**d, is not reported in his experiments. Apart from conformer switching no newly formed signal appeared throughout the secondary photolysis of S-**1** ranging from UV to IR light (LED light from 365 to 650 nm and a mercury lamp of 254 nm). This points to a high photostability of S-**1**, as observed for the similar CF_3 group containing aromatic carbenes **20** or **50**.[28] If the argon matrix containing S-**1** is annealed up to 25 or 30 K, the absorptions of S-**1**u decreases whereas S-**1**d increases (Figure 9). This is analogous to the effect on the conformer

switching with 254 nm photolysis. Subsequent irradiation with 365 nm results in an increase of species S-**1**u and a decrease of bands assigned to S-**1**d.

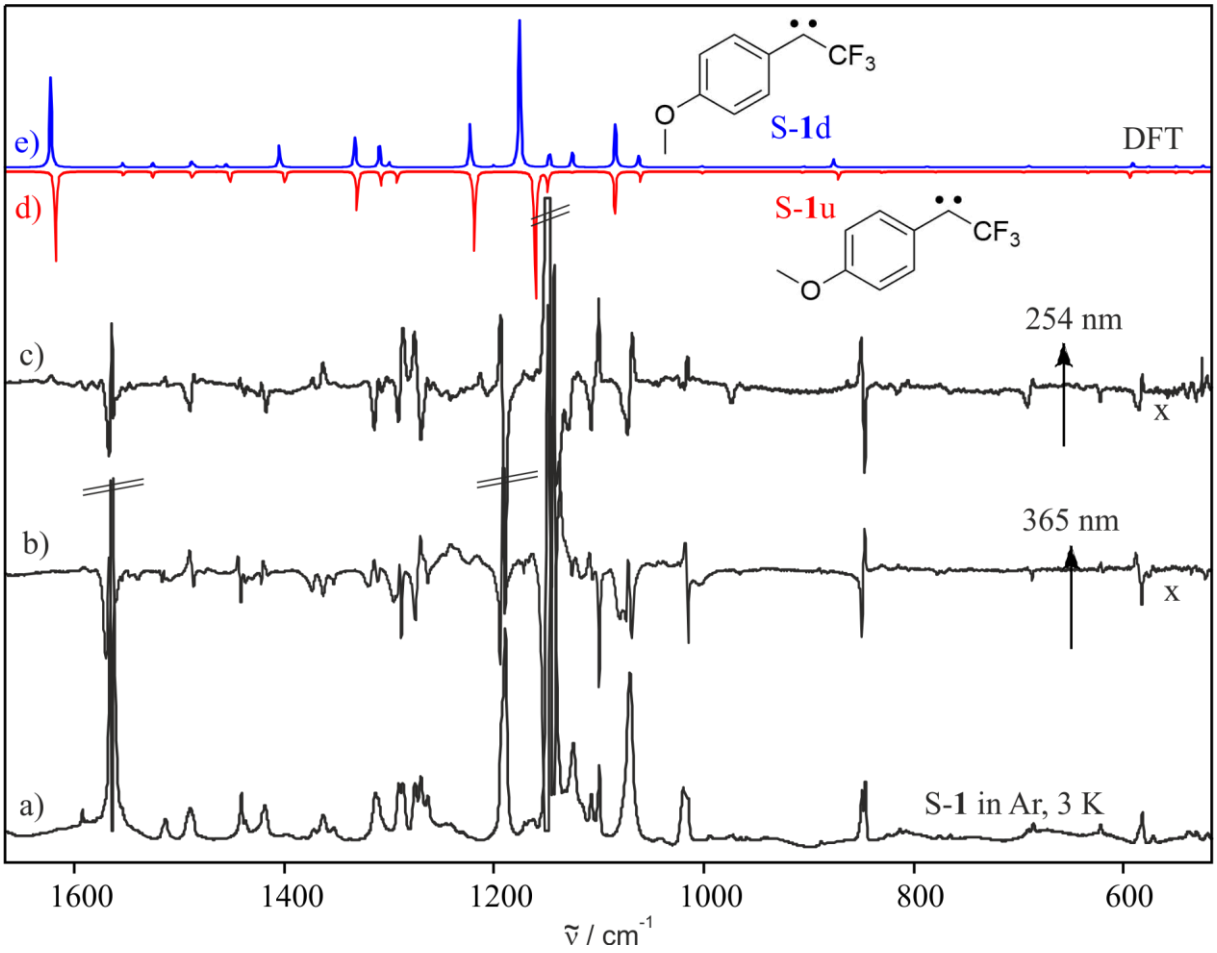

Figure **8:** IR spectra showing the secondary photochemistry of S-**1**. a) IR spectrum obtained after irradiation of the precursor **6** with 450 nm in argon at 3 K. b) IR difference spectrum obtained after irradiation of the matrix containing S-**1** with 365 nm for 10 minutes and c) with 254 nm for 10 minutes. Bands pointing upwards increase in intensity. Bands pointing downwards decrease in intensity. Calculated spectra of both conformers d) S-**1**u and e) S-**1**d (M06-2x /Def2-TZVP//B3LYP/Def2-TZVP). ^{x} represents a magnified difference spectrum.

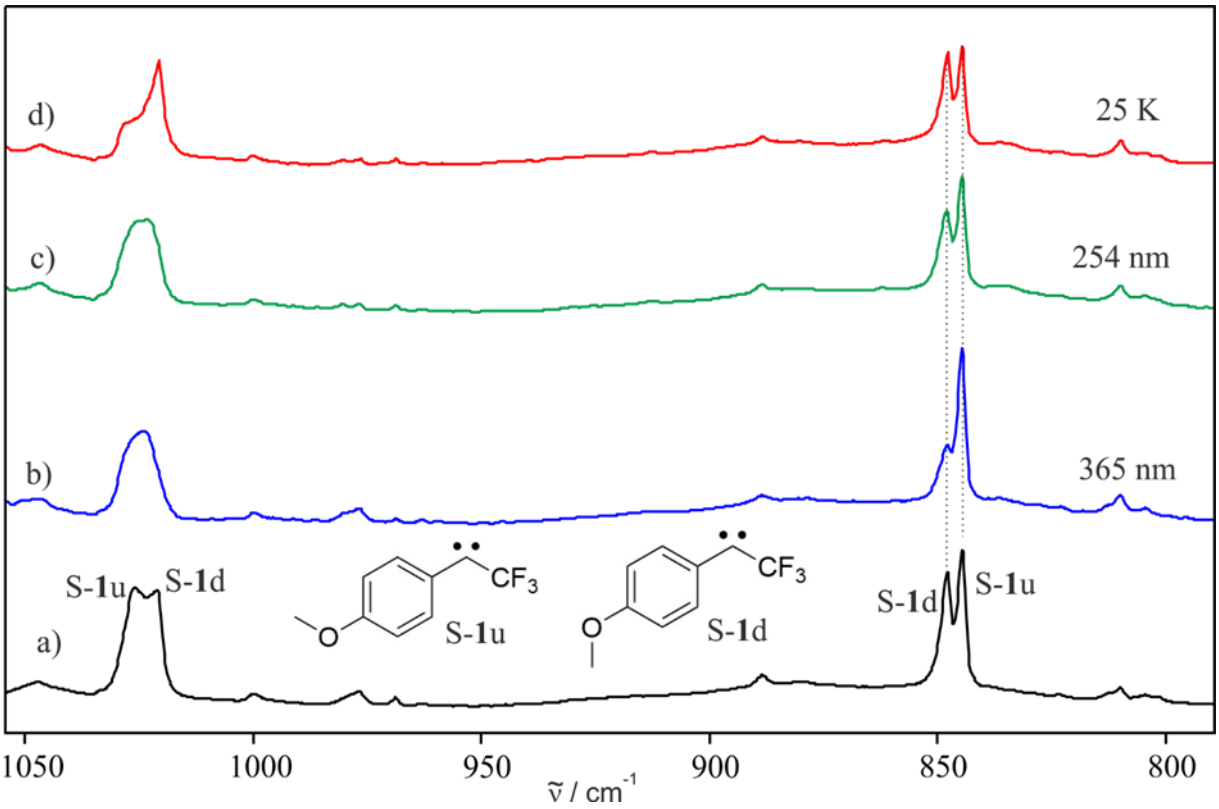

Figure **9**: IR spectra showing the light-induced and thermal behavior of S-**1** in argon at 3 K. IR spectra obtained a) after photolysis of precursor **6** and b) after subsequent 365 nm photolysis (90 minutes), b) after subsequent 254 nm photolysis (90 minutes) and c) after subsequent annealing to 25 K (10 minutes).

In addition to the IR experiments, an experiment was conducted the same way and observed with UV-vis spectroscopy. Singlet carbenes exhibit very informative electronic spectra, which vary as a sensitive function of substituents and geometries.[95]

The UV-vis spectrum of **6** shows an intense absorption at 205, 266 and a small one at 311 nm (Figure 10). Although no visible absorption of **6** at 400 - 500 nm could be detected, irradiation with 450 nm converts the diazo compound **6** to carbene S-**1**. The UV-vis spectrum of S-**1** shows an intense doublet at 335 and 346 nm, as well as smaller bands at 270 nm and 220 nm. The UV-vis spectrum agrees to that reported by Song and Sheridan, however, they could not resolve the band at ~340 nm, presumably due to spectral saturation or since they use 365 nm to produce the carbene from the diazirine. The doublet at 340 nm may be traced back to the presence of the two conformers. The ratio changes by photolysis and annealing congruently to the IR experiment. But calculations of S-**1**u and S-**1**d at the TD-DFT level of theory (B3LYP-D3/6-311+G(d,p)) predict only minor changes for the two conformers (Figure 11).

2.3. p-Methoxyphenyl-1-(trifluoromethyl)carbene

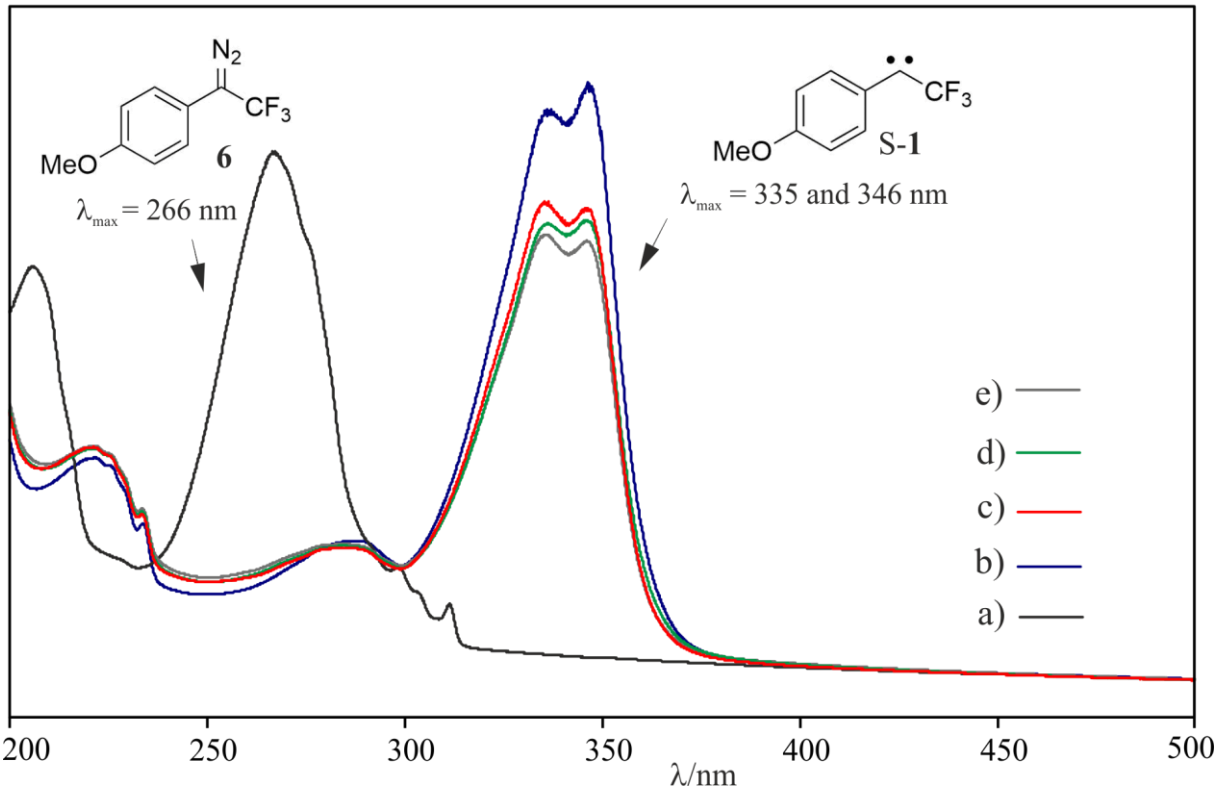

Figure **10:** UV-vis spectra of a) **6** in argon at 8 K and b) after 450 nm photolysis. c) After subsequent 365 nm photolysis, d) after subsequent 254 nm photolysis and e) after subsequent 365 nm photolysis.

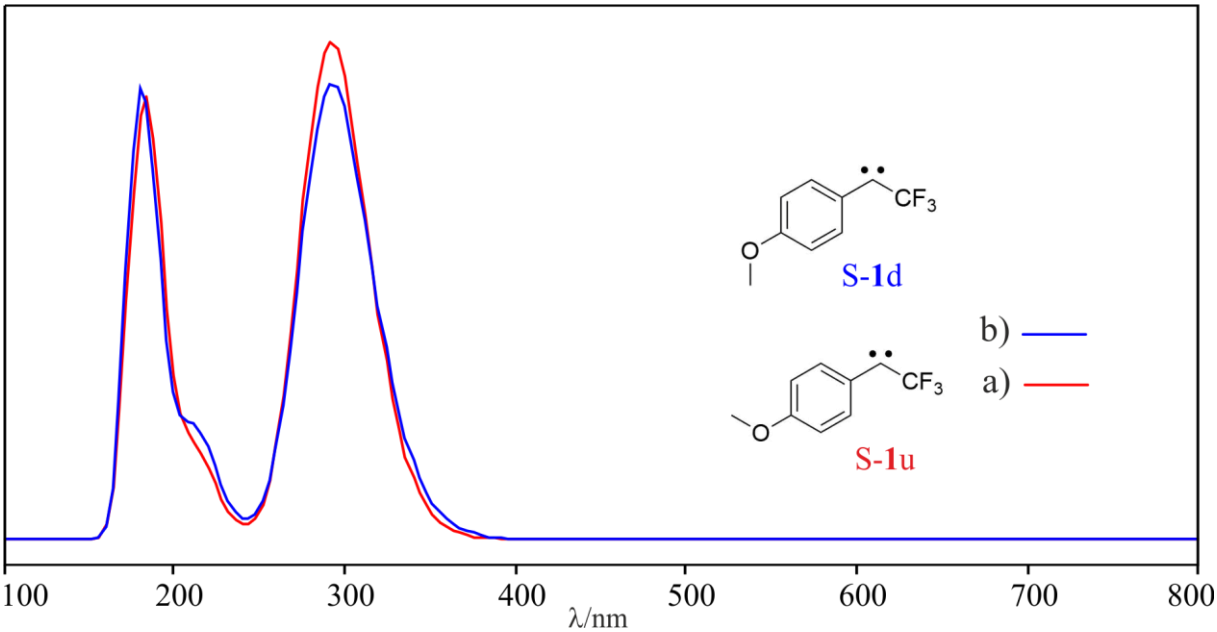

Figure **11:** UV-vis spectra of a) S-**1**u and b) S-**1**d calculated at TD-B3LYP-D3/6-311+G(d,p) level of theory.

2.3.1.3. DFT Calculations

To explain the observed interchanging of the conformers S-**1**u and S-**1**d with light and temperature, DFT calculations were performed. In principle, annealing would populate the more stable conformer if the separating energy barrier can be overcome. Whilst photolysis can lead to a population of both conformers depending on the wavelengths.[30, 96, 97] The transition state (TS) between the two conformations was computed with B3LYP-D3/6-311+G(d,p) level of theory. It suggests a TS with the methoxy group rotating with 115° out of the aromatic plane (Chart 9) and an energy difference of 6.17 kcal mol^{-1} referring to S-**1**u. This energy barrier can possibly overcome with (photo)annealing but is, regarding literature, unlikely to be passed at 30 K. However, as the calculations do not implement the solvation of the carbene in argon and the possible effects on the energies, the activation barrier may be lower and then possibly able to be overcome at 30 K. A second aspect is, that the computations suggest S-**1**u to be the more stable conformer, unless it was found experimentally that S-**1**d is increasing upon annealing and thus indicates this conformer to be the most stable one at least in argon matrices. This can be rationalized with the energetical degeneracy of the conformers of S-**1**u and S-**1**d (0.2 kcal mol^{-1} (B3LYP/Def2-TZVP)) causing that the most stable conformer cannot be derived from the DFT calculations. Thus, it may be concluded that the calculations do not support the experimental observations from the annealing experiment, but this may potentially be traced back to the limits of DFT calculations and also to the not implied solvation or matrix effects.

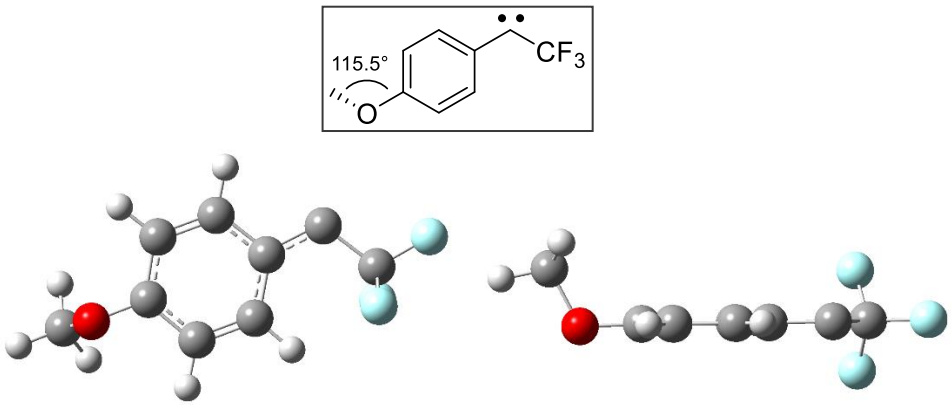

Chart **9:** Calculated structure of the transition state for the conversion from S-**1**u to S-**1**d.

2.2.1.4. Conclusions

Before studying bimolecular reactions of carbene **1**, the chemistry and photolysis of **1** was characterized in inert argon matrices at 3 K. The IR and UV-vis experiments revealed that diazo compound **6** is converted with 450 nm light to carbene S-**1** in its singlet state (Scheme 16). At 3 K both conformers S-**1**u and S-**1**d are formed in a ratio of approximately 1:0.8, according to the IR experiment. These two conformers can be interconverted by photolysis and annealing. DFT calculations predict S-**1**u and S-**1**d to be nearly degenerate in energy. It is noteworthy that no intramolecular rearrangements were observed upon secondary photolysis.

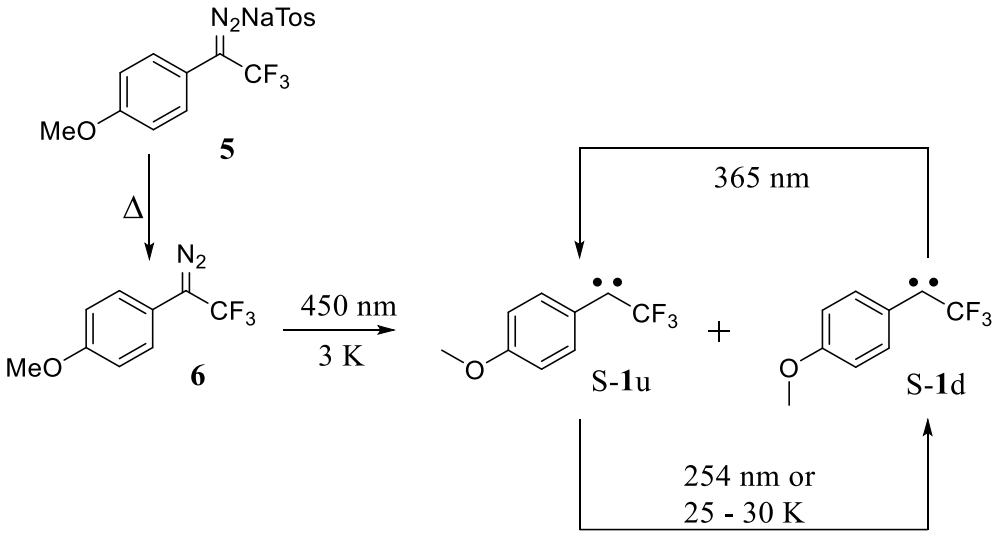

Scheme **16:** Generation of S-**1** and the observed behavior at 3 K in argon upon photolysis and annealing.

2.3.2. Complexation with water in doped matrices

2.3.2.1. Introduction

To observe the complexation of carbenes via matrix isolation, the matrix host can be doped with e.g. Lewis acids like H_2O. The reactive guest molecule is generated by photolysis and isolated in the rigid matrix at 3 K. By softening the matrix through low-temperature annealing, diffusion of small molecules is enabled and leads to interactions and agglomerations. The expected interaction of singlet carbenes with a single molecule of H_2O is the formation of hydrogen-bonded complexes, as observed before with chlorophenyl carbene **90** and fluorophenyl carbene **91** (Scheme 17).[5] Complexes S-**90**--H_2O and S-**91**--H_2O are stable in argon matrices at 3 K, but can be converted to the carbene and H_2O by visible light irradiation. Upon irradiation with UV light they rearrange further to the corresponding aldehyde complexed with HCl or HF. The corresponding alcohols could not be observed due to their instability.

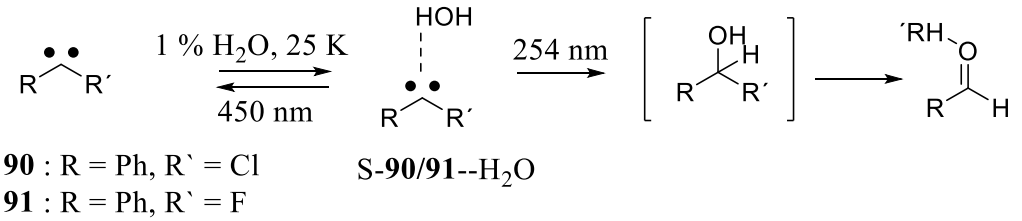

90 : R = Ph, R` = Cl
91 : R = Ph, R` = F

S-**90**/**91**--H_2O

Scheme **17:** Observed reactions of **90** and **91** in argon matrices doped with 1 % of H_2O.[5]

As explained before a similar reactivity was found for triplet carbenes with low lying S-T gaps (**60**, **50, 80**).[12, 13, 28] Those carbenes are stabilized in their singlet states by complexation with H_2O and showed a further rearrangement to the corresponding OH insertion products by photolysis.

2.3.2.2. Results and discussion

To study the complexation of carbene S-**1** and H_2O, **6** was deposited together with argon doped with 1 % of H_2O at 3 K. Subsequent 450 nm photolysis of **6** resulted in the IR signals of singlet carbene S-**1** and H_2O shown in Figure 12. To allow diffusion of small molecules like water, the argon matrix was subsequently annealed to 25 K. The IR absorptions assigned to S-**1** and H_2O decrease, and new bands appear: 1402, 1265, 1210 and 1090 cm^{-1} are the most prominent ones. A closer look at the fingerprint region in Figure 13 shows that the decreasing bands, obtained after annealing to 25 K, can be assigned to S-**1** (u and d) and H_2O. The increasing bands are, compared to the absorptions of S-**1**, broader and slightly shifted, which is characteristic for hydrogen-bonded complexes of singlet carbenes.[5] Therefore, the new bands were assigned to hydrogen-bonded complex S-**1**--H_2O. The antisymmetric C–C–C stretching vibration of S-**1** at

1384 cm^{-1} is blue-shifted in case of S-**1**--H_2O by +20 cm^{-1} compared to S-**1** (Table 1). DFT calculations confirm this assignment by showing a shift of +14 cm^{-1}. Likewise, the intense symmetrical C–C–C stretching vibrations of S-**1** at 1160 and 1155 cm^{-1} are blue-shifted by +10 cm^{-1} relative to the conformer S-**1**u and by +5 cm^{-1} relative to the conformer S-**1**d. The DFT calculations corroborate this by predicting similar shifts of +23 cm^{-1} (S-**1**u) and +10 cm^{-1} (S-**1**d). Another blue-shift can be observed for the C–F antisymmetric stretching which is shifted by +11 cm^{-1} to 1090 cm^{-1} in S-**1**--H_2O (DFT: shift = +14 cm^{-1}). The observed blue-shifted signals reflect a strengthening of the corresponding bonds which can also be validated by the calculated shortening of bond lengths shown in Chart 10. For example, the C_{Aryl}–$C_{Carbene}$ distance in S-**1**--H_2O is shortened by -0.008 Å compared to the distance in the monomer S-**1**. The experimentally obtained signals of S-**1**--H_2O do not allow an assignment to the two conformers.

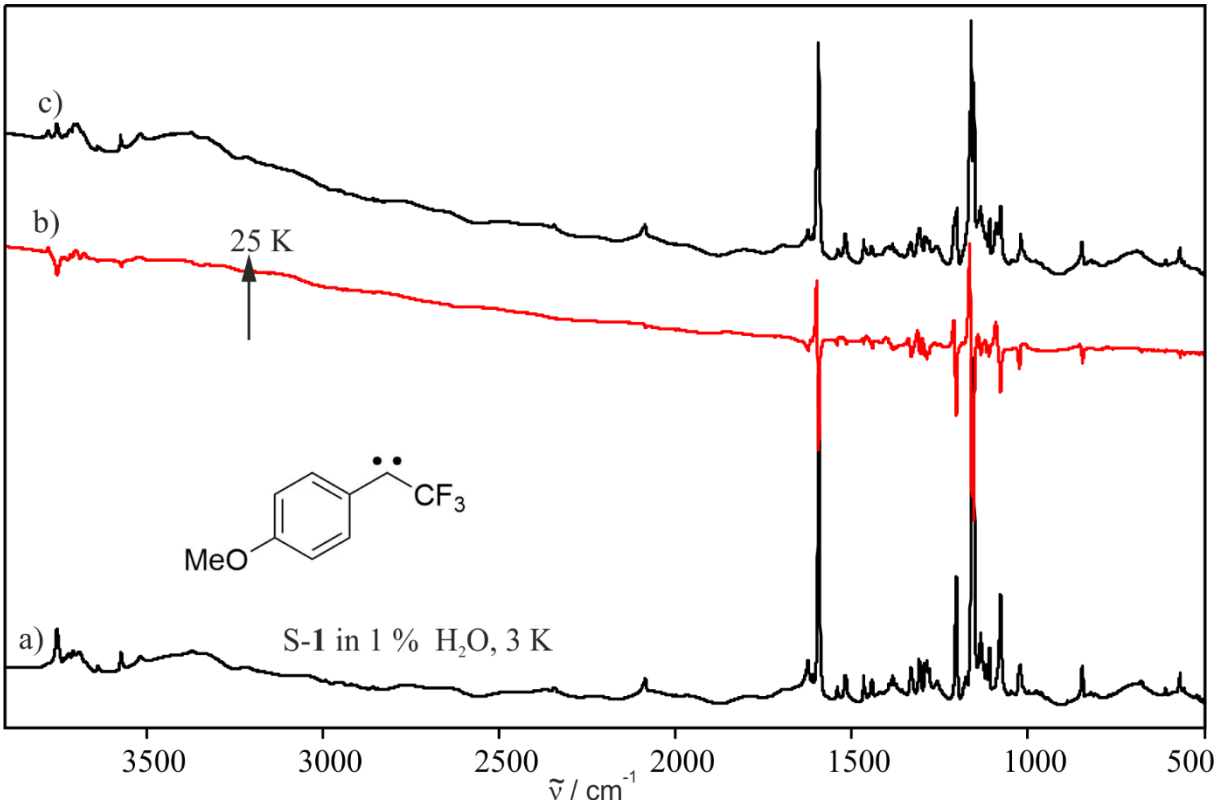

Figure **12:** Annealing of a matrix containing 1 % of H_2O and S-**1** in argon. a) IR spectrum obtained after photolysis of **6**. b) IR difference spectra obtained after annealing the same matrix from 3 to 25 K. Bands pointing upwards increase in intensity and are assigned to complex S-**1**--H_2O. Bands pointing downwards decrease in intensity and are assigned to carbene S-**1** (both conformers) and H_2O. c) Corresponding absolute IR spectrum.

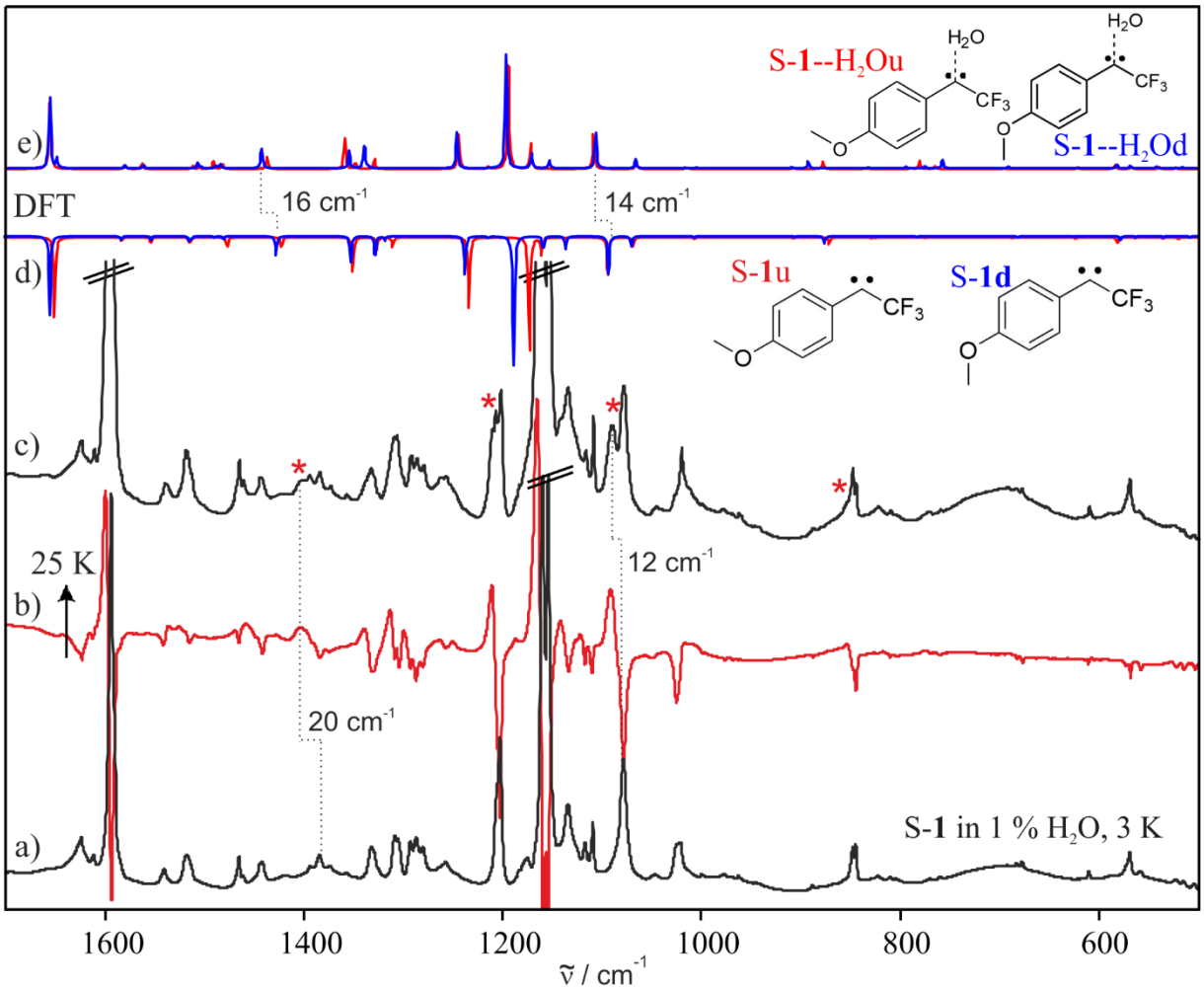

Figure **13:** IR-spectra showing the thermal reaction of water and S-**1** in an argon matrix. a) IR spectrum obtained after irradiation to generate carbene S-**1**. b) IR difference spectrum obtained after annealing the same matrix to 25 K. Bands pointing upwards increase in intensity and are assigned to complex S-**1**--H_2O. Bands pointing downwards decrease in intensity and are assigned to S-**1** (u + d). c) The corresponding IR spectrum. *The asterisks mark the most prominent new bands. IR spectra of d) S-**1** (u and d) and e) S-**1**--H_2O (u and d) calculated at M06-2x/Def2-TZVP//B3LYP/Def2-TZVP level of theory.

Table **4:** Experimental and calculated vibrational frequencies of S-**1**--H_2Ou:

Exp. [a]		Calc. [b] S-**1**--H_2Ou		Assignment [c]
$\tilde{\nu}$	$I_{rel.}$	$\tilde{\nu}$	$I_{rel.}$	
3215	5	3319.6	100	O-H str.
1600	100	1656.1	41	O-H bend. + C=C Ring str.
1538	3	1580.1	3	C=C Ring str.
1526	2	1563.1	4	C=C str.
1457	6	1491.4	6	C-H scissoring (CH_3)
1404	10	1437.3	9	C-C-C str. antisym.
1313	16	1359.1	22	C-H bend.
1299	6	1329.2	7	C=C Ring def.
1210	28	1244.3	27	C-H bend.
1165	90	1194.5	92	C-H bend.
1143	14	1171.9	18	C-F str.
1090	30	1108.7	27	C-F str.
1012	9	1065.8	6	C-O str. (CH_3)
854	3	878.3	5	C-H bend. out of plane
774	1	780.8	6	O-H bend.
608	1	621.4	1	Ring def.
564	1	584.1	3	Ring def.

[a] Calculated at M06-2x/Def2-TZVP//B3LYP/Def2-TZVP level of theory. [b] In argon doped with 1 % of H_2O at 3 K. [c] Tentative assignment.

Table **5:** Experimental and calculated vibrational frequencies and shifts of S-**1**--H_2Ou:

Calculated [a]			Experimental			Assignment [e]
S-**1** (u)	S-**1**--H_2Ou		Argon [c]	Agon/H_2O [d]		
ν/cm^{-1} ($I_{abs.}$)	ν /cm^{-1} ($I_{abs.}$)	shift[b]	ν /cm^{-1} ($I_{abs.}$)	ν /cm^{-1} ($I_{abs.}$)	shift[b]	
870.8 (6)	878.3 (5)	+8	844 (7)	854 (3)	10	C-H bend. out of plane
1093.4 (34)	1108.7 (27)	+15	1079 (31)	1090 (30)	+11	C-F str.
1233.2 (59)	1194.5 (92)	+39	1203 (30)	1165 (90)	+38	C-C-C str. sym.
1421.7 (8)	1437.3 (9)	+16	1384 (9)	1404 (10)	+20	C-C-C str. antisym.
1649.9 (66)	1656.1 (41)	+6	1595 (60)	1600 (100)	+5	C=C Ring str.

[a] Calculated at M06-2x/Def2-TZVP//B3LYP/Def2-TZVP level of theory. [b] Shifts relative to monomers (cm^{-1}). [c] In argon matrix at 3 K. [d] In argon matrix doped with 1 % H_2O at 3 K. [e] Tentative assignment.

Because the complexation also affects the bonding of the involved water molecule, additional evidence for a complexation can be found in the IR region between 3900 to 3000 cm^{-1} where the O–H stretching vibrations are located. If the water molecule is involved in hydrogen-bonding, the OH attached to the hydrogen-bond is weaker and the corresponding IR vibration

is shifted to lower frequencies (red-shifted), whereas the other O–H is strengthened and its IR vibration is shifted to blue.

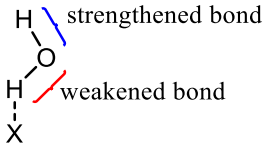

Figure 14 shows a comparison of the IR difference spectra obtained after annealing of 1 % of H_2O in argon, as well as S-**1** in an argon matrix doped with 1 % of H_2O. Apart from the diffusion induced complexation of water to dimers, trimers and polymers, the broad absorption at 3215 cm^{-1} increasing after annealing of S-**1** in a water-doped argon matrix and decreasing upon irradiation is tentatively assigned to the O–H stretching vibration of S-**1**--H_2O. The stretching vibration of O–H in one molecule of H_2O in an argon matrix at 3 K is experimentally found at 3638 cm^{-1}.[86, 98] A shift of $\Delta\nu$ = 425 cm^{-1} indicates that S-**1** is forming a moderate hydrogen-bond with water.[99, 100] For the singlet chlorophenyl carbene **90**, the complexation with H_2O resulted in a red-shift of the O–H stretching, compared to free H_2O, of $\Delta\nu$ = 438 cm^{-1}.[86] Thus, the hydrogen-bond in complex S-**1**--H_2O is, compared to the strongly hydrogen-bonded complex of **90** and H_2O, weaker. This can be explained with a lower basicity of carbene S-**1** than **90**.

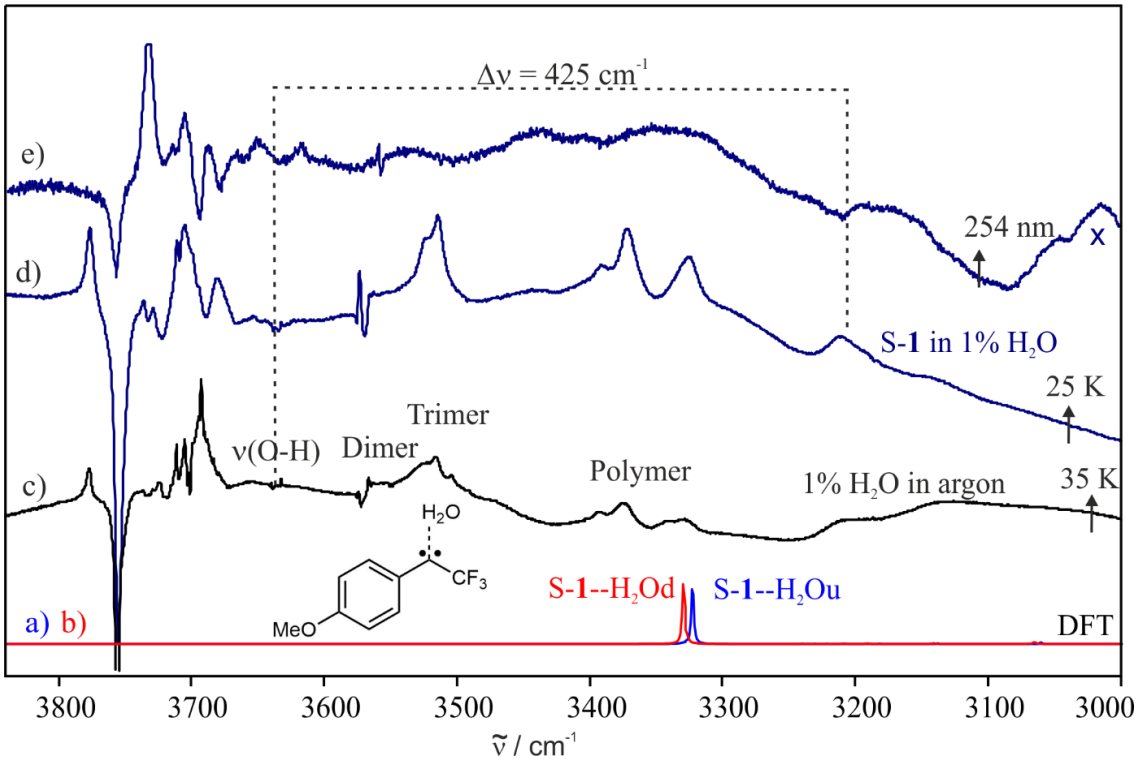

Figure **14:** The shift of the O–H stretching in free H_2O and hydrogen-bonded to S-**1** (presumably). Calculated frequencies of a) S-**1**--H_2Ou and b) S-**1**--H_2Od (M06-2x/Def2-TZVP//B3LYP/Def2-TZVP). c) IR difference spectrum obtained after annealing of an argon matrix doped with 1 % of H_2O. d) IR difference spectrum obtained after annealing of an argon matrix containing S-**1** and 1 % of H_2O and e) obtained after subsequent irradiation. Bands pointing upwards increase in intensity. Bands pointing downwards decrease in intensity. ^{x} represents a magnified difference spectrum.

To gain more information on the stability of complex S-**1**--H_2O under matrix isolation conditions, secondary photolysis was performed. S-**1**--H_2O is stable at 3 K and irradiation (e.g. 365 nm (LED), 256 nm (mercury lamp) or 410 nm (OPO Laser)) is needed to decrease the signals assigned to S-**1**--H_2O and observe an increase of a new set of signals (Figure 15). The newly formed IR absorptions are matching well to the IR spectrum of independently synthesized and characterized 2,2,2-trifluoro-1-(*p*-methoxyphenyl)ethanol **8** isolated in argon at 3 K. The formation of OH insertion products was observed in similar experiments with carbene water complexes (**60**--H_2O, **70**--H_2O, **50**--H_2O).[3, 4, 28] Also, the photolysis of the complex of chlorophenyl carbene **90** and water results in the benzaldehyde HCl complex, which is build-out of the corresponding transient alcohol (see Chapter 2.1. Introduction).

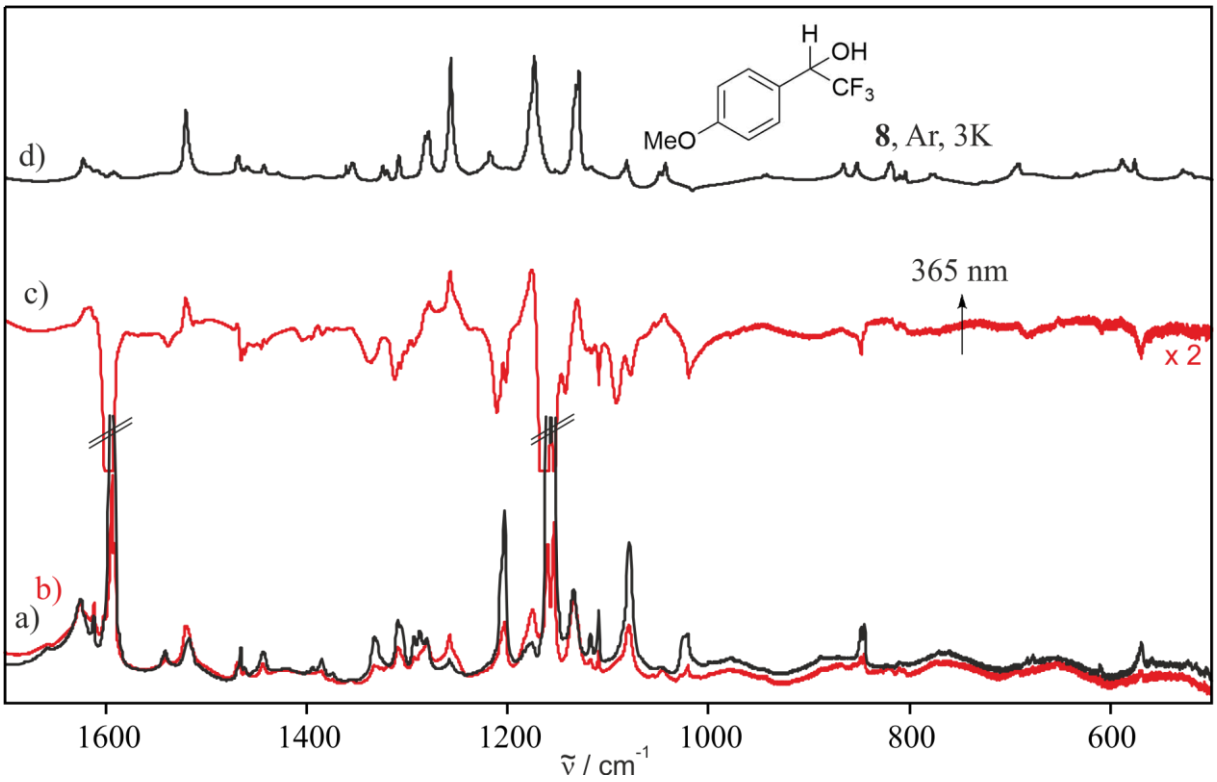

Figure **15:** a) IR spectrum obtained after annealing of a matrix containing S-**1** and 1 % of water. b) IR spectrum obtained after 80 minutes of 365 nm photolysis and c) the corresponding IR difference spectrum. Bands pointing upwards increase in intensity and are assigned to **8**. Bands pointing downwards decrease in intensity and are assigned to S-**1**--H_2O. d) IR spectrum of **8** matrix isolated in argon at 3 K. ^{x} represents a magnified difference spectrum.

UV-vis experiments were carried out in the same manner as the IR studies. The UV-vis spectrum of carbene **1** in 1 % of water is showing a doublet at 335 and 346 nm and smaller signals at 270 nm and 220 nm (Figure 16). With annealing to 25 K, the doublet at 335 and 346 nm appears to be slightly broadened. Nonetheless, it can be assigned to complex S-**1**--H_2O,

since the UV-vis patterns of singlet carbenes and their water complexes are not expected to show huge differences.[5] Upon secondary photolysis, the signals assigned to S-**1**--H_2O are decreasing and absorptions at 230 and 280 nm are growing. These absorptions can be assigned to insertion product **8** by comparison to the UV-vis spectrum of a synthesized and characterized sample of insertion product **8** in argon at 8 K. Overall, the UV-vis experiments support nicely the results of the IR experiment.

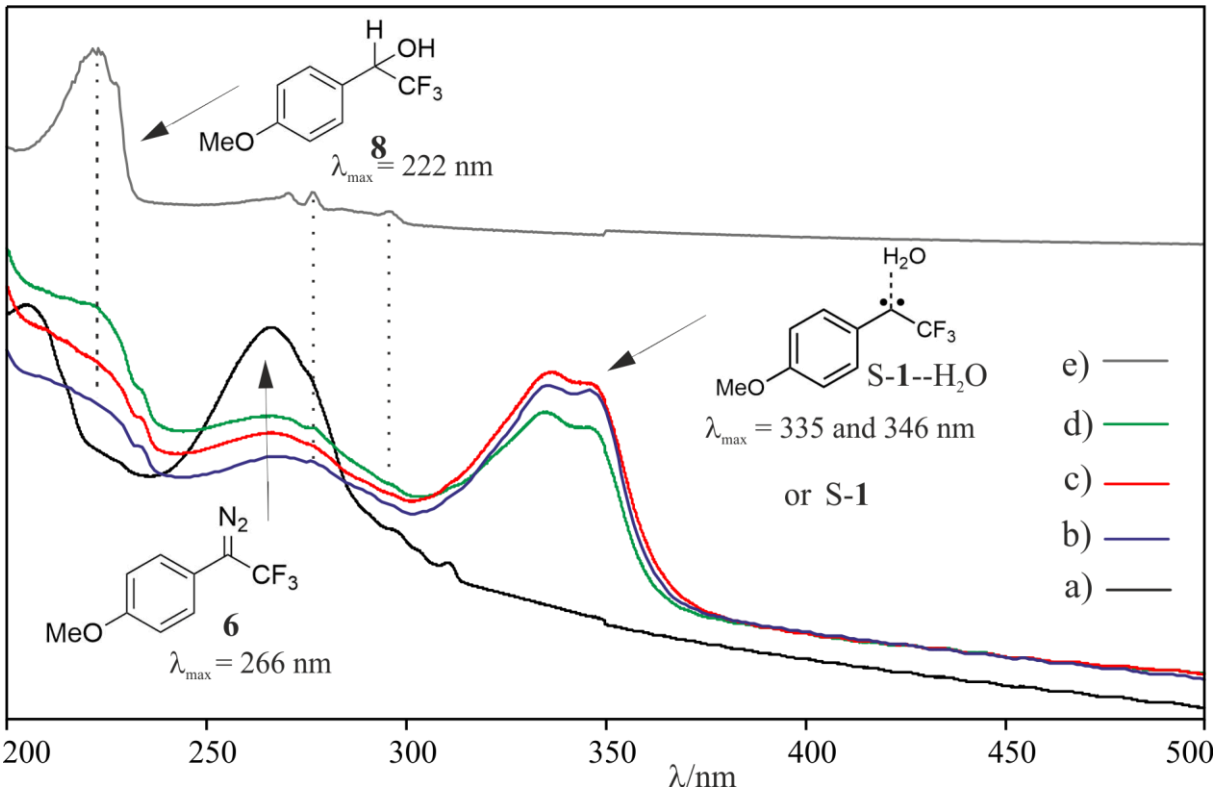

Figure **16:** UV-vis experiment of **1** in argon matrices doped with 1 % of water at 8 K. UV-vis spectra obtained a) after the deposition of **6** in an argon matrix doped with 1 % of water and b) after the subsequent photolysis of **6** to generate S-**1**. c) UV-vis spectra obtained after annealing of the same matrix to 25 K and after d) secondary photolysis with 365 nm. e) UV-vis spectrum of **8** in argon at 8 K.

2.2.2.3. DFT calculations

Calculated structures and relative energies for singlet complexes S-**1**--H_2Ou and S-**1**--H_2Od and the triplet complexes T-**1**--H_2Ou and T-**1**--H_2Od are depicted in Chart 10. The DFT calculations (B3LYP/Def2-TZVP) show, that conformer S-**1**--H_2Ou is the most stable with an energy difference of 0.48 kcal mol^{-1} to conformer S-**1**--H_2Od. The triplet water complex T-**1**--H_2Ou is 6.47 kcal mol^{-1} less stable than S-**1**--H_2Od. For the complexes selected geometrical parameters (bond lengths and C–C–C angle) are shown. The bond lengths of the most stable conformer S-**1**--H_2Ou are compared to the ones of S-**1**u as well. Due to the correlation of the H–OH distance with the strength of the hydrogen-bond, the strengths of the bond between carbene **1** and H_2O was classified using the data provided by literature.[100] With a computed length of 1.97 Å and a difference in H–O bond distances of +0.026 Å, the hydrogen-bonding of S-**1**--H_2O can be considered as a moderate hydrogen-bond. The triplet states of **1** are calculated to form radical-like weak van-der Waals complexes with H_2O, which is reflected in a longer distance of the carbene-carbon to H_2O.

To gain more insights on the mechanism of the rearrangement of complex S-**1**--H_2O to insertion product **8**, the transition state and the intrinsic reaction pathway (IRC) were calculated at the B3LYP/Def2-TZVP level of theory (Figure 17). Following the pathway from S-**1**--H_2Ou to **8**, an activation barrier (E_a) of 7.5 kcal mol^{-1} (8.5 kcal mol^{-1} with B3LYP-D3/6-311++G(d,p) level of theory) has to be overcome to form **8**p. Barriers like this are too large to be overcome thermally below 20 K as similar activation barriers for similar insertion reactions indicate (S-**50**--H_2O, S-**90**--H_2O, Chart 11). Thus, the calculations support the experimental observation that the reaction needs photochemical excitation to go over the **TS** and form **8**. Additionally, the calculations are in good agreement with the experimental results showing the complexation of S-**1** with H_2O to form hydrogen-bonded complex S-**1**--H_2O is thermodynamically stabilized.

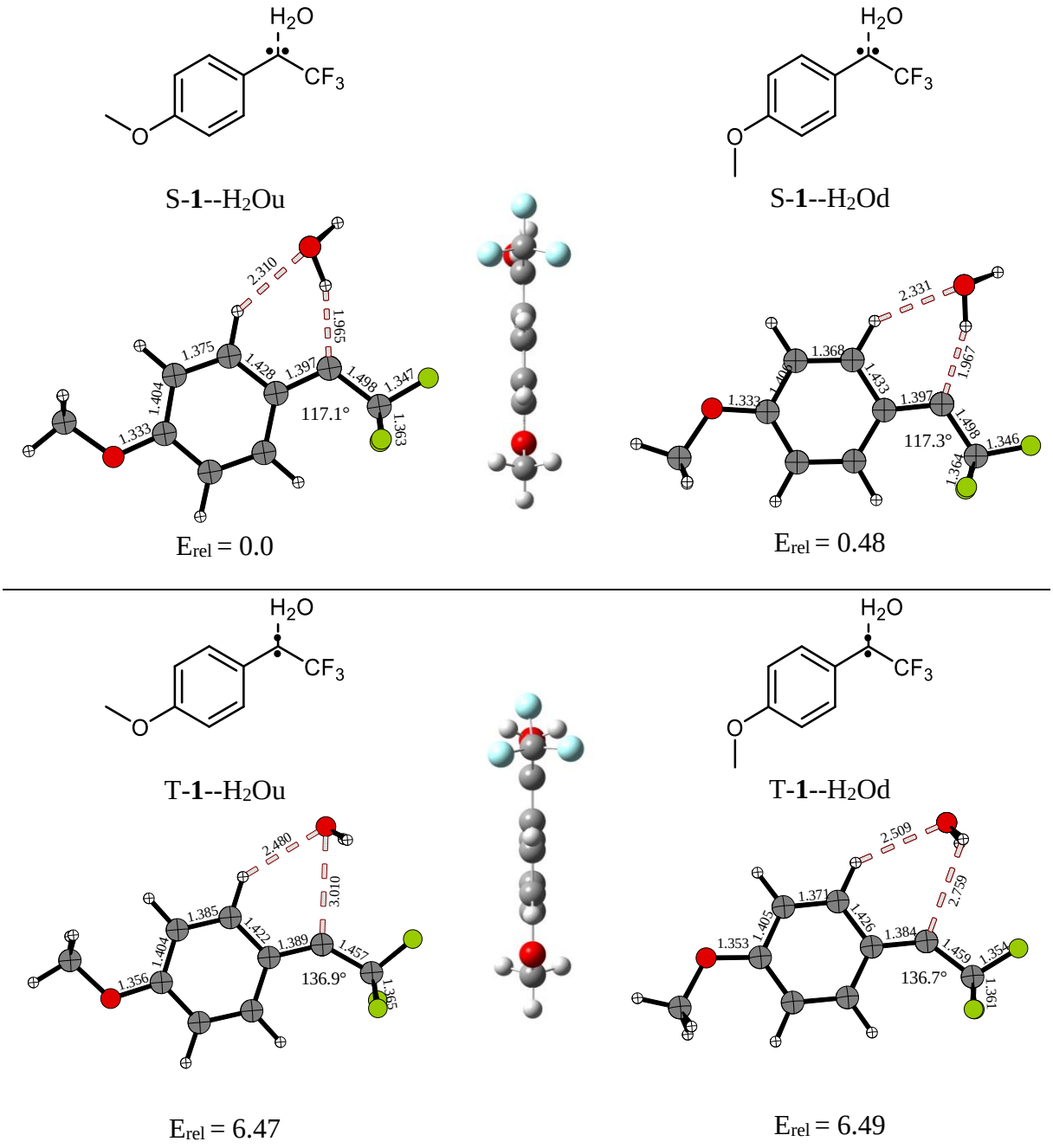

Chart **10:** Structures and relative energies of singlet and triplet hydrogen-bonded complexes S-**1**--H_2Ou, S-**1**--H_2Od, T-**1**--H_2Ou and T-**1**--H_2Od optimized at B3LYP/Def2-TZVP level of theory. For S-**1**--H_2Ou selected geometrical parameters are depicted. Bond lengths in Å.

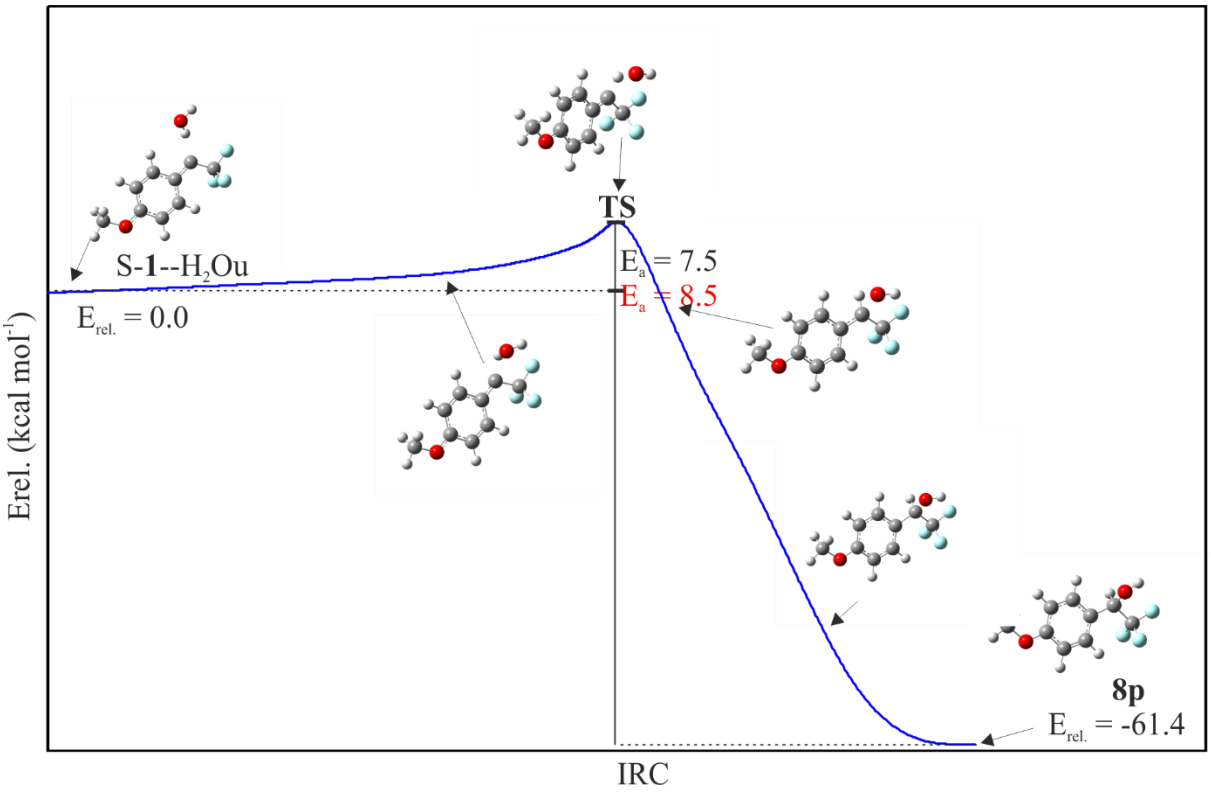

Figure **17:** Intrinsic reaction coordinate (IRC) for the rearrangement of the complex S-**1**--H_2Ou to **8p** calculated at the BLYP-D3/Def2-TZVP level of theory. Energies in kcal mol^{-1}. The activation barrier (Ea) was calculated with separate structures at the BLYP-D3/Def2-TZVP level of theory and with B3LYP-D3/6-311++G(d,p) shown in red.

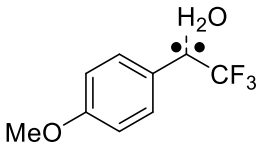

S-**1**--H_2O

E_a = 8.5 kcal mol^{-1}

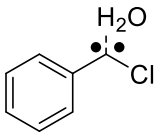

S-**90**--H_2O

E_a = 11.1 kcal mol^{-1}

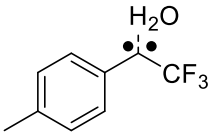

S-**50**--H_2O

E_a = 9.2 kcal mol^{-1}

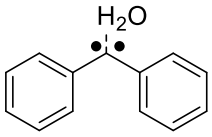

S-**60**--H_2O

E_a = 6.6 kcal mol^{-1}

Chart **11:** Activation barriers (E_a) for the OH insertion of selected carbene water complexes calculated at the B3LYP-D3/6-311++G(d,p) level of theory.

2.2.2.4. Conclusions

The findings of the UV-vis and IR experiments of carbene **1** in interaction with 1 % of H_2O at matrix isolation conditions, are summarized in Scheme 18**.** After photolysis of **6**, both conformations of carbene S-**1** were observed via IR spectroscopy. Annealing of the argon matrix to 25 K results in hydrogen-bonded complex S-**1**--H_2O. Upon photolysis of S-**1**--H_2O, alcohol **8** is generated by OH insertion at the former carbene center. The formation of OH insertion products is a typical reaction for singlet carbenes.[5] The hydrogen-bond in complex S-**1**--H_2O was classified as moderate bond according to DFT calculations and also by the experimental OH shifts.[100]

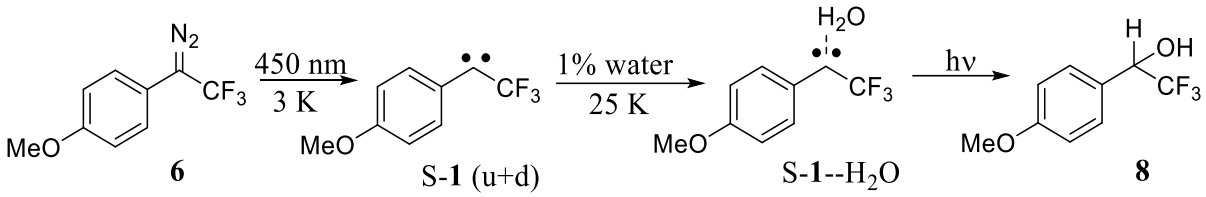

Scheme **18:** Generation and reaction of **1** in argon matrices doped with 1 % of water.

2.3.3. Complexation with ammonia in doped matrices

2.3.3.1. Introduction

Following the experiments of singlet carbene S-**1** in H_2O-doped argon matrices and bistable carbene **50** and others in 1 % of NH_3-doped argon matrices,[28, 41, 85] the reaction of S-**1** was studied in NH_3-doped matrices in a similar way and monitored via IR spectroscopy. Singlet carbenes can be considered as Lewis bases are found to form hydrogen-bonded complexes with Lewis acids.[5, 101] Also carbene **50** was observed to form hydrogen-bonded singlet complexes with water and ammonia after annealing the matrices to 25 K. The complex with ammonia S-**50**--HNH_2 is weaker and in contrast to the complex with water, it is not stable at 3 K and generates the NH_2 insertion product via quantum mechanical tunneling (QMT). Photolysis results in a back formation of **50** and NH_3 (Scheme 19). A similar reactivity was found for another bistable carbene 3-methoxy-9-fluorenylidene, as well.[93] However, only few carbenes are known to activate NH_3, which is based on the high N–H bond strengths (107 kcal mol^{-1}) and its basicity (pK_a = 38).

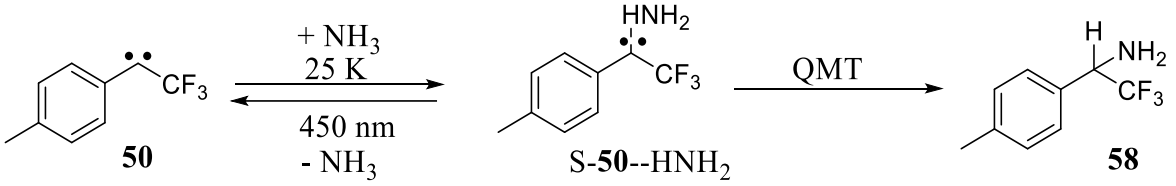

Scheme **19:** Observed reaction of S-**50** with NH_3.

2.3.3.2. Results and discussion

The experiment was conducted analogously to the experiments in H_2O-doped matrices. After deposition of **6** with an excess of argon doped with 1 % of ammonia, the matrix was irradiated with 450 nm LED light to obtain singlet carbene S-**1**. The corresponding IR spectra are shown in Figure 18. The matrix was subsequently annealed to 25 K for 10 minutes and cooled back to 3 K. It was observed that the IR signals assigned to ammonia and S-**1** decrease and new signals increase. The diffusion of ammonia in the softened argon matrix can be confirmed by the formation of dimers, trimers and multimers.[102] But basically, the IR difference spectrum obtained after annealing is very similar to the one obtained in the water experiment. A comparison of these two experiments is shown in Figure 20. As calculations confirm (Figure **19**), both hydrogen-bonded complexes S-**1**--HNH_2 and S-**1**--H_2O are not expected to show observable differences in their IR vibrations. Thus, it can be suggested that singlet carbene S-**1** is forming a singlet complex S-**1**--HNH_2 with NH_3. The two conformers S-**1**--HNH_2u and S-**1**--HNH_2d are very close in energy (ΔE = 0.40 kcal mol^{-1}) and could not be separated IR

spectroscopically. The triplet complexes T-**1**--HNH_2u and T-**1**--HNH_2d are destabilized by 2.8 kcal mol^{-1} compared to the singlet complexes and are therefore not expected to be formed. Like also observed for the complexation of S-**1** with water, the C–F antisymmetric stretching, C–C–C symmetric stretching, C–C–C antisymmetric stretching and the aryl C–C deformation vibration are blue-shifted compared to the monomer and chlorophenyl carbene **90** and H_2O.[5] The blue-shift reflects a strengthened bond, which is also observed in the calculated bond distance between the carbene carbon to the aryl carbon with a slight shortening of 0.005 Å. For S-**1**--H_2O the corresponding shortening is calculated to 0.008 Å. The H–O bond lengths is 2.3 Å and therefore longer than in S-**1**--H_2O (1.9 Å). This signalizes a weaker hydrogen-bond which is expected for a complexation of S-**1** with a weaker Lewis acid such as ammonia.

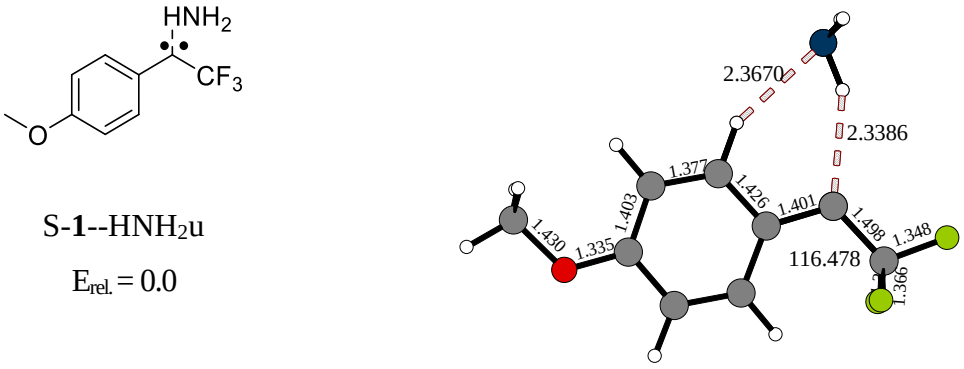

S-**1**--HNH_2u

$E_{rel.}$ = 0.0

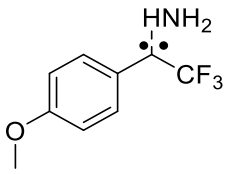

S-**1**--HNH_2d

$E_{rel.}$ = 0.48

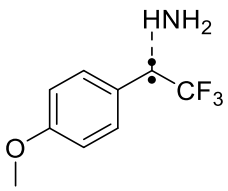

T-**1**--HNH_2d

$E_{rel.}$ = 2.82

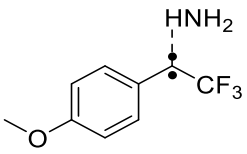

T-**1**--HNH_2u

$E_{rel.}$ = 2.85

Chart **12:** Structure of S-**1**--HNH_2u and relative energies of singlet and triplet hydrogen-bonded complexes S-**1**--HNH_2u, S-**1**--HNH_2d, T-**1**--HNH_2u and T-**1**--HNH_2d optimized at B3LYP/Def2-TZVP level of theory. For S-**1**--H_2Ou selected geometrical parameters are depicted. Bond lengths in Å. In brackets: change in bond lengths compared to the monomer in Å.

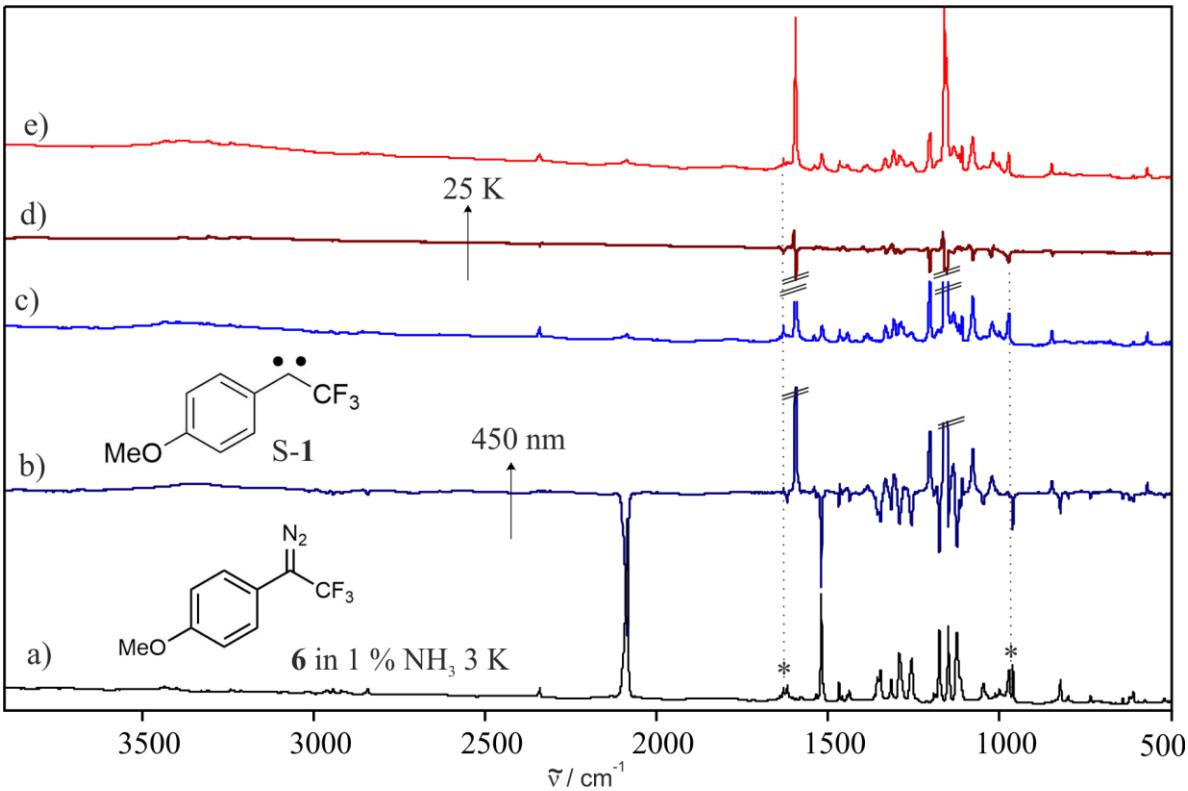

Figure **18:** a) IR spectrum obtained after deposition of **6** in argon doped with 1 % of NH_3 at 3 K. b) IR difference spectrum and c) the absolute spectrum obtained after photolysis of **6**. Bands pointing downwards decrease in intensity and are assigned to **6**, the bands pointing upwards increasing in intensity and are assigned to S-**1**. d) IR difference spectrum obtained after annealing to 25 K and e) the absolute IR spectrum. Bands pointing downwards decrease in intensity and are assigned to S-**1** and NH_3, bands pointing upwards increasing in intensity and are assigned to complex S-**1**--HNH_2. * NH_3.

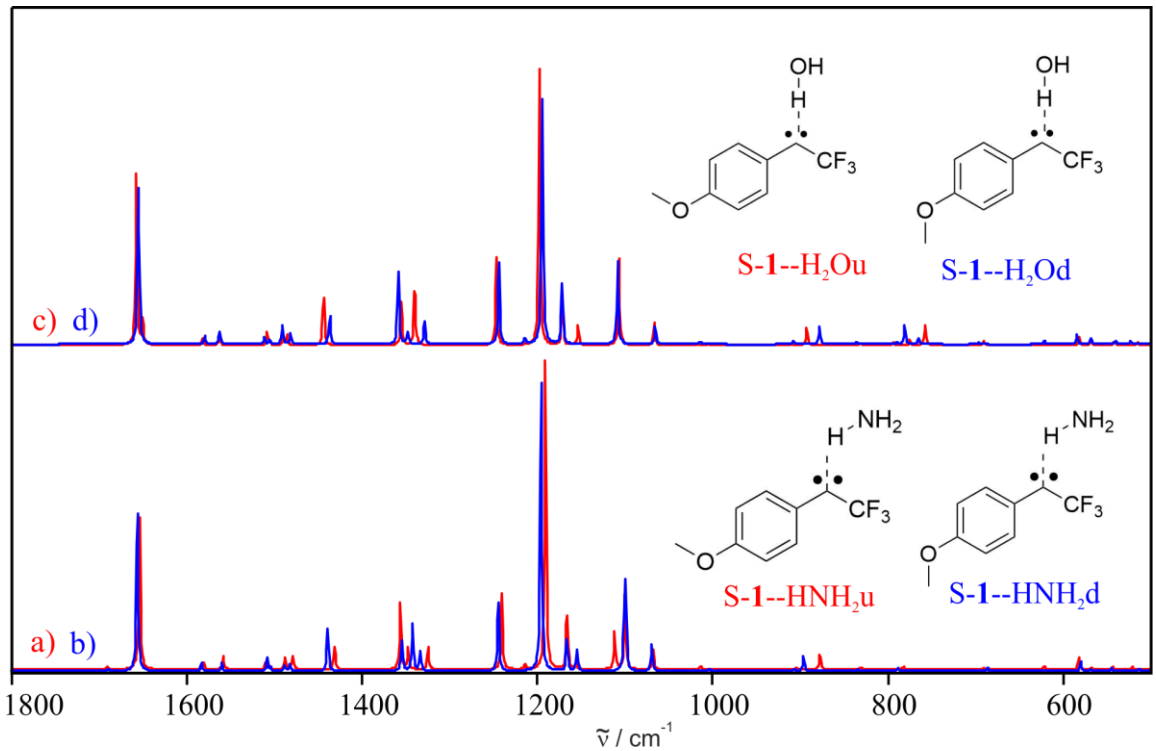

Figure **19:** IR spectra of a) S-**1**--HNH_2u and b) S-**1**--HNH_2d and c) S-**1**--H_2Ou and d) S-**1**--H_2Od computed at the M06-2x/Def2-TZVP//B3LYP/Def2-TZV level of theory.

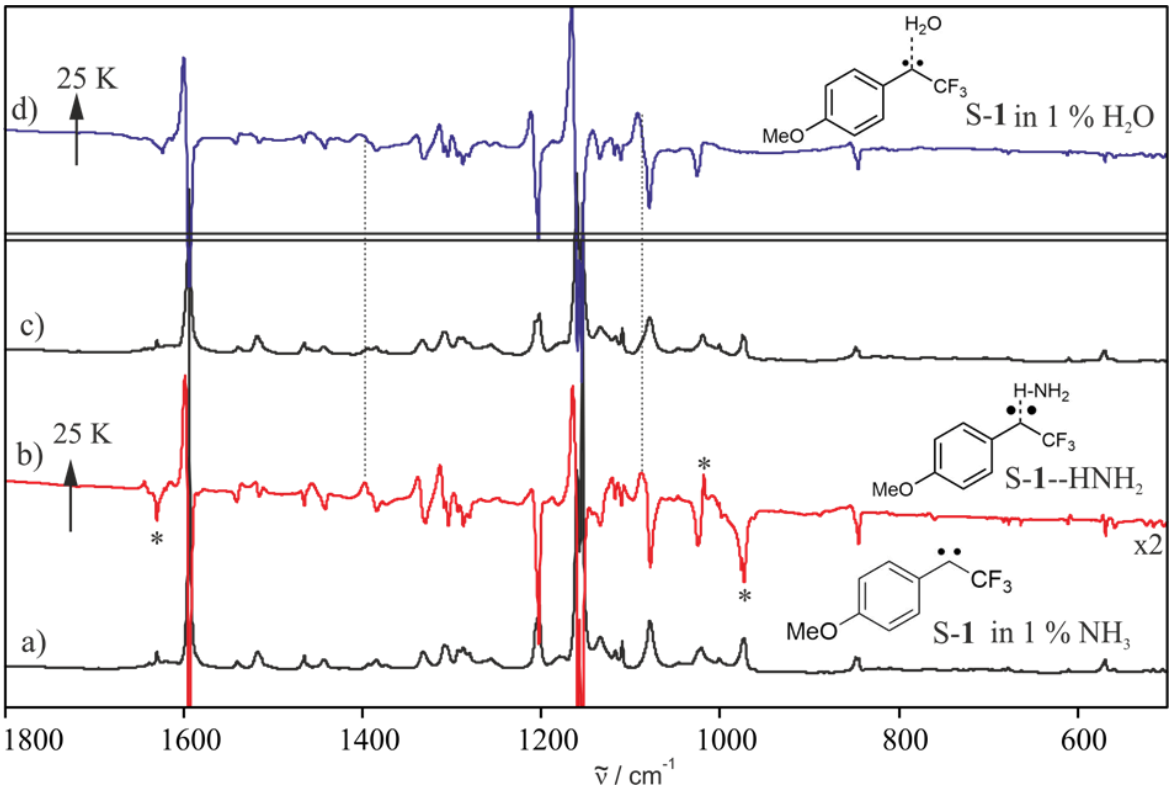

Figure **20:** a) IR spectrum of S-**1** in an NH_3-doped argon matrix. b) IR difference spectrum and c) the absolute IR spectrum obtained after subsequent annealing to 25 K. Bands pointing upwards increase in intensity and are assigned to S-**1**-HNH_2. Bands pointing downwards decrease in intensity and are assigned to S-**1** and NH_3. d) IR difference spectrum obtained after annealing of S-**1** in a H_2O-doped argon matrix to 25 K. Bands pointing upwards increase in intensity and are assigned to S-**1**--H_2O. Bands pointing downwards decrease in intensity and are assigned to S-**1** and H_2O. The * mark the signals assigned to NH_3. ^{x} represents a magnified difference spectrum.

Contrary to S-**1**--H_2O, complex S-**1**--HNH_2 is not stable at 3 K and is converted very slowly, via QMT, to insertion product **8a** (Figure 21). Amine **8a** was identified by comparison of the very weak signals obtained after letting the matrix 30 hours in the dark at 3 K to an authentic IR spectrum of **8a** in argon at 3 K. In contrast to the water complex S-**1**--H_2O, photolysis of S-**1**--HNH_2 did not result in a formation of insertion product **8a** (used photolysis conditions: 650 nm - 365 nm LED, 254 nm mercury lamp).

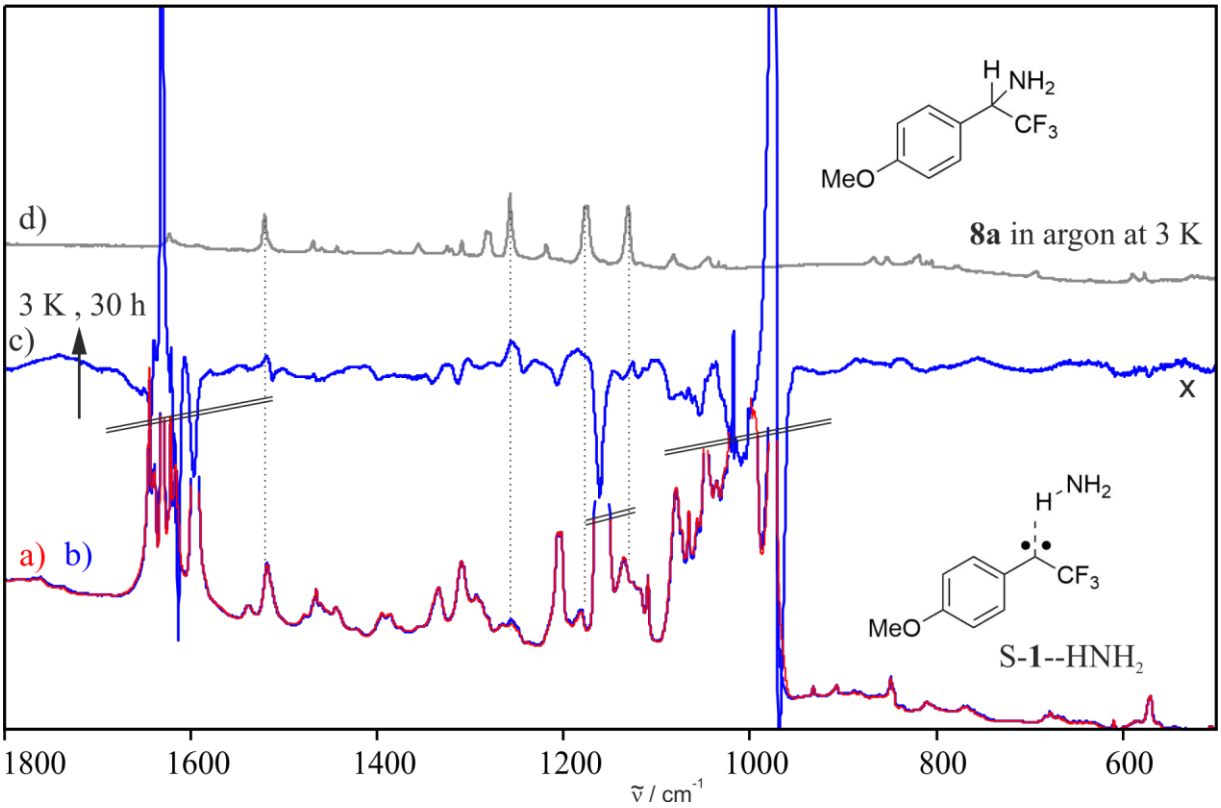

Figure **21:** a) IR spectrum obtained after annealing of a matrix containing S-**1** and 1 % of ammonia. b) IR spectrum obtained after 30 hours darkness at 3 K and the c) corresponding IR difference spectrum. Bands pointing upwards increase in intensity and are assigned to **8a**. Bands pointing downwards decrease in intensity and are assigned to S-**1**--HNH_2. ^{x} represents a magnified difference spectrum.

The experiment was conducted in an analogous way in 1 % ND_3 doped argon matrices. The only difference observed is, that complex S-**1**--DND_2 is stable at 3 K and does not form the insertion product. This results in a large isotope effect and supports a quantum mechanical tunneling (QMT) from S-**1**--HNH_2 to the amine **8a**. These finding is congruent to the experiments of *p*-tolyl(trifluoromethyl) carbene **50** in NH_3- and ND_3-doped argon matrices.[28]

2.2.3.3. Conclusions

The experiment of S-**1** in NH_3 and ND_3-doped matrices, demonstrated that the hydrogen-bonded complexes S-**1**--HNH_2 and S-**1**--DND_2 are formed at elevated temperatures and could be detected via IR spectroscopy. The complex S-**1**--HNH_2 formed with ammonia is weaker than with the stronger Lewis acid H_2O and is metastable and rearranges at 3 K slowly to NH_2 insertion product **8a**. The deuterated complex S-**1**--DND_2 instead is stable at 3 K. This indicates the involvement of QMT. Also structural parameters, e.g. hydrogen-bond lengths, derived from DFT calculations revealed that the complexation with ammonia S-**1**--HNH_2 is weaker (H-bond = 2.3 Å), compared to the water complex S-**1**--H_2O (1.9 Å).

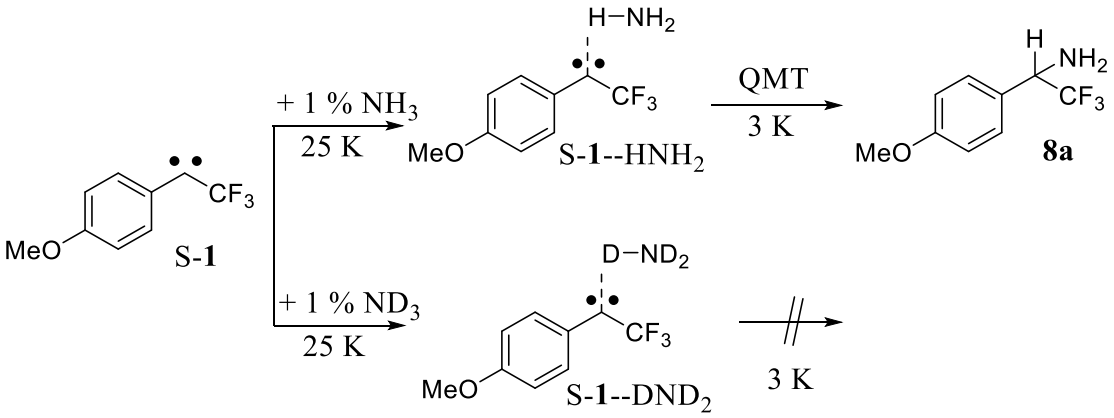

Scheme **20:** Observed reaction of S-**1** matrices doped with NH_3 and 1 % of ND_3.

2.3.4. Direct reaction in solid water

2.3.4.1. Introduction

The reactivity of **1** in direct contact to H_2O was studied by using low-density-amorphous water ice as a matrix host.[3, 26, 103] Thus, the carbene is generated directly in proximity to water molecules and usually no diffusion is needed to observe a reaction of the highly reactive carbene. The reaction of carbenes trapped in LDA water ice matrices differs depending on the carbene, as discussed in Chapter 1.2. Carbene **1**, is computed to be more proton affine than carbene **50**, for which the corresponding cation could not been observed in LDA water ice. Therefore, it is interesting to study the reaction of **1** in a similar manner and examine the correlation of the proton affinity to the formation of cations in LDA water ices further. The corresponding cation **2** is destabilized by an inductive effect ascribed to the fluorine in β-position to the cationic carbon. Nonetheless it has, in contrast to **52**, a better ability to delocalize the positive charge to the methoxy substituted aryl ring. The pK_R^+ value of cation **2** is estimated

to be even higher than of the antiaromatic destabilized cation fluorenyl cation **72** (**2** = -20.8 kcal mol^{-1}; **72** = -15.9 kcal mol^{-1})[10, 89] and thus **2** is expected to react more rapidly with the OH^- to the insertion product. A correlation of the pK_R^+ to thermal stability of cations isolated in amorphous water ices was observed in recent experiments (Scheme 13).[4, 85]

In a previous experiment, cation **2** was observed via laser flash photolysis.[8] Richard *et al.* studied different 4-methoxyphenylethyl cations bearing β-fluorine substituents with structures as shown in Scheme 21. The cations were generated photolytically from precursors (X = Cl or Br). The transient absorption spectra of precursor **6c** (R = CF_3, R´= H, X = Br) upon irradiation in 2,2,2-trifluoroethanol indicates the generation of two intermediate species. One was identified as cation **2** (quenched by nucleophiles), the other as the corresponding radical **4** (quenched by oxygen). Cation **2** shows its maximum UV absorption (λ_{max}) at 320 nm and **4** at 290 nm.

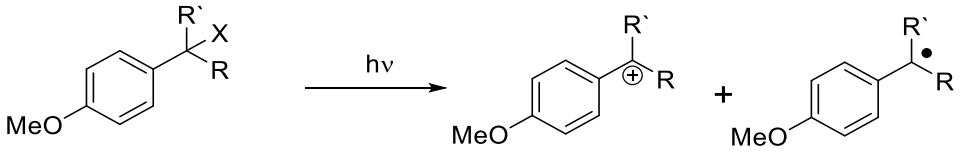

Scheme **21:** Photolysis experiments studied in literature. (X = Br, R = CF_3 or CHF_2; R´= H or CF_3).[8]

A general influence of the methoxy substitution on the stability of a carbene and a cation was found greater for the carbene than the cation.[1] Thus, regarding previous studies and the calculated PA it is conceivable for the protonation of carbene **1** in solid water ice to obtain a resonance stabilized cation which can be spectroscopically studied. On the contrary, the pK_R^+ value indicates a rapid reaction of **22** to the insertion product.

2.2.4.2. Results and discussion

Precursor **6** was co-deposited with an excess of water vapor at 50 K and subsequently cooled to 8 K. The obtained UV-vis spectrum is shown in Figure 22. To study the direct reaction of S-**1** in LDA H_2O ice, precursor **6** is irradiated with 450 nm light. The UV-vis spectrum obtained after 18 hours of photolysis shows that the UV signals of **6** at 280 nm and 210 nm are depleted after photolysis, whereas new signals are at 320 nm (broad) and 230 nm and weaker signals are at 280 and 290 nm. With a synthesized, characterized and matrix isolated sample of insertion product **8**, the two signals at 280 and 290 nm and the one at 230 nm were assigned to **8**. Depending on the lengths of photolysis, the broad signal at 320 nm (marked by *) is showing a different shape (Figure 23). This may indicate the presence of two different species. A comparison to the water complex S-**1**--H_2O observed in 1 % H_2O-doped argon matrices shows absorptions at 335 and 346 nm and may thus be one of the species responsible for the broad

absorption. This would be similar to the experiments of singlet carbenes **96** and **95** in LDA water ices, which also showed weak signals of their strongly hydrogen-bonded complexes S-**90**/**91**--H_2O. The other absorption at around 320 nm fits to the reported value of cation **2**.[8] In this study, **2** was generated and observed with LFP. The strongest absorption (λ_{max}) of **2** is found at 320 nm. In the LFP experiment, cation **2** is accompanied by radical **4** with λ_{max} at 295 nm. Based on an EPR experiment performed analogously, radical **4** is most likely not generated in the experiments of this work, by not showing an increase in the radical region during annealing. Additionally, the EPR experiment confirms the singlet state of the observed species, as during the whole experiment, no signal of a triplet species could be detected. The structures of both conformers **2**u and **2**d were calculated with DFT and are shown in Chart 13. The two conformers are nearly degenerate in energy. Both are computed to have a for cations preferred planar geometry. Another broad and weak signal at 250 nm may possibly be assigned to cation **2** as well or to another species. This absorption is formed upon photolysis of **6** and is not present in the experiment without water.

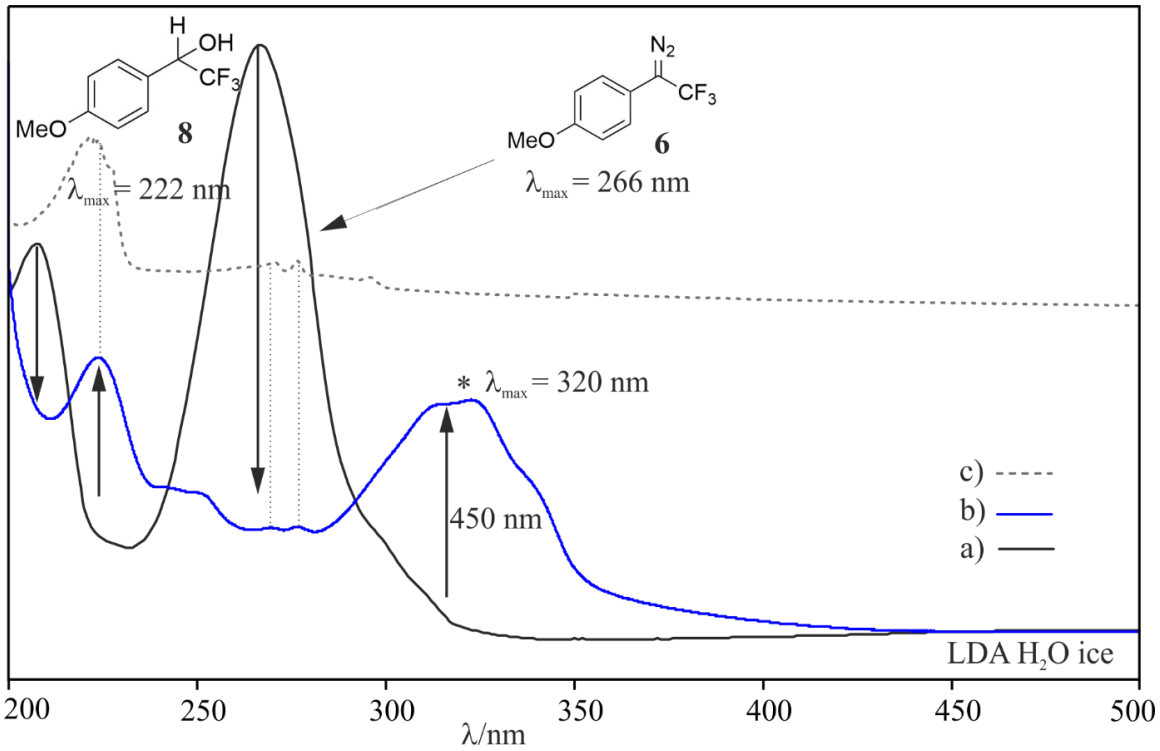

Figure **22:** UV-vis experiment showing the photolysis of precursor **6** in LDA water ice. a) UV-vis spectra obtained after the deposition of **6** in LDA water ice at 8 K and b) after the subsequent photolysis of **6**. c) UV-vis spectrum of insertion product **8** in LDA water ice at 8 K. * Presumably cation **2**.

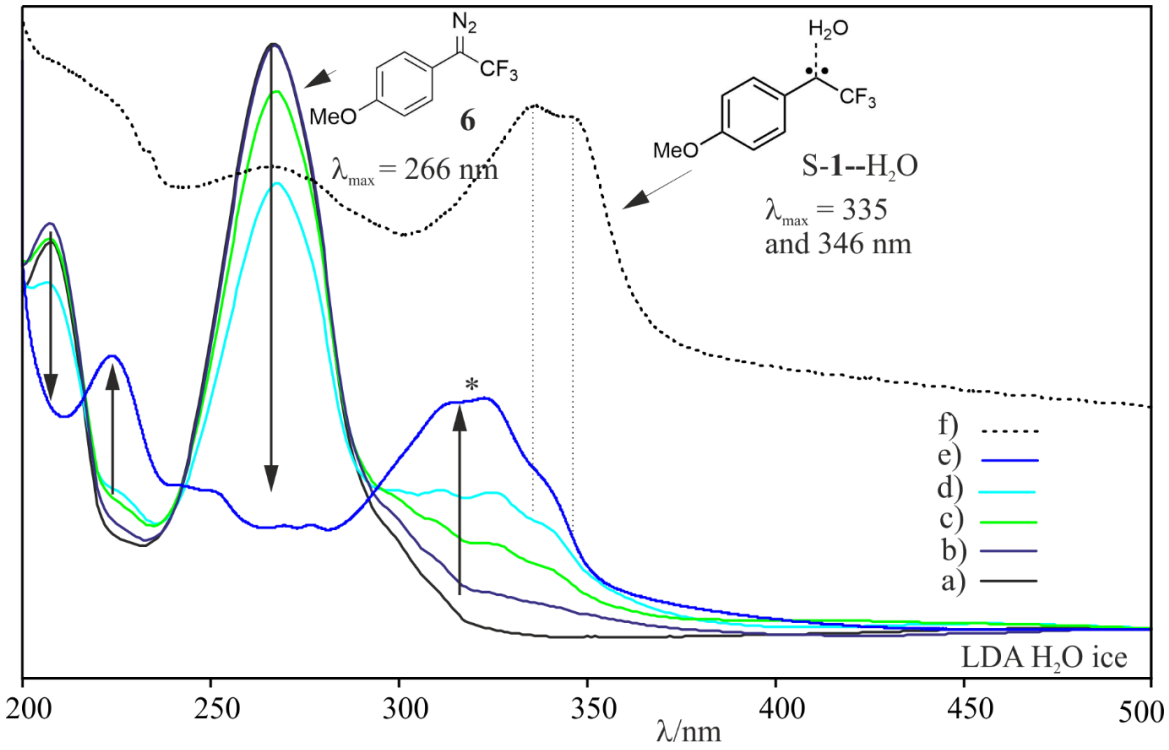

Figure **23:** UV experiment showing the stepwise photolysis of precursor **6** in LDA water ice at 8 K. a) UV-vis spectrum of **6** in LDA water ice. UV-vis spectrum obtained after b) 5 minutes, c) 20 minutes, d) 1 hour and e) 18 hours of 450 nm irradiation. f) UV-vis spectrum obtained after annealing in an argon matrix doped with 1 % H_2O (assigned to S-**1**--H_2O). * Signal at 320 nm.

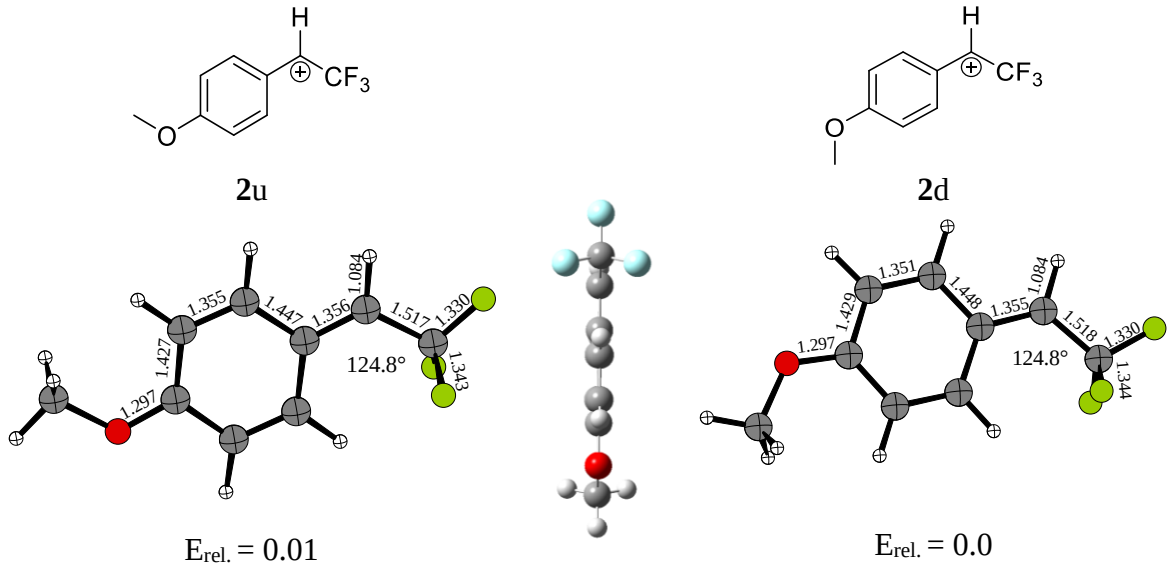

Chart **13:** Structures and selected parameters of cation **2**u and **2**d, optimized at B3LYP/Def2-TZVP level of theory. Energies in kcal/mol.

To gain more information of the reaction, additionally to the UV-vis experiment of singlet carbene S-**1** in low density amorphous H_2O ice, the reaction was observed via IR spectroscopy. Precursor **6** was co-deposited together with H_2O at 50 K to ensure good optical properties of

the LDA H_2O ice matrix. The spectrum obtained after cooling down to 9 K is shown in Figure 24. Apart from the intense broad features of LDA water ice at ~3200 and 750 cm^{-1}, the spectrum is similar to the deposition spectrum of **6** in argon matrices.

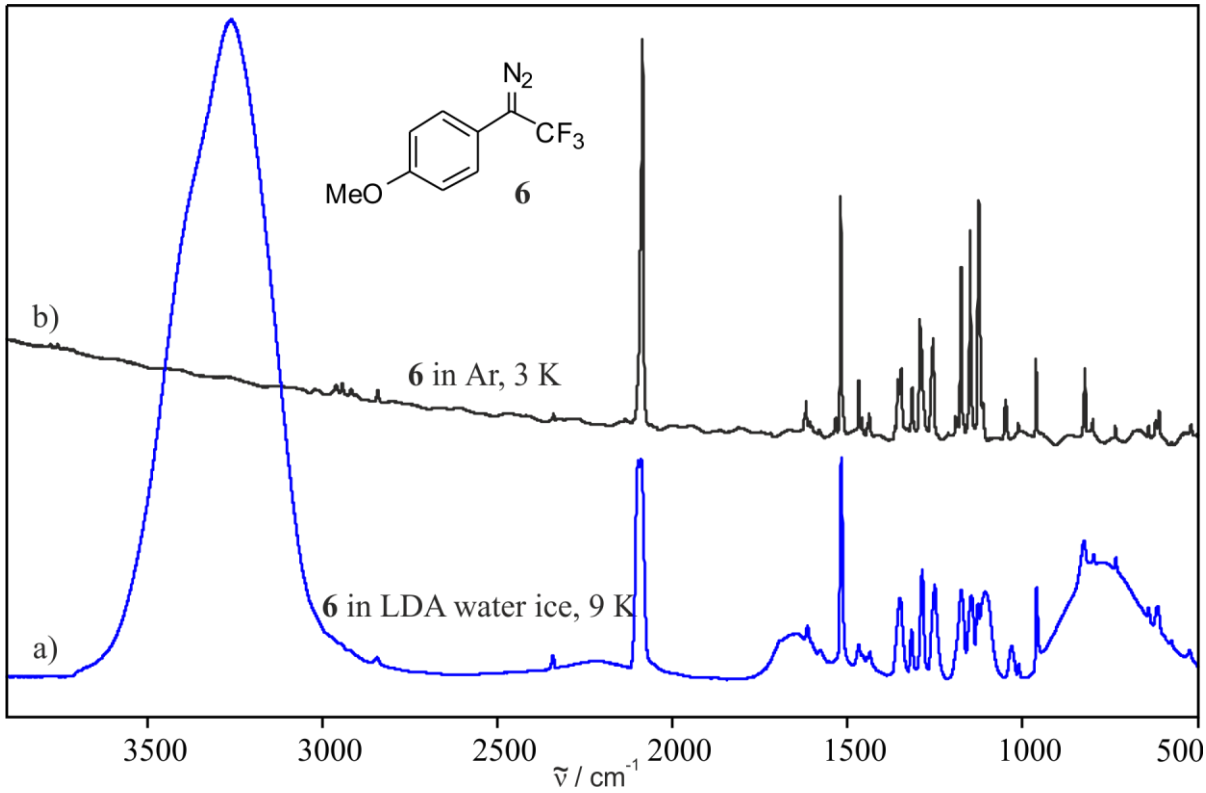

Figure **24:** a) IR spectrum obtained after deposition of **6** in a) LDA water ice at 9 K and b) in argon doped with 1 % of water at 3 K.

The photolysis of **6** in LDA H_2O ice was observed via IR spectroscopy as shown in Figure 25. The difference spectrum obtained after 18 hours of photolysis is shown together with the IR normal spectrum. The decreasing signals are assigned to **6**. Most of signals obtained after the photolysis could be assigned to the OH insertion product **8** by comparison to an authentic spectrum of **8** in LDA H_2O ice. See Figure 83 in Appendix for a comparison of **8** in argon and in solid water ice. The IR experiment is congruent with the UV-vis experiment, showing the formation of **8** after photolysis of **6**. The broadness of the signals does not allow a more detailed analysis, and hence, to study if other products, like cation **2**, are underneath the signals, an annealing experiment was performed.

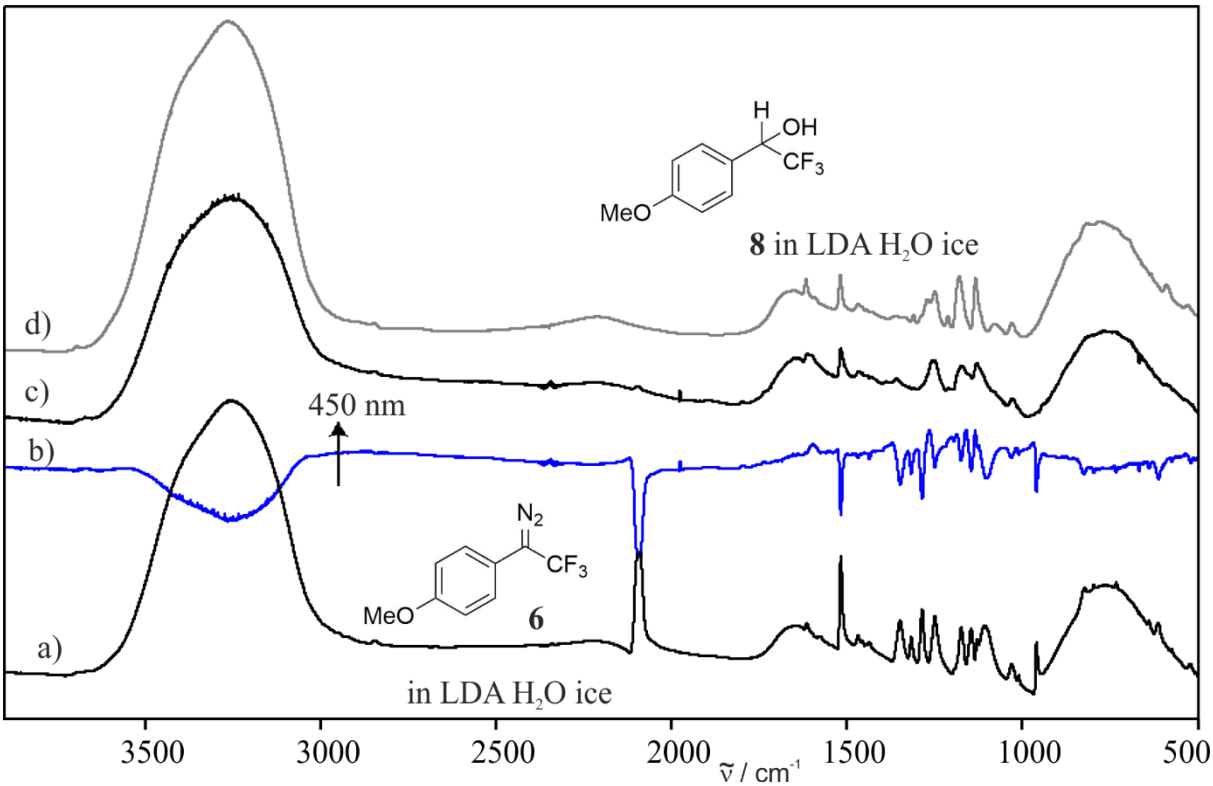

Figure **25:** Photolysis of **6** in LDA water ice. a) IR spectrum of **6** in LDA water ice at 9 K and b) the IR difference spectrum obtained after 18 hours of irradiation and c) the corresponding IR spectrum. d) For comparison: IR spectrum of **8** in LDA water ice at 9 K.

The LDA water ice matrix can be tempered up to 150 K to allow the observation of thermal reactions between the guest molecules and the LDA H_2O ice.[26] In Figure 26 the IR experiment showing the free annealing up to 85 K is depicted. The spectra were taken without cooling down or pausing the heat up, but the heat up took around ~1 minute per 1 K. The IR difference spectra show that some signals start decreasing slowly at 40 K and decrease further up to 85 K. The difference spectrum obtained after annealing to 85 K was also used to compare to a calculated IR spectrum of cation **2**u (M06-2x/Def2-TZVP//B3LYP/Def2-TZVP) as shown in Figure 27. The signals match well to the calculated vibrations of **2**u. The strongest vibration of **2**u is the C–F stretching vibration calculated at 1277 cm^{-1}, this vibration is assigned to the signal at 1258 cm^{-1} in the experiment. Another strong vibration at 1519 cm^{-1} is assigned to the C=C ring deformation vibration calculated at 1554 cm^{-1}. The assignment indicates, that the broad UV-vis absorption at 320 nm may be traced back to cation **2**, as literature suggests.[104] An indication of the presence of complex S-**1**--H_2O, as observed in the UV-vis experiment, has not been detected. The assignment of the increasing IR signals obtained after annealing to 85 K is due to their weakness and broadness difficult, but may fit to insertion product **8**, like observed in the UV-vis experiment Figure 27.

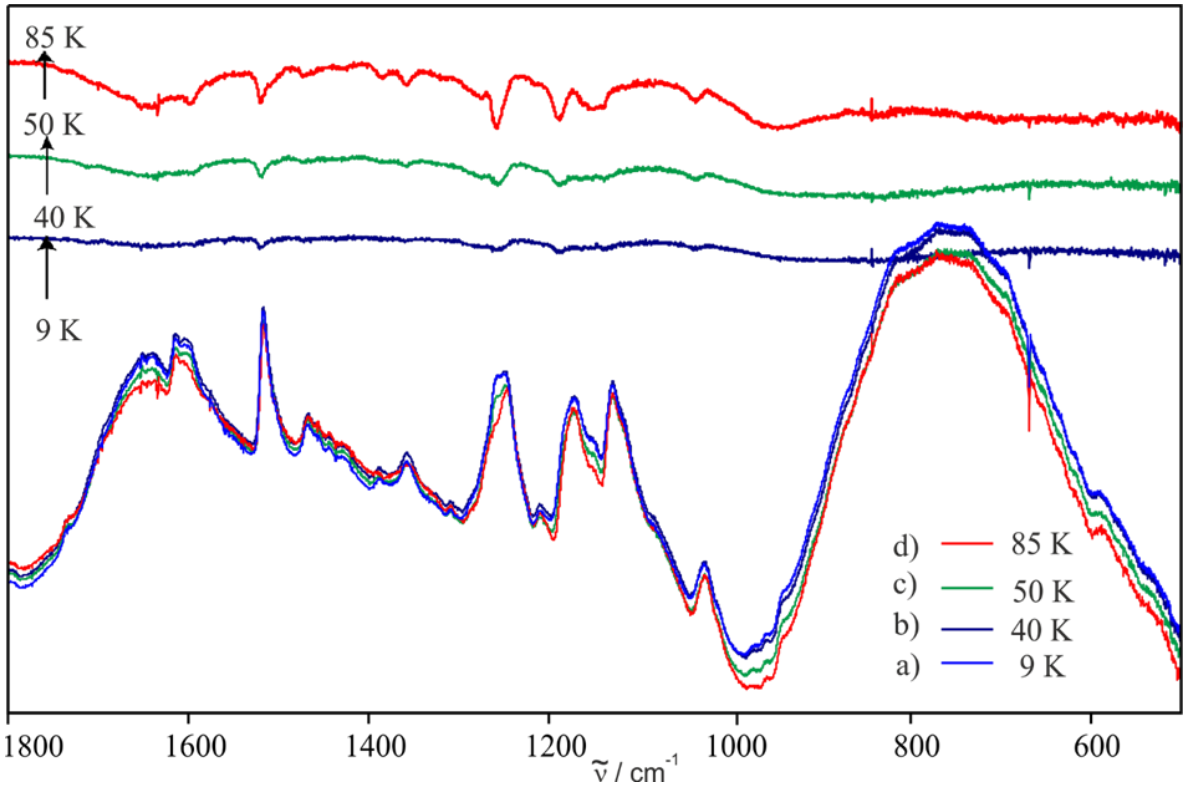

Figure **26:** Experiment in LDA water ice. a) IR spectrum obtained after photolysis of **6** in LDA water ice at 9 K. IR and IR difference spectra obtained after annealing from b) 9 to 40 K, c) 40 to 50 K and d) from 50 to 80 K. Bands pointing upwards increase in intensity. Bands pointing downwards decrease in intensity.

Table **6:** Experimental and calculated vibrational frequencies of cation **2**u:

Exp.[b]		Calc.[b] **2**u		Assignment [c]
$\tilde{\nu}$	$I_{rel.}$	$\tilde{\nu}$	$I_{rel.}$	
1639	35	1707.5	60	C=C str.
1602	25	1659.0	67	C=C str.
1519	34	1554.3	86	C=O str.
1469	14	1511.4	13	C=C str.
1384	22	1418.7	26	C-H bend.
1358	25	1396.4	70	C=O str.
1276	5	1312.7	34	C-C-C str. sym.
1259	77	1276.6	100	C-F str.
1189	79	1212.2	71	C-H bend.
1148	100	1203.2	62	C-F str.
1036	15	1196.3	12	C-H bend.

[a] Calculated at M06-2x/Def2-TZVP//B3LYP/Def2-TZVP level of theory. [b] In LDA water ice at 9 K. [c] Tentative assignment.

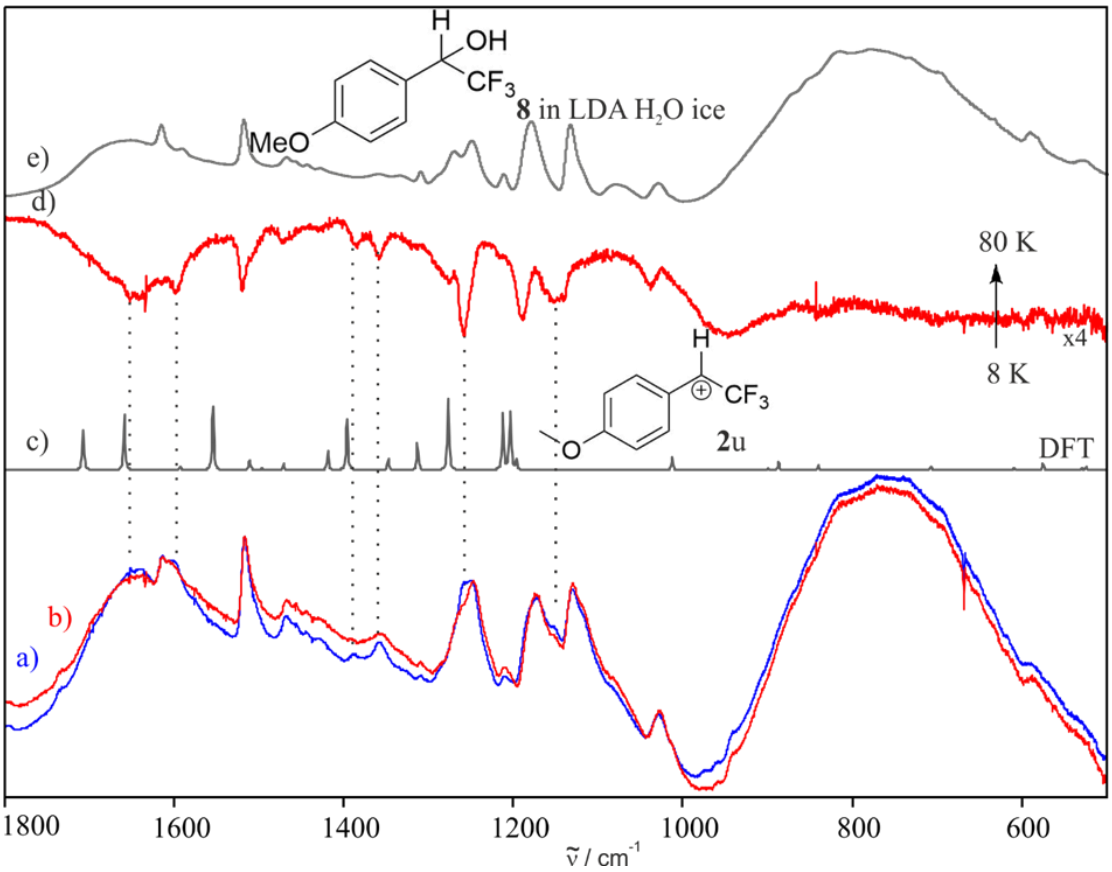

Figure **27:** IR spectra obtained a) after photolysis of **6** in LDA water ice at 9 K and b) after subsequent annealing to 80 K. c) Calculated IR spectrum of **2**u at M06-2x/Def2-TZVP//B3LYP/Def2-TZVP level of theory. d) IR difference obtained after annealing to 80 K. Bands pointing upwards increase in intensity. Bands pointing downwards decrease in intensity. e) IR spectrum of **8** in LDA water ice. ^{x} represents a magnified difference spectrum.

The annealing was also monitored via UV-vis spectroscopy. After photolysis of **6** in LDA water ice, the matrix was annealed as described before in the IR experiment. In Figure 28 the obtained UV-vis spectra during warming up stepwise from 8 to 80 K are shown. It is noticeable that one part of the broad feature at ~340 nm (complex S-**1**--H_2O) decreases almost completely during annealing to 40 K. The part at 300 - 330 nm (presumably **2**) is slowly decreasing further up to 70 - 80 K. This observation indicates the presence of two species. It can be assumed that S-**1**--H_2O is present in low amounts after photolysis of **6** and due to this only observed in the more sensitive UV-vis experiment. Both species are transformed mostly to insertion product **8**.

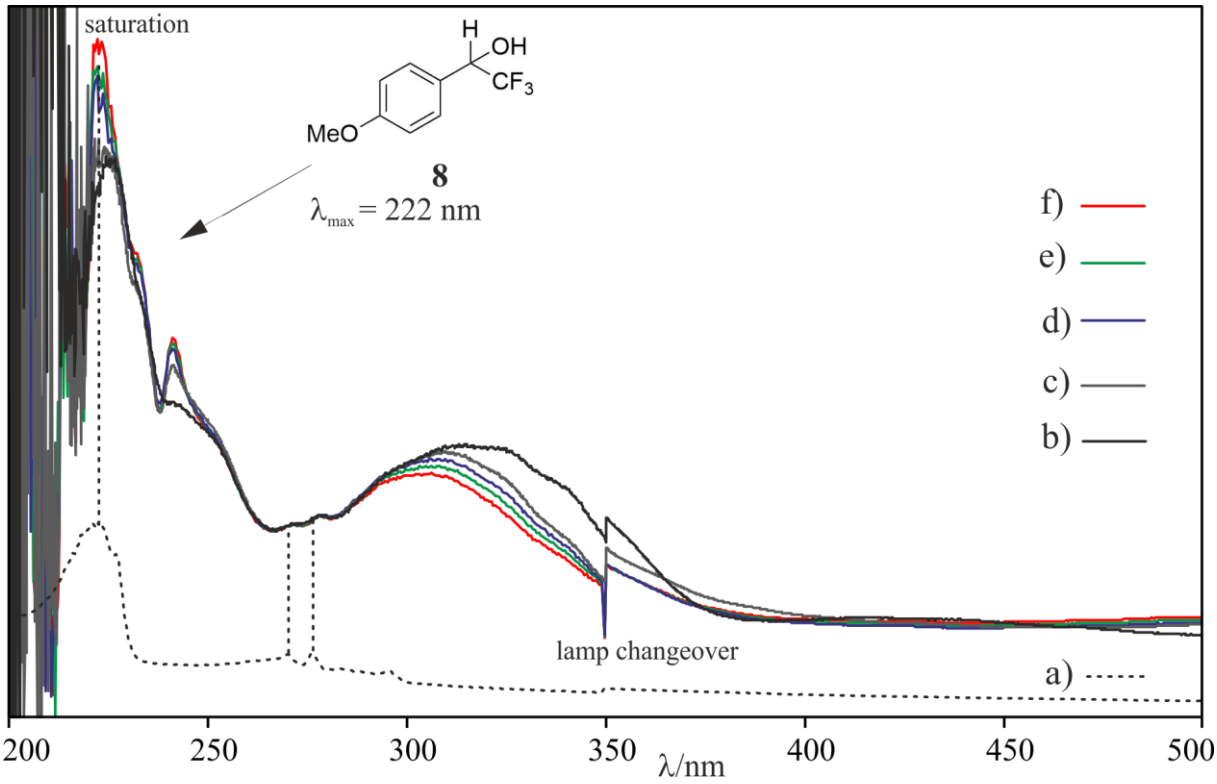

Figure **28:** Free annealing experiment after 450 nm photolysis in LDA ice observed via UV-vis spectroscopy. a) UV-vis spectrum of **8** in LDA water ice at 8 K. b) UV-vis spectrum obtained after photolysis of **6** in LDA H_2O ice. UV-vis spectra obtained at c) 40 K, d) 60 K e) 70 K and f) 80 K.

To elucidate the reaction further, secondary photolysis was observed via UV-vis spectroscopy. Figure 29 shows the UV-vis spectra before and after secondary photolysis of S-**1**--H_2O with 365 nm light in LDA water ice, as well as in a 1 % of water-doped matrix. In the case of the experiment in 1 % of water, photolysis results in a decrease of the absorptions assigned to complex S-**1**--H_2O and an increase of alcohol **8**. In the case of the UV-vis experiment in LDA water ice, mostly the part at ~340 nm of the broad absorption decreases. This observation corroborates the presence of two species underneath the broad feature centered at 320 nm. Thus, it was concluded that one part of the broad feature can be assigned to S-**1**--H_2O, since analogous to the experiment in 1 % of water, secondary photolysis of S-**1**--H_2O produces insertion product **8**. The region assigned to cation **2** decreases only marginally during photolysis and thus secondary photolysis indicates a high photolytic stability of **2** under the used conditions (365 nm LED, 254 nm mercury lamp) by showing no further reaction. This surprising photostability may be explained with the inability to find a light source (300 – 320 nm) selectively applying for the cation **2**.

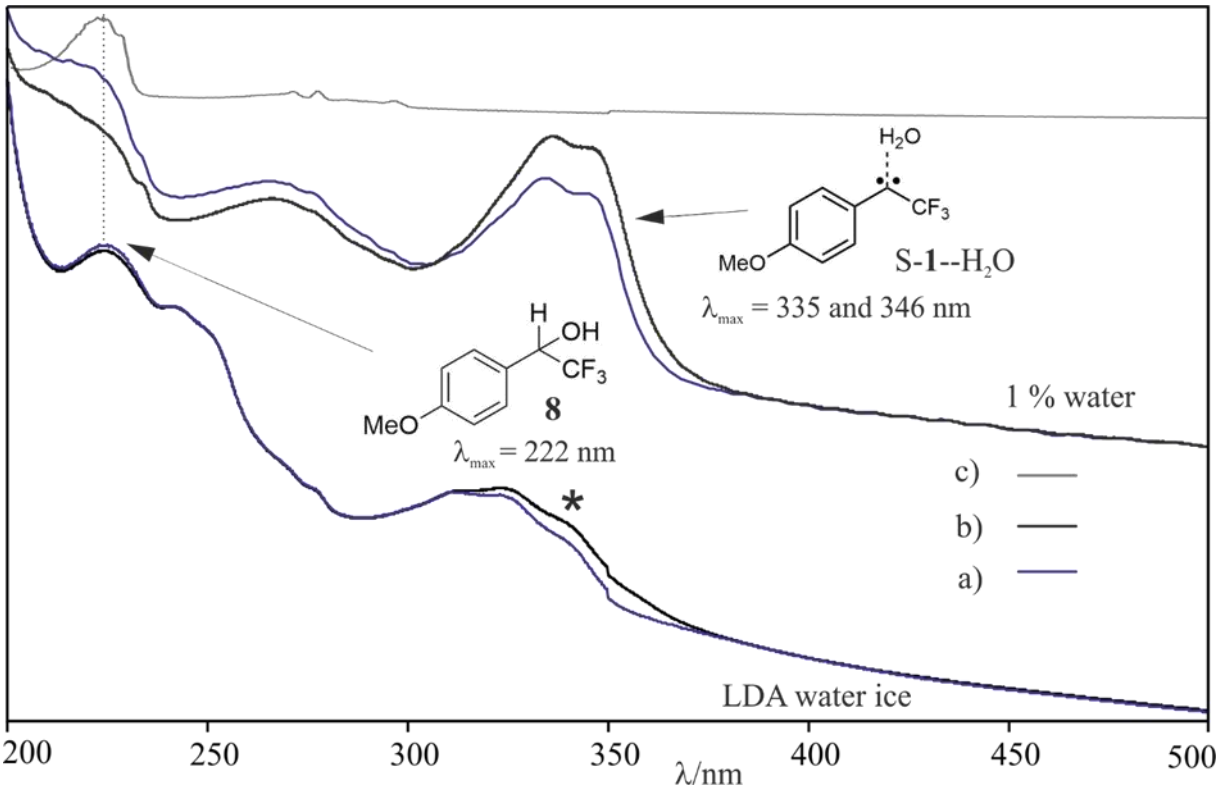

Figure **29:** a) Primary (450 nm) and b) secondary (365 nm) photolysis in LDA water ice at 9 K. Above: a) Primary (450 nm) and b) secondary (365 nm) photolysis in argon doped with 1 % of water at 8 K. c) a) UV-vis spectrum of **8** in LDA water ice at 8 K.

Overall, the UV-vis, IR and EPR experiments of **6** in LDA water ice indicate that more than one species is formed upon 450 nm photolysis (Scheme 22). All species have a singlet multiplicity, according to the EPR measurements. The IR and UV-vis experiments indicate, that **8** is generated in a high yield, whereas cation **2** and especially complex S-**1**--H_2O are formed in lower yields. As with 1 % of water-doped matrices, hydrogen-bonded complex S-**1**--H_2O is transformed via secondary photolysis to OH insertion product **8**. Additionally, by tempering to 40 K, S-**1**--H_2O decreases and **8** is formed. Cation **2** stays unaffected to the used photolysis conditions and decays slowly at annealing above 40 K. The product formed out of **2** by annealing may probably be assigned to **8**.

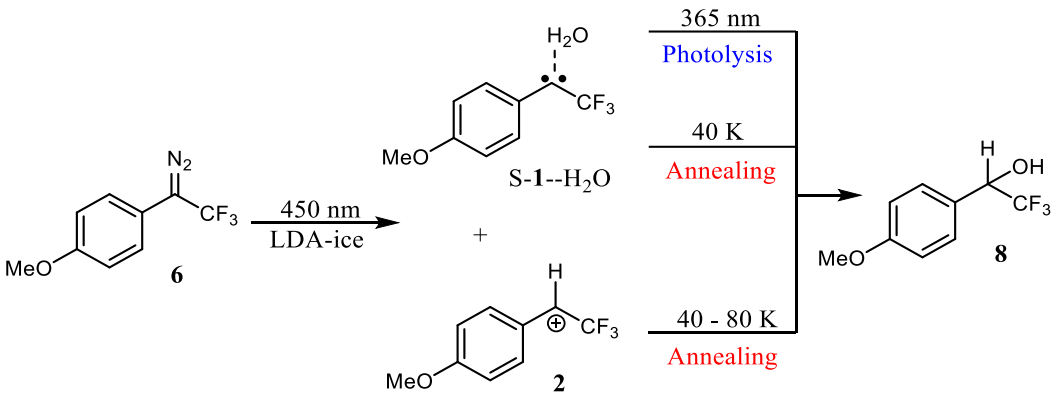

Scheme **22:** Observations in LDA water ice after photolysis of **6**.

To validate the findings of the UV-vis, EPR, and IR experiments, an experiment with heavy water LDA ice was conducted. The deuteration of cation **2** is expected to show differences in the IR spectrum. Especially the vibrations which are involving the H or D atom at the former carbene center.

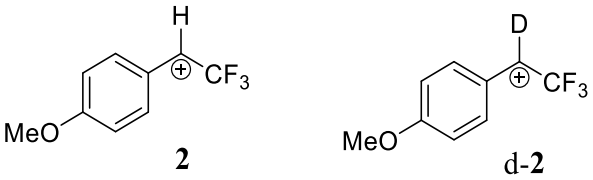

Chart **14:** Structures of cation **2** and deuterated cation d-**2**.

The experiment in LDA D_2O ice was performed analogously to the LDA H_2O ice experiment. The broad absorptions centered at 2500 and 550 cm^{-1} are attributed to the amorphous D_2O ice. The signals of diazo compound **6** are, like in the case of H_2O ice due to interactions with the matrix, broadened but still very similar to the IR spectrum in argon (Figure 30).

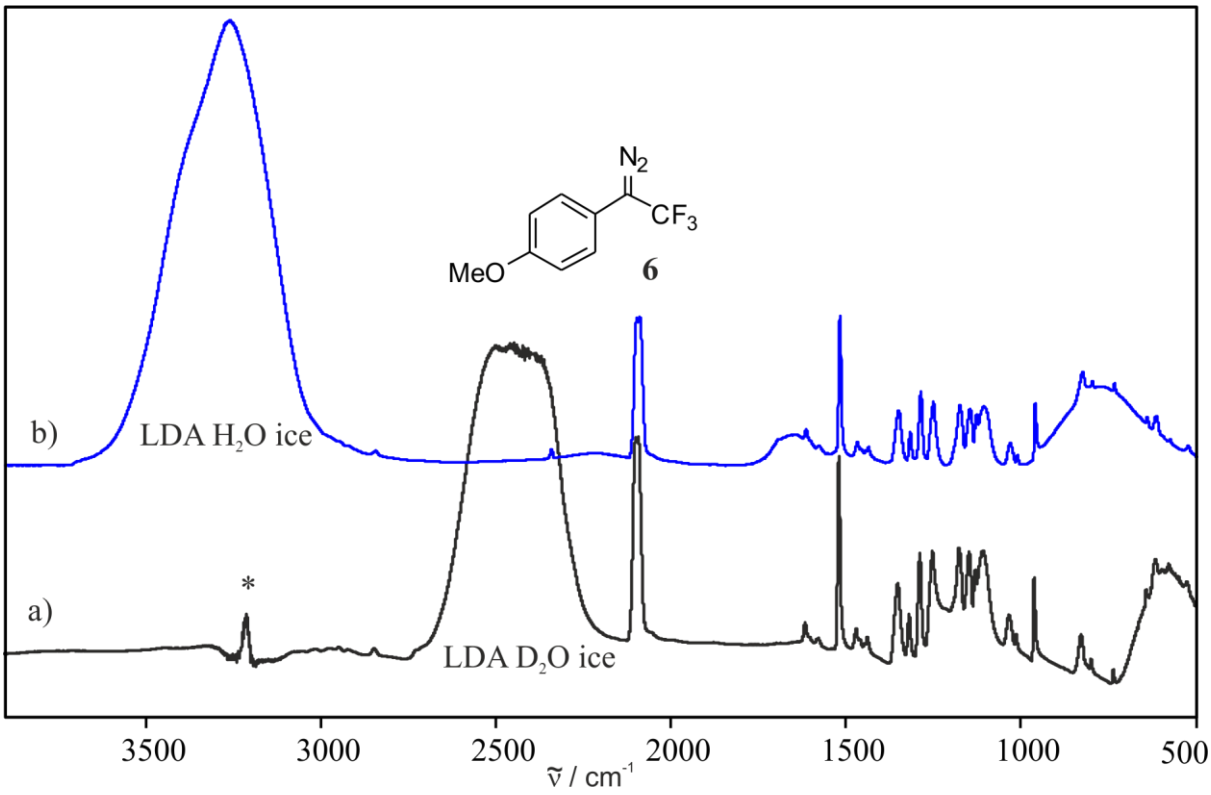

Figure **30:** IR spectra obtained after deposition of precursor **6** in a) LDA D_2O ice and in b) LDA H_2O ice at 9 K. * Traces of H_2O.

Diazo compound **6** was photolyzed with 450 nm and the obtained IR difference spectrum after photolysis is shown in Figure 31, as well as the IR spectrum of independently synthesized d-**8** in argon at 3 K for comparison. The IR difference spectrum shows a decrease of the bands assigned to **6** and an increase of new signals. A comparison of the obtained IR signals to the IR spectrum of d-**8** in argon at 3 K indicates that most of these new signals can be traced back to insertion product d-**8**. Simultaneously to the experiment in LDA H_2O ice, the matrix was subsequently annealed to 80 K. A comparison of the IR spectra obtained in solid D_2O ice to the ones in solid H_2O ice, as well as to the calculated IR spectra of **2** and d-**2**, are shown in Figure 32. The corresponding absolute IR spectra before and after annealing can be found in a separate Figure 33. The difference spectra in D_2O and H_2O ice obtained after the annealing from 9 to 80 K are showing similarities, but some differences are present as well: For example, the absorption at 1386 cm^{-1} (marked by *) decreasing with annealing to 80 K in the H_2O experiment, is not visible in the equally conducted D_2O experiment. DFT calculations predict the C=C antisymmetric stretching vibration for **2** to be at 1419 cm^{-1}, whereas for d-**2** to be very weak and shifted to 1401 cm^{-1}. Also, the vibration at 1205 cm^{-1} (marked by *) in D_2O (calc. 1253 cm^{-1}) C–D–F scissoring) is blue-shifted to 1258 cm^{-1} (calc. 1276 cm^{-1}) in H_2O. The IR difference spectra obtained after annealing to 80 K show the differences more distinct. The

comparison to the calculated spectra of the cation **2** and the deuterated cation d-**2** are fitting well and do support the results of the IR and UV-vis experiments.

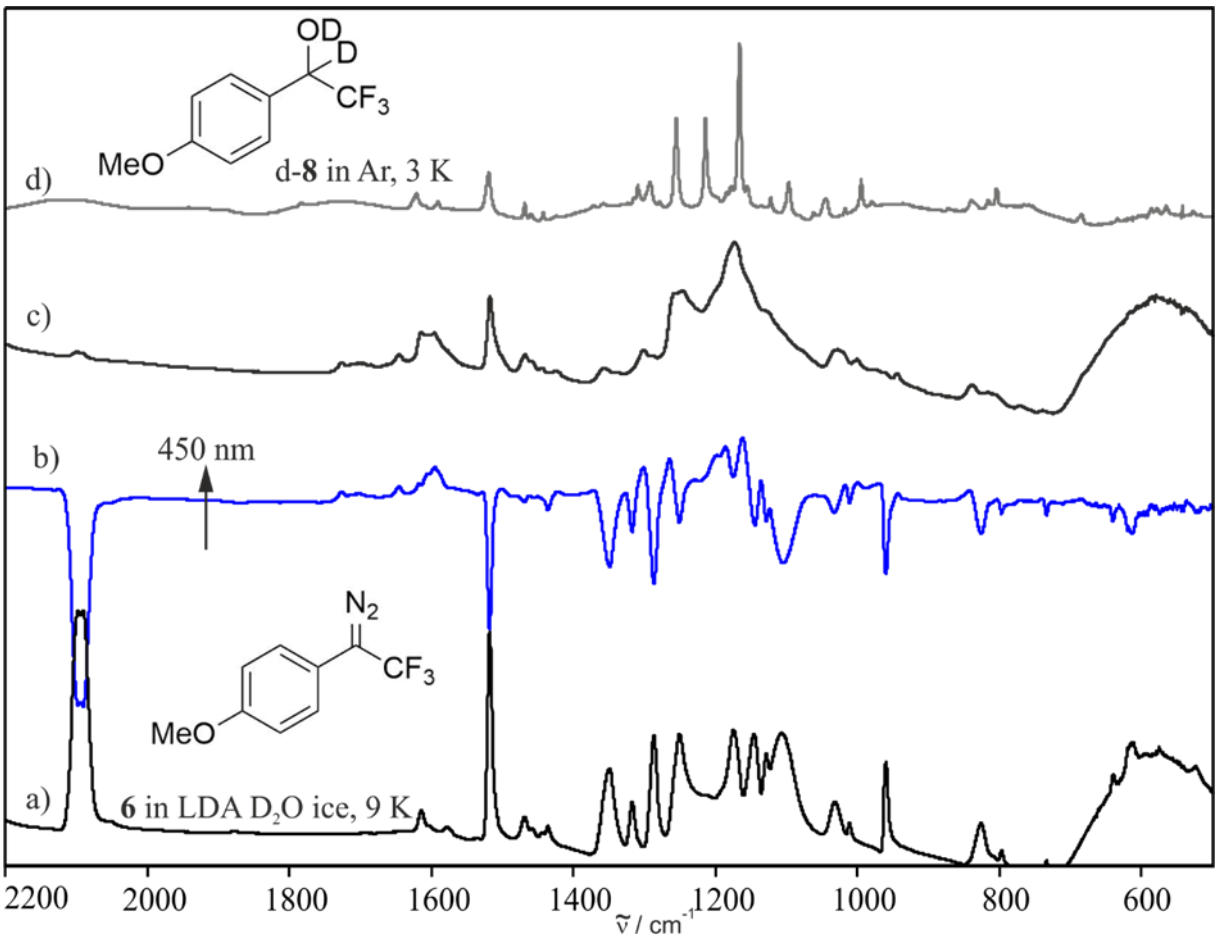

Figure **31:** a) IR spectrum obtained after deposition of precursor **6** in LDA D_2O ice at 9 K. b) IR difference spectrum obtained after subsequent 450 nm irradiation and the c) corresponding IR spectrum. Bands pointing upwards increase in intensity. Bands pointing downwards decrease in intensity. d) IR spectrum of d-**8** in argon at 3 K.

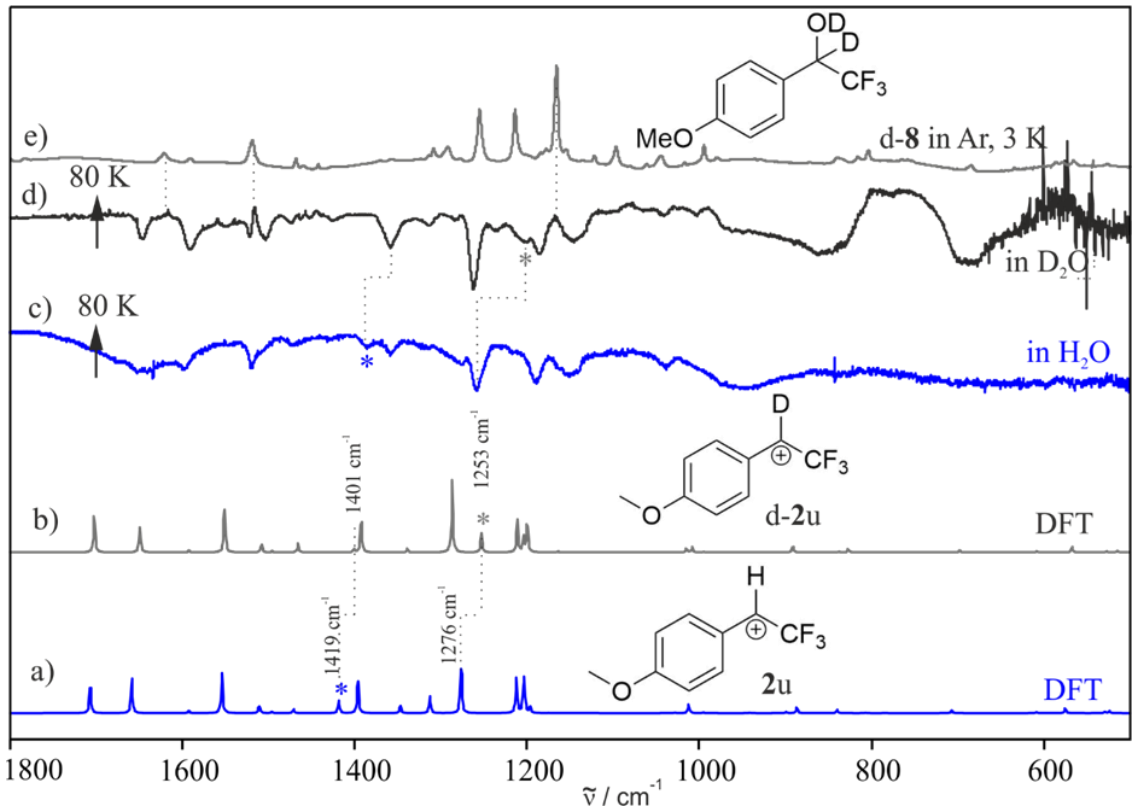

Figure **32:** Comparison of the LDA D_2O ice to the LDA H_2O ice experiment. Calculated spectra of a) cation **2**u and b) of the deuterated d-**2**u (M06-2x/Def2-TZVP//B3LYP/Def2-TZVP). c) IR difference spectrum obtained after annealing the H_2O matrix from 9 to 80 K. d) IR difference obtained after annealing the D_2O matrix from 9 to 80 K. Bands pointing upwards increase in intensity. Bands pointing downwards decrease in intensity. e) IR spectrum of d-**8** in argon at 3 K.

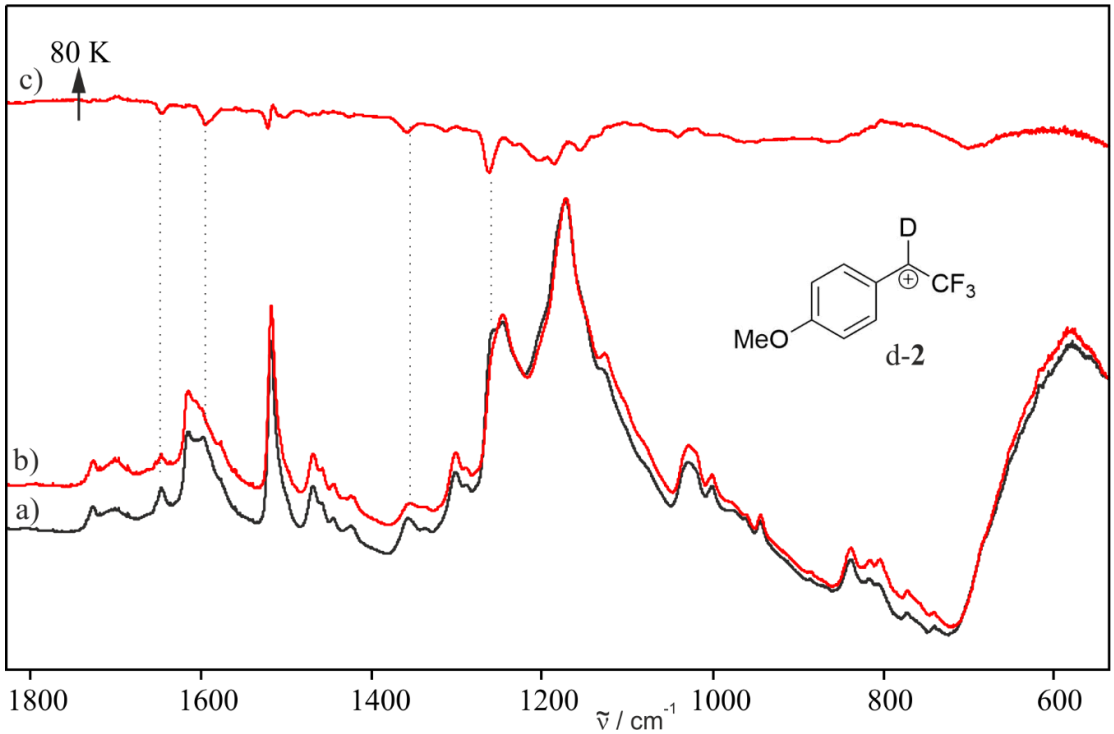

Figure **33:** IR spectra obtained a) before and b) after annealing the D_2O matrix containing d-**2** from 9 to 80 K. c) IR difference obtained after annealing the D_2O matrix from 9 to 80 K. Bands pointing upwards increase in intensity. Bands pointing downwards decrease in intensity.

2.2.4.3. Conclusions

The direct reaction of carbene **1** with H_2O was studied in LDA water ices via IR, UV-vis and EPR spectroscopy (Scheme 23). The motivation was to produce and trap the corresponding α-trifluoromethyl cation **22** in the polar and nucleophilic environment of amorphous water ice. The photolysis of precursor **6** in reactive amorphous water ices results in a high concentration of insertion product **8**. Alcohol **8** was identified by comparison to an authentic sample of **8** isolated in amorphous water ice. The generation of **8** is explainable by the, relative to **62** and **82,** high pK_R^+ value of **2**, which increases the reactivity toward nucleophiles and shifts the equilibrium further to the insertion product. Additionally to **8**, cation **2** and hydrogen-bonded complex S-**1**--H_2O are present in lower yields after photolysis of **6**. S-**1**--H_2O rearranges at temperatures below 40 K and at 365 nm photolysis to alcohol **8**. The presence of traces of complex S-**1**--H_2O is congruent to the experiments of chlorophenyl carbene **90** in LDA water ices. The UV-vis absorptions assigned to **2** are in good agreement to reported values.[8] Moreover, the calculated IR vibrations of **2** are matching the experimentally obtained spectra. Whereas cation **52** was not observed in similar experiments, **2** is the first α-trifluoromethyl bearing carbocation observed in matrix isolation experiments. The enhanced stability may be traced back to its possibility to delocalize the positive charge towards the *para*-methoxy substituted aromatic ring and thus prevent the direct insertion of OH^-. Probably due to the high pK_R^+ value, destabilizing effect of the ß-fluorination and the lower PA, the stability of **2** in LDA water ice is found to be less than matrix isolated aryl cations (**72**, **62** and **82**) and at annealing to ~40 K the insertion product **8** is generated. Cation **2** is found to be stable at the used photolytic conditions and in contrast to benzhydryl cation **62** and dihydrodibenzotropylium cation **82** in amorphous water ice,[3, 85, 105] cation **2** is not found to photolytically rearrange to a radical species. This may be traced back to the proximity of the UV-vis absorption of **2** and radical **4** (295 nm for **4** and 320 nm for **2**) and the difficulty to find a wavelength which is selectively exciting only one species. IR spectroscopic experiments in LDA D_2O ice are supporting the finding that a protonation of S-**1** results in the generation of **2**, which is stable in LDA water ices up to 40 K.

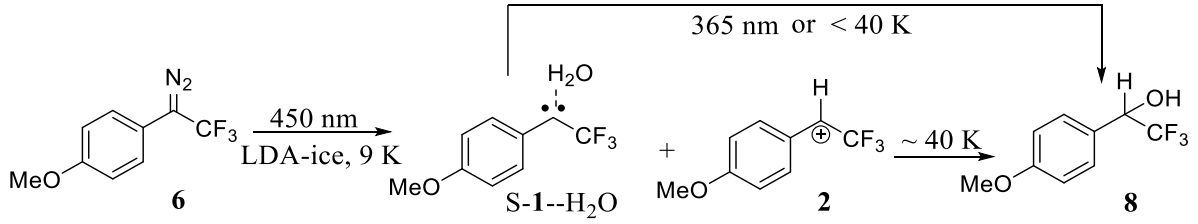

Scheme **23:** Generation of S-**1** and assumed mechanism of the direct reaction of S-**1** in LDA ices.

Overall, the experiments suggest that cation **2** with a PA of - 260 kcal mol^{-1} can be generated and stabilized in LDA water ice as found for cations **72**, **62** and **82** and unlike **52** and **92**. Therefore the optimal PA value to isolate cations in LDA ices might be in between -260 and -253 kcal mol^{-1} (B3LYP-D3/6-311+G(d,p)).

2.4. *p*-Dimethylaminophenyl-1-(trifluoromethyl)carbene

2.4.1. Characterization in argon matrices

2.4.1.1. Introduction

p-Dimethylaminophenyl-1-(trifluoromethyl)carbene **20** is bearing an inductively electron-withdrawing trifluoromethyl group (CF_3) attached to the carbene center and a strong electron-donating *para*-dimethylaminophenyl group (NMe_2). The trifluoromethyl group pulls the electron density away from the carbene carbon by an inductive effect, whereas the *p*-dimethylaminophenyl group pushes electron density through a mesomeric effect towards the carbene center. Thus, **20** is an example of a push-pull substituted carbene. As explained in Chapter 1.2, carbenes with this substitution patterns are found to be stabilized in their singlet states.

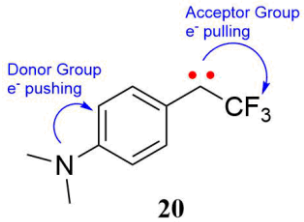

20

In this work, the reactivity of carbene **20** with water and other protic solvents is studied by the matrix-isolation technique coupled with IR, UV-vis and EPR spectroscopy and quantum chemical calculations. For carbene **20** and the corresponding diazo precursors **26**, no matrix isolation studies could be found in the literature.

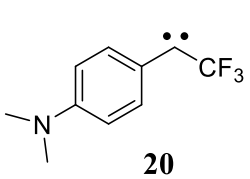

20

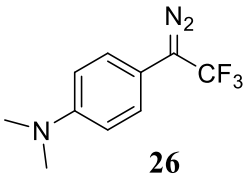

26

2.3.1.2. Results and discussion

Before studying bimolecular reactions of carbene **20**, the photochemical generation of **20** from *p*-(dimethylamino)phenyl(trifluoromethyl)diazomethane **26**, as well as the ground state multiplicity (singlet or triplet) of **20**, and its photolytic and thermal stability must be investigated. Therefore, the molecule was isolated in an inert matrix environment such as argon without reaction partners. Thus precursor **26** was deposited with an excess of argon onto a CsI window at 3 K. The IR spectrum obtained after deposition is shown in Figure 34. The IR spectrum of **26** is in good agreement with frequencies of **26** calculated at M06-2x/Def2-TZVP//B3LYP/Def2-TZVP level of theory. As described in the previous Chapter 2.2., due to poor harmonic frequency predictions of the B3LYP functional for molecules with fluorine-containing groups, it was found necessary, to use the M06-2x functional.[91] The N=N stretching vibration of **26** is found experimentally at 2084 cm^{-1} and is the most intense signal of the spectrum. Another intense vibration at 1533 cm^{-1} is assigned to the C=C antisymmetric stretching vibration. The intense IR vibration at 1124 cm^{-1} is assigned to the antisymmetric stretching of C–F (Table 7).

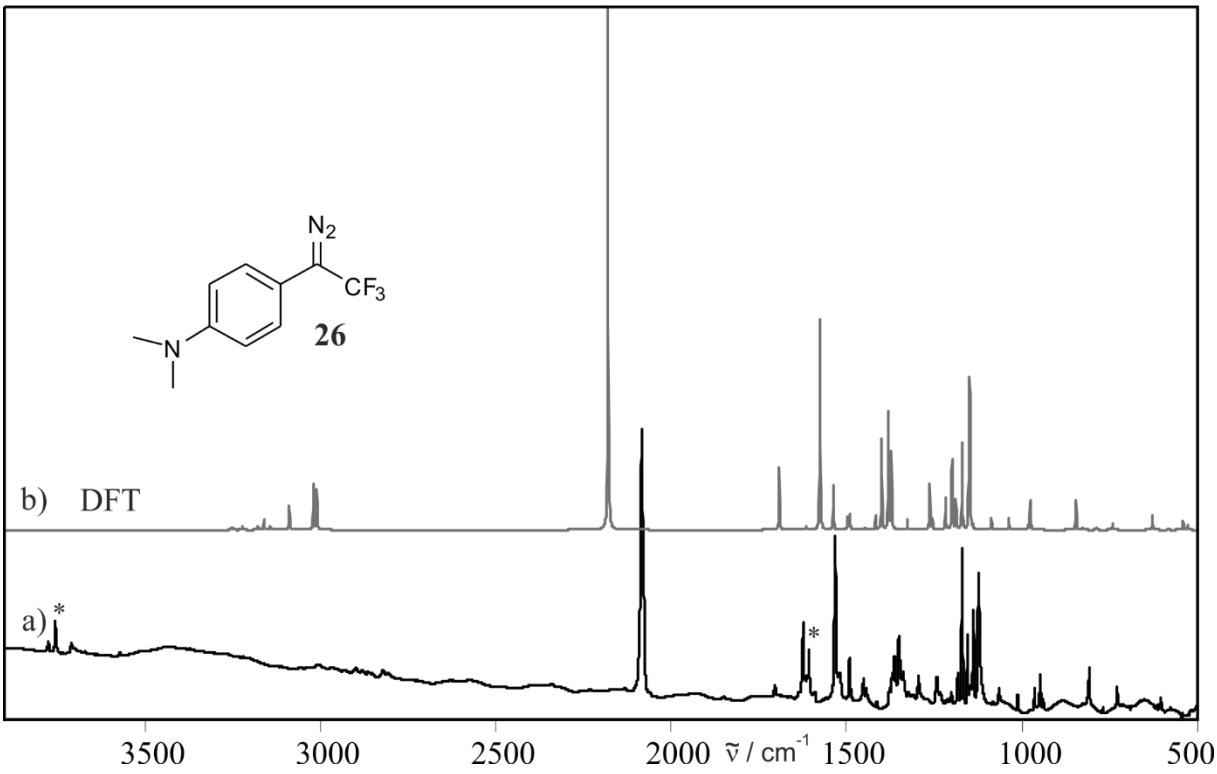

Figure **34:** Assignment of **26**. a) IR spectrum obtained after deposition of **26** at 3 K in argon, b) calculated IR spectrum of **26** (M06-2x/Def2-TZVP//B3LYP/Def2-TZVP). * Traces of water.

Table **7:** Experimental and calculated vibrational frequencies of **26.**

Exp.[b]		Calc.[a] **26**		Assignment [c]
$\tilde{\nu}$	$I_{rel.}$	$\tilde{\nu}$	$I_{rel.}$	
		3160.6	2	C-H str. (CH_3)
		3088.7	4	C-H str. (CH_3)
		3019.9	8	C-H str. (CH_3)
		3009.8	7	C-H str. (CH_3)
2084	100	2179.4	100	N=N str.
1624	2	1691.2	11	C=C Ring str.
1533	45	1575.3	38	C=C Ring str.
1491	6	1537.0	7	C-H bend.
1452	3	1496.6	2	C-H bend. (CH_3)
1443	1	1494.8	2	C-H bend. (CH_3)
1364	8	1399.8	16	N-C str.
1351	10	1380.2	21	C-C-C antisym. str.
1339	2	1371.2	13	C-H bend.
1296	5	1325.8	2	Ring def.
1243	11	1262.5	10	Ring def.
1233	3	1254.1	2	C-H bend.
		1217.2	6	C-C-C sym. str.
1182	6	1198.4	14	C-H bend. (CH_3)
1171	27	1187.9	5	C-H bend.
1155	9	1170.4	17	C-F str
1124	37	1148.6	30	C-F str
1066	3	1086.9	2	C-H bend. (CH_3)
1011	2	1036.9	2	Ring def.
965	2	982.5	1	Ring def.
948	5	975.8	5	Ring def.
939	1	974.3	1	Ring def.
808	7	845.3	5	C-H bend. out of plane
728	2	740.4	1	C-CF_3 bend.
605	2	627.1	2	Ring def.

[a] Calculated at M06-2x/Def2-TZVP//B3LYP/Def2-TZVP level of theory. [b] In argon at 3 K. [c] Tentative assignment.

Carbene **20** is generated upon visible light photolysis (λ = 450 nm) of **26**. The IR spectra obtained before and after photolysis are shown in Figure 35. Since the IR spectrum of carbene **20** was not reported in literature, the obtained spectrum after photolysis of **26** was compared to the calculated vibrations of carbene **20** in its singlet S-**20** and triplet state T-**20** (Figure 36). The IR spectrum is in a good agreement to the calculated vibrations of S-**20** (Table 8), whereas for T-**20** a strong signal calculated at 1390 cm^{-1} cannot be found in the experimental spectrum. The singlet state of **20** was confirmed by an analogously conducted EPR experiment, which did not show any signal assignable to a triplet carbene after photolysis of **26** at 3 K, nor during

annealing or photolysis of **20**. This strong evidence of the singlet state of carbene **20** is further supported by DFT calculations (Chart 15) predicting S-**20** to be energetically more stable (ΔE_{S-T} = -3.3 kcal mol^{-1} (B3LYP/Def2-TZVP)). The most intense IR signals assigned to S-**20** are the aromatic antisymmetric stretching vibration at 1602 cm^{-1} and the C–C–C symmetric stretching vibration at 1160 cm^{-1}.

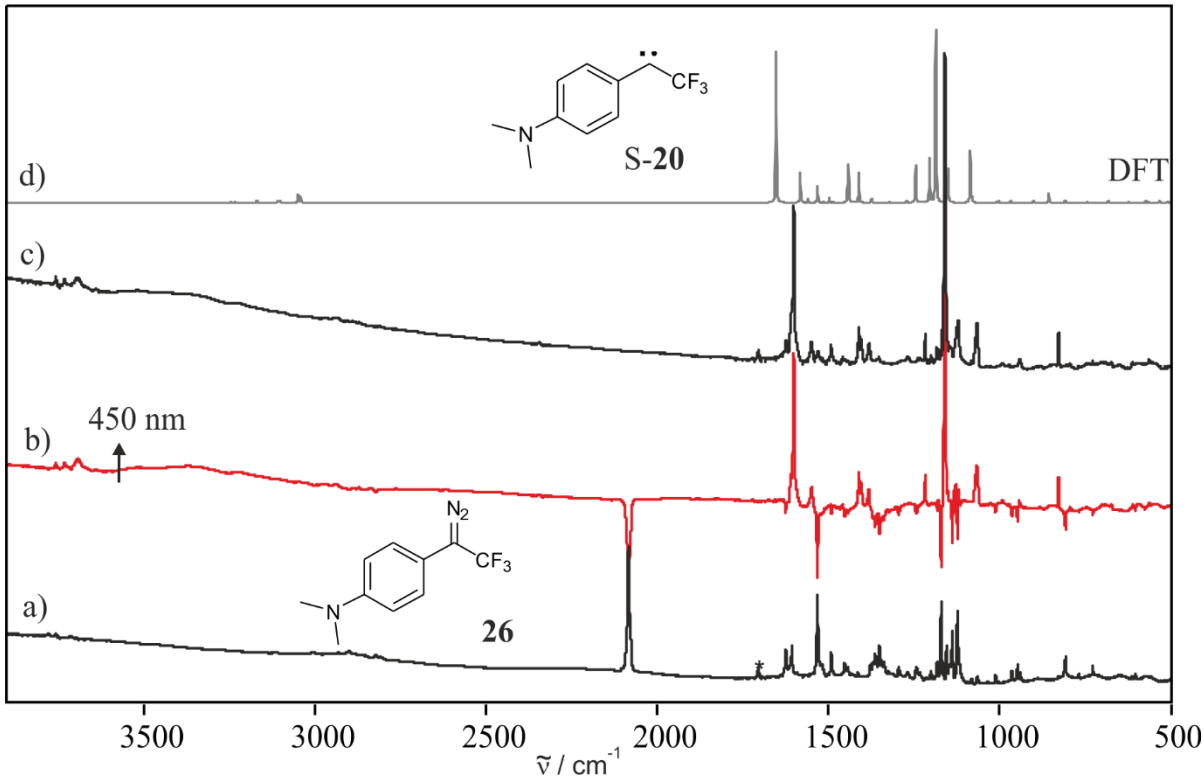

Figure **35:** Photolysis of **26**. a) IR spectrum of **26** in argon at 3 K. b) IR difference spectrum obtained after photolysis. The decreasing signals were assigned to **26**, the increasing signals to S-**20**. c) Absolute IR spectrum obtained after photolysis and d) computed IR spectrum of S-**20** (M06-2x/Def2-TZVP//B3LYP/Def2-TZVP).

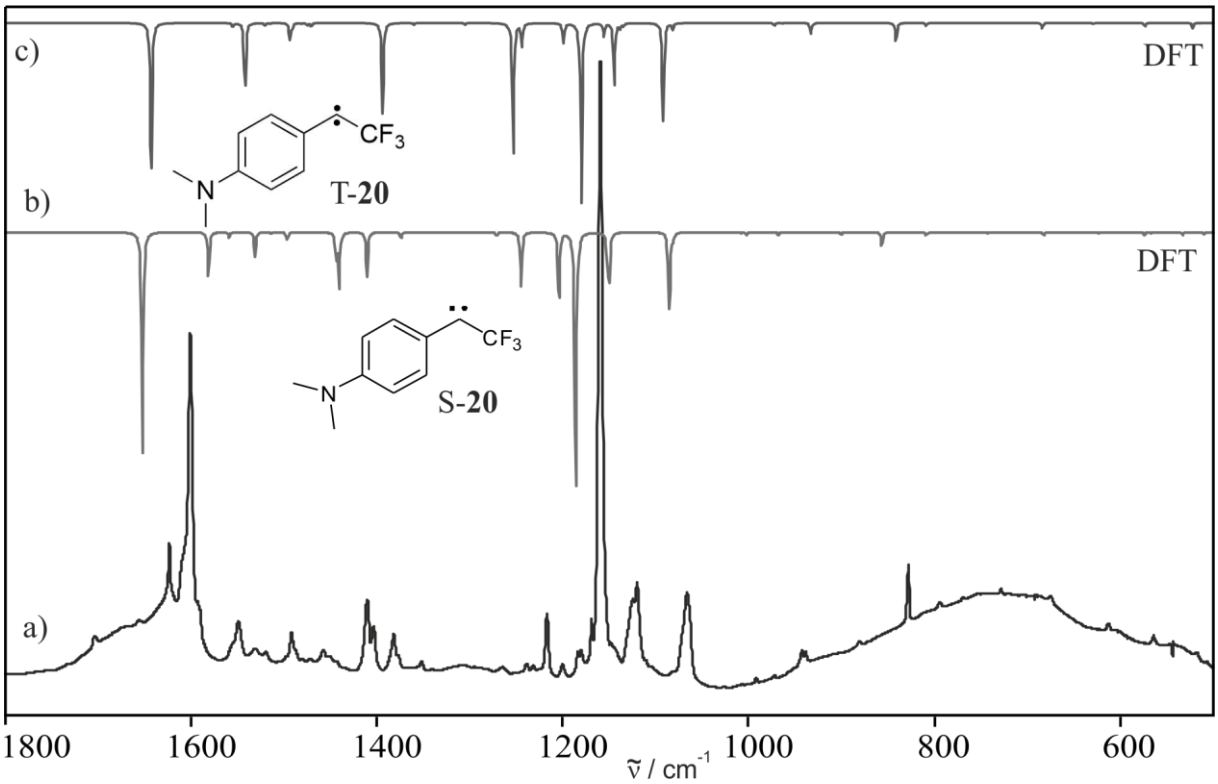

Figure **36:** a) IR spectrum obtained after photolysis of **26** in an argon matrix at 3 K. Calculated IR spectra of b) S-**20** and c) T-**20** (M06-2x/Def2-TZVP//B3LYP/Def2-TZVP).

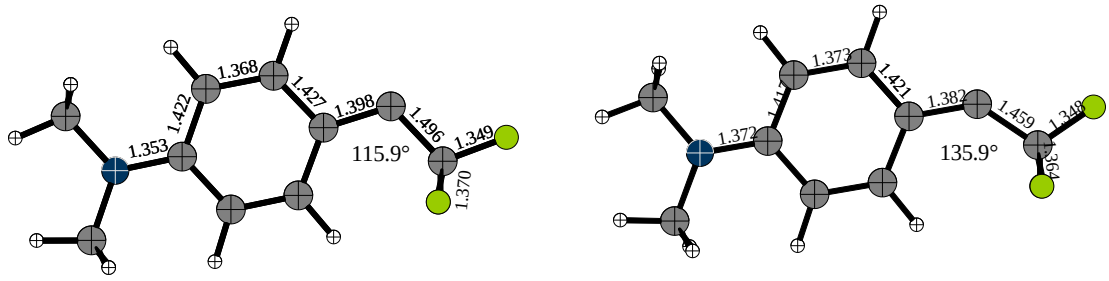

S-**20** T-**20**

$E_{rel.}$ = 0.0 $E_{rel.}$ = 3.3

Chart **15:** $\Delta E_{rel.}$ in kcal mol^{-1}. Bond lengths in Å. Structures and energies are calculated at B3LYP/Def2-TZVP level of theory.

Table **8:** Experimental and calculated vibrational frequencies of S-**20**.

Exp.[b]		Calc.[a] S-**20**		Assignment [c]
$\tilde{\nu}$	$I_{rel.}$	$\tilde{\nu}$	$I_{rel.}$	
		3048.6	5	C-H str. (CH_3)
		3041.5	4	C-H str. (CH_3)
1602	57	1652.8	81	C=C Ring str.
1549	8	1581.7	17	C=C str.
1532	1	1532.0	9	C-H bend. (CH_3)
1493	5	1497.7	2	C-H bend. (CH_3)
1458	2	1496.6	1	C-H bend. (CH_3)
1412	7	1444.2	9	C-H def. (CH_3)
1405	2	1441.0	20	C-C-C antisym. str.
1383	7	1411.2	17	C-H bend. (CH_3)
1352	1	1374.4	2	C-N str.
1218	6	1245.3	21	C-H def.
1160	100	1186.3	100	C-C-C str. sym.
		1152.3	12	C-F str.
1121	27	1150.3	17	C-H def. in plane
1067	22	1085.7	30	C-F str.
880	2	900.7	1	C=C str.
830	4	856.6	5	C-H bend. out of plane
675	1	682.3	1	C-F bend. sym.
613	1	623.1	0	C=C Ring def.
564	1	573.8	1	N-C def.

[a] Calculated at M06-2x/Def2-TZVP//B3LYP/Def2-TZVP level of theory. [b] In argon at 3 K. [c] Tentative assignment.

An UV-vis experiment was conducted in analogy to the IR experiments. The UV-vis spectrum obtained after deposition of diazo compound **26** at 8 K shows its most intense signal at λ_{max} = 290 nm. After 450 nm photolysis of **26**, new absorptions at 260 and 350 – 400 nm (doublet) are present. Those are matching to the calculated absorptions of S-**20** (Figure 37). The strongest of S-**20** is at 350 - 400 nm as a doublet.

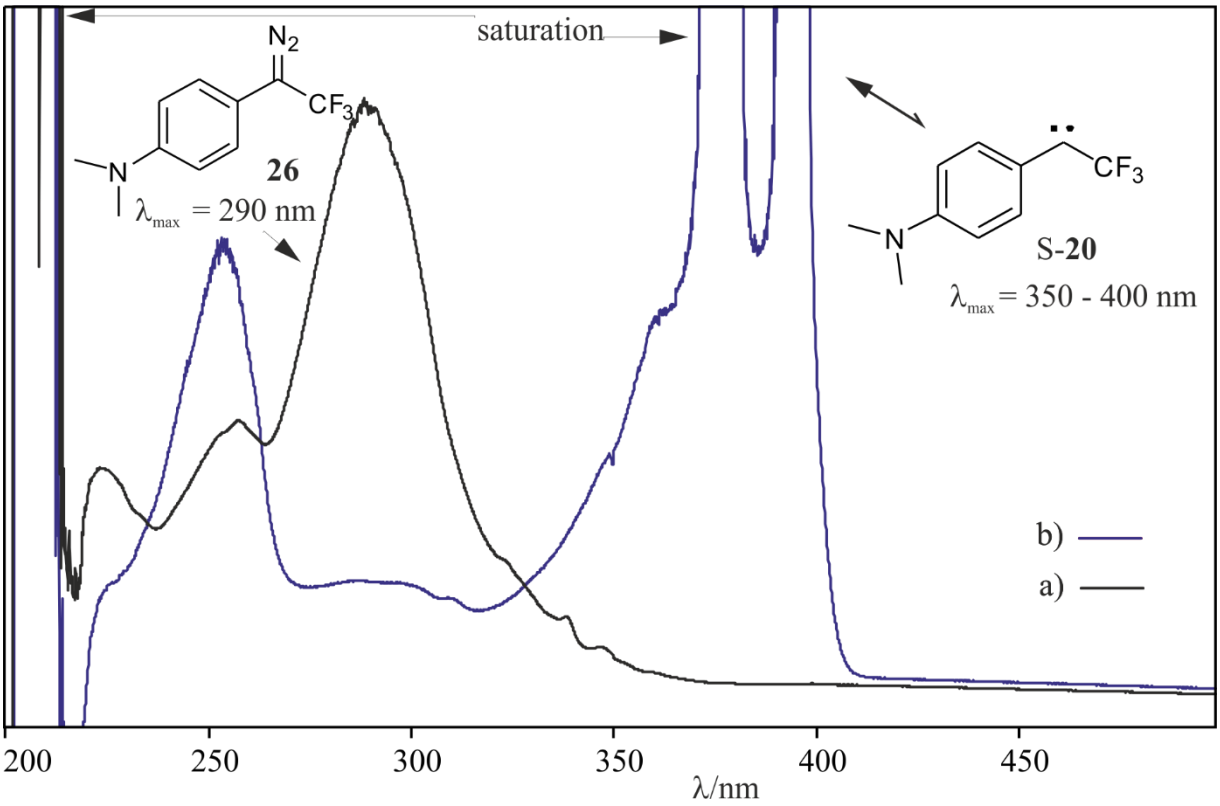

Figure **37:** UV-vis spectrum obtained a) after deposition of **26** in argon at 8 K and b) after subsequent photolysis to generate S-**20**. UV-vis absorptions calculated at the TD-B3LYP/Def2-TZVP level of theory: 184 nm (90%), 238 nm (10%), 318 nm (100%)).

Aryl carbenes are well known for photochemically induced carbene-carbene rearrangements.[106, 107] For CF_3 substituted aromatic carbenes a greater photolytic stability is found.[28] Phenyl(trifluoromethyl)carbene **11a** is, in contrast to phenylcarbene**,** photostable under UV light, and only prolonged irradiation with visible 450 nm LED light results in the rearrangement to the corresponding cycloheptatriene (Scheme 24). Derivates **11c** and **11d** are stable under UV and visible light and for the methyl substituted compound **50** the carbene-carbene rearrangement product is generated only with intense, highly monochromatic light of an OPO laser (434 - 444 nm).[28] As observed in the previous Chapter, *p*-methoxyphenyl-1-(trifluoromethyl)carbene **1** is stable upon IR, UV and visible light irradiation (LED light ranging from 365 to 650 nm and a mercury lamp of 254 nm).

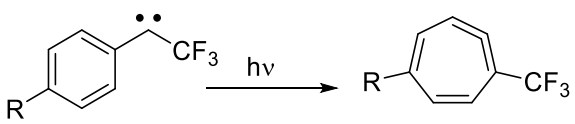

Scheme **24:** Cycloheptatriene formation observed after photolysis for: R = H (**11a**)[28] with hν = 450 nm LED. R = CH_3 (**50**)[28] with hν = 434 - 444 nm Laser. R = F (**11c**)[28], Ph (**11d**)[28] and OCH_3 (**1**) no conversion.

To extend the investigation of *para*-substituted phenyl carbenes containing a trifluoromethyl group, the secondary photolysis on carbene **20** with LED light ranging from 365 to 650 nm was investigated as well as with 254 nm light. As expected, S-**20** shows a high photolytic stability and no cycloheptatriene derivate or the formation of other products were observed via IR spectroscopy.

The thermal behavior of S-**20** was tested by annealing a matrix containing S-**20** in argon from 3 to 25 K for some minutes. There were slight changes in the shape and widths of the IR signals, but no newly formed peaks. These changes may be explained by the rotation of the methyl-group at elevated temperatures accompanied by a change in the equilibrium between the different rotamers. Calculations support this assumption by predicting a barrier of less than 1 kcal mol^{-1} (B3LYP/Def2-TZVP) for the rotation of methyl. Such small barriers can be overcome thermally even below 20 K.[108, 109]

2.3.1.3. Conclusions

To characterize carbene **20** and its photochemistry beforehand studying bimolecular reactions, the carbene was isolated in an inert host. Scheme 25 summarizes the findings of the experiments of diazo compound **26** in argon matrices. Carbene **20** is generated by 450 nm irradiation of **26** in its singlet state S-**20**. Carbene S-**20** could be characterized with IR and UV-vis spectroscopy supported by DFT calculations. The experiments revealed that the strong π-electron donating *p*-dimethylaminophenyl group stabilizes the singlet state. Furthermore, the photolysis of **20** did not show a further photo reactivity. Similar to other trifluoromethyl aryl carbenes, intramolecular rearrangements are suppressed due to the strengths of the C–F bond. and.

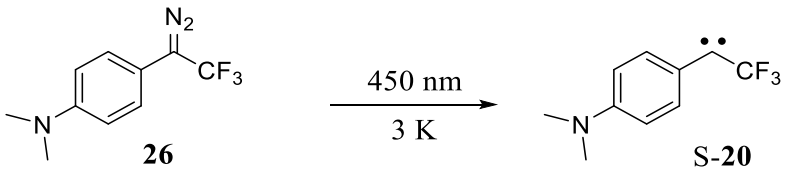

Scheme **25:** Photolytic generation of singlet carbene S-**20** from precursor **26**.

2.4.2. Complexation with water and methanol in doped matrices

2.4.2.1. Introduction

H_2O is able to form hydrogen-bonded complexes with the singlet state of carbenes as explained in Chapter 2.1..[5] A similar chemistry was found with other Lewis acids such as MeOH as well.[12, 13, 86] The experiment of diphenyldiazomethane **66** in matrixes doped with methanol revealed that triplet carbene **60** switches to the singlet state upon complexation with methanol and reacts further via insertion of OH^- to generate the corresponding diphenyl methyl ether **68** (Scheme 26). An earlier study of Kirmse on the photolysis of **66** in methanol solutions also found the ether **68** as product. This product of OH insertion indicates that the protonation of the carbene by methanol occurred through a cationic species **62** followed by OH insertion at the former carbene carbon.[74]

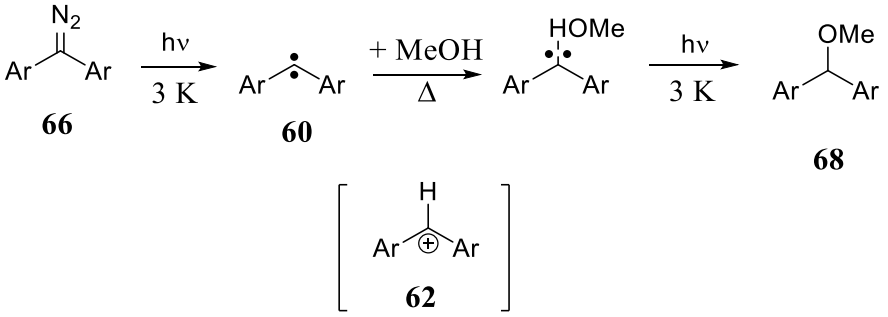

Scheme **26:** The reaction of **60** with methanol.[74]

Although studies of carbene S-**20** and its reactivity towards Lewis acids are not reported in literature, the carbene might be expected to react in a similar way as other singlet carbenes and forms a hydrogen-bonded complex with water or methanol. Furthermore, due to the strong electron-donating *p*-dimethylaminophenyl group, the protonation is potentially more favored than for carbene **1** with a *p*-methoxyphenyl substitution. This is also reflected by the higher PA (Table 1, page 13). Indications of an enhanced stability of the corresponding cation **22** can be found in a number of studies.[11, 110-112] In a solvolysis study on the aromatic substitution reaction of precursors **a** with dimethylamine (Chart 16), the analysis of the reaction rates and the derived products led to the conclusion that the intermediary 1-phenyl-2,2,2-trifluoroethyl carbocations **b** are kinetically stabilized. Richard found a "… *greater stability of 4-Me_2NArCH(CF_3)$^+$ than 4-MeOArCH(CF_3)$^+$ …*".[103] The author explains this with the greater electron delocalization emerging from the substitution with CF_3 compared to alkyl or aryl substitution. Furthermore, he states that "*… destabilizing electrostatic interaction between the positive charge and the positive end of the CF_3 dipole may act to "drive" the positive charge into the aromatic ring*

…".[110] In another paper the authors state that "*…the combination of the 4-(dimethylamino)phenyl and CF_3 groups at the … carbocation … gives a carbocation with a lower reactivity and selectivity than that obtained from the substitution of three phenyl groups. [They] find the power of (dimethylamino)phenyl group as a carbocation stabilizing substituent to be notable and surprising."*[9]

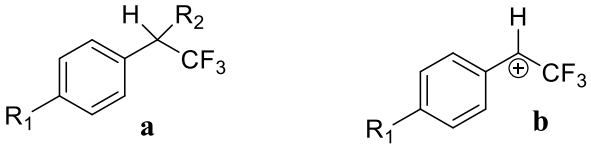

Chart **16:** R_1 = NMe_2 or OMe, R_2 = Br or Tos.[110]

In addition to the experimental studies, a computational study is found in literature, regarding rate constants of the reaction of cations with nucleophiles estimated by the No-Barrier-Theory where the authors report for cation **22** a pK_R^+ value in water of -9.3 proposing a reduced reactivity towards nucleophiles (Scheme 13).[10]

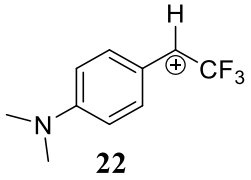

Overall, because of the calculated relatively high PA of carbene **20** (-272 kcal/mol (B3LYP-D3/6-311+G(d,p)), see Chapter 2.1.), the estimated low pK_R^+ value and the resonance stabilization of cation **22**, it is interesting to study the protonation of **20** by Lewis acids.

2.4.2.2. Results and discussion

1 % H_2O

In order to investigate the reactivity of S-**20** with the hydrogen-bond donor H_2O, precursor **26** was deposited together with 1 % of H_2O in argon onto a sapphire window at 8 K. The obtained UV-vis spectrum of **26** is shown in Figure 38. Irradiation with 450 nm light results in the formation of singlet carbene S-**20** with the UV-vis features at 350 - 400 nm (doublet) and a smaller one at 250 nm. To study bimolecular reactions, the argon matrix can be annealed up to 35 K to enable diffusion of small molecules. Interestingly, the matrix containing S-**20** and water turned from white to an intense blue color during tempering to 30 K. The color of the matrix before and after annealing are shown in Picture **3**. As reported in the previous Chapter, the blue color is not observed without the H_2O dopant. Therefore, it can be concluded that the interaction or reaction of S-**20** with water leads to the blue color. The UV-vis spectrum obtained after annealing of the matrix to 30 K for ten minutes is showing a broad triplet between 500 and 650 nm. This absorption confirms the blue color of the newly formed species **u2**. Besides that, the doublet at 350 - 400 nm assigned to S-**20** is decreasing and an absorption at 290 nm is increasing.

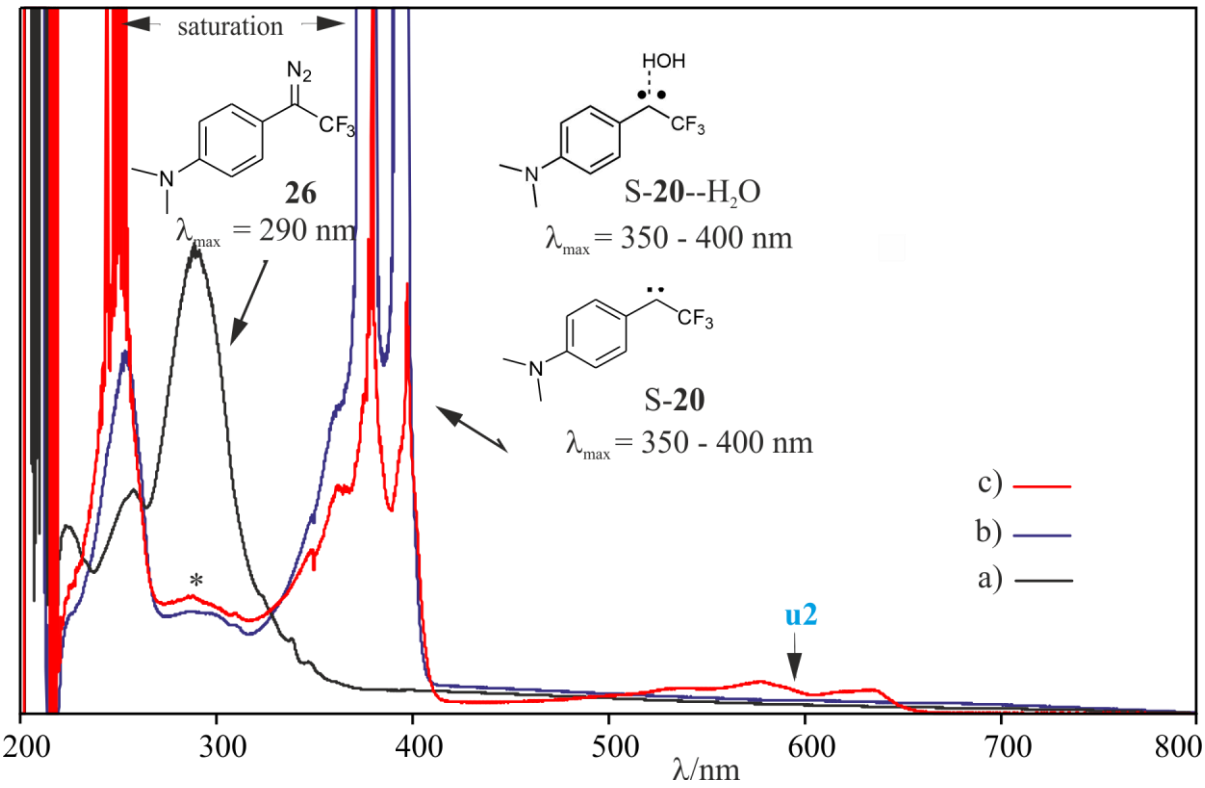

Figure **38:** UV-vis experiment of **26** in an argon matrix doped with 1 % of water. a) UV-vis spectrum obtained after deposition of **26** in argon at 8 K and b) after subsequent photolysis to generate S-**20**. c) UV-vis spectrum obtained after annealing of the same matrix to 30 K for ten minutes. * Signal at 290 nm.

before annealing. after annealing to 30 K.

Picture **3:** The color change of the matrix containing S-**20** and 1% water upon annealing to 30 K.

To investigate the photolysis of **26** and the subsequent annealing IR spectroscopically, diazo compound **26** was deposited together with 1 % of H_2O and an excess of argon onto a CsI window at 3 K. Irradiation with 450 nm light results in the formation of carbene **20** in its singlet state .Figure 39 A signal at 1265 cm^{-1}, which is not observed in the IR experiment without water, is increasing during photolysis. The fingerprint region shows that some other additional weak bands can be assigned to the OH insertion product **28a**, but the signal at 1265 cm^{-1} cannot be assigned to **28a** (Figure 40). In the following, this signal was assigned to a photoproduct **u3**.

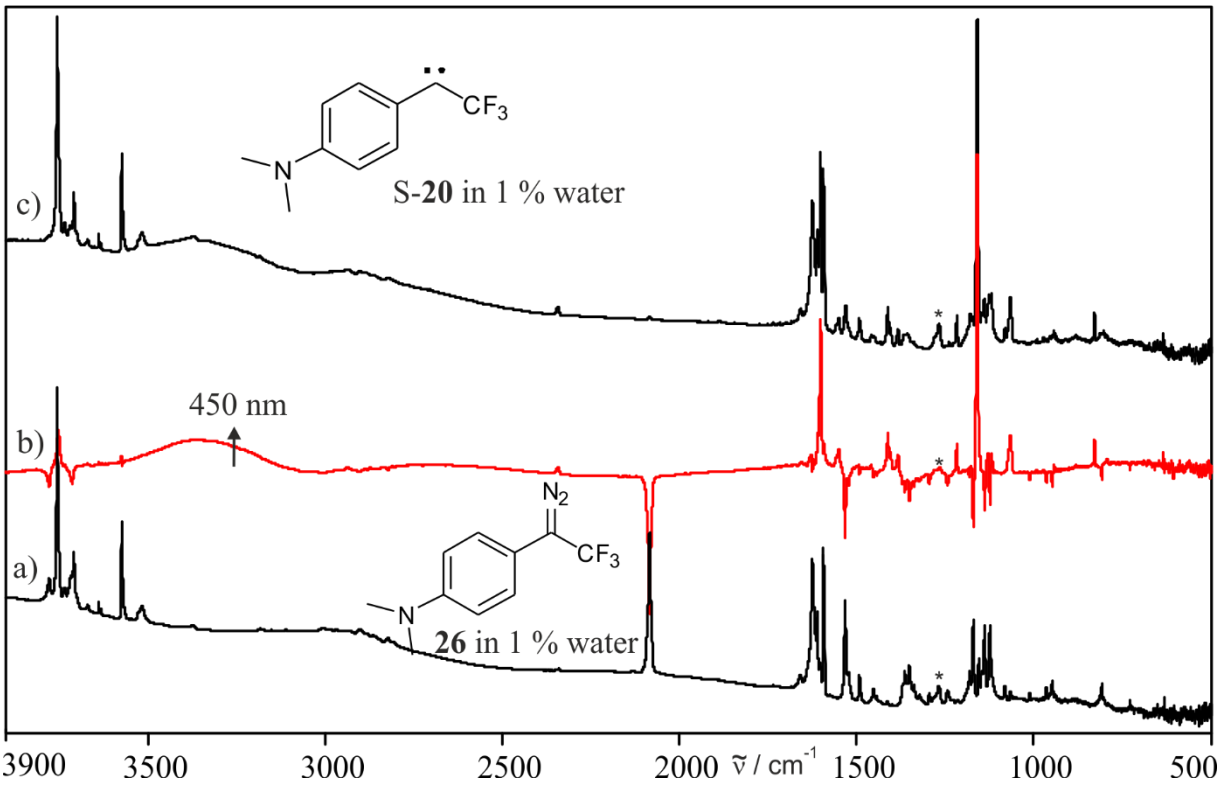

Figure **39:** Deposition and photolysis of **26** in an argon matrix doped with 1 % of water. a) IR spectrum obtained after photolysis of **26** at 3 K. b) IR difference spectrum obtained after photolysis. The decreasing signals were assigned to **26**, the increasing signals to S-**20** and c) the corresponding IR spectrum. * Signal at 1265 cm^{-1} (**u3**).

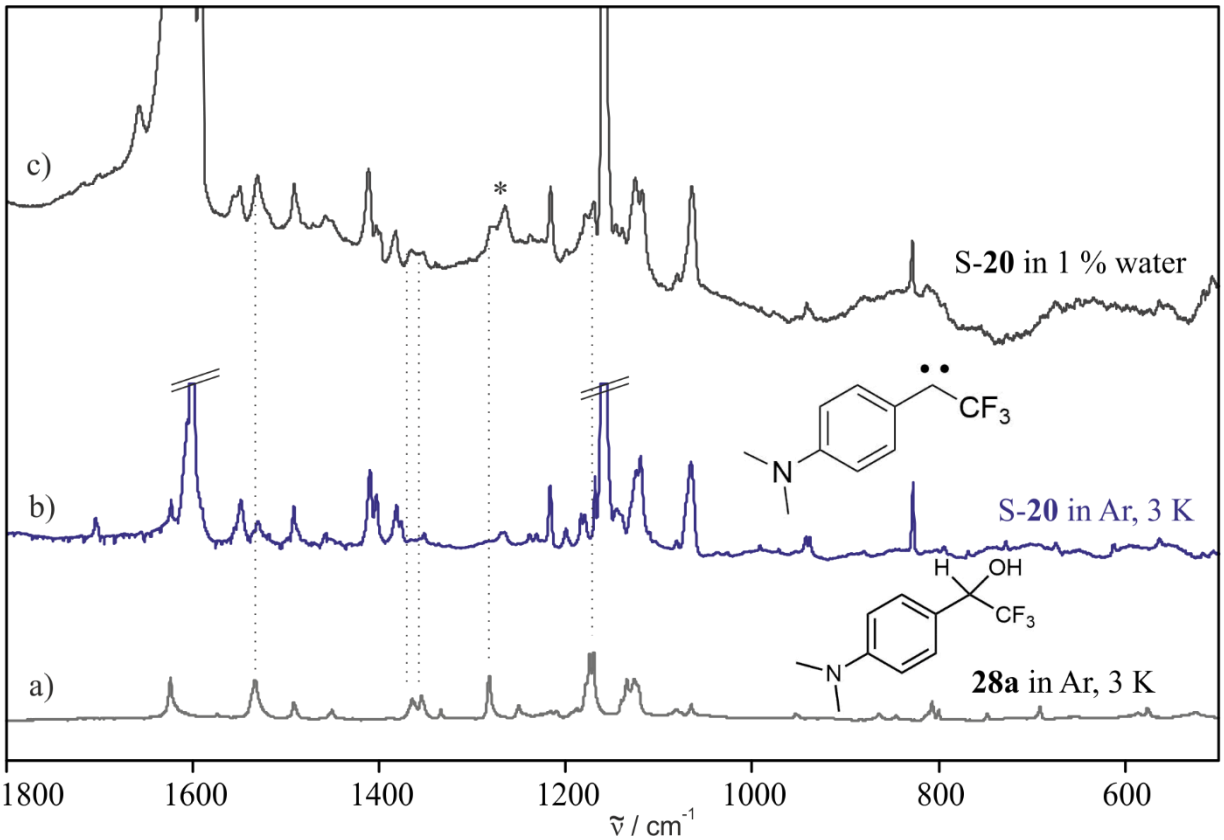

Figure **40:** IR signals obtained after photolysis of **26** in argon matrix doped with 1 % of water. a) IR spectrum of **28a** in argon at 3 K. b) IR spectrum of S-**20** in argon at 3 K. c) IR spectrum of S-**20** in 1 % of water at 3 K. * Signal at 1265 cm^{-1} (**u3**).

The matrix containing S-**20** and water was annealed up to 30 K for ten minutes analogously to the UV-vis experiment and the color of the matrix turned to blue. The obtained IR spectrum before and after annealing is shown in Figure 41. The IR signals which are decreasing during annealing can be assigned to S-**20** and water, indicating a conversion from the carbene and H_2O to a new product. An observation during the whole tempering is, that the blue color is weakly present after annealing to 20 K and intensifies during tempering to 30 K. To observe the spectral changes at different temperatures, the IR difference spectra obtained after annealing to 20, 25 and 30 K are depicted in an additional Figure 42. The IR difference spectra indicate that more than one species is arising. After the first annealing to 20 K, intense signals at 1608 and 1170 cm^{-1}, as well as some smaller ones at 1262, 1231, 1081 and 834 cm^{-1} are present. The IR difference spectrum obtained after annealing to 30 K shows no signals at 1608 and 1170 cm^{-1} anymore, but the smaller vibrations at 1262 and 1231 cm^{-1} are increasing further. Using this information, the obtained signals are separated and assigned to two species **u1** (arising at 20 K) and **u2** (increasing throughout the whole tempering). The list in Table 9 summarizes the IR spectroscopic observations and the derived assignment to the species **u1**, **u2** and the later discovered photoproduct **u3**. The signals of **u1** at 1608, 1170, 1081 and 834 cm^{-1}, which are

increasing on annealing and are slightly shifted compared to S-**20**, were assigned to hydrogen-bonded complex S-**20**--H_2O (Chart 17). A minor shift of IR frequencies of singlet carbene-water complexes relative to the monomers frequencies is expected.[5, 13] The comparison of those IR signals to the calculated spectrum of S-**20**--H_2O (M06-2x/Def2-TZVP//B3LYP/Def2-TZVP) is in a good agreement as well (Figure 43, Table 10, Table 11).

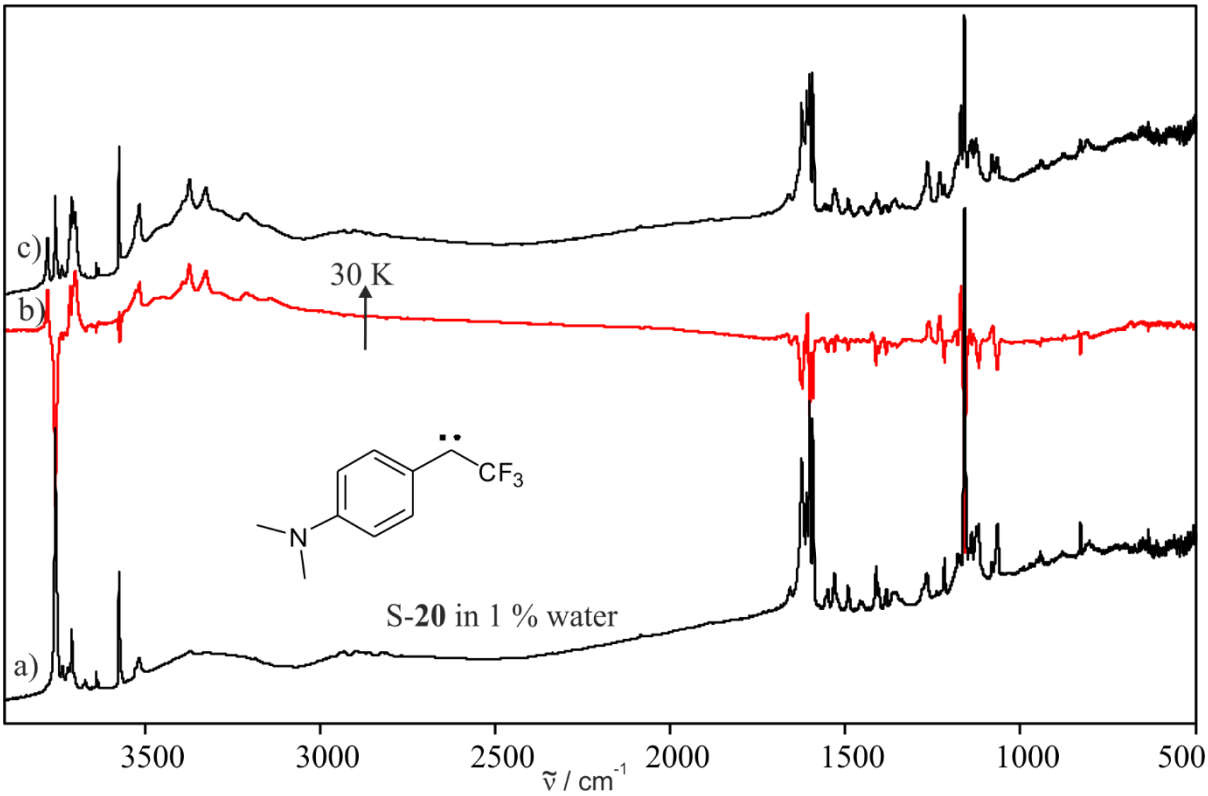

Figure **41:** IR spectra of S-**20** in an argon matrix doped with 1 % of water obtained before and after annealing to 30 K. a) IR spectrum obtained after photolysis of **26**. b) IR difference spectrum obtained after annealing to 30 K. Bands pointing upwards increase in intensity and are assigned to S-**20**--H_2O and **u2**. Bands pointing downwards decrease in intensity and are assigned to S-**20** and water. c) Corresponding absolute IR spectrum.

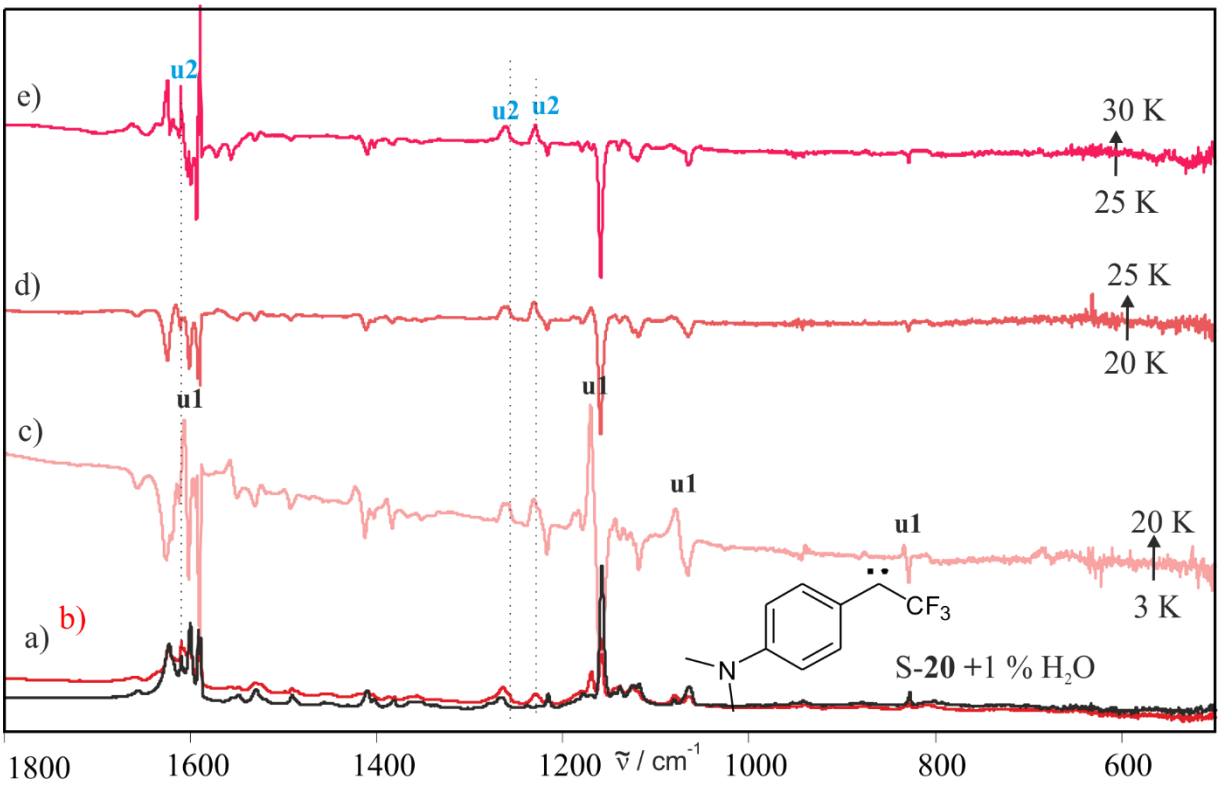

Figure **42:** IR spectra obtained by stepwise annealing of S-**20** in an argon matrix doped with 1 % of water a) at 3 K, b) after annealing and cooling back from 30 to 3 K. IR difference spectra obtained after annealing c) from 3 to 20 K, d) from 20 to 25 K and e) from 25 to 30 K. Bands pointing upwards increase in intensity. Bands pointing downwards decrease in intensity and are assigned to S-**20** and water.

2.4. p-Dimethylaminophenyl-1-(trifluoromethyl)carbene

Table **9:** Separation of the IR signals obtained after annealing to species **u1**, **u2** and **u3**.

Exp.[a]		Observations [b]				Assignment [c]		
		annealing		photolysis				
$\tilde{\nu}$	$I_{rel.}$	20 K	20 -30 K	365 nm	650 nm			
1188-1183	17	+		-		**u1**		
1082-1079	34	+		-		**u1**		
1608		+		-		**u1**		
1608	26		+		-		**u2**	
1536	18		+		-		**u2**	
1525	6	+		-		**u1**		
1501	4	+		-		**u1**		
1485	1	+		-		**u1**		
1467	2	+		-		**u1**		
1423	20	+		-		**u1**		
1410	23		+		-		**u2**	
1390	1	+		-		**u1**		
1334	3	+		-		**u1**		
1334	6		+		-		**u2**	
1265					+			**u3**
1264	63	+		-		**u1**		
1258	10		+		-		**u2**	
1231	80		+		-		**u2**	
1170	100	+		-		**u1**		
1168	26		+		-		**u2**	
1144	11	+		-		**u1**		
1135	10	+		-		**u1**		
1127					+			**u3**
1109	13		+		-		**u2**	
939	2	+		-		**u1**		
876	5	+		-		**u1**		
875	9		+		-		**u2**	
834	4	+		-		**u1**		
686	4		+		-		**u2**	
685	6	+		-		**u1**		

[a] In argon doped with 1 % of H_2O. The IR difference obtained after annealing to 30 K was used for analysis.
[b] **+** represents an increase, **-** represents a decrease in the respective IR difference spectrum. [c] Tentative assignment.

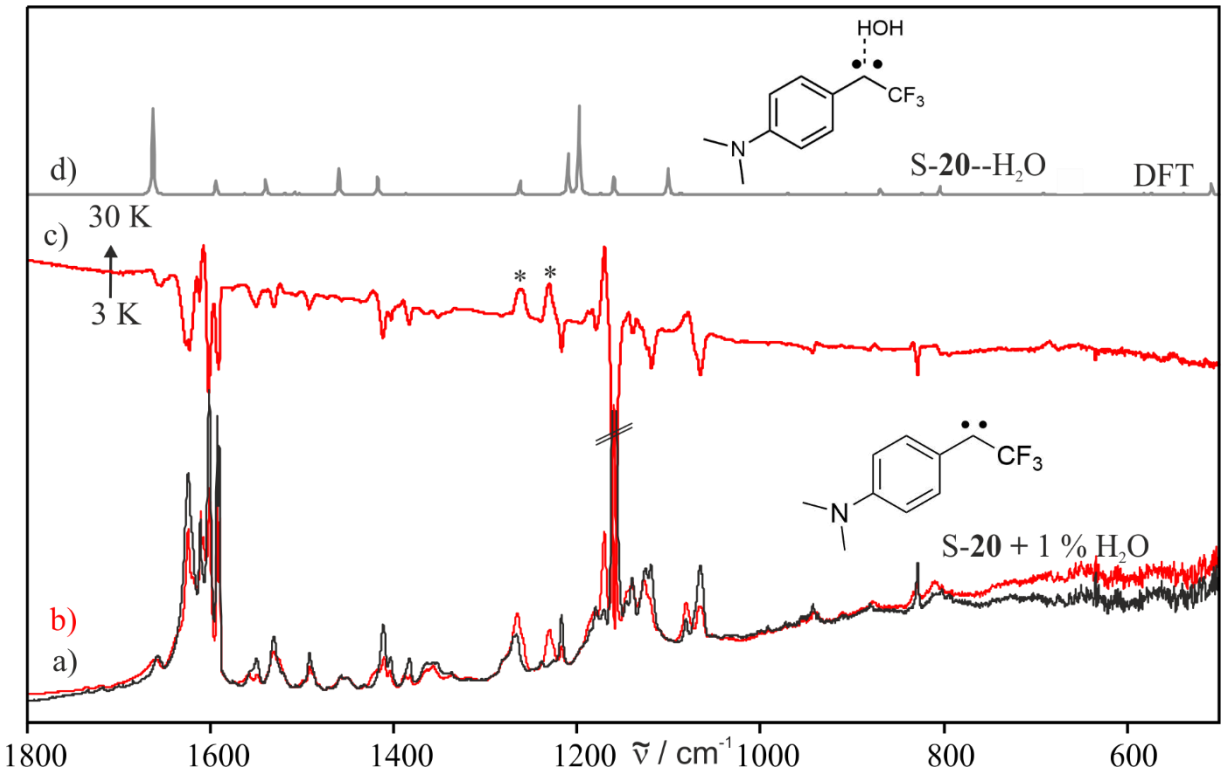

Figure **43:** Comparison of the IR spectrum obtained after annealing of S-**20** and 1 % of water to the calculated spectrum of S-**20**--H_2O. a) IR spectrum obtained after photolysis of **26** and b) IR spectrum obtained after subsequent annealing. c) IR difference spectrum obtained after annealing. The decreasing signals were assigned to S-**20** and water, the increasing signals were assigned mostly to S-**20**--H_2O (* most intense signals assigned to **u2**). d) Calculated IR spectrum of S-**20**--H_2O at M06-2x/Def2-TZVP//B3LYP/Def2-TZVP level of theory.

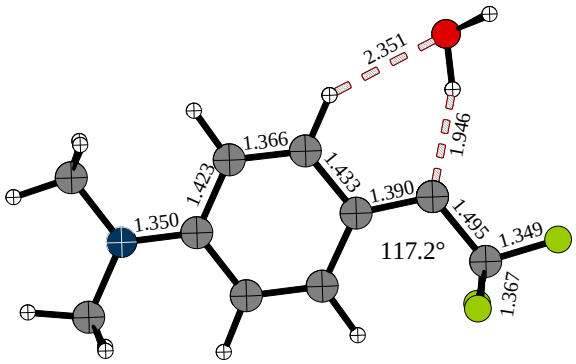

S-**20**--H_2O

Chart **17:** Computed structures and selected parameters of S-**20**--H_2O. Bond lengths in Å. Structure optimized at B3LYP/Def2-TZVP level of theory.

Table **10:** Experimental and calculated vibrational frequencies of S-**20**--H_2O.

Exp.[b] **u1**		Calc.[a] S-**20**--H_2O		Assignment [c]
$\tilde{\nu}$	$I_{rel.}$	$\tilde{\nu}$	$I_{rel.}$	
		3256.0	91	O-H str.
1608	65	1663.1	95	C=C Ring str. + O-H bend.
1525	6	1594.1	16	C=C + C-N str.
1501	4	1539.8	17	C-H bend. (CH_3)
1485	1	1508.0	3	C-H bend. (CH_3)
1467	2	1503.7	2	C-H bend. (CH_3)
1423	20	1459.9	29	C-C-C str. antisym.
1390	1	1417.6	23	C-N str. + C-H bend.
1334	3	1387.4	1	C-H bend.
1264	63	1262.3	16	C-H bend.
1189-1184	17	1210.0	44	C-H bend. + C-F str.
1170	100	1197.9	100	C-C-C str. sym.
1144	11	1174.3	2	C-H bend.
1135	10	1159.6	23	C-F str. sym.
1083-1079	34	1100.6	33	C-F str. antisym.
939	2	970.3	2	Ring def.
876	5	906.2	2	Ring def.
834	4	869.2	7	C-H bend. out of plane
685	6	507.7	13	O-H bend.

[a] Calculated at M06-2x/Def2-TZVP//B3LYP/Def2-TZVP level of theory. [b] In argon doped with 1 % of H_2O at 3 K. [c] Tentative assignment.

Table **11:** Experimental and calculated vibrational frequencies and shifts of S-**20**--H_2O:

Calculated [a]			Experimental			Assignment [e]
S-**20**	S-**20**--H_2O		Argon [c]	Argon/H_2O [d]		
ν/cm^{-1} ($I_{abs.}$)	ν /cm^{-1} ($I_{abs.}$)	shift[b]	ν /cm^{-1} ($I_{abs.}$)	ν /cm^{-1} ($I_{abs.}$)	shift[b]	
1652.8 (81)	1663.1 (95)	+10	1602 (57)	1608 (65)	+6	C=C Ring str.
1085.7 (30)	1100.6 (33)	+14.9	1067 (22)	1081 (34)	+14	C-F str.antisym.
1186.3 (100)	1197.9 (100)	+11.6	1160 (100)	1170 (100)	+10	C-C-C str. sym.

[a] Calculated at M06-2x/Def2-TZVP//B3LYP/Def2-TZVP level of theory. [b] Shifts relative to monomers (cm^{-1}). [c] In argon matrix at 3 K. [d] In argon matrix doped with 1 % of H_2O at 3 K. [e] Tentative assignment.

A useful information helping the assignment was found during subsequent photolysis: If the matrix (after the annealing experiments) is irradiated with red LED light, the color of the matrix bleaches within five minutes. Therefore, the species responsible for the blue color should match the IR frequencies decreasing upon 650 nm photolysis. The obtained difference spectrum after 650 nm irradiation is shown in Figure 44, as well as the IR spectra obtained

after annealing. The signals at 1616, 1262 and 1231 cm^{-1}, which are decreasing during IR photolysis should be traced back to the species accountable for the blue color and were assigned to **u2**. To get more insights especially on the species **u2**, an EPR experiment was conducted the same way. The experiment did not show any signals of a triplet species during the whole experiment, therefore **u2** and **u1** must be singlet species. A triplet radical species was ruled out since there is no increase in the EPR radical region during annealing (However in Appendix

Figure 84 and Figure 85 the IR and UV-vis spectra of radical pair **24 OH** are presented). Potentially, the blue colored species may be a cation **22**, a singlet radical pair, ylide **23a** or dimer **25** (Scheme 28). Dimer **25** is not expected to be generated from S-**20**, due to good isolation conditions in the argon matrix. Nonetheless, UV-vis and IR spectra of **25** were calculated and compared to the experimental spectra. The TD-DFT-calculated UV-vis absorptions of **25** did not show absorptions in the region 500 - 600 nm, nor are the calculated IR frequencies in a good agreement to the observed IR frequencies Figure 44 and thus **25** was ruled out. Due to the singlet state of S-**20** and the electron-donating properties of the *p*-dimethylaminophenyl group, an O-ylide formation may be considered, as oxygen can interact with an empty p orbital of the carbene (Scheme 27).[113-115] But DFT calculations (B3LYP/Def2-TZVP) for the H_2O ylide did not result in a converged structure, whereas the calculated structure of the ylide derived from a reaction with MeOH predicted an energetic destabilization of +2.32 kcal mol^{-1} compared to the monomers. Thus and because of a bad UV-vis and IR spectral congruency (see Figure 85 and Figure 86 in Appendix), an ylide formation was ruled out as well.

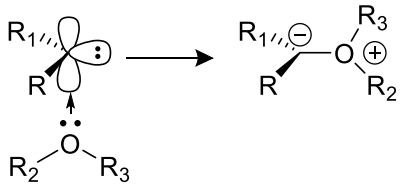

Scheme **27:** Formation of an O-ylide from a singlet carbene.

As the IR signals of **u2** show a better matching to the calculated frequencies of cation **22** (Figure 44**,** Chart 18, Table 12) and considering that the cation is expected to show a huge resonance stability associated with a kinetic stability,[11] **u2** was preliminary assigned to **22**. The experimental IR signals are difficult to interpret, as they overlap with others and thus the IR difference obtained after 650 nm irradiation was used. Here as well, overlapping with the newly formed signals are complicating the evaluation, especially of the intensities of the frequencies at 1231 cm^{-1} and 1258 cm^{-1}. Those two are the strongest signals of **22** (**u2**) and are assigned to

the C–F antisymmetric and symmetric stretching vibrations, respectively. The exact structure of **22** has to be evaluated further as other factors such as an interaction of the OH or a Charge-transfer may be involved (see Chapter 2.4.2.3. DFT Calculations).

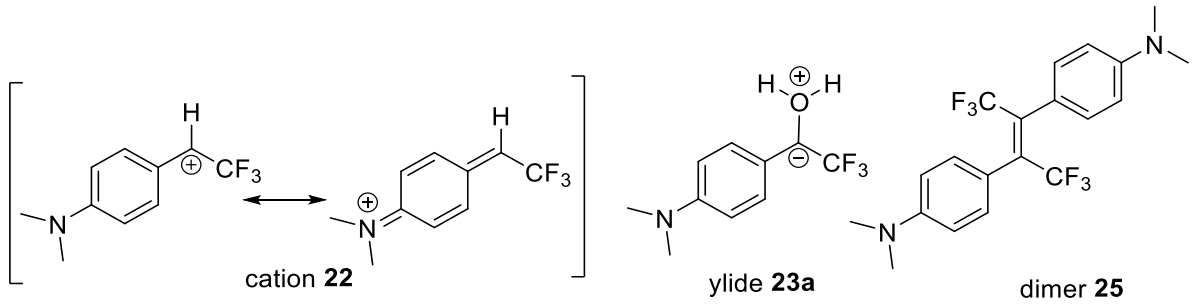

Scheme **28:** Possible singlet species formed by interaction of carbene **20** with water, which may be assigned to **u2**.

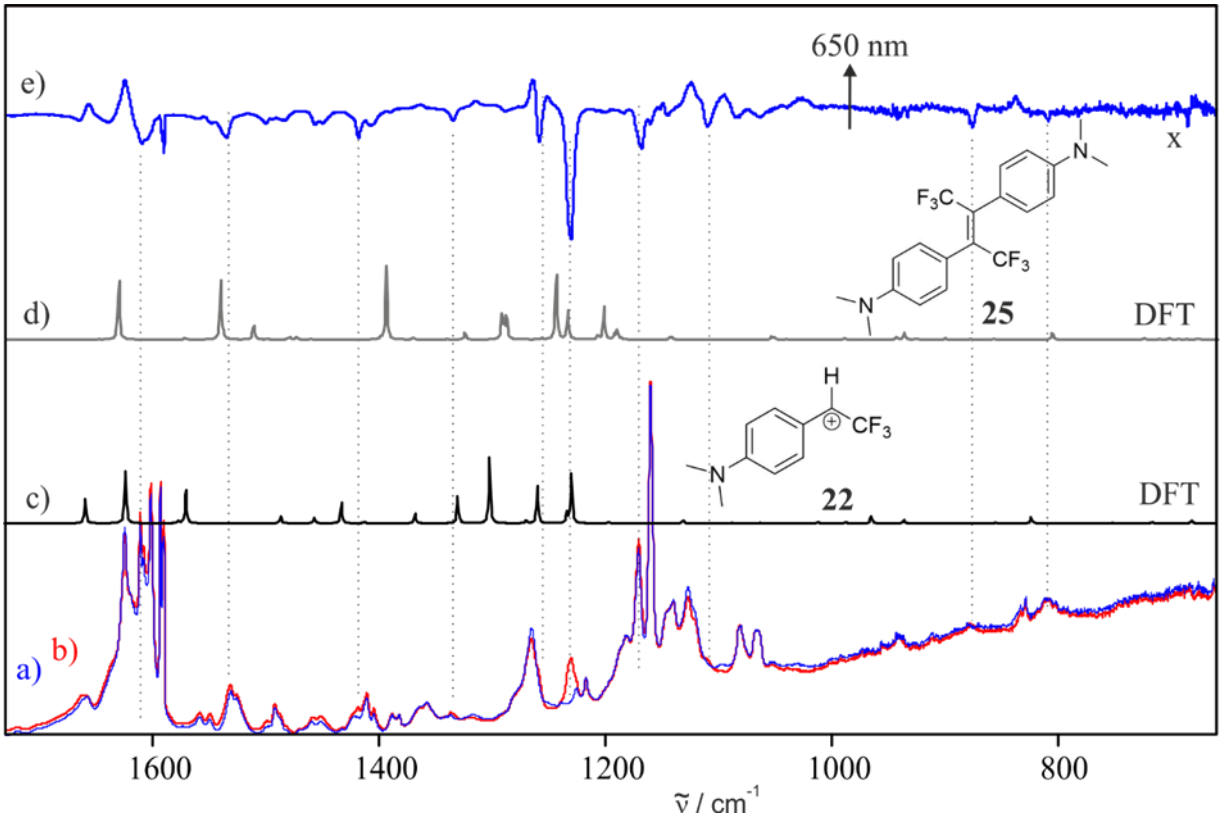

Figure **44:** a) IR spectrum obtained after annealing of S-**20** in a 1 % water-doped argon matrix to 30 K and b) the IR spectrum obtained after subsequent 650 nm photolysis. Calculated IR spectra c) of **22** and d) of **25** (M06-2x/Def2-TZVP//B3LYP/Def2-TZVP). e) IR difference spectrum obtained after 650 nm photolysis. Bands pointing upwards increase in intensity. Bands pointing downwards decrease in intensity and are assigned to **u2**.

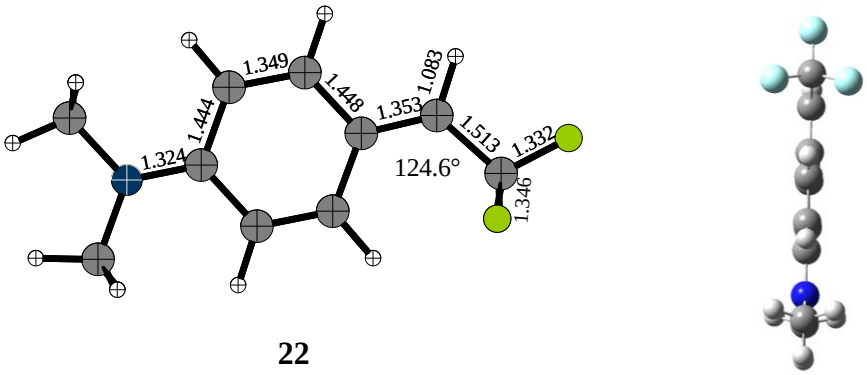

22

Chart **18:** Computed structure and selected parameters of **22**. Bond lengths in Å. Structure optimized at B3LYP/Def2-TZVP level of theory.

Table **12:** Experimental and calculated vibrational frequencies of **22**.

Exp.[b] **u2**		Calc.[a] **22**		Assignment [c]
$\tilde{\nu}$	$I_{rel.}$	$\tilde{\nu}$	$I_{rel.}$	
1608	32	1670.4	93	C=C str.
1536	22	1605.4	58	C-N str.
1419,1405	29	1438.2	32	C-H bend.
1334	7	1359.1	15	C-H bend.
1258	13	1313.3	45	C-F str.
1231	100	1279.0	100	C-F str.
1168	32	1227.8	58	C-H Ring def.
1109	16	1190.9	67	C-F def.
875	11	869.1	11	C-H Ring def.
686	5	697.2	10	C-H bend. out of plane

[a] Calculated at M06-2x/Def2-TZVP//B3LYP/Def2-TZVP level of theory. [b] In argon doped with 1 % of H_2O at 3 K. The intensities derived from an IR difference spectrum and thus are estimated. [c] Tentative assignment.

To investigate the thermal behavior of S-**20** in H_2O-doped argon matrices starting at temperatures below 20 K and secondly to confirm the correlation of the blue colored species to the IR vibrations of **u2**, the experiment was repeated using IR and UV-vis spectroscopy simultaneously. In Figure 45 the UV-vis and IR spectra obtained during stepwise annealing from 3 to 10, 15, 20, 25, and 30 K, for ten minutes each time, are shown. After staying at 30 K the matrix was cooled to 3 K. UV-vis and IR spectra show that **u2** starts to grow at 20 K and increases further throughout 25 K annealing. S-**20**--H_2O (**u1**) behaves differently and its IR signals start increasing at 10 K, and at 15, 20, 25 and 30 K the increase is still observable but weakens with higher temperatures giving rise to **u2**. The UV-vis spectra obtained at 10 and 15 K are showing signals at 250 nm and between 300 and 400 nm. Those signals can be

assigned to S-**20** or S-**20**--H_2O since singlet carbenes and their hydrogen-bonded water complexes are expected to show very similar UV-vis spectra. The calculated UV-vis spectra of S-**20** and S-**20**--H_2O shown in Figure 46 are underlining this expectation. Above 20 K another signal at 500 - 650 nm rises, which is attributed to the blue colored species **u2**. The corresponding IR signals, which rise above 20 K are found at 1262 and 1231 cm^{-1}. Noteworthy, at 30 K the absorptions at 300 - 400 nm and 250 nm increase again accompanied by an absorption at 290 nm. This different behavior at 30 K is also observed in the IR difference spectrum: the signal at 1262 cm^{-1}(**u2**) is growing faster than the signal at 1231 cm^{-1}. This indicates that underneath the band at 1261.8 cm^{-1} might be the absorption of another species. This might be the same species **u3** (signal at 1265 cm^{-1}) observed increasing during the photolysis of **26** in 1 % of water or a separate species. Assuming that **u2** is cation **22**, the calculated UV-vis absorptions of **22** should match the UV-vis absorption at 500 - 650 nm. However, this is not the case for TD-DFT calculations of **22** with B3LYP/Def2-TZVP and B3LYP/6-31+g(d,p) level of theory (Figure 47). Hence those TD-DFT calculations are not supporting this theory. Potentially, this may be traced back to the difficulty to obtain reliable UV-vis spectra with TD-DFT calculations, especially for excited states such as Charge-transfer complexes.[116, 117] See the Chapter 2.4.2.3. DFT Calculations for further information.

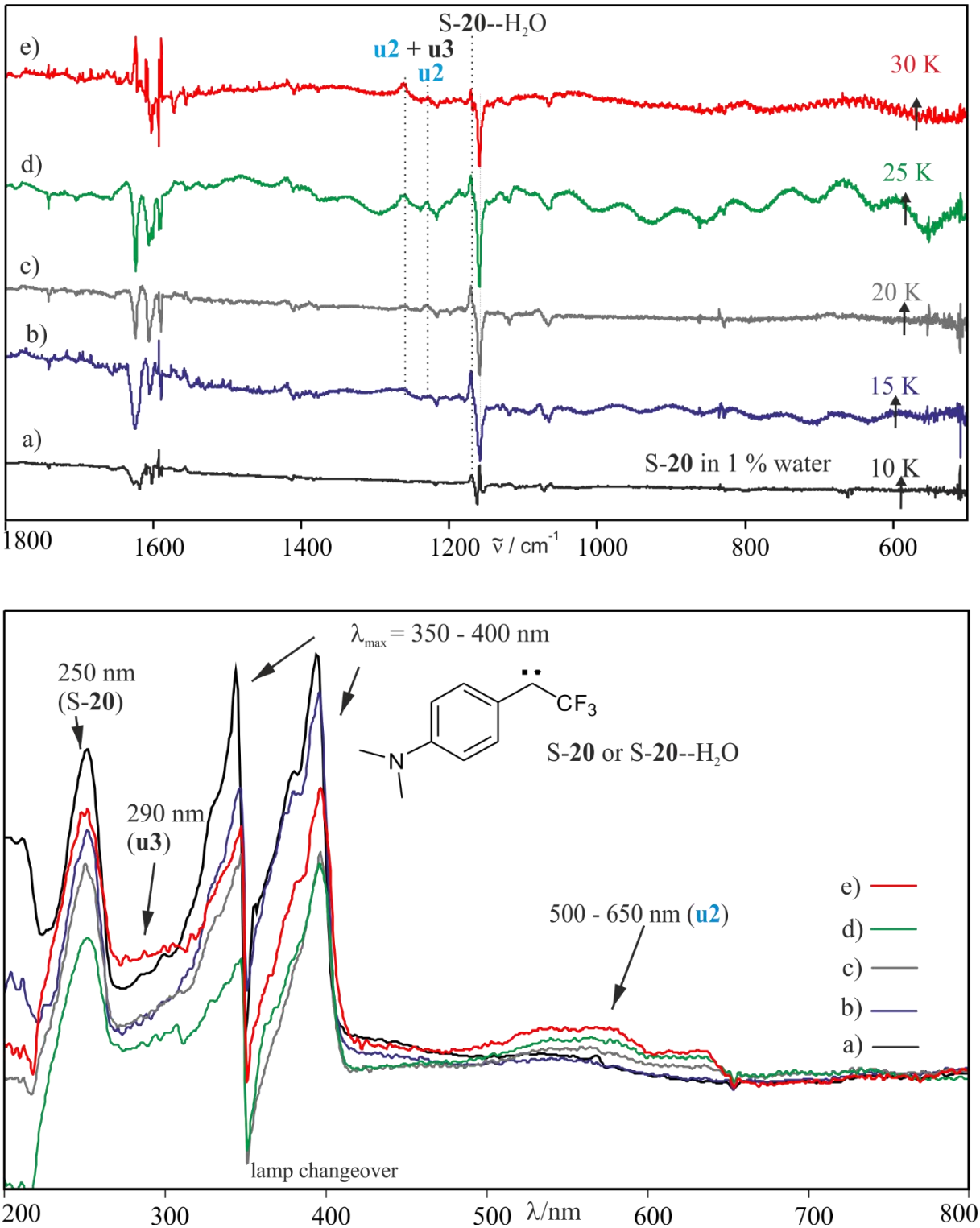

Figure **45** IR (upper part) and UV-vis (bottom part) spectra taken simultaneously. Spectra obtained during a stepwise free annealing experiment of S-**20** in 1 % H_2O. UV: a) UV-vis spectrum obtained after annealing from 3 to 10 K, b) 15 K, c) 20 K, d) 25 K and e) 30 K for ten minutes at each temperature. At 340 nm the lamp changeover of the spectrometer induces a strong cut. IR: IR difference spectra showing the changes between 5 K steps. a) 10 K, b) 15 K, c) 20 K, d) 25 K and e) 30 K. Bands pointing upwards increase in intensity. Bands pointing downwards decrease in intensity.

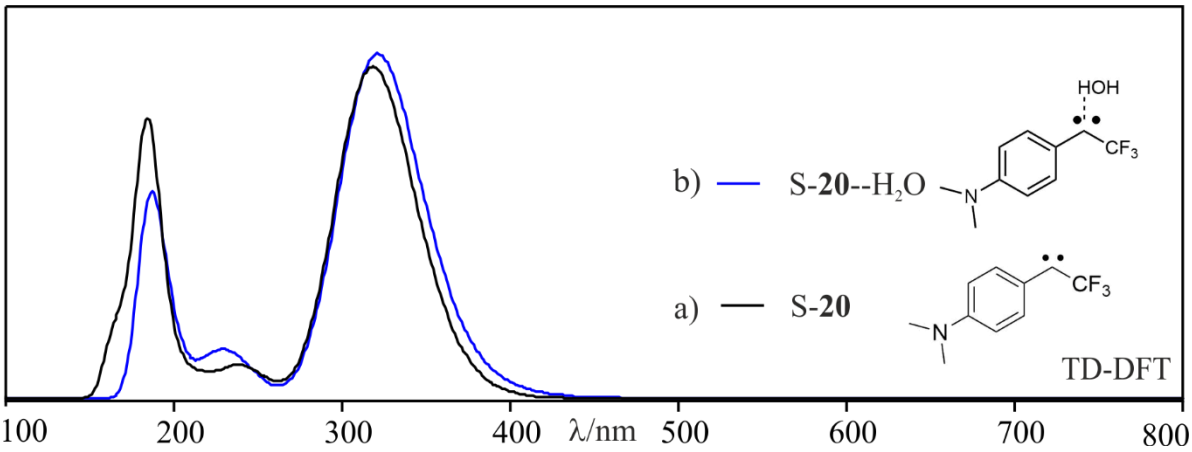

Figure **46** Calculated UV-vis absorptions of a) S-**20** and b) S-**20**--H_2O calculated at TD-DFT (B3LYP/Def2-TZVP) level of theory.

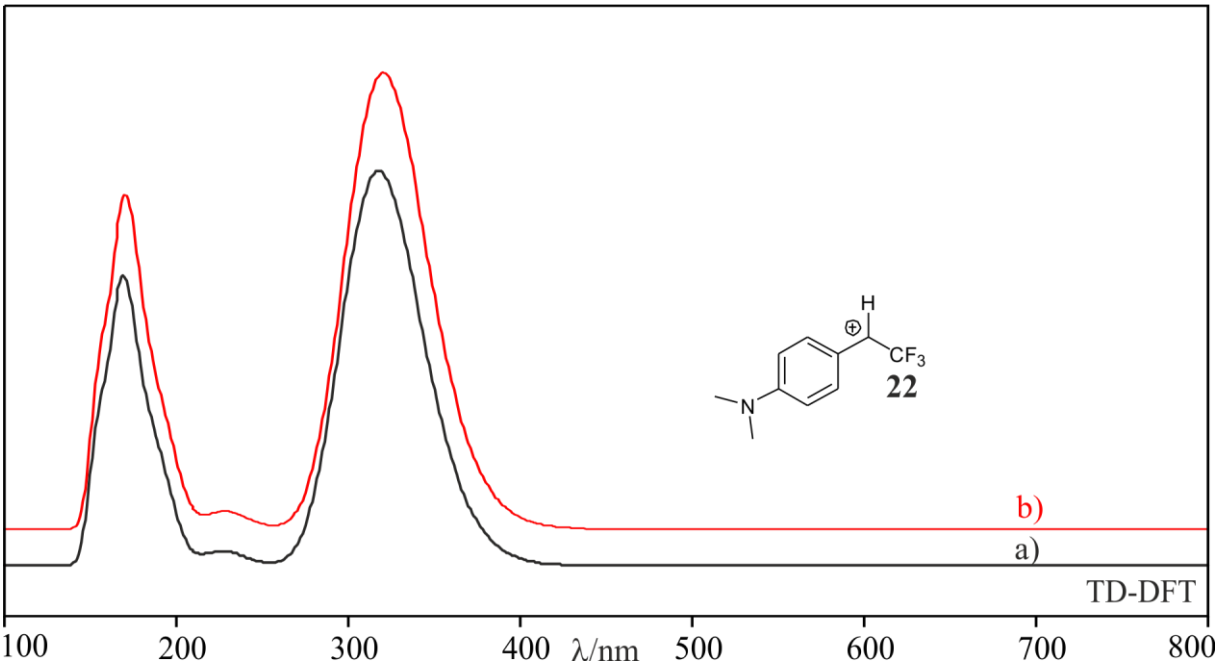

Figure **47** UV-vis spectra of **22** calculated at TD-DFT (a) B3LYP/Def2-TZVP and b) B3LYP/6-31+g(d,p) level of theory.

To get more information on the generated species, photolysis was performed after annealing and observed via IR spectroscopy. As mentioned before, the blue colored species **u2** is light-sensitive and bleaches fast if exposed to 650 nm light (Figure 48). The newly generated photoproduct **u3** shows its strongest IR vibration at 1265 cm^{-1}. This signal was found to increase already upon photolysis of precursor **26** in matrices doped with water and by annealing to 30 K as mentioned before, (see Figure 49) thus those vibration may be assigned to photoproduct **u3**. As the signal at 1265 cm^{-1} shows no decrease throughout the experiments, it was assumed that the responsible species is not showing any further reactivity. The usual OH insertion product **28a**, resulting from insertion at the C-1 carbon (Chart 19), can be ruled out by comparison to a

reference spectrum of **28a** in an argon matrix at 3 K (Figure 48). As cation **22** is possibly kinetically hindered to insert OH at the C-1 position induced by a repulsion of the negative CF_3 group and by charge delocalization over the aromatic ring,[11, 118] other OH insertion products were calculated (Chart 20). The energetically most stable alcohols besides **28a**, are **29a2** and **29a4**. Insertion products **29a1** and **29a3** were ruled out due to energetical and spectroscopic reasons. The formation of hemiacetals and hemiaminals like **29a4** were discussed in literature as a result of a C-5 insertion to cations with a very delocalized charge and sterically hindered C-1 carbons.[110] Moreover, the calculated IR signals of **29a4**, are showing a good agreement to the obtained spectrum. Alcohol **29a2** (C-3 insertion) is showing a reasonable IR spectroscopically matching as well, but no previous experimental evidence for this compound was found. However a simulation (QM/MM MD) on the reaction of aryl carbene **60** in water observed an C-3 insertion (*ortho*-hydroxylation) as a possible side reaction.[118, 119] Because of the experimental congruency and the mentioned literature results, **29a4** was considered as most probable assignment of **u3**, although **29a2** may not be ruled out.

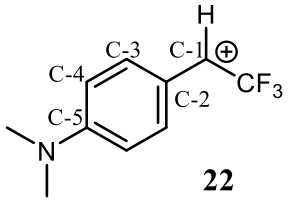

22

Chart **19:** Possibilities for OH insertions at cation **22**.

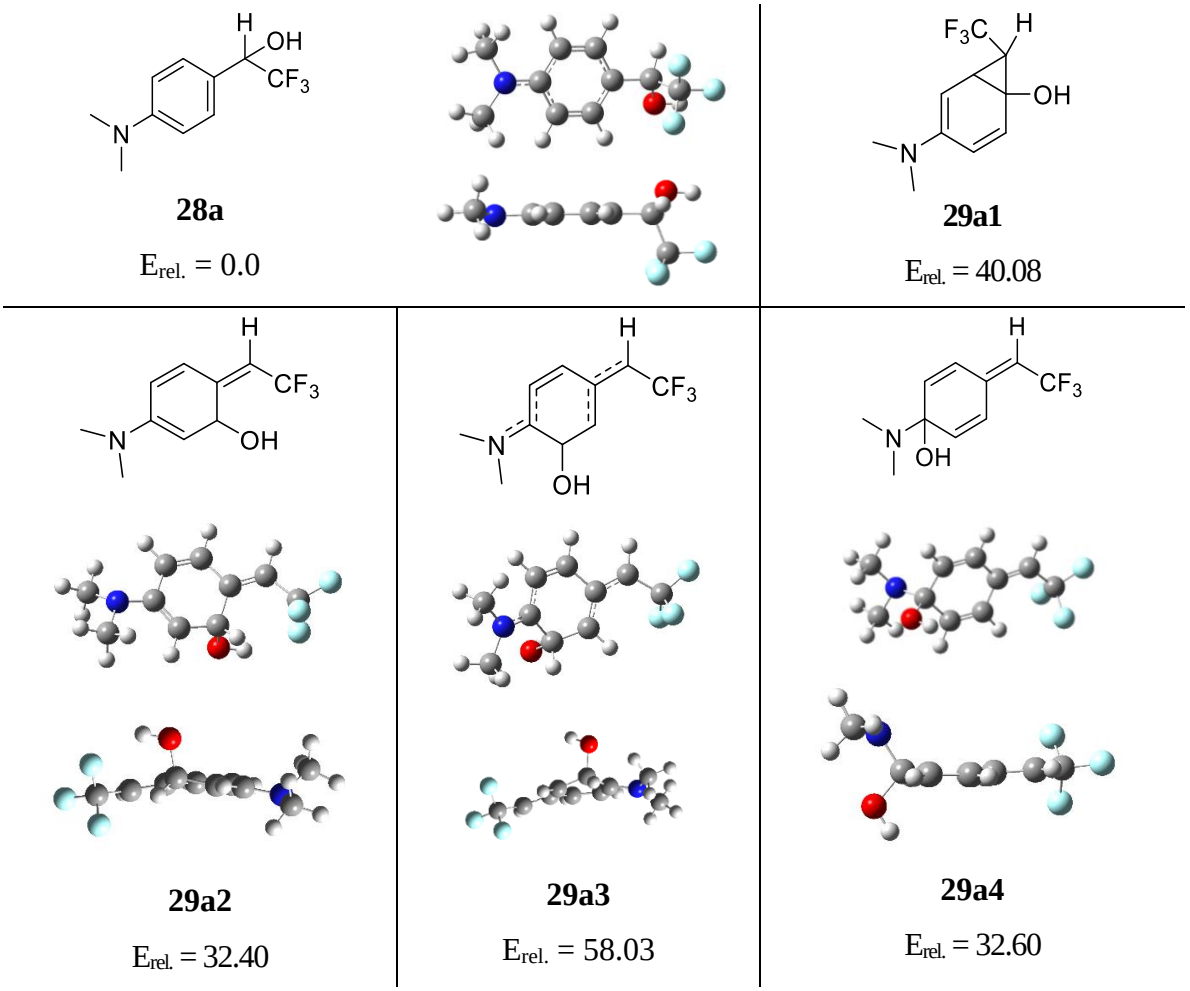

Chart **20:** Calculated structures and relative energies of potential OH insertion products (B3LYP/Def2TZVP). $E_{rel.}$ in kcal mol^{-1}.

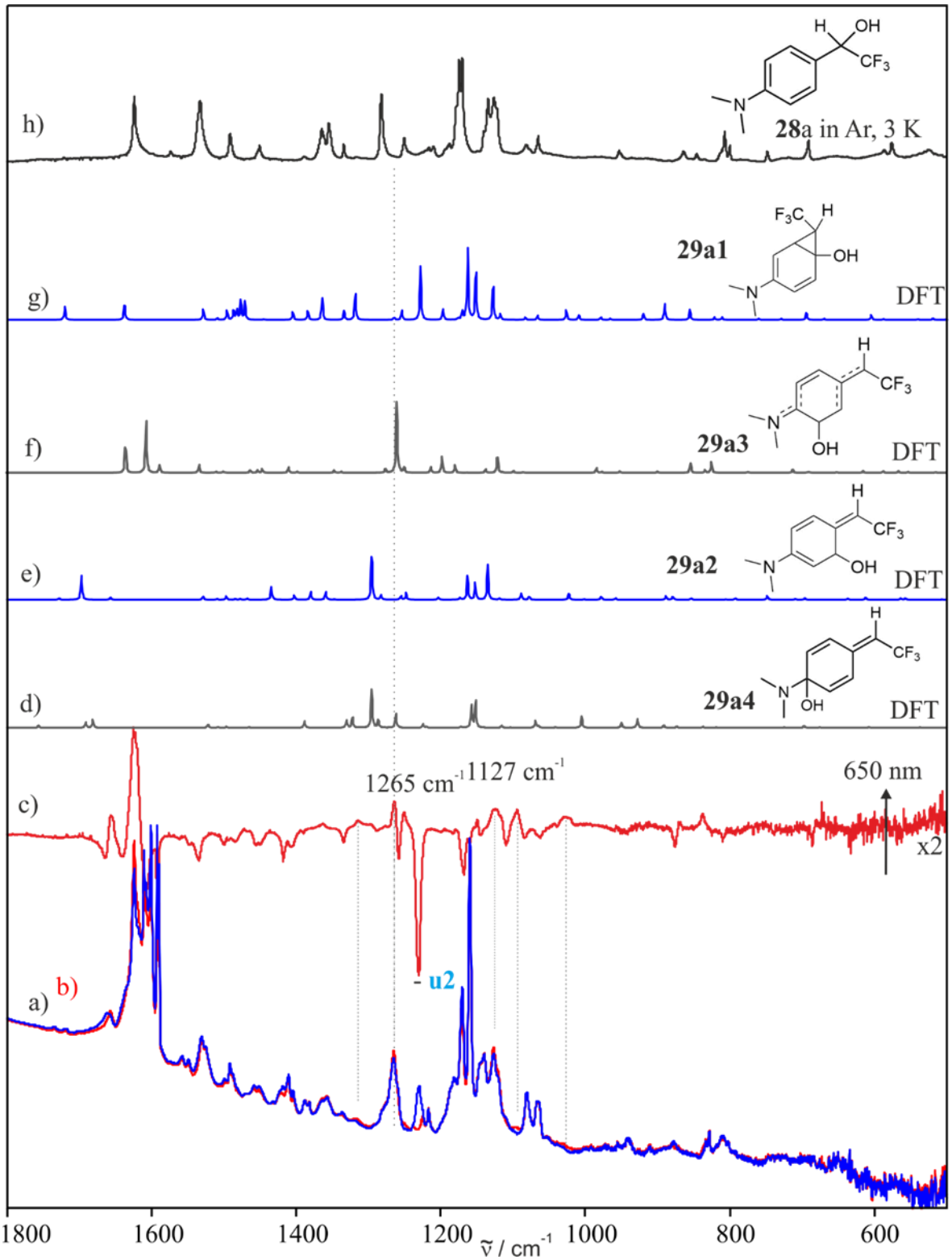

Figure **48:** IR spectra showing the effects 650 nm photolysis of **u2** in an argon matrix doped with 1 % of water at 3 K and calculated spectra of potential OH insertion products. IR spectra obtained a) before and b) after 650 nm photolysis. c) Corresponding IR difference spectrum. Bands pointing upwards increase in intensity and are assigned to **u3**. Bands pointing downwards decrease in intensity and are assigned to **u2**. d) - h) Calculated IR spectra of **29a4**, **29a2**, **29a3**, **29a1** (M06-2x/Def2-TZVP//B3LYP/Def2-TZVP). i) IR spectrum of **28a** in argon at 3 K. ^{x} represents a magnified difference spectrum.

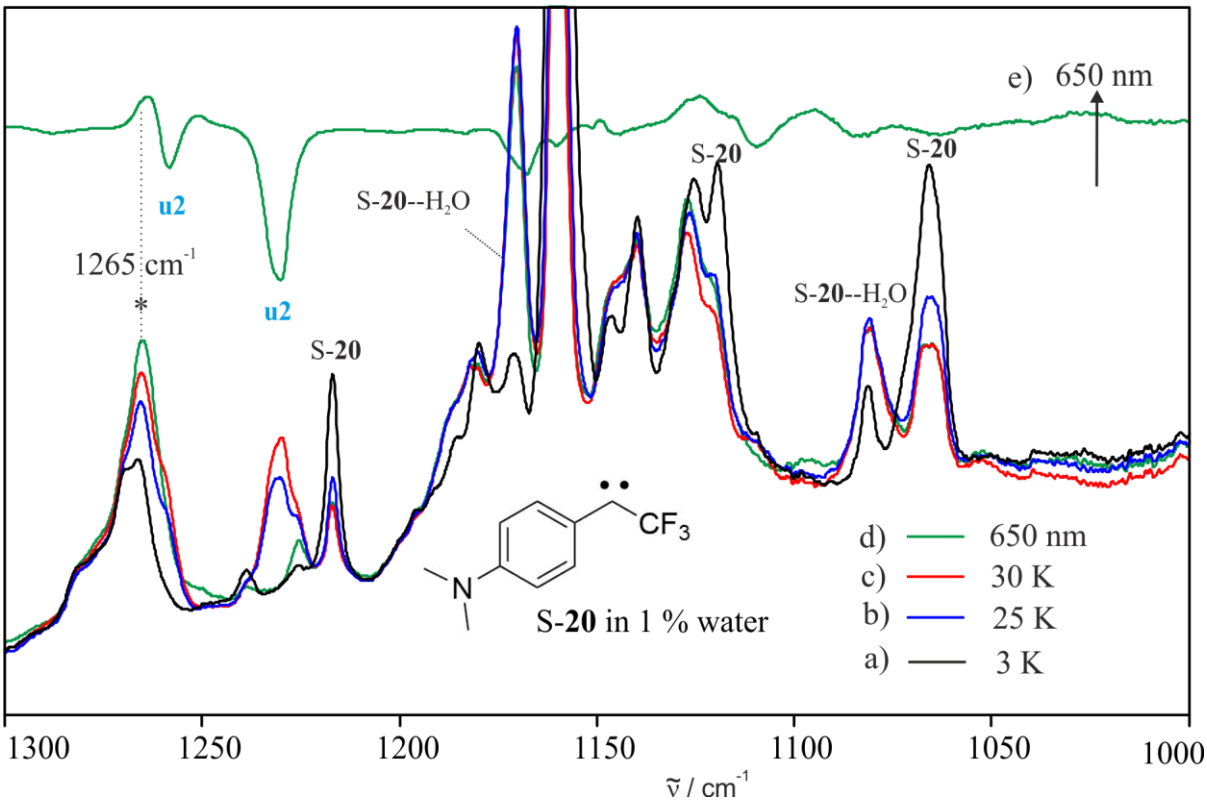

Figure **49:** Increase of the IR signal at 1265 cm^{-1} (**u3**) during annealing and photolysis of S-**20** in 1 % of water. Absolute IR spectra obtained a) after photolysis of **26**, b) after annealing to 25 and c) to 30 K and d) after 650 nm irradiation and e) the corresponding IR difference spectrum. Bands pointing downwards decrease in intensity and are assigned to **u2**. The signal at 1265 cm^{-1} is marked by *. The decreasing signals during annealing are assigned to S-**20**.

As cations are observed to be converted to their corresponding radicals by photoinduced electron capture, a radical formation on irradiation of **22** may also be assumed.[105] Thus, an EPR experiment was conducted analogously. The radical region is showing a slight increase after 650 nm irradiation of **u2** (Figure 50), but since unstructured radical signals are frequently observed during photolysis and no additional signals are observed in the EPR spectrum, it might most likely not be assigned to radical **24**. The calculated IR frequencies (M062x/def2TZVP//B3LYP/def2TZVP) and a calculated UV-vis spectrum of **24** were compared to the experimental spectra (Appendix Figure 88 and Figure 89). The IR signals show a matching, although the intense vibration calculated at 1400 cm^{-1} is not observed in the experimental spectrum. The calculated UV-vis absorptions of **24** instead are not supporting the experimental UV spectrum as after photolysis no absorption above 400 nm can be found. Overall, because of the results of the EPR and UV-vis experiments and because no further reactivity of **u3** was observed a radical species was ruled out.

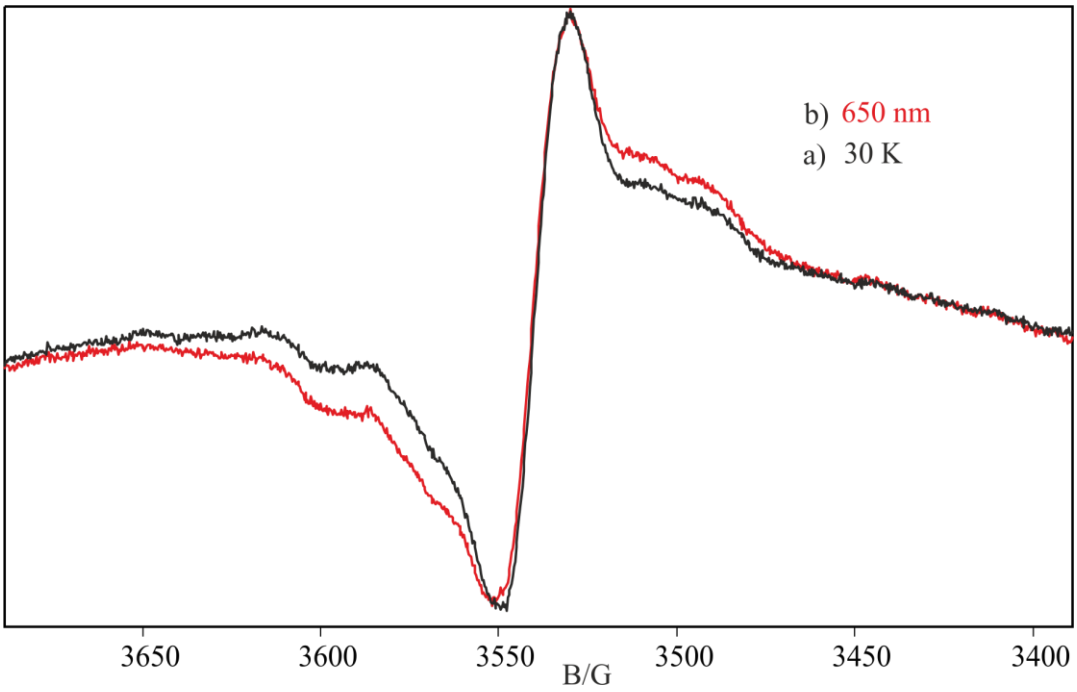

Figure **50:** EPR experiment of S-**20** in a water-doped argon matrix. a) EPR obtained after annealing to 30 K and subsequent cooling down to 3 K. b) EPR signal obtained after subsequent 650 nm photolysis.

Complex S-**20**--H_2O undergoes a different photochemistry compared to **u2** and is stable upon IR irradiation. Instead, the IR signals assigned to S-**20**--H_2O decrease with UV light of 365 nm (Scheme 29). The newly formed IR signals fit well to the IR signals of an independently synthesized and well-characterized sample of insertion product **28a** (Figure 51).

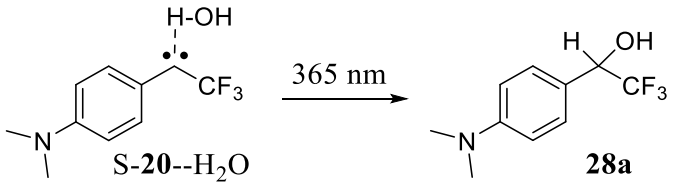

Scheme **29:** Photochemistry of S-**20**--H_2O.

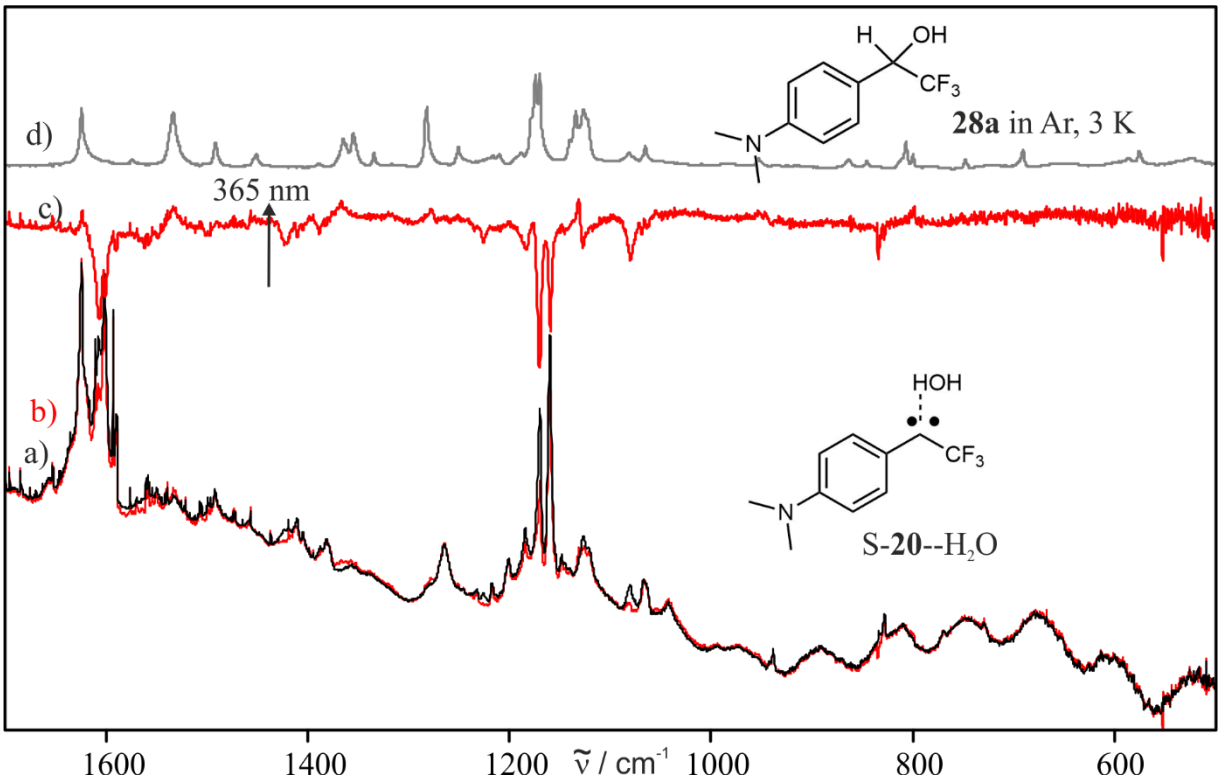

Figure **51:** Photochemistry of S-**20**--H_2O at 3 K. a) IR spectrum obtained after annealing a matrix containing S-**20** and 1 % of water and b) IR spectrum obtained after subsequent 365 nm irradiation. c) IR difference spectrum obtained after 365 nm irradiation. Bands pointing upwards increase in intensity and are assigned to **28a**. Bands pointing downwards decrease in intensity and are assigned to S-**20**--H_2O. d) IR spectrum of **28a** in argon at 3 K.

The secondary photolysis was studied with UV-vis spectroscopy as well. In Figure 52, the UV-vis spectra obtained after photolysis of precursor **26**, after annealing and after subsequent 650 nm irradiation is shown. After 650 nm photolysis the features at 250 and 500 - 650 nm are decreasing and support the observation that cation **22** is converted by 650 nm photolysis to another product. The remaining UV-vis absorptions after 650 nm irradiation at 250 nm and 350 - 400 nm can be assigned to a mixture of S-**20** and S-**20**--H_2O (as observed IR spectroscopically). The feature at 290 nm (marked by *) is increasing after annealing and photolysis and can be assigned to photoproduct **u3**. This is congruent to the coupled IR and UV-vis experiment, which showed that **u3** is already building up during annealing to 30 K and increases upon photolysis. As the IR experiments shows, the usual OH insertion product **28a** is not the photoproduct of **u2** (**22**). But a differentiation based on the UV-vis spectra of OH insertion product **28a** and potential compounds **29a4** and **29a2** is not possible due to their computed similarity (Figure 53). It can be concluded that the UV-vis experiments support the observation of a blue-colored transient species (**u2**) which is generated after annealing of a matrix containing S-**20** and water and decreases upon 650 nm photolysis. The UV-vis experiment suggests that **u2** shows absorptions at 250 nm and 500 - 650 nm. The absorption at

350 - 400 nm can be assigned to S-**20** and S-**20**--H_2O. Another species **u3** shows a signal at 290 nm increasing during annealing to 30 K and further increasing with photolysis.

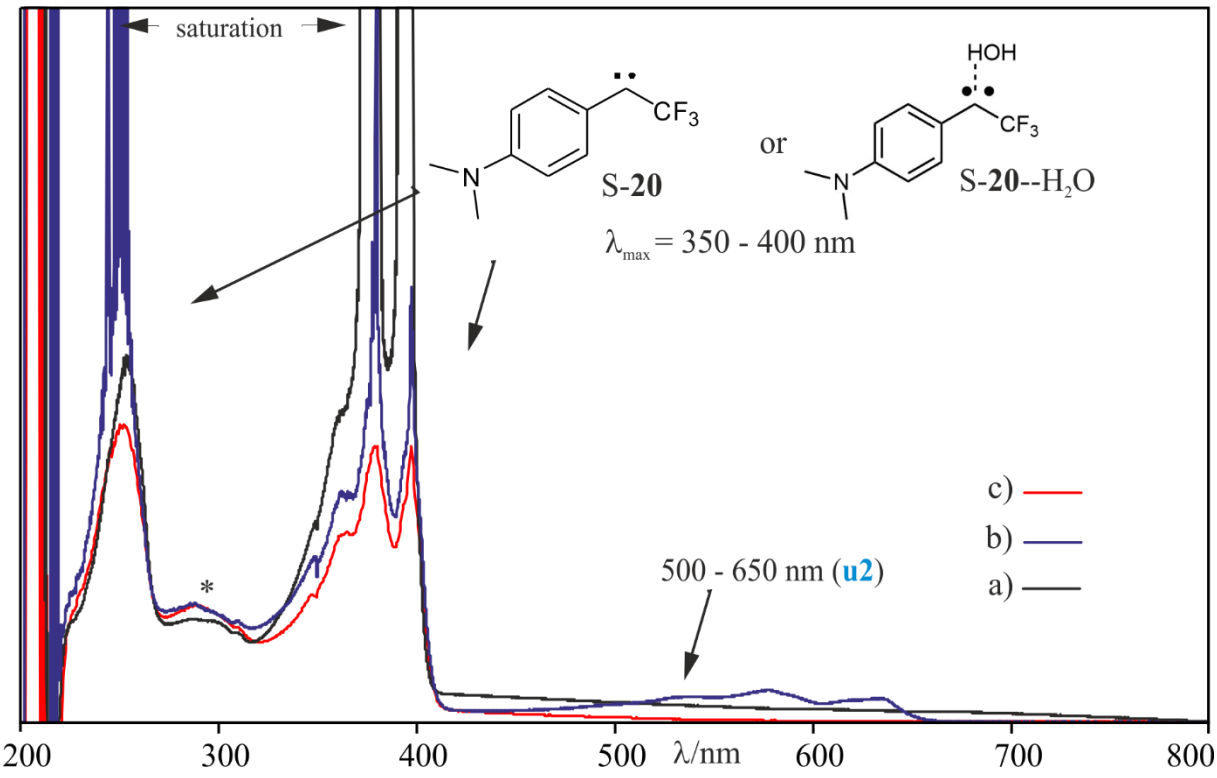

Figure **52:** UV-vis experiment of **26** in argon doped with 1 % water at 8 K before and after secondary photolysis. a) UV-vis spectrum obtained after photolysis of **26**. b) UV-vis spectrum obtained after annealing the same matrix to 30 K and c) after 650 nm irradiation. * Signal at 290 nm.

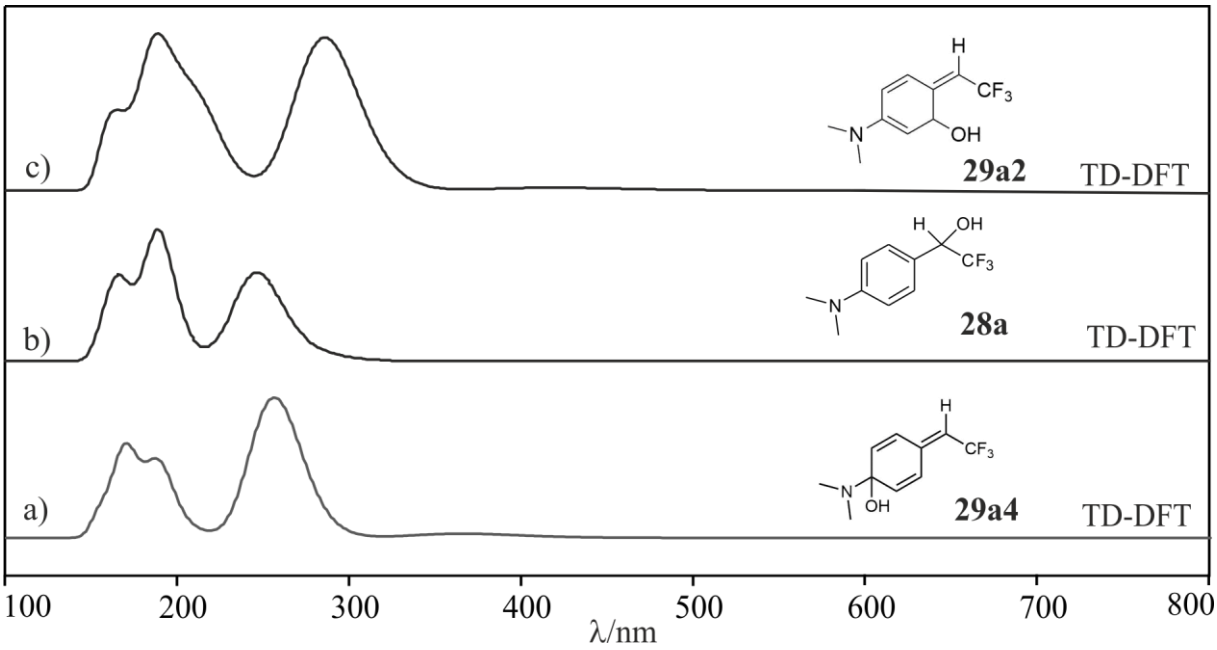

Figure **53**: Calculated UV-vis spectrum of possible photoproducts a) **29a4** b) **28a** and c) **29a2** (TD-B3LYP/Def2-TZVP).

Scheme 30 summarizes the results so far: The IR experiments in 1 % water-doped argon matrices show the presence of two species generated during annealing. According to EPR experiments, all species including **u1,** **u2** and **u3** have a singlet ground-state. With the help of IR and UV-vis spectroscopy combined with DFT calculations, **u1** is assigned to singlet complex S-**20**--H_2O. S-**20**--H_2O is build out of S-**20** and H_2O mostly at temperatures up to 20 K. With UV photolysis, S-**20**--H_2O is converted to OH insertion product **28a.** The blue colored species **u2** is formed out of S-**20** and H_2O as well and increases continuously during annealing above 20 K. Upon photolysis with 650 nm light, **u2** is converted to photoproduct **u3**. **u2** and its photoproduct **u3** could not be assigned with certainty so far. IR, UV-vis, and EPR spectroscopy in combination with DFT calculations and observations from literature[110, 120] suggest that **u2** is cation **22** and **u3** the quinoid OH insertion product **29a4**. Alcohol **294a2** is another possible assignment to **u3**. In the following, experiments such as 3 % of H_2O doping, MeOH and D_2O doping should elucidate the reaction further.

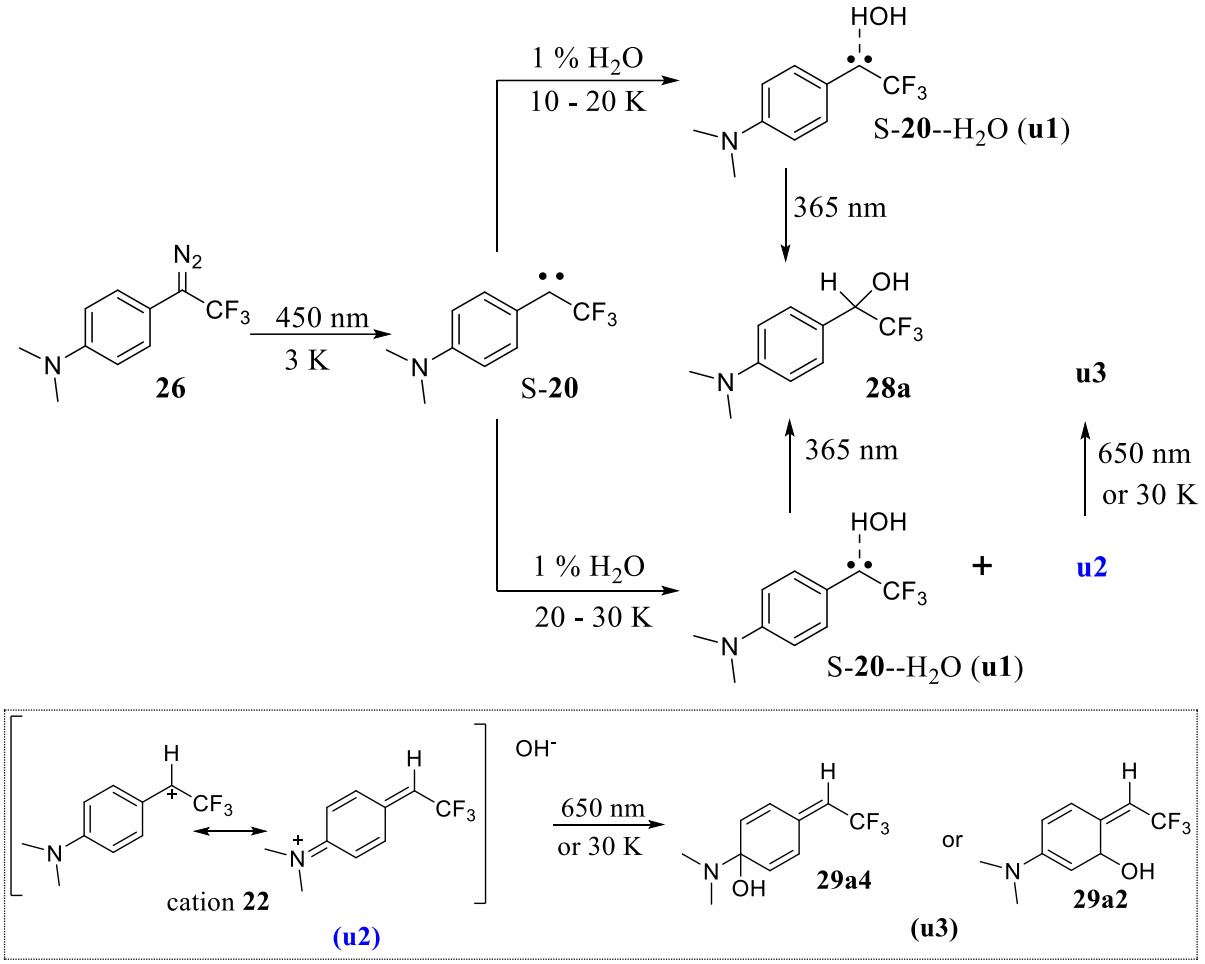

Scheme **30:** The observed reaction of S-**20** in an argon matrix doped with 1 % of water. The assignment of the blue colored species **u2** and its photoproduct **u3** are still preliminary. A possible assignment and reactivity of **u2** and **u3** is shown at the bottom part.

3 % of H_2O

An increase of the amount of H_2O could have different effects on the reactivity of **20**. With an increased amount of water the carbene is statistically not surrounded by one molecule of H_2O (like approximately in 1 %) anymore, but by several, which can lead to aggregation of the dopant and may change its chemical behavior.[121] The experiment in argon matrices doped with 3 % of H_2O was conducted analogously to the experiment in 1 % of H_2O. After annealing a matrix containing S-**20** and 3 % of H_2O, the color changes to blue, as observed with 1 % of H_2O. The IR spectra obtained after photolysis of **26**, annealing to 30 K, and secondary photolysis are shown in Figure 54. The IR spectra show congruency to the experiments in 1 % of H_2O: photolysis of **26** results in IR signals assigned to carbene S-**20** and **u3**, with annealing of the matrix, **u2** and S-**20**--H_2O are formed. **u2** is converted to **u3** by secondary 650 nm photolysis. Increasing the amount of H_2O does therefore not result in a different reactivity of S-**20**. But Figure 55 shows that after 450 nm photolysis, **u3** (IR signal at 1265 and 1127 cm^{-1}) and **28a** (IR signal at 1170 cm^{-1}) are produced in a higher yield relative to S-**20** than in the experiment with 1 % of H_2O. Regarding the IR experiments it can be concluded, that increasing the amount of water leads to a higher amount of **u3** and **28a** directly after photolysis of **26**. This may be explained by a direct insertion of OH occurring if more than one molecule of water surrounding the carbene or by close contact of the molecules.

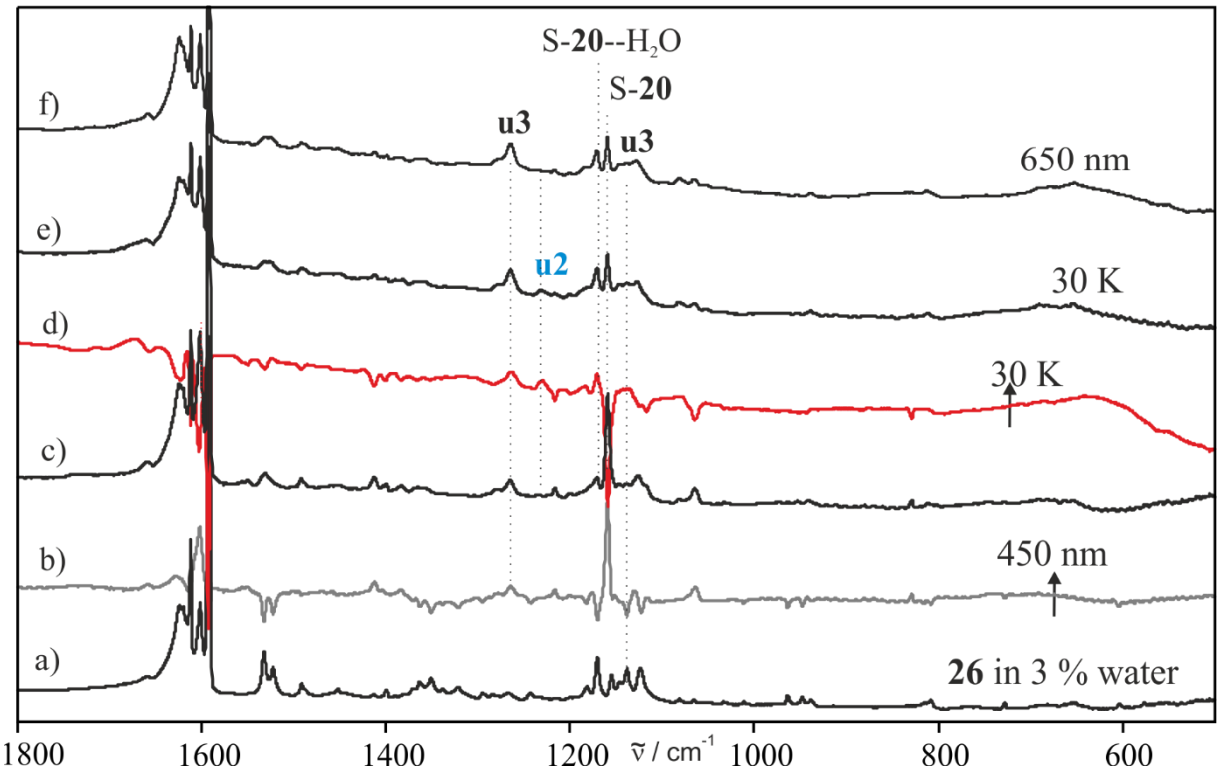

Figure **54:** IR spectra obtained for **26** in an argon matrix doped with 3 % of water. a) IR spectrum obtained after deposition of **26** b) IR difference spectrum obtained after photolysis of **26**. Bands pointing upwards increase in intensity. Bands pointing downwards decrease in intensity. c) The corresponding absolute IR spectrum. d) IR difference spectrum obtained after annealing to 30 K and cooling back to 3 K. e) The corresponding absolute IR spectrum. f) IR spectrum obtained after subsequent 650 nm photolysis.

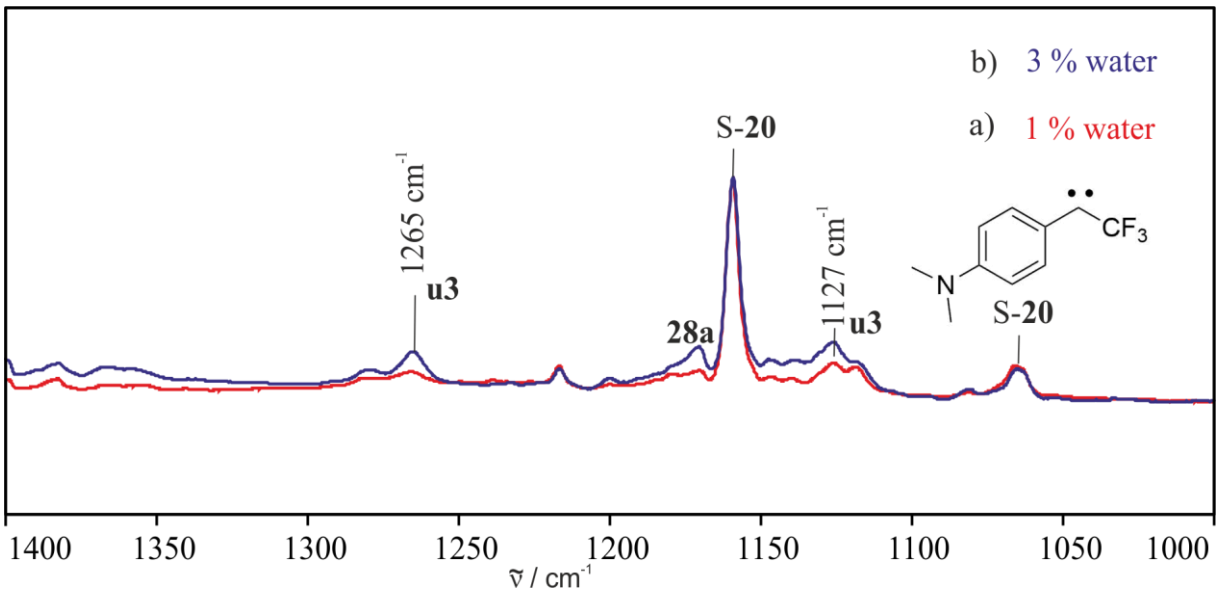

Figure **55:** Comparison of the IR spectra with a) 1 % and b) 3 % of water doping. Both IR spectra are obtained after 450 nm photolysis of **26** at 3 K and are relative to carbene S-**20**.

1 % MeOH

To investigate if carbene S-**20** is showing a similar reactivity towards the weaker Lewis acid methanol and forms a hydrogen-bonded complex accompanied by a protonation of S-**20** to form cation **22**, an experiment in an argon matrix doped with MeOH was performed analogously to the H_2O-doped experiment. Thus, precursor **26** was deposited with 1 % MeOH-doped argon on a CsI window at 3 K and irradiated with 450 nm light. Subsequent annealing enables the diffusion of small molecules. Like in the water case, the matrix window turns from colorless to blue during annealing to 30 K. The IR spectra obtained before and after annealing of the water- and the methanol-doped matrices are shown in Figure 56. Except for the signals assigned to water or methanol, there are not many obvious differences in the IR spectra. Likewise, the IR absorption of **u2** at 1231 cm^{-1} (marked by dashed line in Figure 56) seems very similar in H_2O and MeOH. This is in line with the assumption that cation **22** is generated out of S-**20** and MeOH or H_2O during annealing. The calculated frequencies of complex S-**20**--H_2O and the complex S-**20**--MeOH are shown in Figure 57, together with the IR difference spectra obtained after annealing of the argon matrix containing S-**20** and 1 % of H_2O and 1 % of MeOH, respectively. The calculated IR frequencies of both complexes S-**20**--H_2O and S-**20**--MeOH show very similar IR vibrations, differing just slightly in the area between 1100 and 700 cm^{-1}. This is consistent with the very similar IR spectra obtained after annealing with MeOH and H_2O doping.

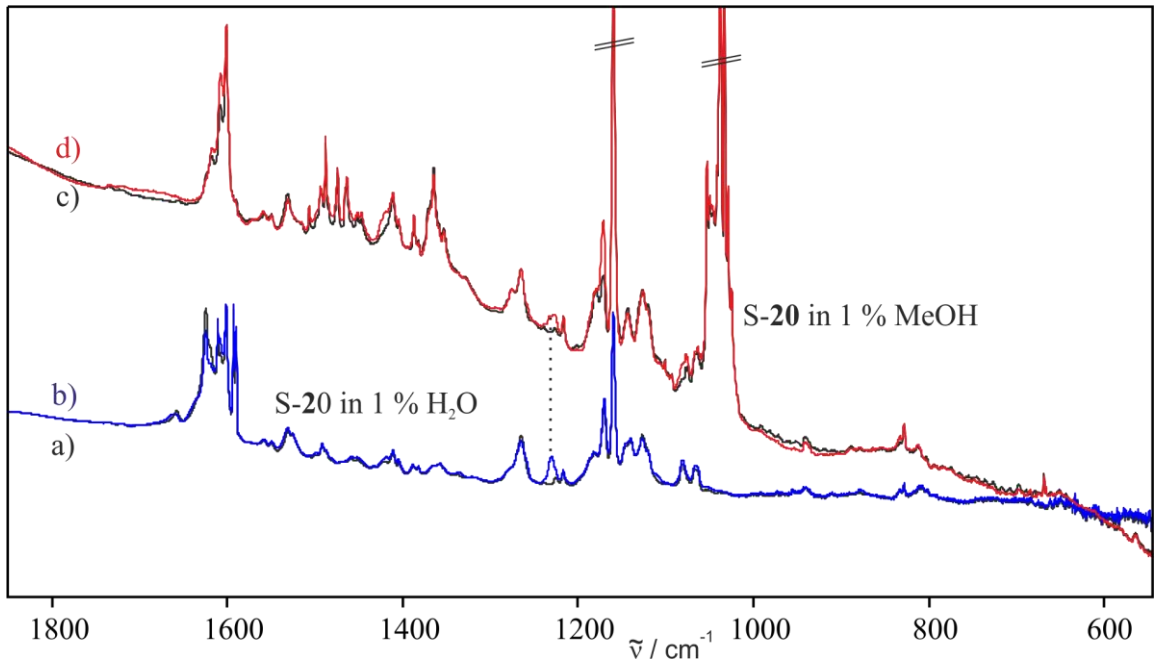

Figure **56:** Comparison of the experiment in H_2O- to MeOH-doped matrices. IR spectra obtained after annealing of an argon matrix doped with 1 % of water containing S-**20** to the experiment with a 1 % of MeOH-doped matrix. The IR spectra a) and c) are obtained after photolysis of **26** in H_2O and MeOH, respectively, b) and d) after annealing to 30 K in H_2O and MeOH, respectively.

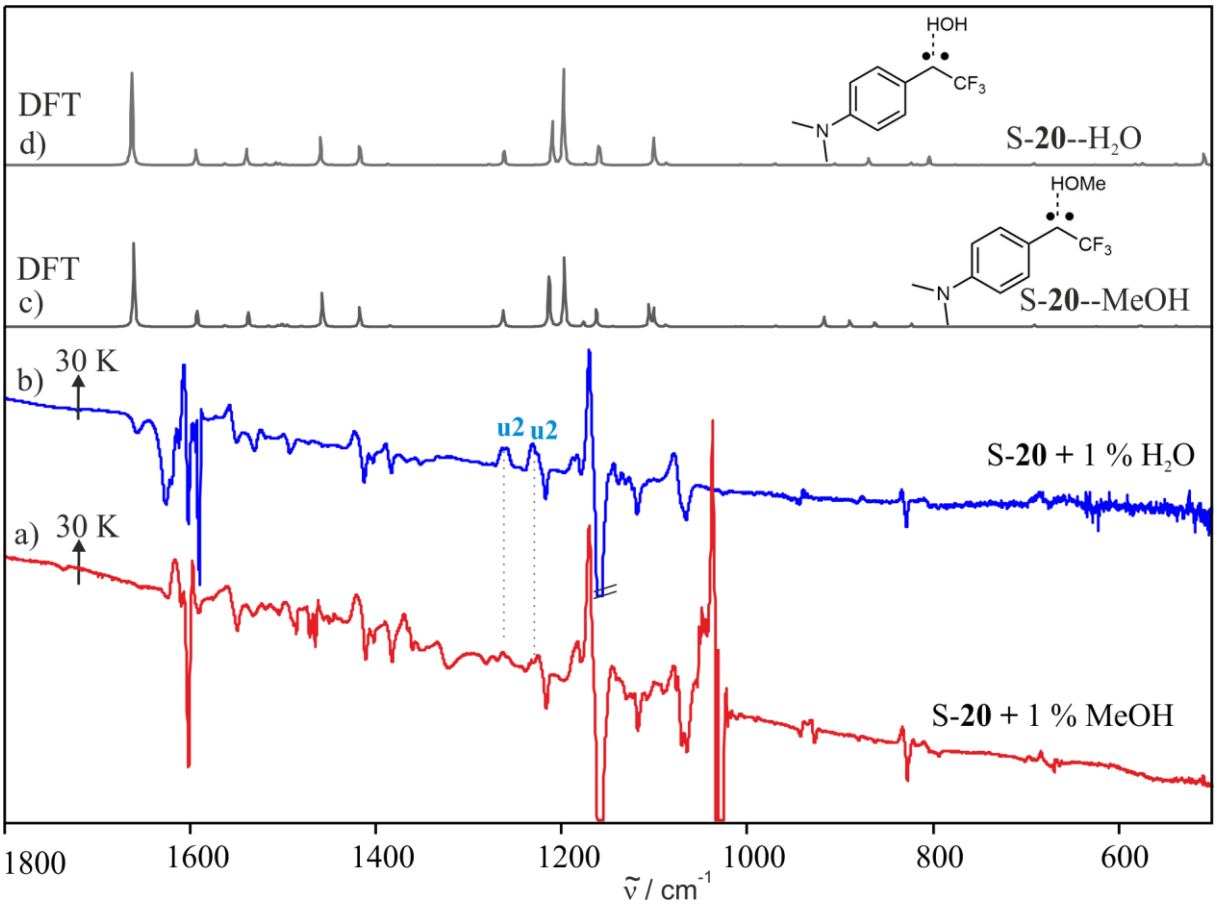

Figure **57:** IR difference spectra obtained after annealing in experiments in argon matrices doped with a) methanol and b) water. Bands pointing upwards increase in intensity. Bands pointing downwards decrease in intensity and are assigned to S-**20** and methanol or water, respectively. c) and d) calculated spectra of S-**20**--MeOH and S-**20**--H_2O (M06-2x/Def2-TZVP//B3LYP/Def2-TZVP).

Interestingly, photolysis with 650 nm light shows differences for H_2O- and MeOH-doped matrices. Whereas in H_2O- and MeOH-doped argon matrices the signals assigned to **u2** are decreasing with 650 nm light, with methanol, additional signals assigned to complex S-**20**--MeOH are decreasing with 650 nm irradiation as well (Figure 58). This indicates that S-**20**--H_2O is stable upon 650 nm photolysis, whereas the methanol complex S-**20**--MeOH is photolabile. The formed product on 650 nm irradiation of S-**20**--MeOH is fitting nicely to the calculated IR spectrum of **28b**. The weak signals of photoproduct **u3b**, which is generated out of **22** (**u2**) could not be assigned due to the weak signal intensities and overlapping's.

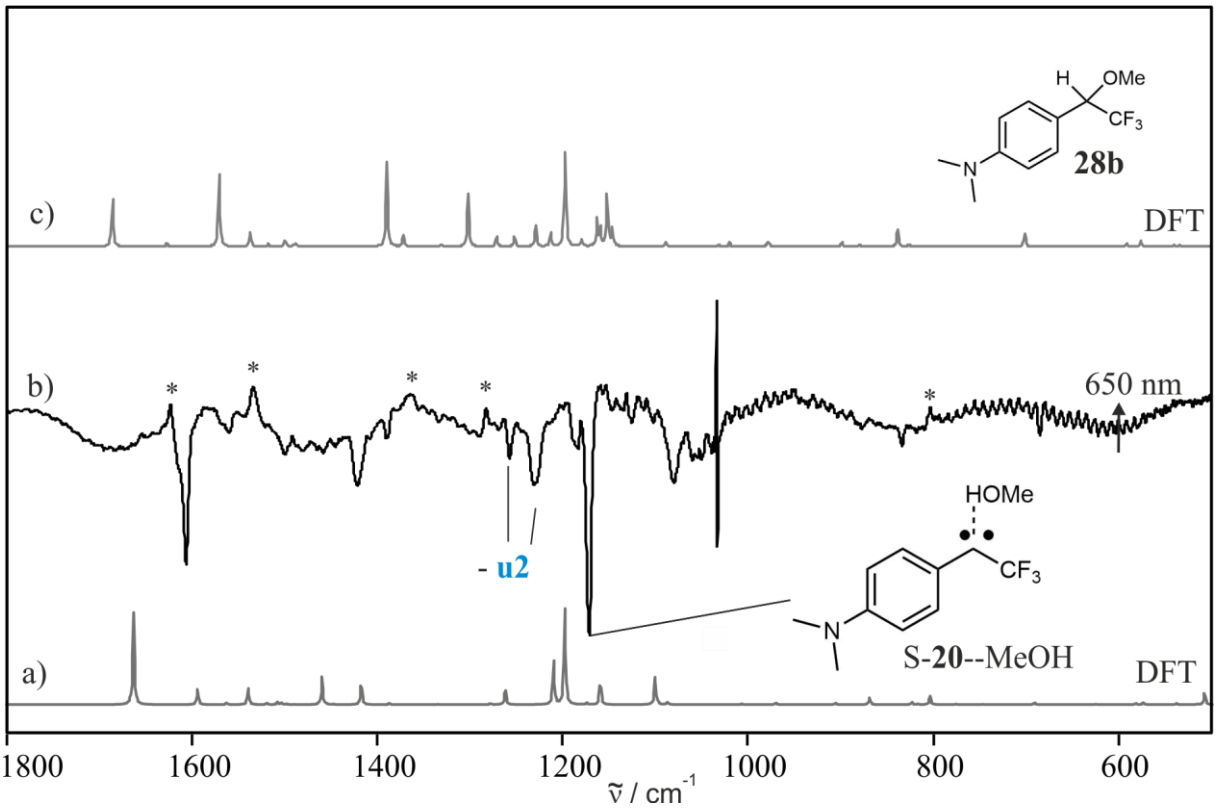

Figure **58:** a) Calculated IR spectrum of S-**20**--MeOH and b) IR difference spectrum obtained after photolysis in an argon matrix doped with 1 % methanol at 3 K. Bands pointing upwards increase in intensity. Bands pointing downwards decrease in intensity and were assigned to S-**20**--MeOH and **u2**. Calculated IR spectra of c) **28b** (M06-2x/Def2-TZVP//B3LYP/Def2-TZVP). * Signals preliminarily assigned to **28b**.

The UV-vis experiments of **26** in argon matrices doped with 1 % of MeOH was conducted analogously to the IR experiments. In Figure 59 the UV-vis spectrum obtained before and after tempering the matrix containing S-**20** and methanol is shown. The feature around 500 and 650 nm is comparable to the water case, suggesting a similar product like cationic species **22**. The results of subsequent photolysis are presented in this Figure as well. Again, the effect is identical to the H_2O experiments and shows the depletion of the 500 - 650 nm feature. In both cases, a growing distinct signal at 290 nm is observed. Based on TD-DFT calculations, this signal can be traced back to both products of secondary photolysis **28b** and **29b4** (Figure 60).

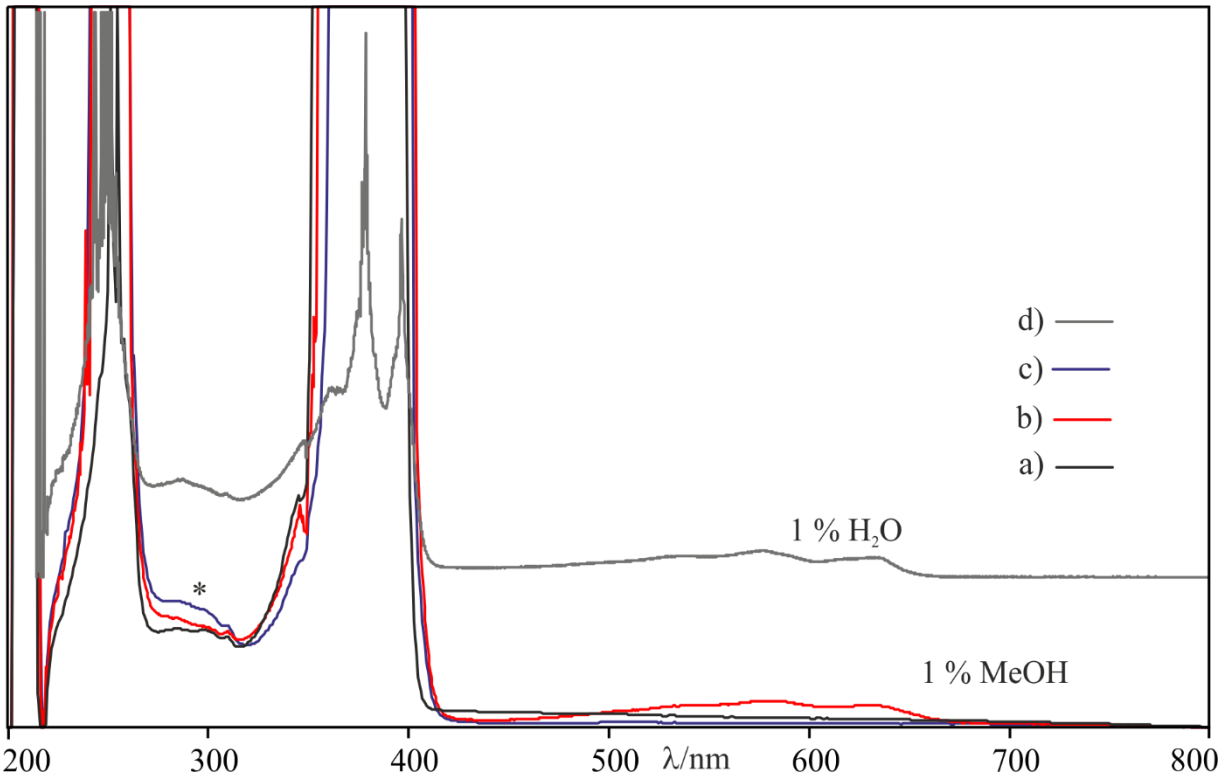

Figure **59:** UV-vis spectra obtained in a 1 % methanol-doped argon matrix containing **26** a) after irradiation of **26** (450 nm, 8 K), b) after annealing to 30 K and c) after 650 nm photolysis. d) UV-vis spectrum obtained after annealing S-**20** to 30 K in a 1 % of water-doped argon matrix. * Signal at 290 nm.

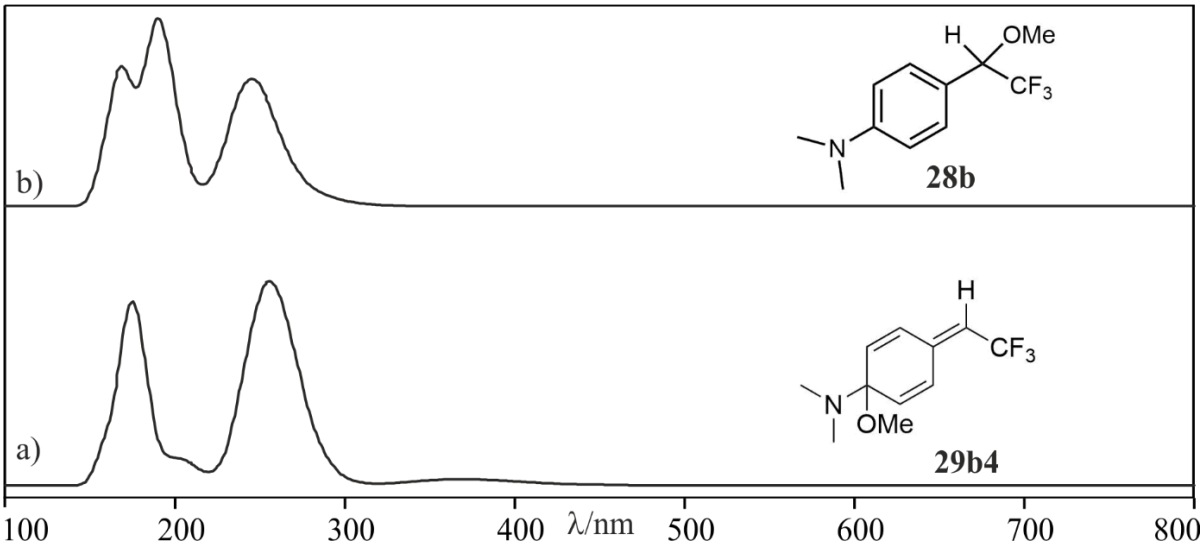

Figure **60:** Calculated TD-DFT UV-vis spectra of a) **28b** and b) **29b** (B3LYP/Def2-TZVP).

Concluding this Chapter, the experiments in MeOH-doped matrices show many similarities to the experiments with H_2O-doping. Annealing of the matrix containing S-**20** and methanol leads to the formation of hydrogen-bonded complex S-**20**--MeOH and a blue colored species **u2** (cation **22**). The UV-vis and IR signals of **u2** are comparable to the ones in the water experiments. This underlines the idea of protonation of S-**20** by methanol and water because in

both cases the same cation **22** would be generated. Like in the water experiments a second species, complex S-**20**--MeOH, is formed during annealing. The IR and UV-vis signals of S-**20**--MeOH are very similar to S-**20**--H_2O, but secondary photolysis of S-**20**--MeOH differs by showing photo-lability to IR light, whereas S-**20**--H_2O shows higher stability and decreases only with UV light. No further information about photoproduct **u3b** were obtained.

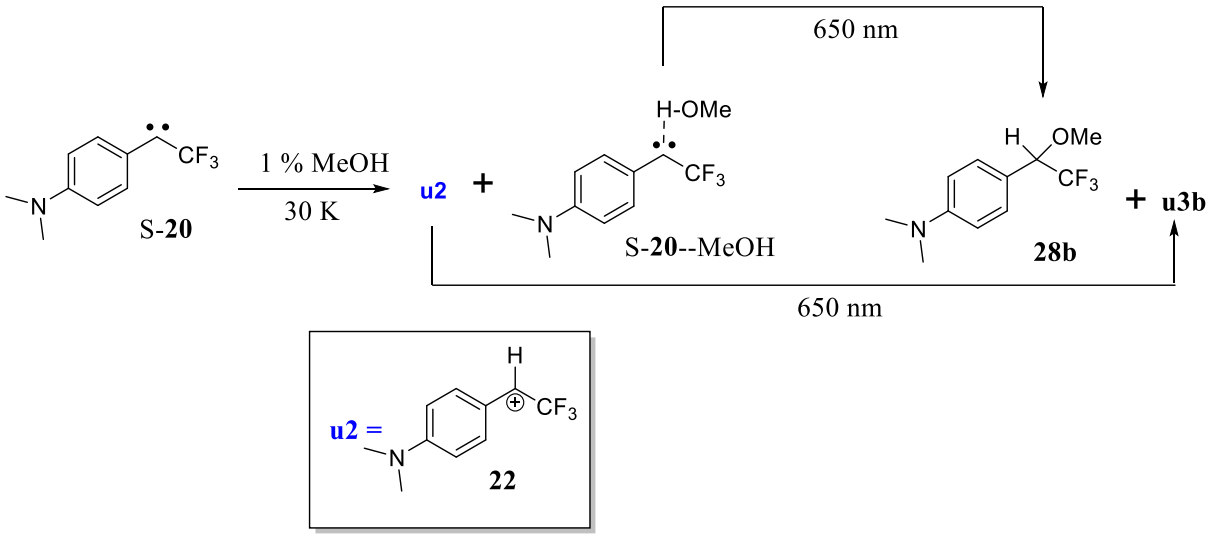

Scheme **31:** Observed reaction of S-**20** in methanol-doped argon matrices. The presumed structures for **u2** is depicted.

1 % of D_2O

To gain more information about the "unassigned" species **u2** and its photoproduct **u3**, the analog experiments in argon with 1 % of D_2O were performed. A protonation at the former carbene carbon to form **22** should show characteristic shifts of the corresponding IR vibrations if the H_2O is exchanged for D_2O.

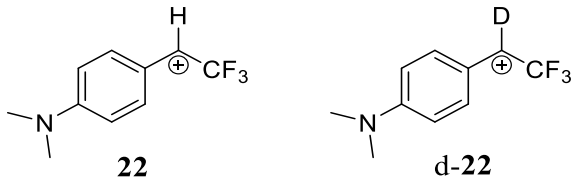

Chart **21:** Structures of cation **22** and deuterated cation d-**22**.

Diazo compound **26** was deposited with 1 % D_2O-doped argon on a cold matrix window, irradiated with 450 nm light and annealed to enable diffusion and interaction of the molecules. Like in water-doped matrices, the color of the matrix changes to blue during annealing. The obtained IR difference spectrum after annealing is shown in Figure 61.There is some amount of water present, hence, for comparison, the experiment in H_2O is depicted as well. The signals assigned to carbene S-**20** and D_2O are decreasing and new signals appear. Some new signals can be assigned to **u2**, but the signal at 1246.7 cm^{-1} cannot be found in the water experiment.

Due to the loss of this signal after 650 nm photolysis, it may be assigned to d-**u2**. The calculated IR vibrations S-**20**--D_2O and S-**20**--H_2O show that the complex is almost not influenced by deuteration (Figure 62), in contrast, the deuteration of cation d-**22** differs from that in the computed IR frequencies compared to **22**. Most shifts are found around 1350 - 1200 cm^{-1} including the vibrations assigned to C–C–C stretching and C–F scissoring, which are most influenced by deuteration. For **22** two medium-sized signals are calculated at 1313 cm^{-1} (C–F scissoring) and 1279 cm^{-1} (C–C–C stretching vibration). For d-**22** one intense vibration is computed between those signals at 1294 cm^{-1} (C–C–C stretching vibration) (Figure 62). The experimentally obtained signals assigned to **22** are at 1258 and 1231 cm^{-1}. The experimentally obtained IR signal in the deuterium experiment at 1246 cm^{-1} (Figure 61) increasing after annealing and decreasing with 650 nm lies in between the two signals of **u2** and may be assigned to the calculated intense C–C–C stretching vibration of d-**22** at 1294 cm^{-1}. In the non-deuterated experiment, the obtained IR signals increasing after annealing and decreasing with 650 nm are at 1258 and 1213 cm^{-1}. Overall, those findings are in line with species **u1** being singlet complex S-**20**--H_2O and species **u2** being cation **22**.

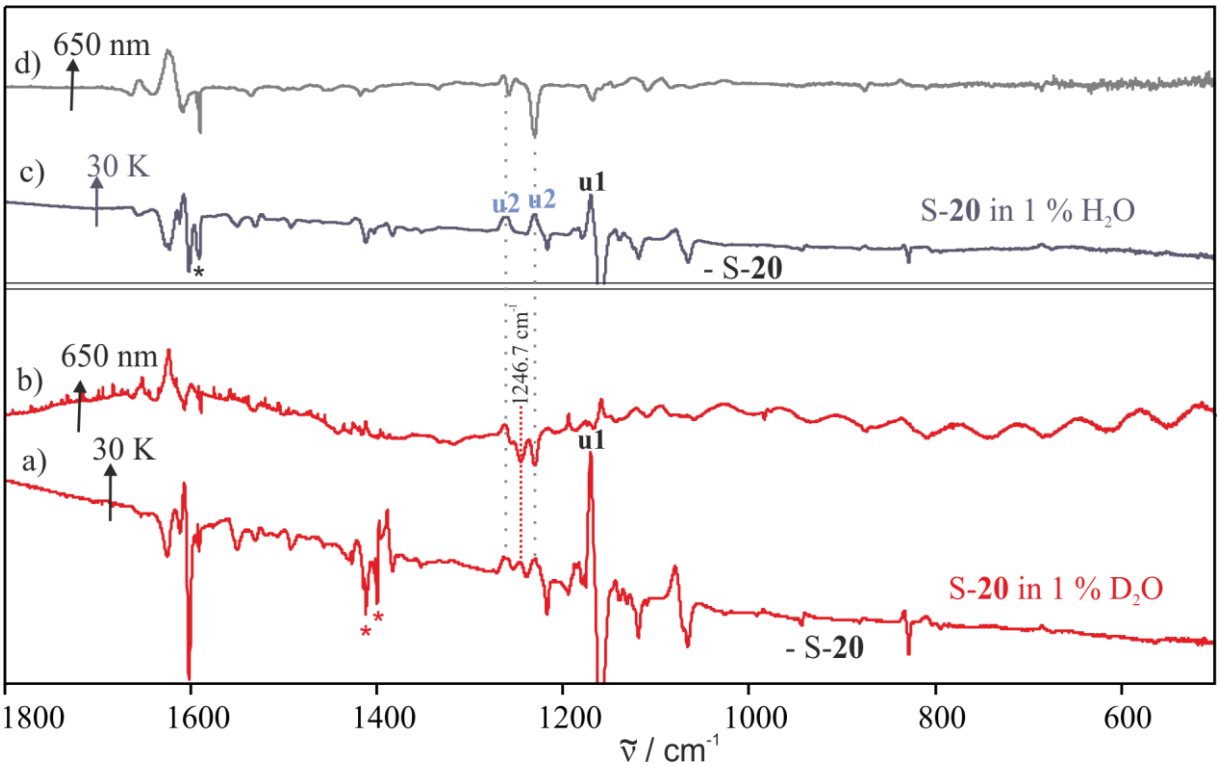

Figure **61**: IR difference spectra obtained after annealing argon matrices containing 1 % of H_2O and 1 % of D_2O, respectively. IR difference spectra obtained after tempering from 3 to 25 K/30 K and cooling back and after 650 nm irradiation for a), b) D_2O and c) d) H_2O. Bands pointing upwards increase in intensity. Bands pointing downwards decrease in intensity. IR signals assigned to * D_2O and * H_2O.

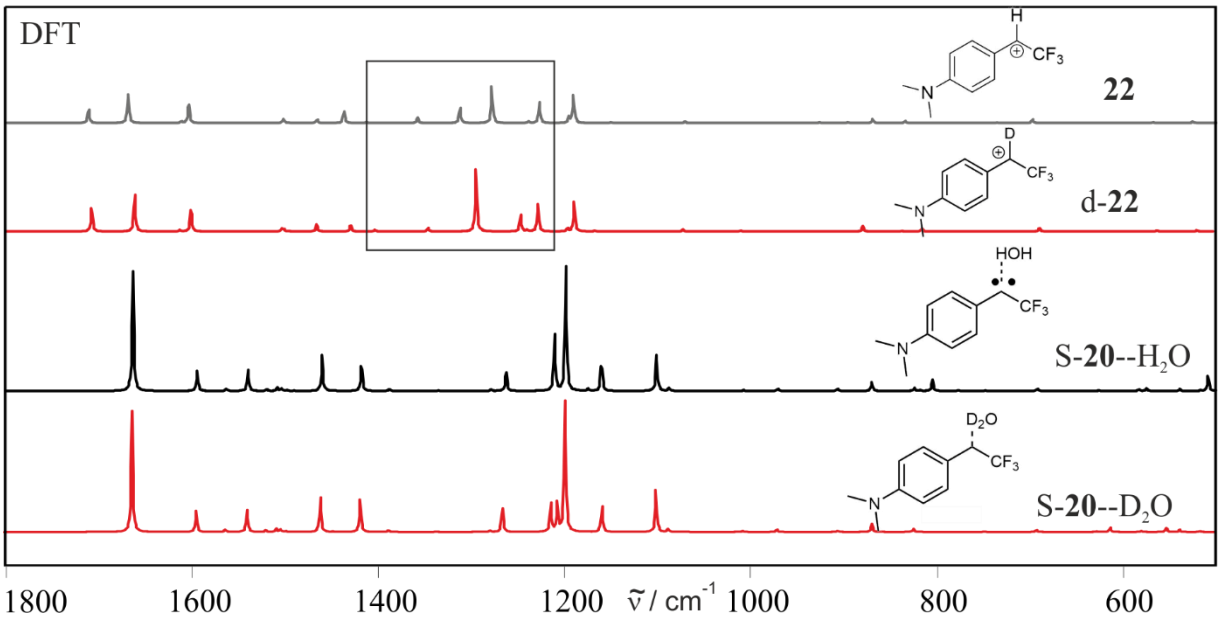

Figure **62:** Calculated spectra of a) S-**20**--D_2O and b) S-**20**--H_2O, as well as deuterated cation c) d-**22** and d) **22** (M06-2x/Def2-TZVP//B3LYP/Def2-TZVP).

The photolysis of **u2** was investigated in more detail and the IR spectra of the corresponding photoproducts **u3** and d-**u3** (potentially **29a4** and d-**29a4** or d-**29a2**, Chart 22) are compared to each other. Calculations suggest that they are different in their IR spectra (Figure 63).

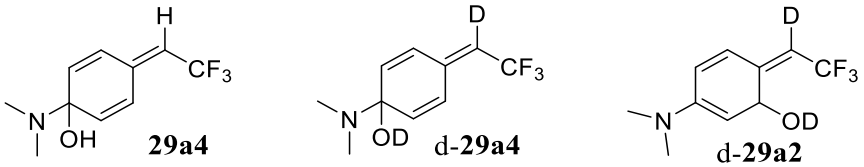

Chart **22:** Structures of hemiaminal **29a4**, deuterated d-**29a4** and d-**29a2**.

In Figure 63 the computed IR spectra of **29a4**, d-**29a4** and d-**29a2** are compared to the IR difference spectra obtained after photolysis in water- and heavy-water-doped matrices, respectively. Those two IR spectra show differences in the signals which are decreasing, as well as in the signals which are increasing. This indicates that deuteration affects **u2** as well as **u3**. The intense signals increasing in the difference spectrum in the D_2O experiment at 1264, 1195, and 1160 cm^{-1} were not observed the water experiment. Thus, these signals were compared to the calculated IR spectra of d-**29a4** and d-**29a2**. Whereas the calculated vibrations of d-**29a4** fit reasonably well to the newly formed peaks, the vibrations of d-**29a2** are matching poorly regarding the intensities and an experimentally not observed vibration calculated at 1407 cm^{-1}. The most intense vibrations of d-**29a4** are calculated to be the C–C–C symmetric stretching at 1294 cm^{-1} and the antisymmetric stretching of C–F at 1152 cm^{-1}.

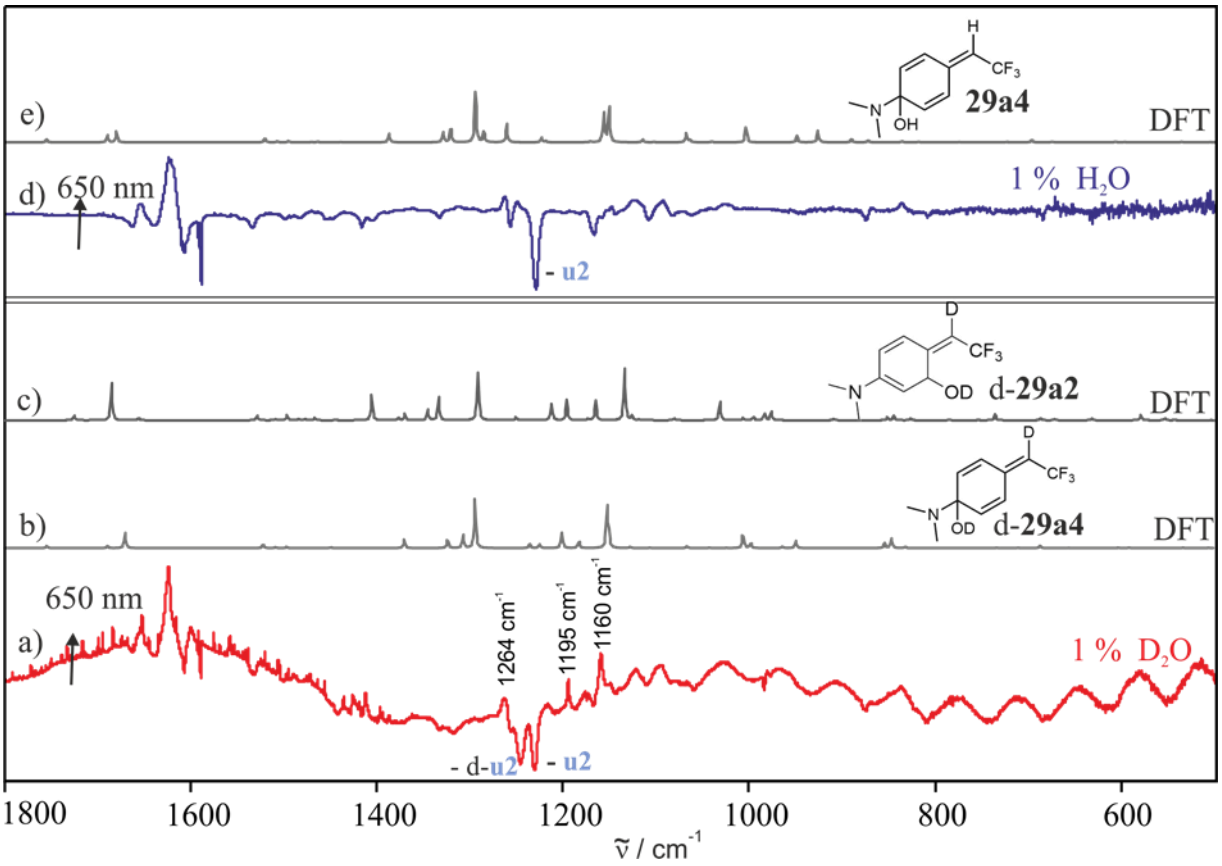

Figure **63:** Comparison of the photolysis in 1 % of H_2O to 1 % of D_2O at 3 K. (bottom) D_2O experiment: a) IR difference obtained after 650 nm irradiation. Bands pointing upwards increase in intensity. Bands pointing downwards decrease in intensity. The decreasing signals were assigned to **u2** and d-**u2**, the increasing to **u3** and d-**u3**. The calculated spectra of b) d-**29a4** and c) d-**29a2** (M06-2x/Def2TZVP//B3LYP/Def2-TZVP). H_2O experiment: d) IR difference obtained after 650 nm irradiation. The decreasing signals were assigned to **u2**, the increasing to **u3**. e) Calculated spectrum of **29a4** (M06-2x/Def2-TZVP//B3LYP/Def2-TZVP).

Concluding the experiments of S-**20** in D_2O-doped matrices, the substitution of water with heavy water results in expected shifts of some characteristic IR vibrations for the protonation of S-**20**. This supports the analysis that during annealing carbene S-**20** abstracts hydrogen (deuterium) from water (deuterated water) to form cation **22** (d-**22**). Upon photolysis of **22** (d-**22**), **u3** (d-**u3**) is generated. **u3** (d-**u3**) could not be assigned with certainty, but quinoid compound **29a4** (d-**29a4**) is the most likely possibility.

2.4.2.3. DFT calculations

To study the reaction computationally the intrinsic reaction pathway (IRC) of the rearrangement S-**20**--H_2O to **28a** was computed at B3LYP/Def2-TZVP level of theory and shows a concerted reaction with a transition state lying 8.6 kcal mol^{-1} above the complex S-**20**--H_2O (Figure 64). This activation barrier has to be overcome to build insertion product **28a**. The reaction is highly exothermic with -64.6 kcal mol^{-1}.

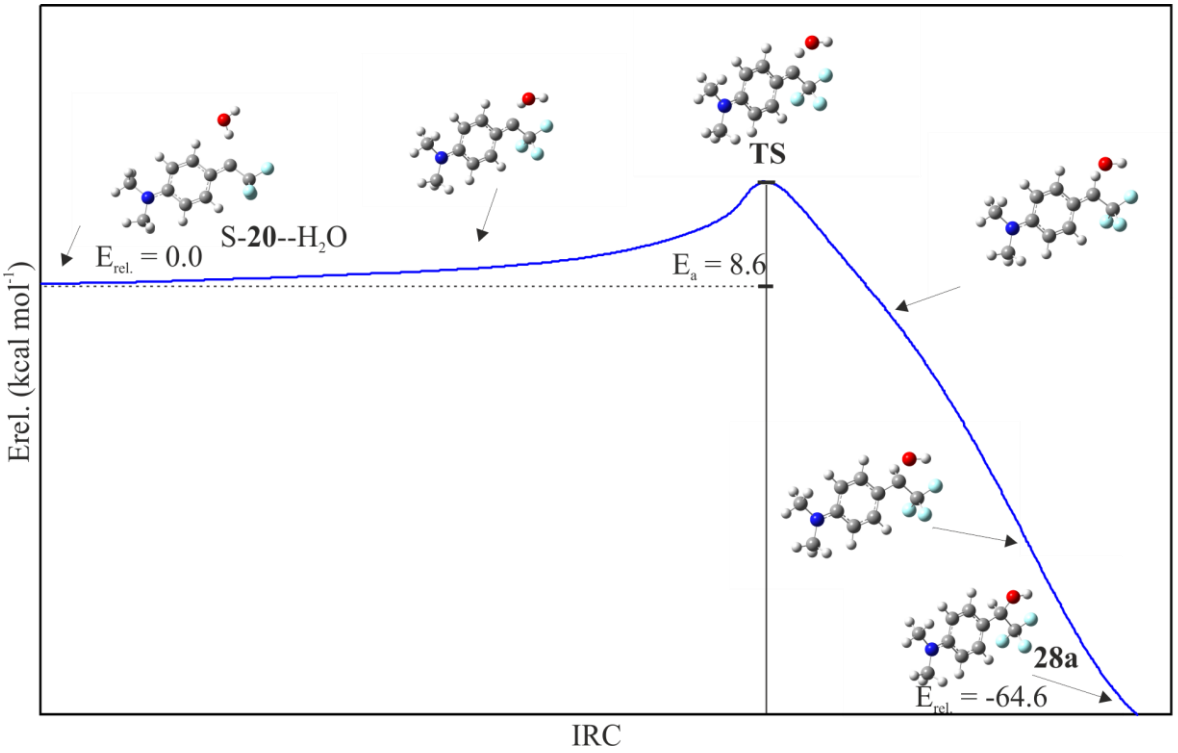

Figure **64:** IRC of the rearrangement of complex S-**20**--H_2O to **28a** calculated at B3LYP/Def2-TZVP level of theory. Energies in kcal mol^{-1}. The activation barrier was calculated with separate structures at the BLYP-D3/Def2-TZVP level of theory.

The IRC of the conversion of S-**20**--MeOH to **28b** is computed at the B3LYP/Def2-TZVP level of theory as well (Figure 65). The reaction is computed to be concerted, as expected from the experiments in argon matrices, and highly exothermic. The activation barrier is with 5.9 kcal mol^{-1} relative to S-**20**--MeOH lower than in the rearrangement S-**20**--H_2O to **28a**. This finding corroborates the experimental results which showed that the conversion of S-**20**--H_2O to **28a** needed higher energetic light (365 nm) compared to S-**20**--MeOH to **28b** (650 nm) (Scheme 32). A similar observation was found in the reaction of phenylchlorcarbene **90** with water.[5]

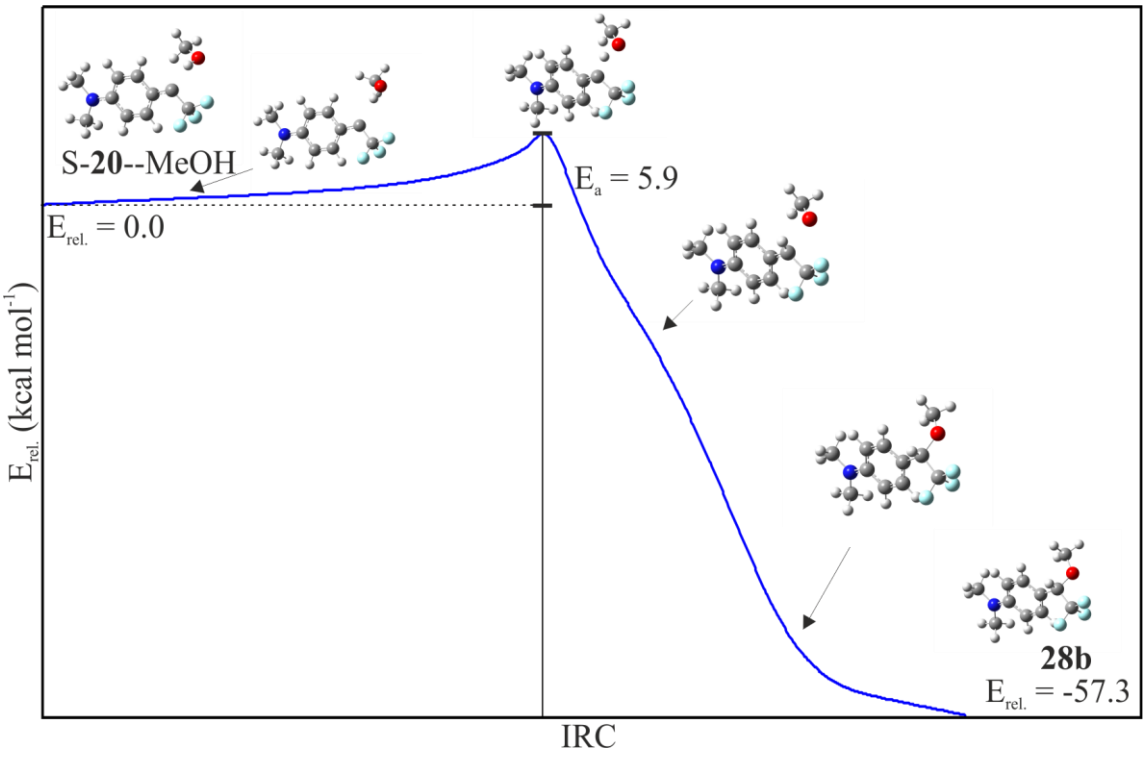

Figure **65:** IRC of the rearrangement of complex S-**20**--MeOH to **28b** calculated at B3LYP/Def2-TZVP level of theory. Energies in kcal mol^{-1}. E_a was calculated with separate structures at the BLYP-D3/Def2-TZVP level of theory.

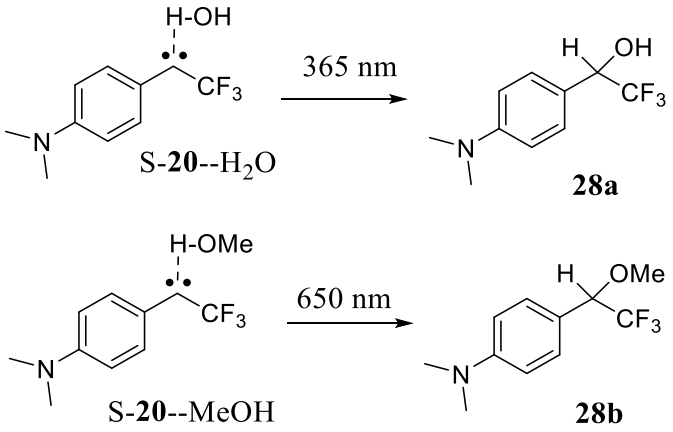

Scheme **32:** Photolysis of S-**20**--H_2O and S-**20**--MeOH.

DFT calculations at B3LYP/Def2-TZVP level of theory on the relative energies of possible products and intermediates out of S-**20** and water are compared (Table 13). Complex S-**20**--H_2O is stabilized with -10.4 kcal mol^{-1} compared to S-**20** and H_2O. The OH insertion product **28a** is stabilized by -66.4 kcal mol^{-1} and is the thermodynamically most stable. **29a4** instead is only stabilized by -33.8 kcal mol^{-1} relative to the carbene S-**20** and water. An "ion-pair" **22a**, discussed in the following, is not stabilized and shows a 2.2 kcal mol^{-1} higher relative energy than carbene S-**20** and water. But as the calculation does not include a possible stabilizing influence of solvation on the ion pair, the number may be lower.

Table **13:** Relative energies of selected molecules.

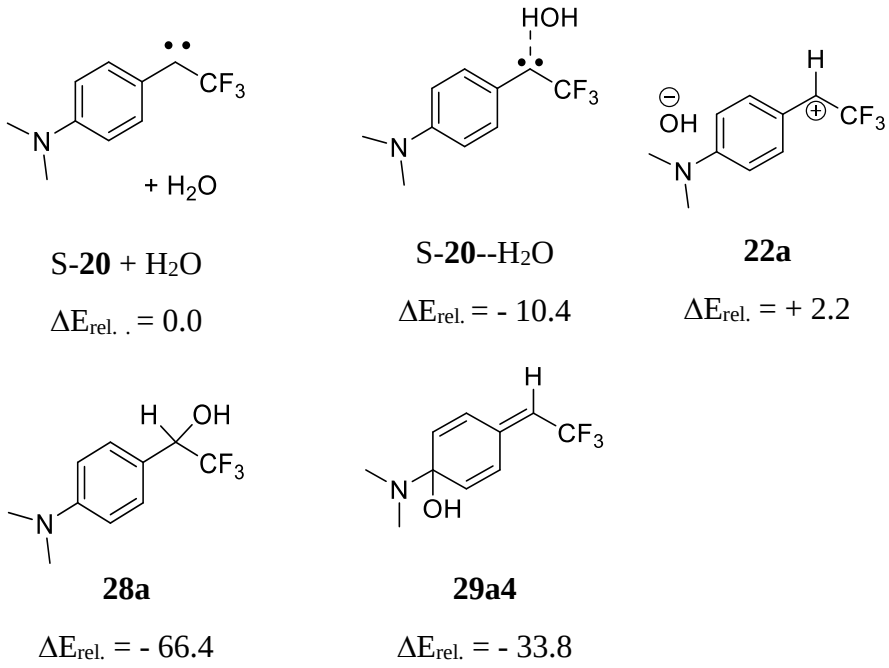

S-**20** + H_2O	S-**20**--H_2O	**22a**
$\Delta E_{rel.}$ = 0.0	$\Delta E_{rel.}$ = - 10.4	$\Delta E_{rel.}$ = + 2.2
28a	**29a4**	
$\Delta E_{rel.}$ = - 66.4	$\Delta E_{rel.}$ = - 33.8	

Relative energies $\Delta E_{rel.}$ in kcal mol^{-1}. Calculated with B3LYP/Def2-TZVP level of theory.

While the calculated IR frequencies of **22** agree with the experimental values, the TD-DFT calculated UV-vis spectrum of cation **22** is not showing absorptions in the 400 - 600 nm range and is not matching the obtained experimental spectrum (Figure 66). Thus, the origin of the observed blue color could not be clarified with TD-DFT calculations so far. To find a possible explanation of why cation **22** is obtaining a blue color, the cation is calculated including an interaction with the counterion OH^-.[122] Singlet **22a**, with the OH positioned 2.14 Å away from the nitrogen is found as a minimum energy structure (Chart 23). "Ion pair" **22a** shows a stabilization compared to **22** and free OH^- of 13 kcal mol^{-1}. Moreover, does the interaction of the anion induce a change in the structure and the charge localization. In **22a** the largest positive charge (except the carbon of CF_3) is located at the carbon atom in the ring next to C–H (0.209). A difference in the structures is the dihedral angle C–N–C–C° in **22** being linear and **22a** slightly bend with 168.24° at the dimethylamino moiety.[123, 124] The calculated UV-vis spectrum of **22a** shows its most intense absorption λ_{max} at 450 nm, whereas the most intense absorption of **22** is computed at 320 nm (Figure 66). Overall, the calculations on **22a** indicate a possible influence of the OH^- ion on the geometry and the UV-vis spectrum. But the nature of **22a**, if it is an ion pair[125, 126] or a singlet radical pair[127-130] has to be evaluated. The IR spectrum of ion-pair **22a** was calculated and compared to the one of cation **22** (Figure 67), but the comparison of **22** and **22a** to the experimental IR spectra does not show conclusively better matching to **22a**

or **22**. Also a Charge-transfer interaction, intermolecular or intramolecular, has to be taken into account.[131, 132]

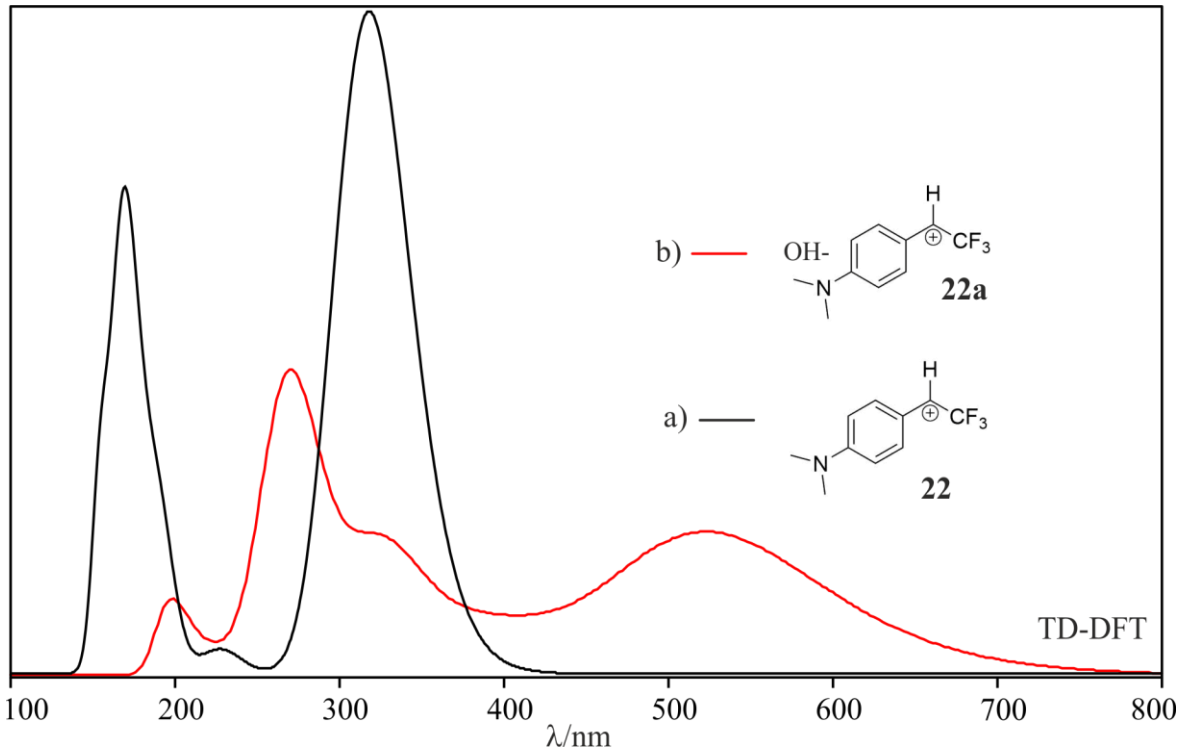

Figure **66:** UV-vis spectra of a) **22** and b) **22a** calculated at TD-DFT (B3LYP/Def2-TZVP) level of theory.

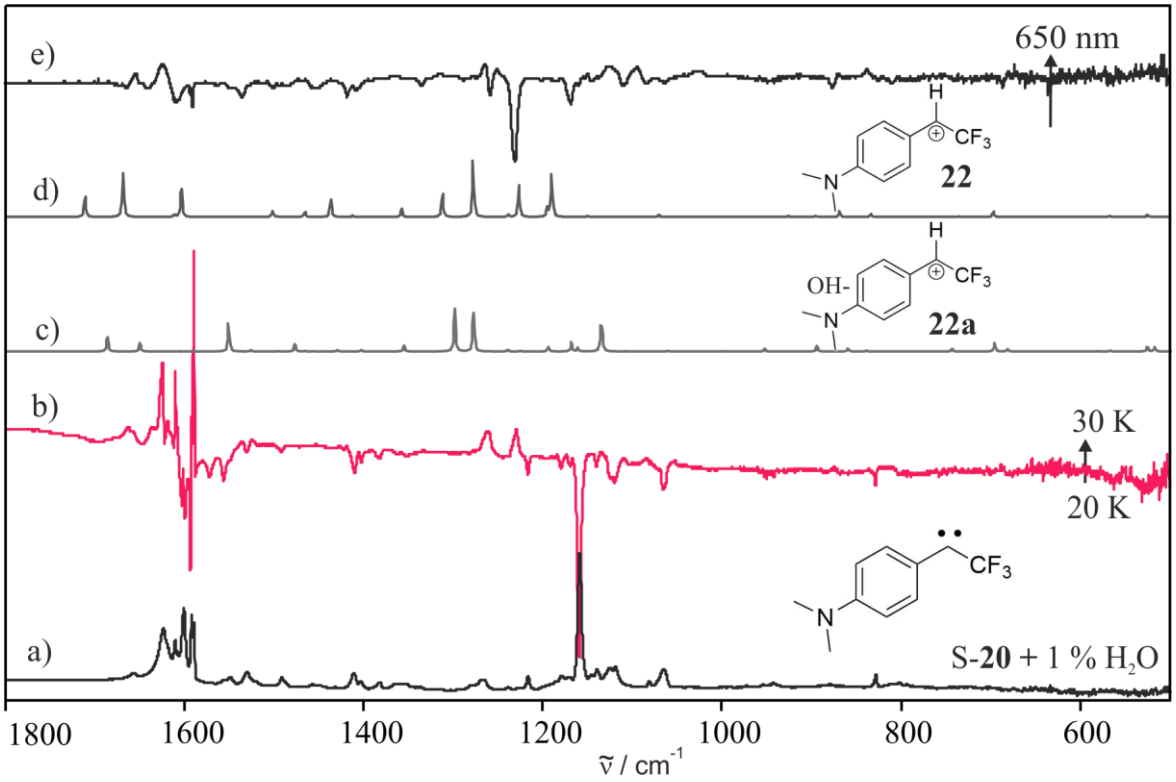

Figure **67:** Comparison of the calculated IR frequencies of **22** and **22a**. a) IR spectrum of S-**20** in argon doped with 1 % water at 3 K. b) IR difference spectrum obtained after annealing from 25 to 30 K. Bands pointing upwards increase in intensity and are assigned to **u2**. Bands pointing downwards decrease in intensity and are assigned to S-**20** and water. Calculated IR frequencies of c) **22a** and d) **22** (M06-2x/Def2-TZVP//B3LYP/Def2-TZVP). e) IR difference spectrum obtained after 650 nm photolysis.

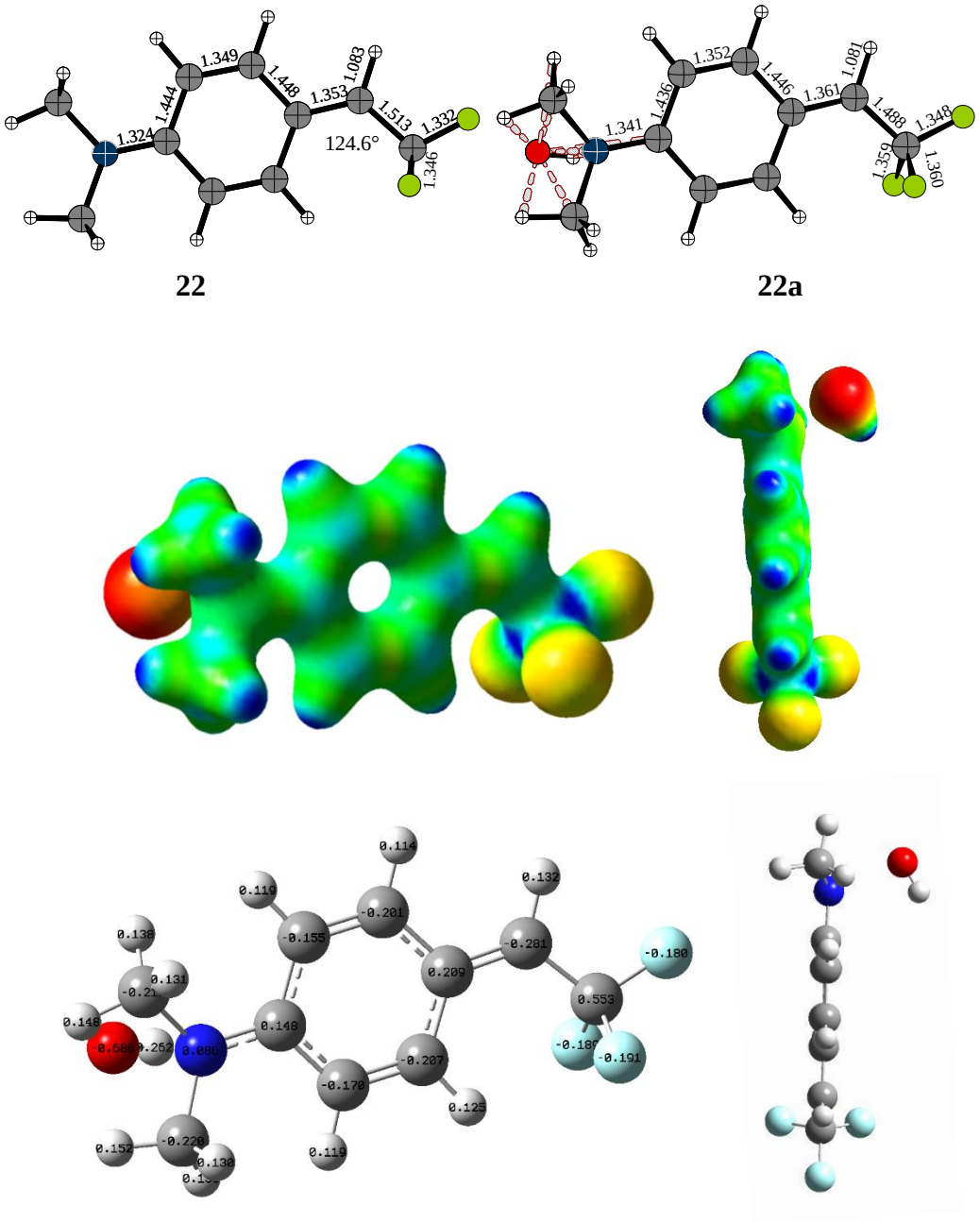

Chart **23:** Structure and electrostatic potential map of **22a** (color range from red with -13.0 kcal mol^{-1} to blue with 318 kcal mol^{-1}; density = 0.07). Selected bond lengths and angles of **22a** and (**22**) and Mulliken charges of **22a**. Bond lengths in Å. (B3LYP/Def2-TZVP).

The corresponding ion pair with counterion MeO^- **22b** was calculated (Chart 24). The calculated UV-vis spectrum of **22b** shows nearly no differences to **22a** (Figure 68), this is fitting to the observation of the UV-vis experiment which shows no difference in the spectrum after annealing in methanol compared to water.

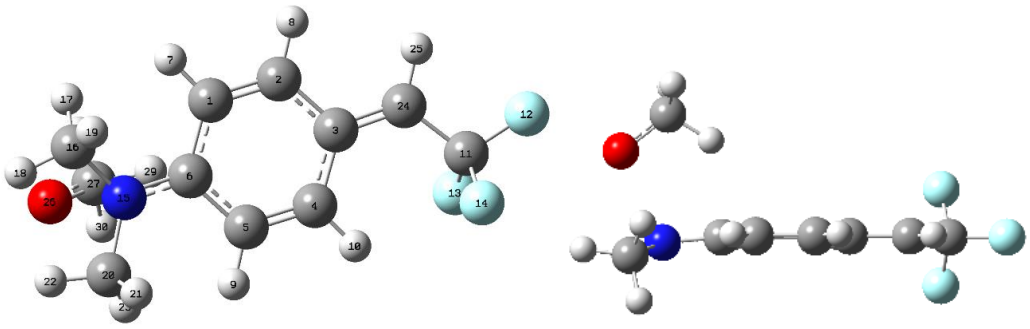

22b

Chart **24:** Structure of **22b** calculated with B3LYP/Def2-TZVP level of theory.

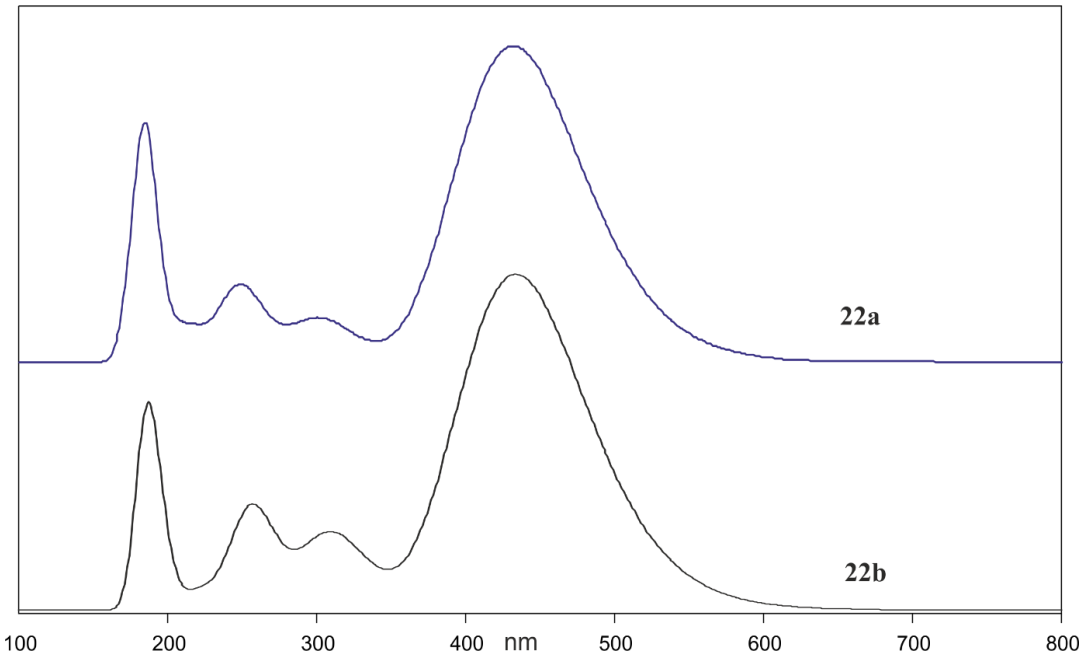

Figure **68:** Calculated UV-vis spectrum of ion pairs **22b** and **22a** (TD-B3LYP/Def2-TZVP).

2.4.2.4. Conclusions and outlook

The IR, UV-vis and EPR experiments of push-pull substituted singlet carbene S-**20** in doped matrices showed a differing chemistry than observed for the similarly substituted carbene S-**1**. Annealing of S-**20** in an argon matrix doped with 1 % of H_2O, D_2O or MeOH results, depending on the temperature, in at least two products. One species which is built mostly at temperatures around 20 K is assigned to the singlet complexes S-**20**--H_2O, S-**20**--D_2O or S-**20**--MeOH, respectively. Insertion product **28a** is generated with 365 nm photolysis out of complex S-**20**--H_2O, whereas S-**20**--MeOH shows a higher light-sensitivity and rearranges upon 650 nm photolysis to insertion product **28b**. The other species **u2** is blue and is built at higher temperatures above 20 K. The EPR experiment, which was conducted in an analog way indicates the singlet multiplicity of both species. With the help of results from literature and by evaluation of IR and UV-vis experiments, **u2** was assigned to cation **22**. DFT calculated IR spectra show a reasonable agreement to the experimentally obtained IR spectra. Photolysis of **22** is not resulting in the usual insertion product **28a**, instead another species **u3** is generated upon 650 nm irradiation. Most likely this species is a result of a OH insertion at another position of the cation **22**. Thus, in this Chapter it was shown that a β-fluorinated cation can be stabilized by introducing a strongly electron donating *p*-dimethylaminophenyl substitution counteracting the destabilization effect of CF_3. As the insertion at C-1 is hindered and the OH^- is likely stabilized by the cation itself, the cation is kinetically stabilized even in argon. With the experimental observations two questions arise: why is a charged and polar cationic species stabilizable in a non-polar argon matrix and why does the OH insertion of this species not take place at the former carbene carbon? The first question seems to contradict the old principle in chemistry "Like dissolves like", as this rule also applies for the matrix hosts as they solvate the trapped guest molecules. For example, matrix isolation experiments of cations **62**,[3] **72**[4], **82**[85] and **2** showed that these cations are not observed in argon matrices, but are stabilized in the polar LDA water ice matrices. Based on DFT calculations, the structure of **22** shows a distance between C_1 and C_2 of 1.353 Å and C_3 and C_4 of 1.349 Å (Chart 25). Those C–C bond lengths suggest a double bond character.[49] Therefore, the structure of cation **22** resembles more the resonance structure depicted in Chart 25. Also, the N–C_5 bond with a distance of 1.324 Å indicates a partial double bond and therefore an iminium ion like structure. Thus, these structural properties suggest firstly that the electrons in **22** are highly delocalized and secondly, that an insertion at C-1 is hindered and may results in a (kinetically) stabilization of **22** potentially even in argon. An illustration of the charge distribution of **22** provides the electrostatic potential map of cation **22** depicted in Figure 2 (page 15). It corroborates that the

positive charge is not only located at the former carbene center but is delocalized over the ring and especially on the C-5 carbon atom. The Mulliken charges of **22** depicted in Chart 25 are showing the most positive charge at C-5 with 0.271 (CF_3 carbon is omitted). This distribution of charge of **22** may also explain why the recombination of cation **22** with OH^- does not result in the usual insertion product **28a**. The charge delocalization throughout the aromatic ring and the repulsive influence of the negative CF_3 group, as also suggested in literature, may explain the stability of **22**.[110, 112] So, it may be suggested that, during annealing a protonation of S-**20** by H_2O occurs, then the highly negative CF_3 group pushes the OH^- ion away to the aryl ring where it is somehow stabilized until it inserts, light- or temperature-induced. Aside from this, the reported pK_R^+ of **22** is with a value of -9.3 relatively low, suggests a decreased reactivity of the cation toward nucleophiles, as found experimentally.

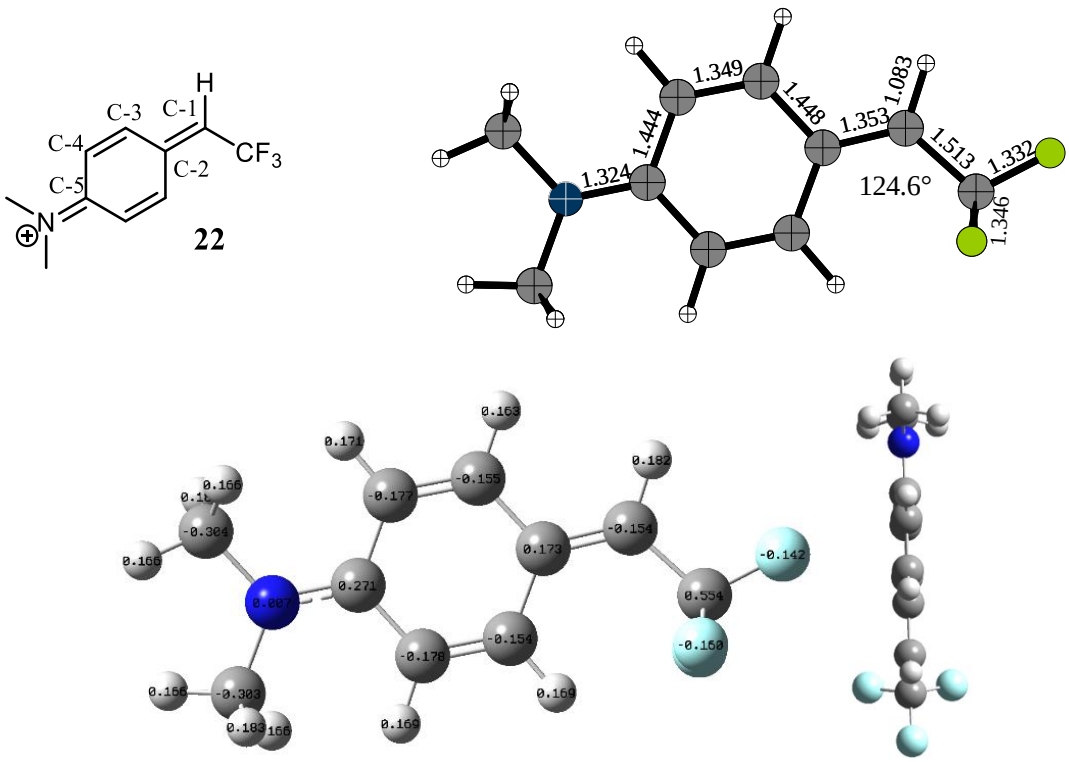

Chart **25:** Structure and Mulliken charges of **22** (B3LYP/Def2-TZVP). Selected bond lengths and angles of **22**. Bond lengths in Å.

To verify the assignment of **u2** to a cationic species like **22** and also to get more information about the generated species **u2** and **u3**, it would be interesting to extend the experimental analysis. For this, the study of the micro-solvolysis of carbene **20** at ambient or temperature reduced conditions in unreactive solvents like e.g. hexafluorobenzene doped with water may be an interesting possibility. The analysis of the final products could be determined with

techniques like NMR spectroscopy or mass spectrometry. Another approach would be ultrafast spectroscopy or LFP to evaluate the lifetime and/or rate constants of the cation. A synthetical approach would be a substitution of the *p*-dimethylamino group with other amino groups like in compound **14**, **15** or **16** as this would potentially change the stabilities and the UV-vis spectra of the cations (Chart 26).[133]

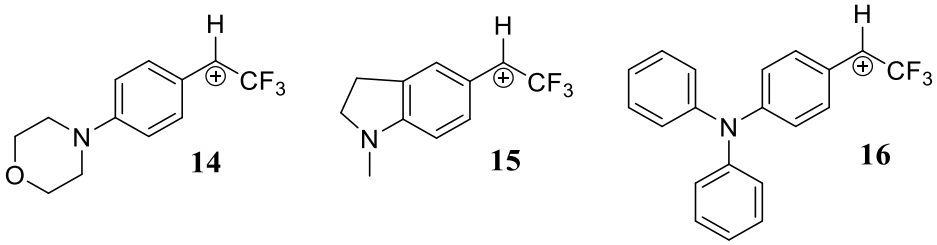

Chart **26:** Cations **14, 15** and **16**.

To analyze if the CF_3 group plays an important role for the reactivity and stability of the cation or if the amino group is the determining factor, other *p*-amino substituted benzhydryl cations like **17** can be analyzed in similar experiments in doped argon matrices. As this compound is already reported in literature[76] the analysis would probably be simplified.

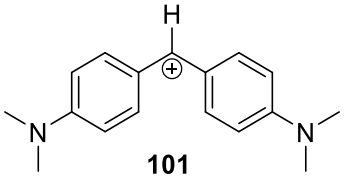

Chart **27:** Cation **101**.

Furthermore, it may be interesting to study, if a change of the matrix host to a more polar solvent (e.g. nitrogen) has an influence on the stability and reactivity of **22**. By using a host with a higher melting point such as xenon or a lower melting point such as neon, the temperature effect of the annealing process can be studied in more detail. A variation of the host may also elucidate if the compound has solvatochromic properties.[134]

2.4.3. Direct reaction in solid water

2.4.3.1. Introduction

By increasing the amount of water to 100 % (as in LDA water ice), the medium in which the molecule is "solvated" is not non-polar like argon anymore. Hence other more polar species like e.g. cations could be stabilized and observable as shown for the benzhydryl cation and others.[3, 4, 85] Secondly, the amorphous water ice matrix is not inert but more reactive. This can result in direct OH insertions. Thus, as explained in Chapter 2.1. Introduction, the photolysis of the diazo precursors in LDA water ices did not result in the corresponding carbenes, but instead the corresponding cations or insertion products[5, 28] are formed. For the photolysis of **26** in LDA water ice it may be expected that the cation **22** is formed and stabilized due to the high PA of the corresponding carbene **20** (272 kcal mol^{-1} (B3LYP/6-311+G(d,p))) and its low pK_R^+ value (- 9.3).[10] But the experiments in 3 % H_2O showed that an increase of water leads to less amount of **22** and an increase of photoproduct **u3**. Thus, it may be expected that an increase of water results in a direct insertion of OH and the direct formation of **u3**.

2.4.3.2. Results and discussion

The experiments are conducted in low density amorphous water ice and performed similarly to the study of **6** (Chapter 2.3.4.) and diphenyldiazomethane **66** in LDA water ice.[3] Deposition of **26** with an excess of water at 50 K onto a matrix window and subsequent cooling to 9 K results in the IR spectrum shown in Figure 69. The IR spectrum shows the IR vibrations of **26** embedded in the characteristic broad features of LDA water ice. The IR spectrum of **26** in argon and 1 % of water is plotted for comparison. Subsequently, the matrix was irradiated with 365 - 450 nm light. The 365 nm photolysis was chosen because traces of **26** remained even after 18 hours of 450 nm photolysis. The fingerprint region of the obtained IR spectrum after photolysis of **26** is shown in

Figure 70. The obtained IR difference spectrum after photolysis shows the decreasing signals of **26**, as well as a set of newly formed signals. The most intense new signals are at 1626 and 1265 cm^{-1}. With the help of a synthesized sample of **28a** matrix isolated in LDA water ice, some characteristic signals may be traced back to alcohol **28a**. In Figure 90 in Appendix the IR spectrum obtained after the deposition of **28a** in argon is compared to the IR spectrum obtained in LDA water ice. It shows that the frequencies of **28a** in LDA water ice are shifted and broadened resulting of weak interactions of the alcohol with the solid water matrix (Appendix Table 16). The signals at 1626, 1533, 1265 and 1140 cm^{-1} can be assigned to **28a**, but the intensities of the signals do not match the intensities of **28a** in LDA water ice. Especially the

signal at 1265 cm^{-1} is extremely intensified. This can be explained by overlapping's to the IR signals of **u3**, which showed its most intense signal at 1265 cm^{-1}. The experiments in LDA water ices do not show a blue color or any sign of cation **22**. Apparently, the direct reaction of **20** with water results in the formation of photoproducts **u3** and **28a**. It is conceivable that the 365 - 450 nm irradiation leads to the decomposition of **22** and S-**20**--H_2O and the direct formation of **u3** and **28a**. The reactivity in LDA water ice also fits to the observations in 3 % water-doped argon matrices and signalize that the contact of **20** to more molecules of water leads to a direct formation of **u3** and **28a**.

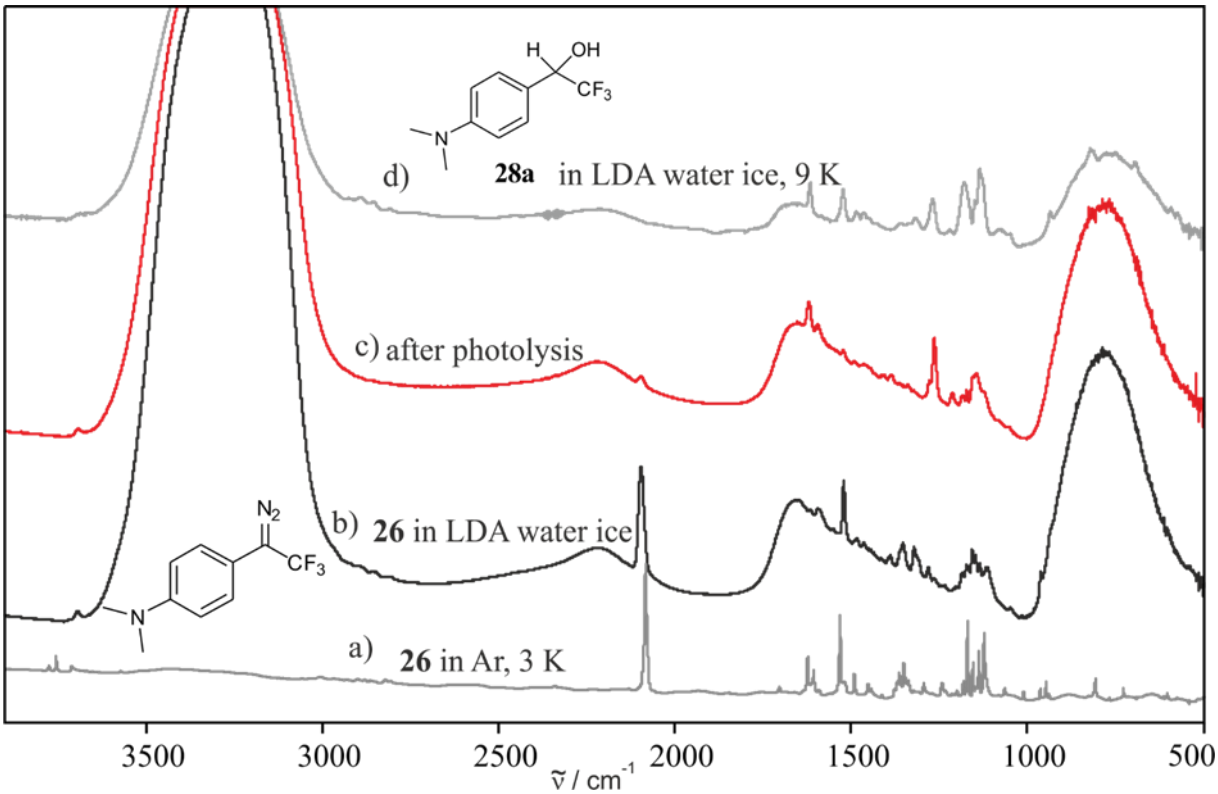

Figure **69:** IR experiment of **26** in LDA water ice. a) IR spectrum of **26** in an argon matrix doped with 1 % of water at 3 K. b) IR spectrum of **26** in LDA water ice at 9 K. c) IR spectrum obtained after 365 - 450 nm photolysis of **26** in LDA water ice. d) IR spectrum of **28** in LDA water ice at 9 K.

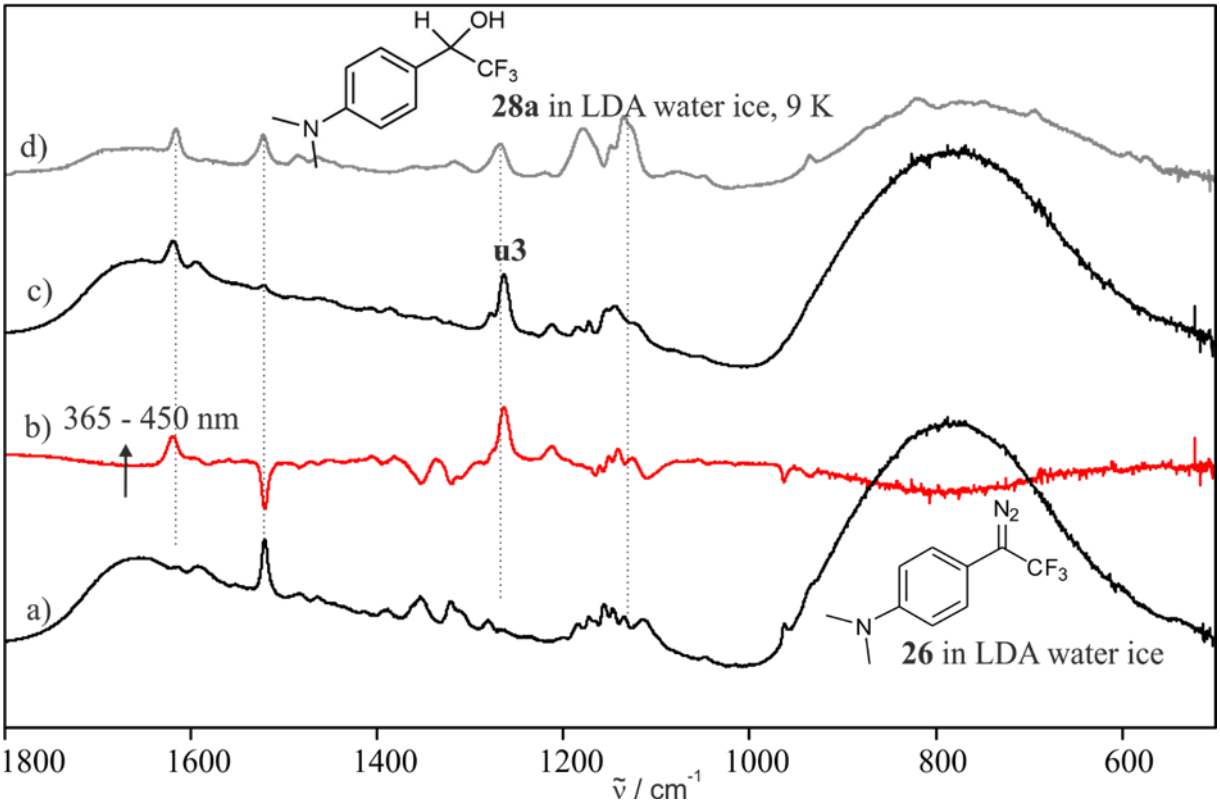

Figure **70:** Fingerprint region of the experiment of **26** in LDA water ice. a) IR spectrum obtained after photolysis of **26** in LDA water ice. b) IR difference spectrum obtained after 365 - 450 nm photolysis of **26** in LDA water ice. Bands pointing upwards increase in intensity. Bands pointing downwards decrease in intensity and are assigned to **26**. c) IR spectrum obtained after photolysis of **26** in LDA water ice. d) IR spectrum of **28a** in LDA water ice.

2.4.3.3. Conclusions

To study the reaction of carbene **20** in direct contact with water, the corresponding diazo precursor **26** was isolated in LDA water ice at 9 K. IR spectroscopic investigations revealed, that in comparison to the results from the annealing controlled complexation of carbene **20** (Chapter 2.4.2.), the photolysis of **26** in solid water did not generate the intermediary species **u2** (preliminarily assigned to cation **22**) and S-**20**--H_2O. Instead photoproducts **u3** and **28a** are present directly (Scheme 33). This is contrary to the reaction of carbene **1** (Chapter 2.3.4.) or diphenylcarbene **60** in amorphous water ice, for which photolysis resulted in the corresponding cations, which were stabilized in water ice and also contrary to the reaction of carbene **50** [28] and **30** (Chapter 2.5.3.) for which photolysis resulted only in the C-1 insertion product.

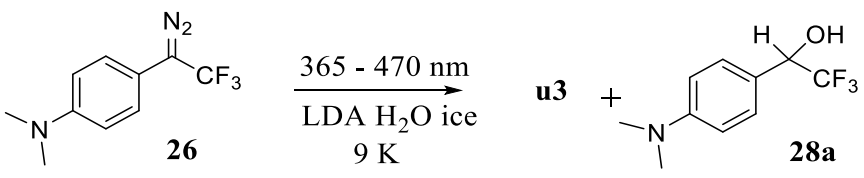

Scheme **33:** The observed reaction of **26** in LDA water ice.

In amorphous water ice the precursor is photolyzed in a surrounding of water molecules close by resulting in a direct reaction of the derived intermediary species. The experiments of **26** in LDA water ice suggest, that the proximity of water molecules results in a direct/concerted reaction of the carbene or the corresponding cation to the insertion products **28a** and **u3**. To understand the generation of **28a** and **u2**, previous experiments must be considered (Chapter 2.4.2.). Here it was shown that insertion product **28a** is formed upon 365 nm photolysis of S-**20**--H_2O. Thus, the direct formation of alcohol **28a** in LDA water ice may be explained by the formation S-**20** which, promptly rearranges to **28a** upon UV irradiation. On the other side, the formation of **u3** may be explained by a direct reaction of the cationic species **u2**. It may be assumed that **u2** directly inserts the OH, triggered by close contact to H_2O molecules or/and by UV irradiation. This was also assumed in Chapter 2.4.2. in the reaction of S-**20** in 3 % of water doped matrices. IR spectroscopic investigations suggest that one molecule of H_2O can stabilize cation **22**, whereas more water molecules lead to the formation of **u3** in a higher amount. To understand how **u3** is produced it is necessary to study the photolysis of **u2** in more detail also using 365 nm light.

2.5. *m*-Methoxyphenyl-1-(trifluoromethyl)carbene

2.5.1. Characterization in argon matrices

2.5.1.1. Introduction

Carbene **30** has an inductively electron pulling *meta*-methoxyphenyl group and an additional electron-withdrawing trifluoromethyl group attached to the carbene center. This results in the carbene center being more electrophilic.

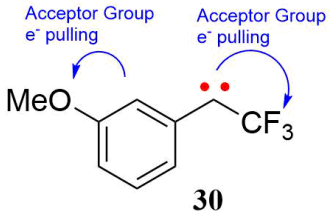

30

Song and Sheridan studied carbene **30** in nitrogen matrices with IR, UV-vis and EPR spectroscopy.[135] The EPR signals obtained for **30** in perfluoro-2-*n*-butyltetrahydrofuran at 90 K indicate a triplet multiplicity. Furthermore, the spin specific reactivity of **30** with oxygen, hydrogen, and hydrogen chloride did affirm the triplet ground-state of **30** by showing a reaction with O_2 and H_2 and no reaction with HCL (Scheme 34).

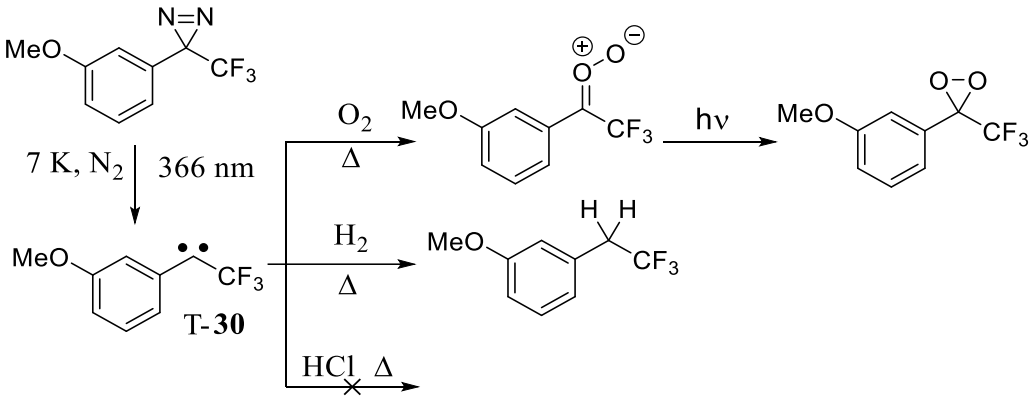

Scheme **34:** Generation and observed reactivity of T-**30** with O_2, H_2 and HCl at low-temperatures.[135]

In this work the reactivity of triplet carbene T-**30** with water is probed by the annealing induced complexation in doped matrices and by the direct reaction in LDA water ice. The carbene was chosen as it is comparable to *para*-methoxyphenyl substituted carbene S-**1**. Due to the *meta*-position, the resonance stabilization effects of the methoxy substitution is absent in **30** compared to **1**. This destabilization is also supported by the calculated lower PA of **30**. Thus, the reactivity of **30** is expected to differ from S-**1**.

2.5.1.2. Results and discussion

m-methoxyphenyl-1-trifluoromethyldiazomethane **36** is obtained by thermolysis of the corresponding tosylhydrazone sodium salt **35** and matrix isolated directly with an excess of argon on a cold CsI window. In Scheme 35 all four conformers of **36** are depicted. As the energy difference between the conformers is calculated to be nearly degenerate (0.26 - 0.29 kcal/mol (B3LYP/Def2-TZVP)) it may be expected that a mix of **36**uu, **36**dd, **36**ud and **36**du is present after deposition. The obtained IR spectrum was compared exemplarily to the calculated spectra of **36**uu and **36**du at M06-2x/Def2-TZVP//B3LYP/Def2-TZVP level of theory as shown in Figure 71. The matching is reasonable, but a further differentiation of the conformers was not performed. The most intense signal in the IR spectrum obtained after deposition of **36** is the N=N stretching vibration at 2092 cm^{-1} (Table 14).

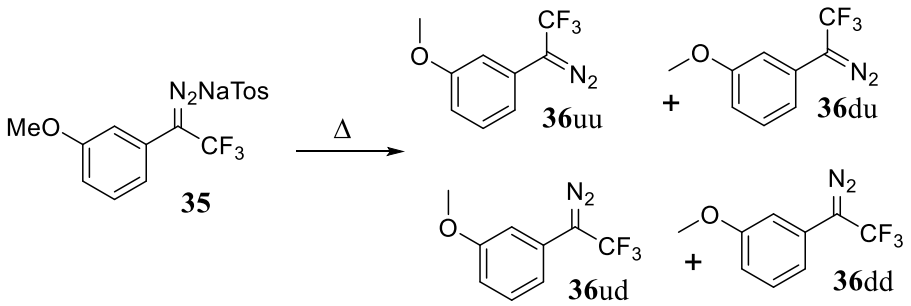

Scheme **35:** Formation of **36** by thermolysis of **35**.

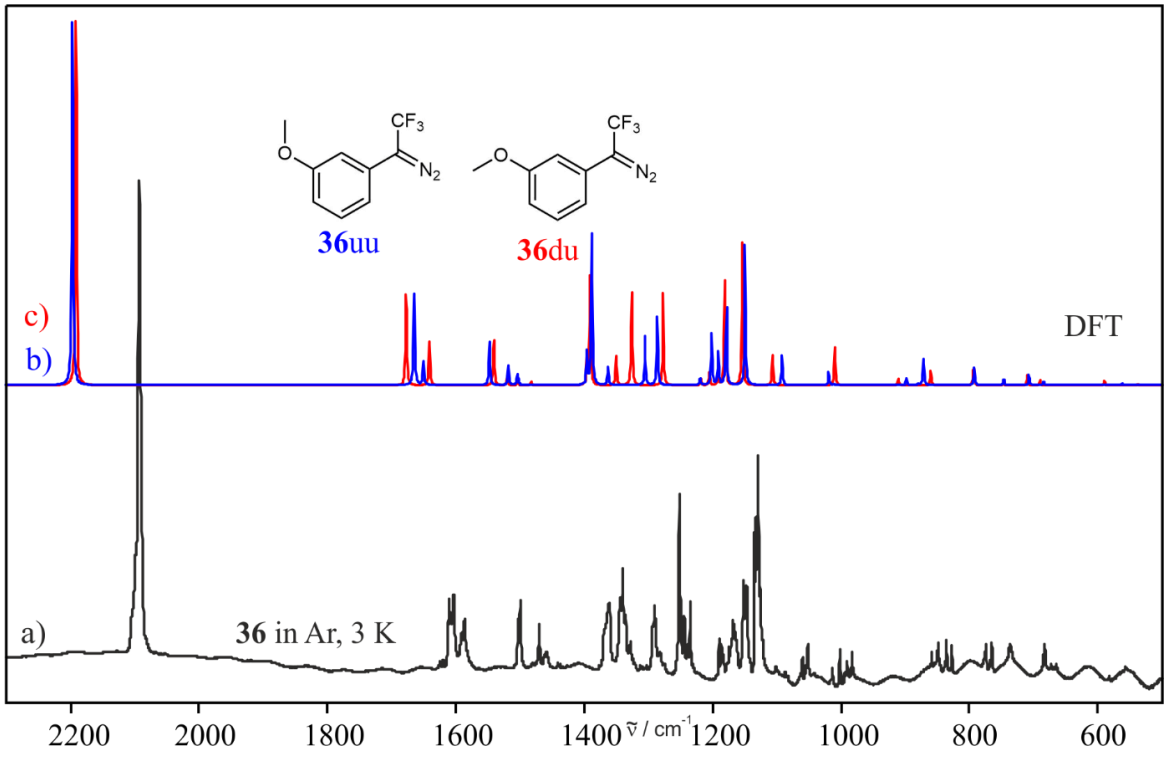

Figure **71:** a) IR spectrum obtained after deposition of the precursor **36** in an argon matrix at 3 K. b) calculated IR-spectra of **36**uu and **36**du at M06-2x/Def2-TZVP// B3LYP/Def2-TZVP level of theory.

Table **14:** Experimental and calculated vibrational frequencies of **36**.

Exp.[b]		Calc.[a] **36**uu		Assignment [c]
$\tilde{\nu}$	$I_{rel.}$	$\tilde{\nu}$	$I_{rel.}$	
2965	2	3111.6	3	C-H str. (CH_3)
2846	1	3045.1	4	C-H str. (CH_3)
2094	100	2196.7	100	N=N str.
1611, 1604	39	1664.5	28	C=C Ring str.
1591, 1586	19	1649.6	7	C=C Ring str.
1504, 1500	22	1547.1	11	C-H bend.
1470	6	1517.6	6	C-H bend. (CH_3)
1460	6	1504.0	2	C-H bend.
1361	41	1502.3	1	C-H bend. (CH_3)
1344, 1340	39	1395.2	8	C=N str.
1328	3	1387.7	40	C-C str.
1290	38	1362.2	5	C-H bend.
1252	32	1304.9	12	C-O str.
1235	10	1286.0	17	C-O str.
1190, 1184	10	1219.5	2	C-H bend. (CH_3)
1153, 1147	43	1201.1	13	C-F str.
1129	100	1190.9	8	C-H bend.
1059	3	1178.2	20	C-F str.
1051	5	1148.9	35	C-F str.
1001	5	1091.9	7	C-O str.
981	3	1018.7	4	C=C Ring str.
849	4	992.9	0	C-H bend. out of plane
836	5	897.5	2	C-H bend. out of plane
829	2	879.5	0	C-H bend. out of plane
774	5	871.6	7	Ring def.
765	3	792.2	4	C-H bend. out of plane
737	14	746.5	2	C-F bend.
684	6	706.7	3	C-H bend. out of plane
582	0	684.5	1	Ring def.

[a] Calculated at M06-2x/Def2-TZVP//B3LYP/Def2-TZVP level of theory. [b] In argon at 3 K. The signals derive from a mixture of conformers and were exemplarily assigned to **36**uu. [c] Tentative assignment.

To generate *m*-methoxyphenyl(trifluoromethyl)carbene **30**, precursor **36** was irradiated with 450 nm LED light overnight. In Figure 72 the obtained IR spectrum after overnight photolysis is depicted. The absorptions are matching nicely to the frequencies of T-**30** reported by Song and Sheridan.[135] Some of the signals show a splitting, which may indicate the presence of similar species, most likely conformers. The calculated frequencies of all four conformers T-**30**uu, T-**30**ud, T-**30**dd and T-**30**du combined are not fitting to the obtained IR intensities in the region 1200 – 1300 cm^{-1} (Appendix Figure 91), This is probably due to a different ratio of

the four conformers. Therefore, the computed IR spectrum of each triplet conformer is compared to the experimental IR spectrum obtained after photolysis of **36** (Figure 72). The IR spectra match nicely to the IR spectrum obtained after photolysis. A separate assignment to the conformers and an evaluation of the ratio of those was not conducted. The most stable conformer regarding DFT calculations is T-**30**uu with the methoxy moiety pointing upwards with respect to the trifluoromethyl group. The singlet-triplet gap for the most stable conformer T-**30**uu is 4.09 kcal mol^{-1} compared to S-**30**uu and thus the results of the calculations are supporting its triplet multiplicity. The calculated structures of the four conformers of the triplet and the singlet state are depicted in Chart 28 and sorted by their relative energies in ascending order.

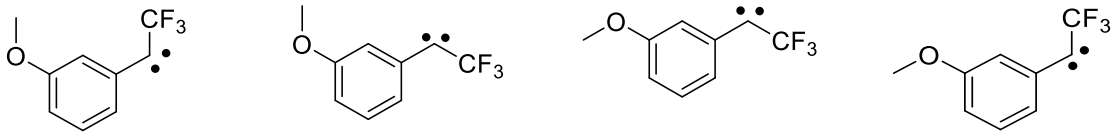

T-**30**uu $E_{rel.}$ = 0.0

T-**30**ud $E_{rel.}$ = 0.20

T-**30**dd $E_{rel.}$ = 0.85

T-**30**du $E_{rel.}$ = 0.93

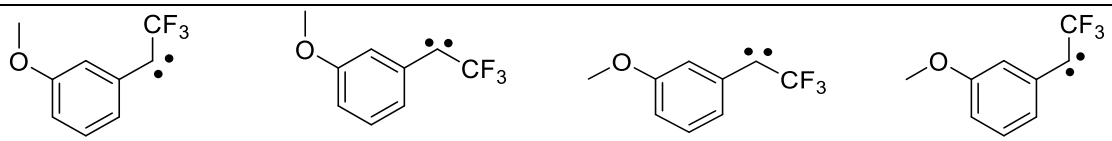

S-**30**uu $E_{rel.}$ = 4.09

S-**30**ud $E_{rel.}$ = 4.46

S -**30**dd $E_{rel.}$ = 5.63

S-**30**du $E_{rel.}$ = 5.66

Chart **28:** Structures and relative energies of the four different conformers of T-**30** and of S-**30** calculated at B3LYP/Def2-TZVP level of theory. Energies in kcal/mol.

.

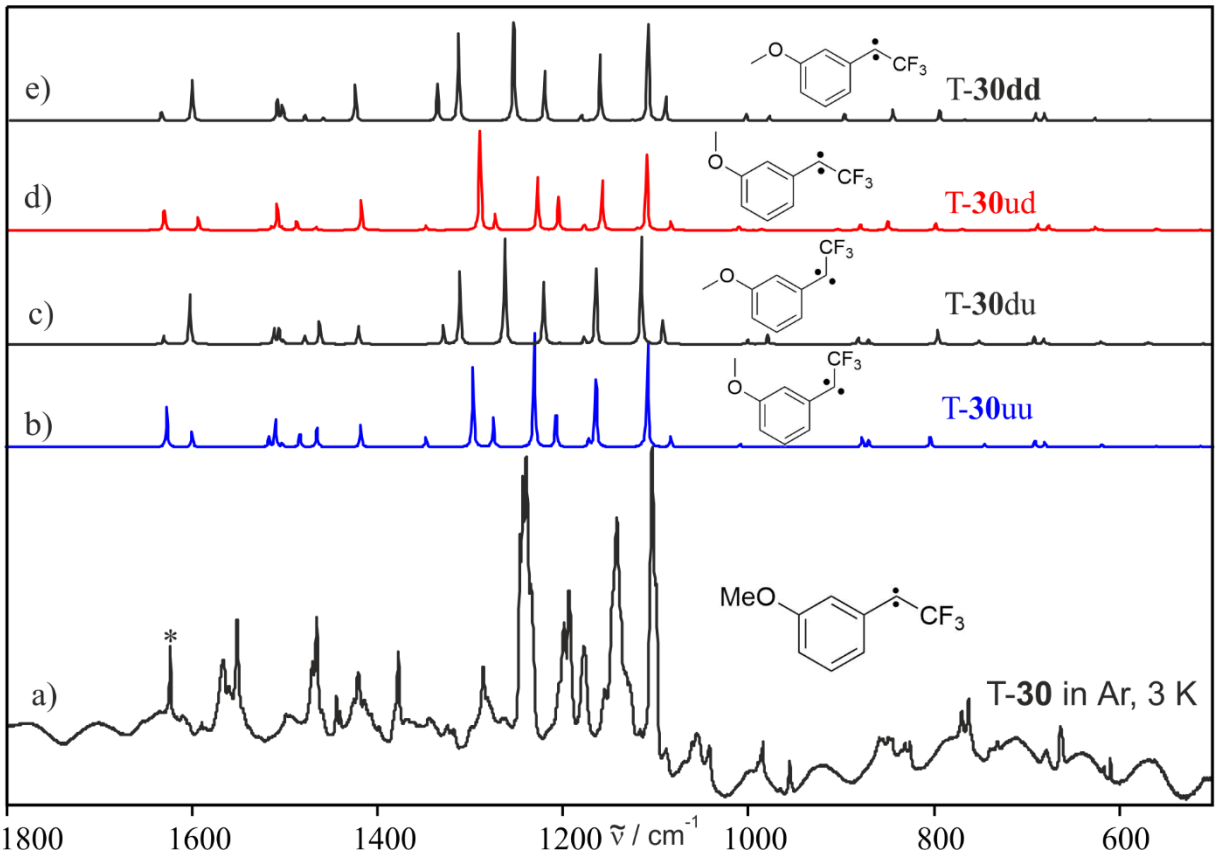

Figure **72:** Comparison of experiment to calculated spectra. a) IR spectrum obtained after photolysis of **36**. Calculated IR spectra of b) T-**30**uu, c) T-**30**du, d) T-**30**ud and e) T-**30**dd (M06-2x/Def2-TZVP//B3LYP/Def2-TZVP). * The signal marked by an asterisk is caused by H_2O.

Table **15:** Experimental and calculated vibrational frequencies of T-**30**.

Exp.[b]		Calc.[a] T-**30**uu		Assignment [c]
$\tilde{\nu}$	$I_{rel.}$	$\tilde{\nu}$	$I_{rel.}$	
2968	8	3105.5	7	C-H str. (CH_3)
2948	7	3037.4	10	C-H str. (CH_3)
1567	8	1627.0	35	C=C Ring str.
1551	9	1599.9	14	C=C Ring str.
1471, 1467	23	1510.1	24	C-H bend. (CH_3)
1445, 1441	3	1483.5	14	C-H str. (CH_3)
1422	22	1465.4	19	C=C str.
1371	10	1418.1	20	C-C-C str. antisym.
1286	14	1296.9	70	C-O str.
1244, 1241	100	1275.2	26	C-O str.
1200, 1194	46	1231.1	100	C-F str.
1179	17	1207.5	34	C-H bend.
1143	92	1164.6	69	C-F str.
1105	62	1109.1	91	C-F str.
1054, 1043	19	1084.1	10	C-O str.
985	5	1009.4	3	Ring def.
956	3	988.1	1	Ring def.
857, 849	8	877.8	9	Ring def.
832, 827	3	870.7	7	C-H bend. out of plane
770	2	804.5	11	C-H bend. out of plane
763	2	745.6	3	C-C-C bend.
680	3	691.5	7	C-H bend. out of plane
664	5	680.9	4	C-F bend.
610	1	619.6	3	Ring def.

[a] Calculated at M06-2x/Def2-TZVP//B3LYP/Def2-TZVP level of theory. [b] In argon 3 K. The signals derive from a mixture of conformers and were exemplarily assigned to T-**30**uu. [c] Tentative assignment.

The four different conformers of T-**30**, similarly to singlet carbene S-**1**, are interconvertible by photolysis and annealing (Figure 73). A distinction between those is not done in this work, due to their similarity and overlapping of the IR spectra. During irradiation of carbene T-**30** with LED light ranging from 365 to 650 nm and a mercury lamp emitting 254 nm light, as well as during tempering the matrix up to 35 K, no signals which would indicate the formation of a new product were obtained.

2.5. m-Methoxyphenyl-1-(trifluoromethyl)carbene

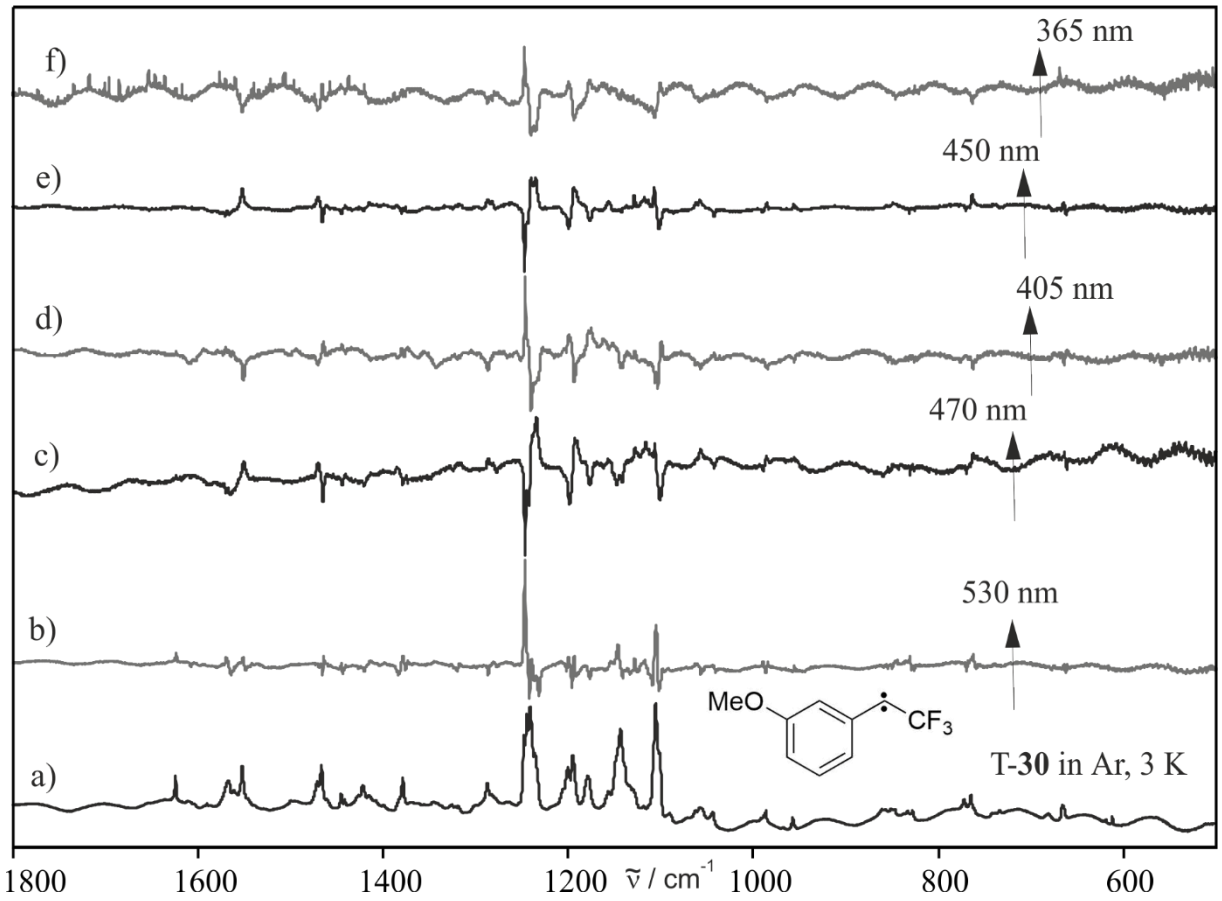

Figure **73:** Photolysis of T-**30** in argon at 3 K. a) IR spectrum obtained after photolysis of **36** and IR difference spectra obtained after b) 530 nm for 30 minutes, c) 470 nm for 30 minutes, d) 405 nm for 45 minutes, e) 450 nm for 45 minutes and e) 365 nm for 1 hours. Bands pointing upwards increase in intensity. Bands pointing downwards decrease in intensity.

2.5.1.3. Conclusions

To understand the chemistry and photochemistry of carbene **30** in an environment without reaction partners, precursor **36** was isolated in an argon matrix at 3 K. The IR experiments showed that triplet carbene T-**30** is generated by 450 nm photolysis of **36** (Scheme 36). The obtained IR spectrum is matching nicely to the reported values of T-**30** by Song and Sheridan.[135] The spectrum indicates the presence of multiple conformers which interconvert via photolysis and annealing. DFT calculations suggest the four conformers to be nearly degenerate in energy. A separation of these species was not performed in this work. Apart from this, T-**30** was photostable upon the used wavelengths in argon matrices at 3 K. Overall, the experiments underline that a pull-pull substitution stabilizes the triplet ground state of carbene **30**. Due to the α-fluorination, the carbene is stabilized kinetically and no further rearrangements were observed.

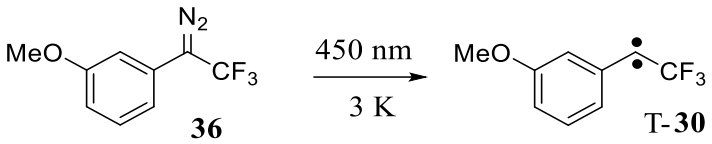

Scheme **36:** Generation of T-**30**.

2.5.2. Complexation with water in doped matrices

2.5.2.1. Introduction

A more detailed introduction can be found in Chapter 2.1.. Matrix-isolation experiments[13] and calculations[119] showed that **60** switches its spin-state from triplet to singlet if the carbene interacts through a hydrogen-bond with one molecule of water to form complex S-**60**--H_2O (Scheme 37). At temperatures between 3 and 12 K the benzhydryl alcohol **68** is produced by quantum mechanical tunneling (QMT). For other triplet carbenes with a low singlet-triplet gap a spin switching could be observed as well (e.g. flourenyliden **70**,[4] *p*-tolyl(trifluoromethyl) carbene **50** [92]). Instead for dibenzocycloheptadienylidene **80** [12] with a higher singlet-triplet gap no singlet complex was observed.

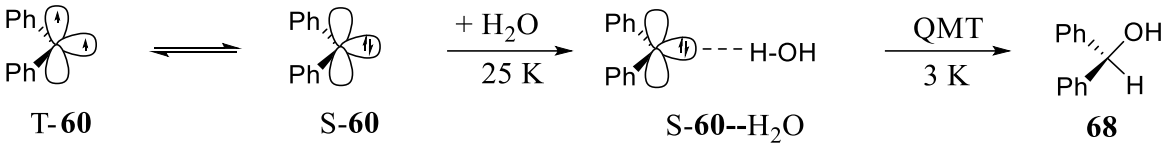

Scheme **37:** Reaction of **60** in argon matrices doped with 1 % of water.

Since the S-T gap of carbene **30** (3.98 kcal mol^{-1} (B3LYP-D3/6-311+G(d,p))) is calculated to be lower in energy than **60** (5.58 kcal mol^{-1} with (B3LYP-D3/6-311+G(d,p))), it is expectable to observe a spin switch from the triplet state to the hydrogen-bonded singlet complex S-**30**--H_2O.

2.5.2.2. Results and discussion

To study the reactivity of T-**30** and 1 % of water UV-vis spectroscopically, **36** was generated by thermolysis of sodium *p*-methoxy-2,2,2-trifluoroacetophenone-*p*-tosylhydrazon **35** and was deposited directly together with an excess of argon doped with 1 % of water on a sapphire window at 8 K. In the UV-vis spectrum depicted in Figure 74, precursor **36** shows a broad absorption at ~250 nm. After photolysis of **36**, signals assigned to T-**30** are present at 240 nm and a weaker broader one at 500 nm. These values are matching the reported UV-vis absorptions of T-**30** by Song and Sheridan.[135] The matrix was annealed to 25 K for 10 minutes and cooled back to 8 K and the obtained UV-vis spectrum shows the decrease of the absorption at 500 nm assigned to T-**30** and an increase of an absorption at ~330 nm. This observation suggests the formation of a new product out of T-**30**. The singlet state of bistable carbene S-**50** showed a similar broad absorption at 326 nm.[28] This information was used to assign the new signal preliminarily to S-**30** or more likely to hydrogen-bonded complex S-**30**--H_2O.[5] Additional weak signals present after photolysis of **36** and increasing during annealing at 218,

270 and 277 nm could be assigned to insertion product **38**, as a comparison to the UV absorptions of **38** isolated in argon at 3 K shown in Figure 75, reveals. This early generation of **38** can be explained with the proximity of some of the isolated carbene S-**30** and water. The interaction of **30** with one water molecule is expected to result in the spin switching of T-**30** to singlet state S-**30** upon formation of a hydrogen-bond with water.

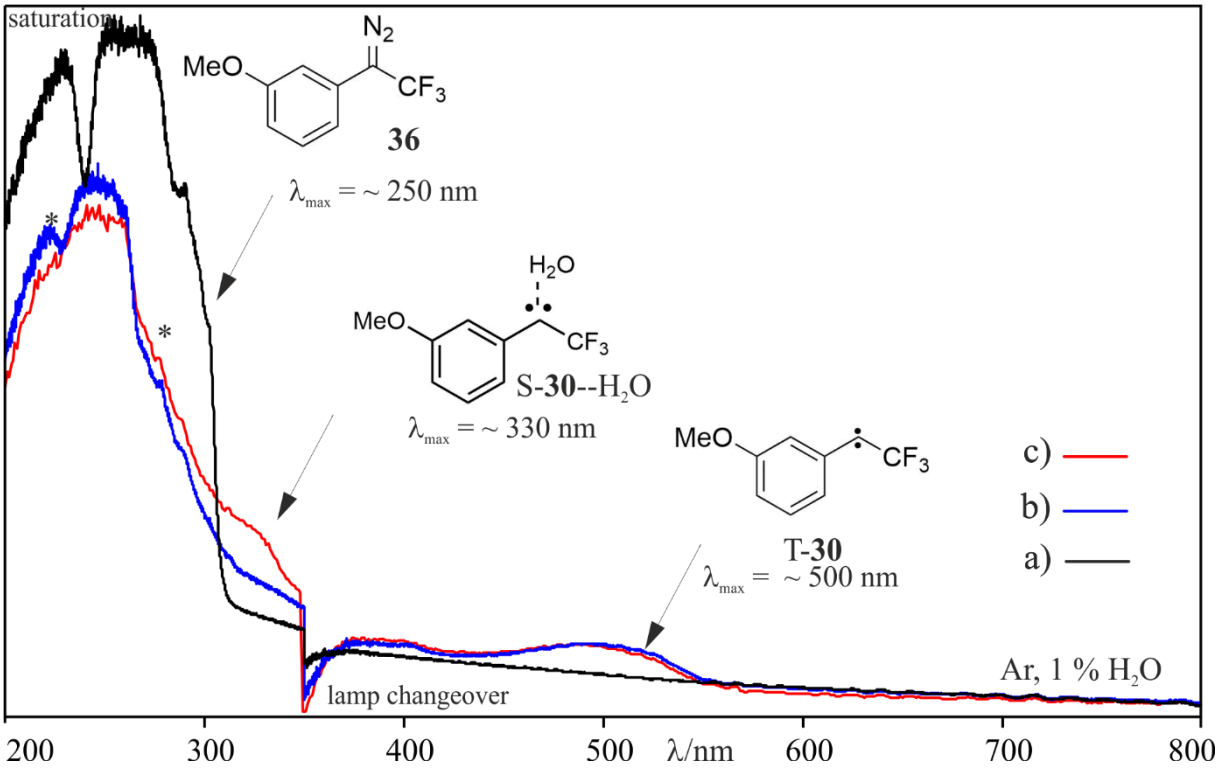

Figure **74:** a) UV-vis spectrum obtained after deposition of **36** with an excess of argon doped with 1 % of water. b) UV-vis spectrum obtained after photolysis of **36** and c) after subsequent annealing to 25 K. * Signals assigned to **38**.

In another analogous experiment, the secondary photochemistry of S-**30**--H_2O was studied. In Figure 75 the UV-vis spectrum of T-**30** and the annealing induced complexation to obtain the spectrum of S-**30**--H_2O are shown. Insertion product **38** is formed in small amounts during annealing as well. During subsequent photolysis with 365 nm light, the signal at ~330 nm decreases and absorptions at 270 and 277 nm increase, these signals could be assigned to OH insertion product **38** by comparison to a separate UV-vis spectrum of **38** in argon at 3 K.

2.5. m-Methoxyphenyl-1-(trifluoromethyl)carbene

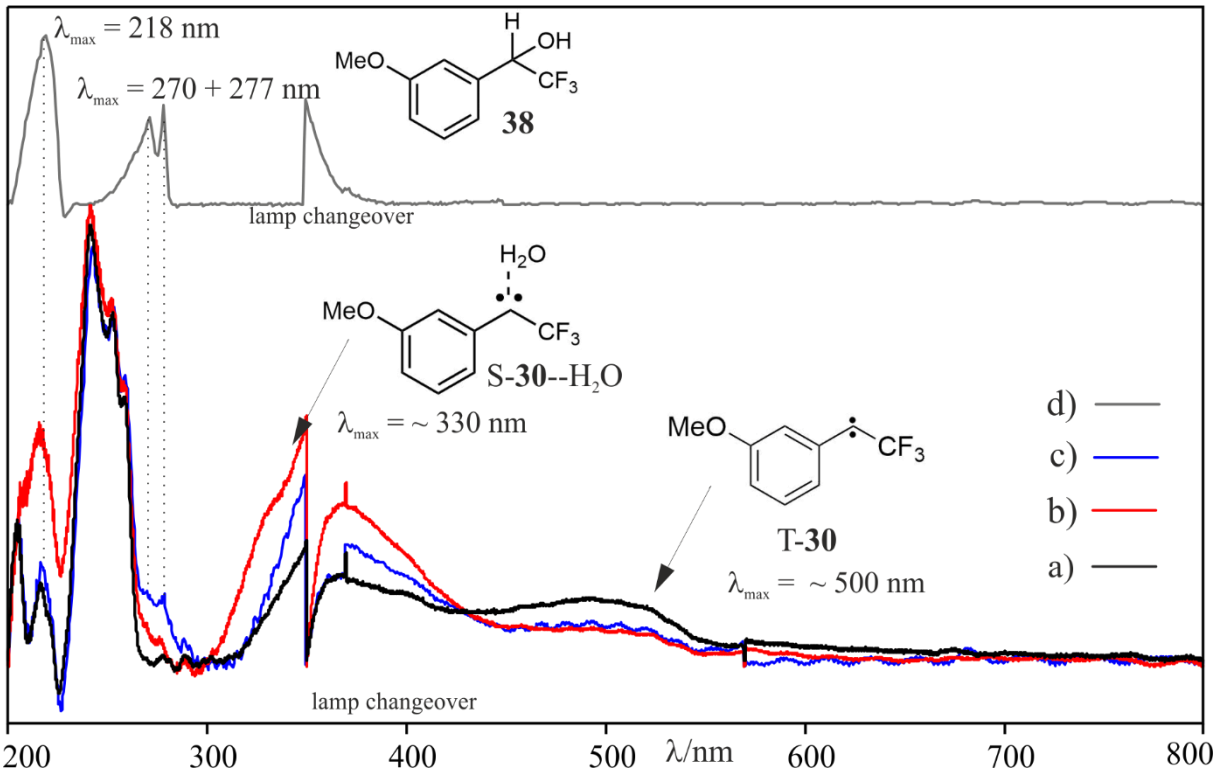

Figure **75:** UV experiment of **30** in in argon doped with 1 % of water. a) UV-vis spectrum obtained after photolysis of **36**. b) UV-vis spectrum obtained after subsequent annealing to 25 K and c) after subsequent 365 nm photolysis and d) UV-vis spectrum of **38** isolated in argon at 8 K.

To validate the findings of the UV-vis experiment, an EPR experiment was conducted in a similar way. An EPR spectroscopic study can be helpful to observe the conversion of a triplet to a singlet species. After the deposition of **36** and argon doped with 1 % of water on the tip of a cooled copper rod, precursor **36** was photolyzed and the EPR spectra shown in Figure 76 was obtained. The obtained signals match the reported ones of T-**30** with |D/hc| and |E/hc| values of 0.519 and 0.030 cm^{-1}, also smaller signals at |D/hc|=0.532 and |E/hc|=0.031cm^{-1}, potentially arising from another conformer of T-**30**, are visible.[48] The spectrum obtained after annealing and subsequent cooling back to 3 K are showing a decrease of the signals of T-**30**. This underlines the findings from the UV-vis experiment and indicates that an interaction of T-**30** and water results in the formation of an EPR silent hydrogen-bonded singlet complex S-**30**--H_2O.

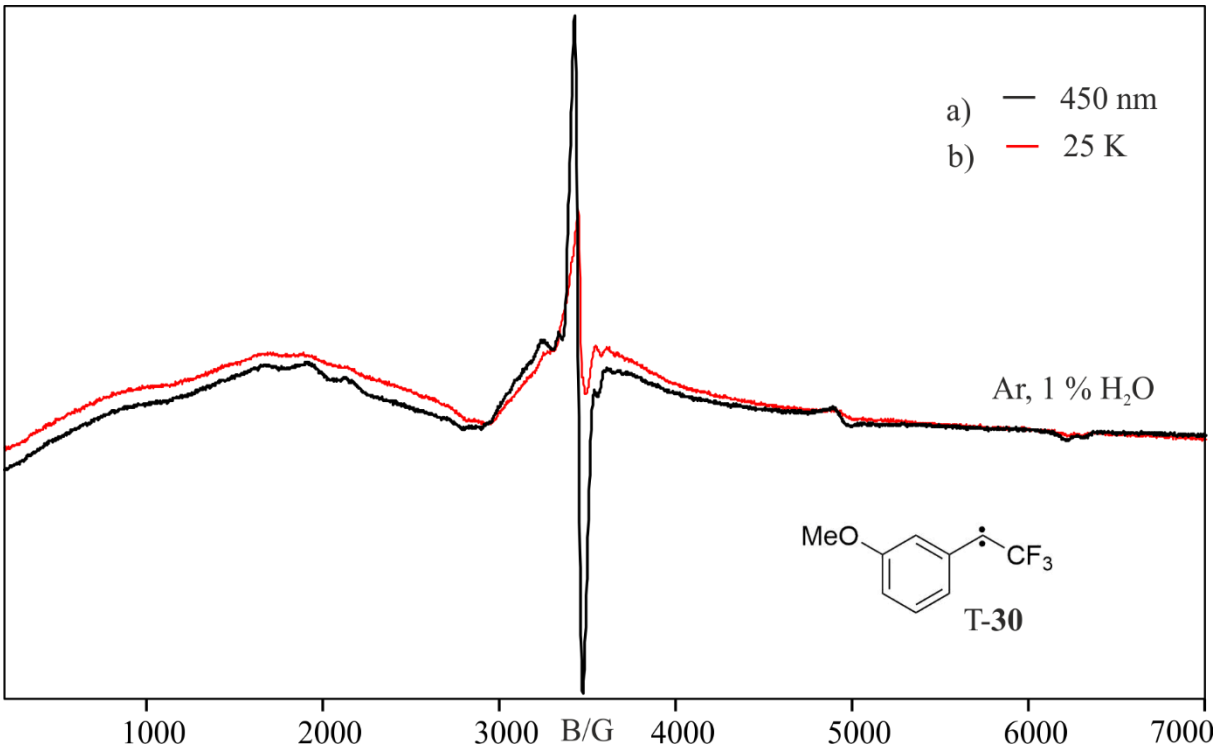

Figure **76:** EPR spectra showing a decrease of signals assigned to T-**30**. Obtained a) before and b) after annealing a matrix containing T-**30** and 1 % water in argon. The strong signal at ~3500 B can be traced back to radicals, which appeared after photolysis of **36**. The other decreasing signals were assigned to T-**30**.

Congruently to the UV-vis and EPR experiments, the reaction of T-**30** and 1 % of H_2O was also studied using IR spectroscopy. Therefore, **36** was deposited on a CsI window at 3 K and then irradiated with 450 nm light overnight to generate T-**30**. The obtained IR spectra are shown in Figure 77. Some additional signals obtained after irradiation can be assigned to insertion product **38**, like also observed in the UV-vis experiment. Subsequent annealing to 25 K and cooling back to 3 K gave only slight changes in the IR spectrum. The corresponding IR difference spectrum shows the decrease of the signals assigned to T-**30** and water and an increase of some new signals. A comparison of the newly formed signals to insertion product **38** was used to separate those from others (Figure 78). An accurate assignment was not possible due to the weak signals. Congruently to the UV-vis experiment, the matrix was subsequently photolyzed with 365 nm. In Figure 78 the obtained IR difference spectrum shows very weak decreasing signals, which may show reasonable agreement to the calculated IR vibrations of S-**30**--H_2O (uu+du+du+dd). The increasing signals obtained after 365 nm photolysis, match nicely to the IR spectrum of **38**, independently synthesized, characterized and isolated in argon at 3 K. The IR experiment corroborates the UV-vis experiment and suggests that S-**30**--H_2O is generated after annealing of T-**30** with H_2O. S-**30**--H_2O is photolabile and forms insertion product **38** during irradiation.

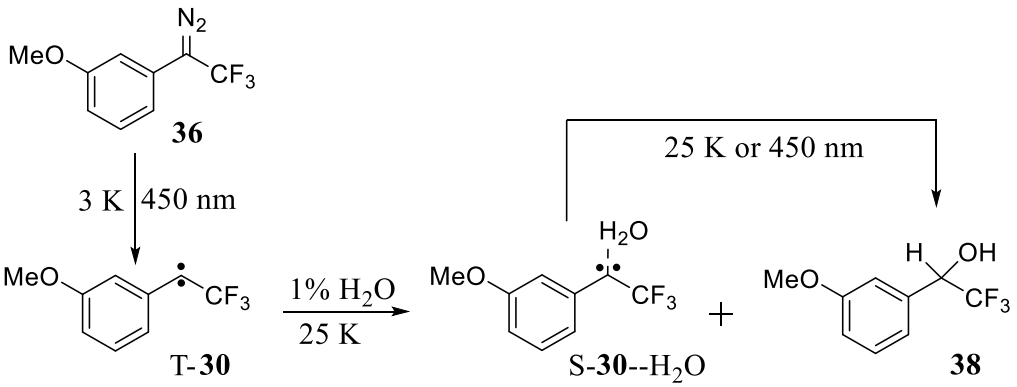

Scheme **38:** Generation and the observed reaction of T-**30** with 1 % of water.

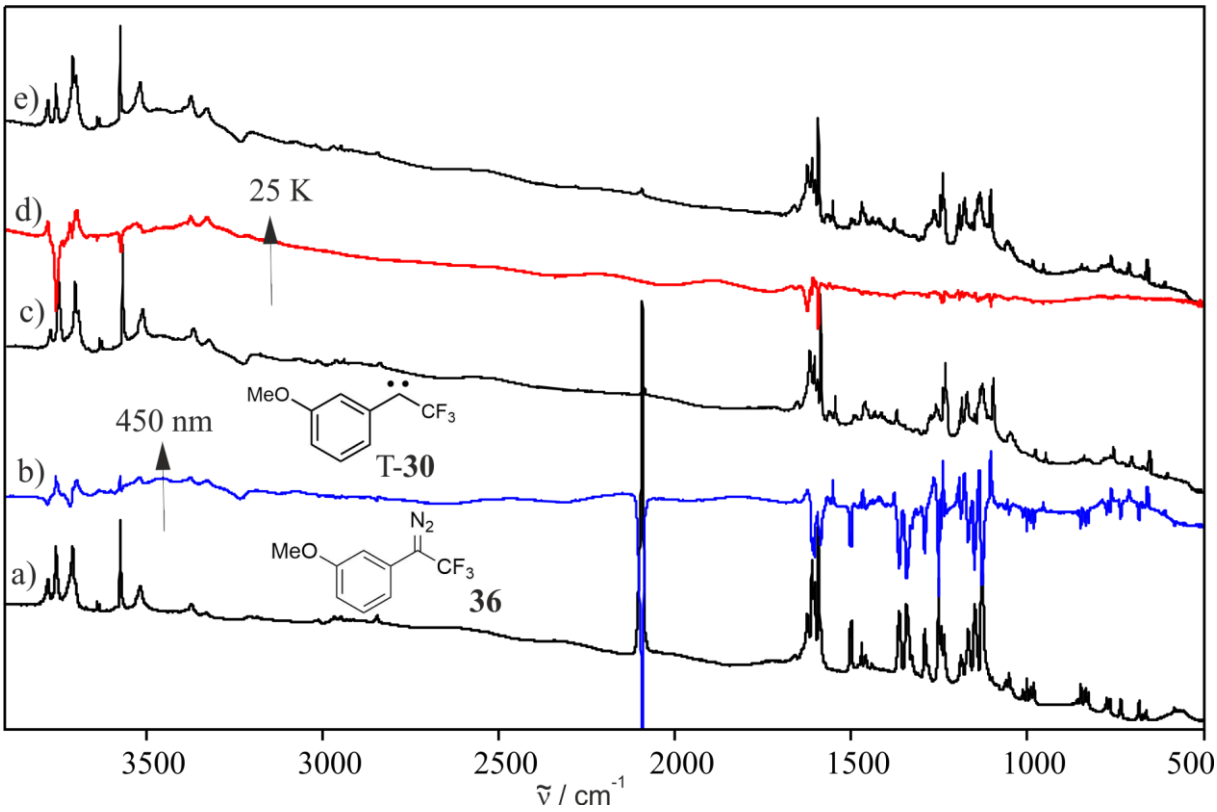

Figure **77:** Photolysis and subsequent annealing of a matrix containing 1 % of water and T-**30**. a) IR spectrum obtained after photolysis of **36** at 3 K. b) IR difference spectra obtained after photolysis and c) the corresponding IR spectrum. d) IR difference spectrum obtained after subsequent annealing to 25 K. Bands pointing upwards increase in intensity. Bands pointing downwards decrease in intensity. e) The corresponding absolute IR spectrum.

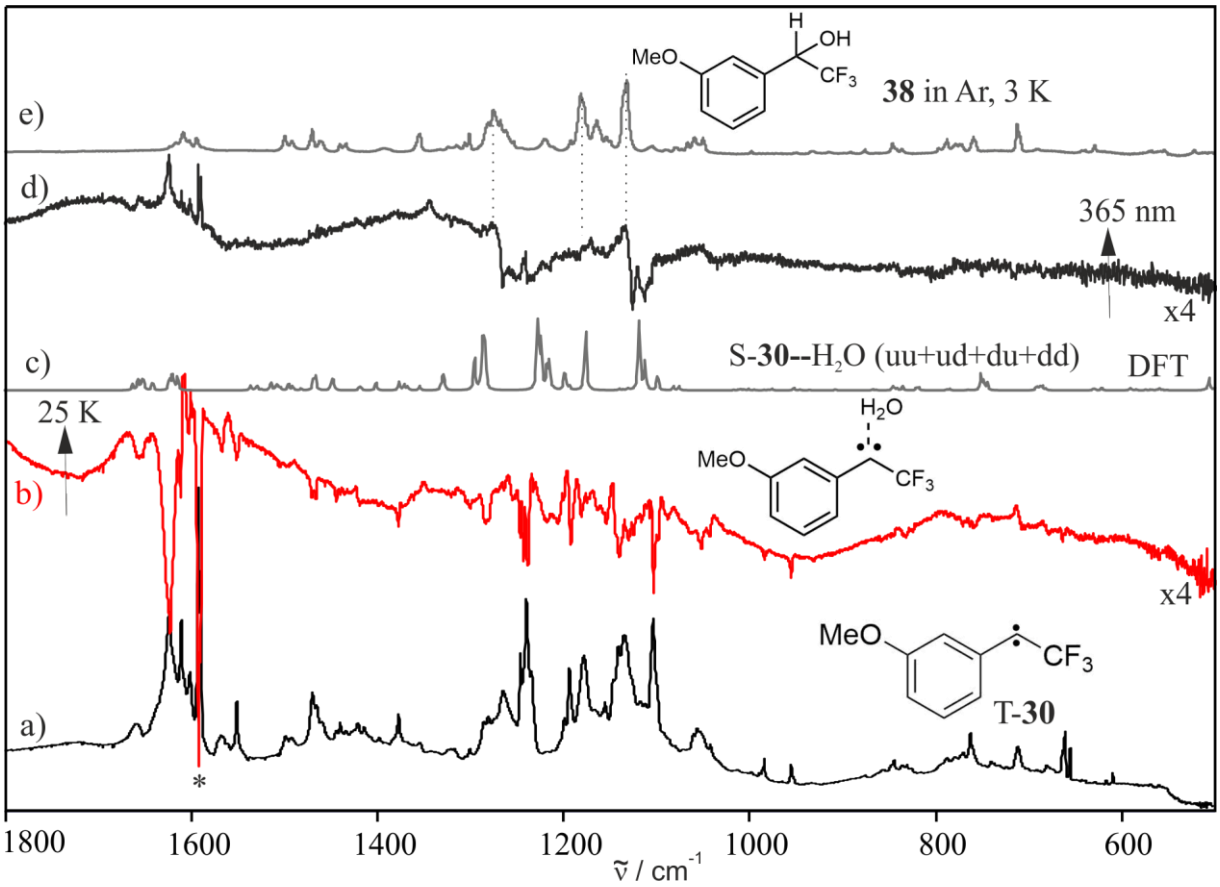

Figure **78:** IR-spectra showing the thermal reaction of H_2O and **30** in an argon matrix. a) IR spectrum obtained after irradiation of **36** in 1 % of H_2O with 450 nm to generate carbene T-**30**. b) IR difference spectrum obtained after annealing of T-**30** and 1 % H_2O to 25 K. Bands pointing upwards increase in intensity. Bands pointing downwards decrease in intensity and were assigned to carbene T-**30** and H_2O. c) Calculated IR spectrum of S-**30**--H_2O (uu+ud+du+dd) at M06-2x/Def2-TZVP//B3LYP/Def2-TZVP level of theory. d) IR difference spectrum obtained after 365 nm irradiation. e) IR spectrum of **38** in argon at 3 K. * Signal caused by H_2O. ^{x} represents a magnified difference spectrum.

2.5.2.3. DFT-Calculations

The complexation of carbene **30** with one molecule of water was investigated computationally to confirm the experimental results. At B3LYP-D3/Def2-TZVP level of theory the S-T gap of the most stable conformer T-**30**uu was computed to -4.09 kcal mol^{-1} relative to S-**30**uu. To investigate the interaction with water, both complexes were computed with one molecule of water attached to the carbene center. Whereas the triplet state of **30** only forms a weak van der Waals complex (C–H distance of 2.81 Å), the basic singlet state interacts by formation of a hydrogen-bonded complex with a C–H distance of 1.98 Å. As shown in Scheme 39, the complexation with H_2O results in a stabilization of the singlet state by 1.23 kcal mol^{-1} relative to T-**30**--H_2O. This corroborates the experimental results.

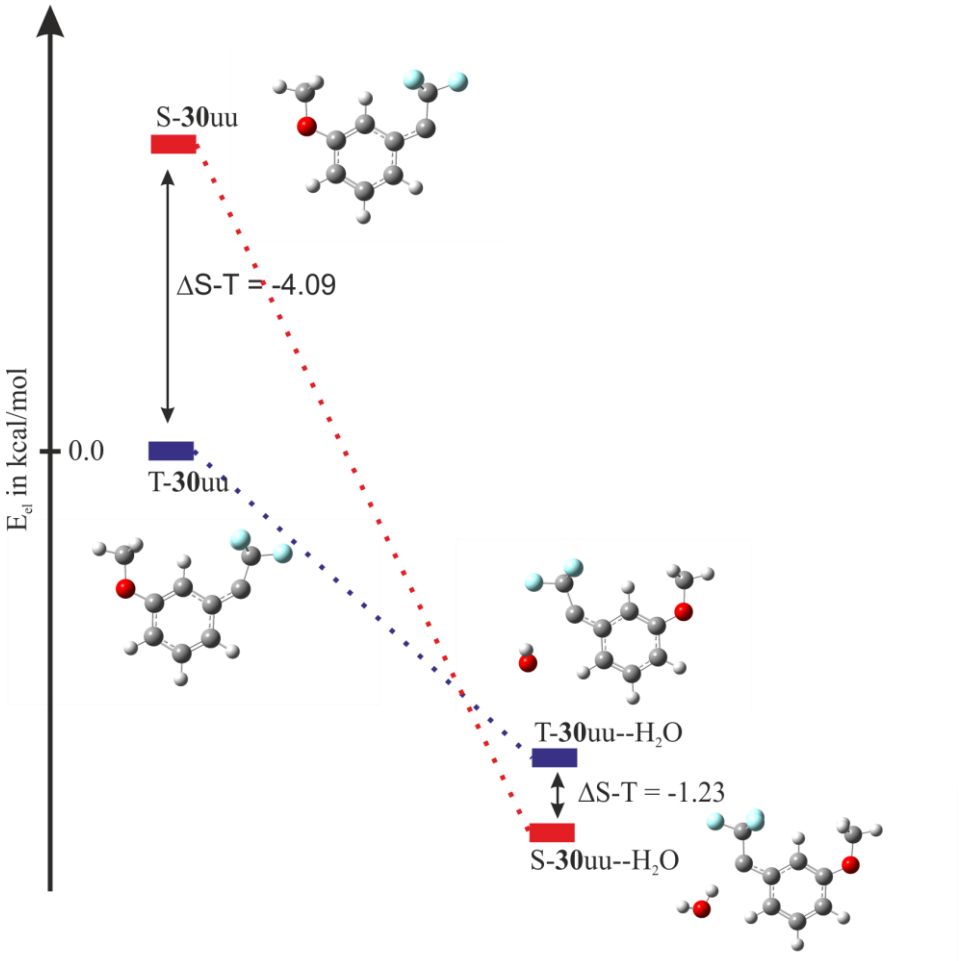

Scheme **39:** Relative energies of T-**30**uu and S-**30**uu and their complexes with water. Calculated at BLYP/Def2-TZVP level of theory, ZPVE included.

The reaction pathway of the rearrangement of S-**30**uu--H_2O to OH insertion product **38** was computed at the B3LYP/Def2-TZVP level of theory and shows that the reaction has to overcome a transition state which lies above the hydrogen-bonded complex by 5.7 kcal mol^{-1}

(Figure 79). The final product **38** is thermodynamically stabilized by -50 kcal mol^{-1} compared to S-**30**uu--H_2O.

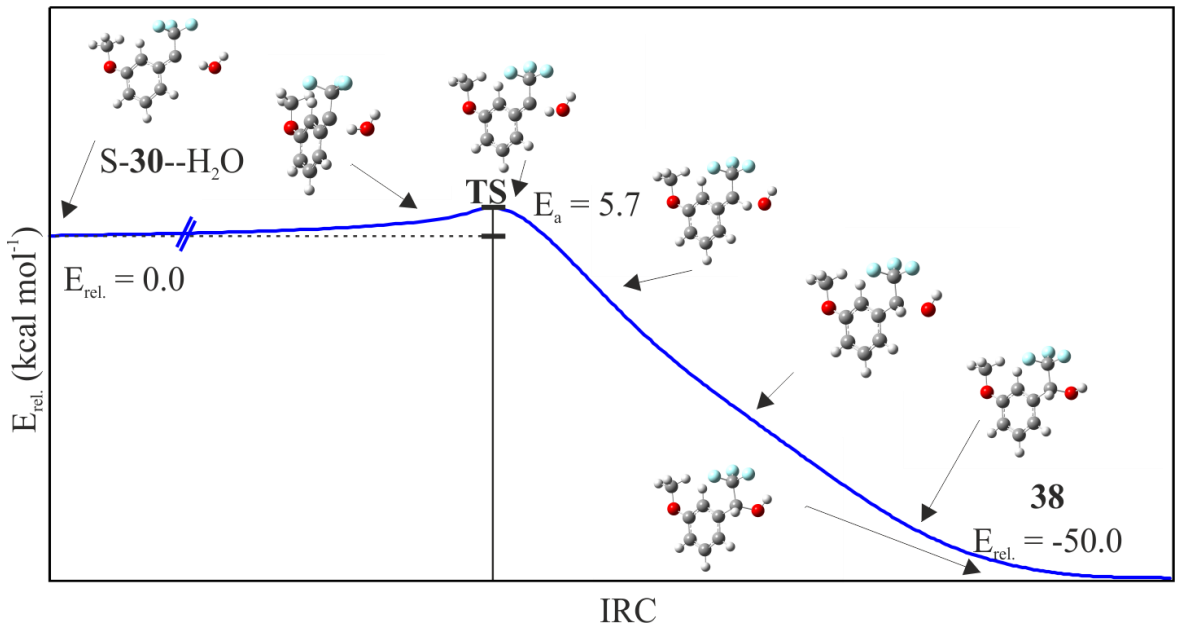

Figure **79:** Intrinsic reaction coordinate for the rearrangement of the complex S-**30**--H_2Ouu to **38** calculated at the BLYP/Def2-TZVP level of theory. Energies in kcal mol^{-1}. The activation barrier was calculated with separate structures at the BLYP-D3/Def2-TZVP level of theory.

2.5.2.4. Conclusions

To get information on the annealing controlled reaction of T-**30** with water, triplet carbene T-**30** was isolated in H_2O-doped argon matrices at 3 K. UV-vis, EPR and IR spectroscopy suggest the formation of singlet complex S-**30**--H_2O after annealing to 25 K. This formation can be explained by intersystem crossing from the triplet to singlet state induced by the complexation with H_2O. This assumption is supported by calculations showing a thermodynamic stabilization of the singlet state with water compared to a complexation in the triplet state. Previous experiments with other triplet carbenes showed that a spin-flip occurs for carbenes with small S-T gaps.[4, 12, 13] DFT calculations suggest a thermodynamically preference of the hydrogen-bonded singlet complex S-**30**--H_2O compared to the triplet complex T-**30**--H_2O by 1.23 kcal mol^{-1}.

2.5.3. Direct reaction with water in solid water

2.5.3.1. Introduction

See Chapter 2.1. for a more detailed introduction. Carbene T-**30** is not expected to form a stable carbocation in LDA water ices due to its computed low proton affinity. With a PA of -250.93 kcal mol^{-1} (B3LYP-D3/6-311+G(d,p)) it may show a comparable behavior in LDA water ice like triplet β-trifluoromethyl carbene **50**. For **50** with a PA of -253.60 kcal mol^{-1} no cationic species was observed after photolysis of the precursor under similar conditions. Instead the OH insertion product was formed directly, no other species apart from traces of singlet carbene S-**50** (or the complex S-**50**--H_2O) could be detected with UV-vis and IR spectroscopy.[28]

2.5.3.2. Results and discussion

Precursor **36** was co-deposited with an excess of water at 50 K and subsequently cooled to 9 K. **36** was irradiated with 450 nm light overnight and the obtained UV-vis spectra before and after photolysis are shown in Figure 80. By comparison to a UV-vis spectrum of alcohol **38** in argon at 3 K, most of the obtained signals could be assigned to **38**. A broad signal at 330 nm may be assigned to remaining complex S-**30**--H_2O. Overall, the experiment shows the expected reactivity similar to **50** in LDA water ice[28] and no cationic species could be detected.

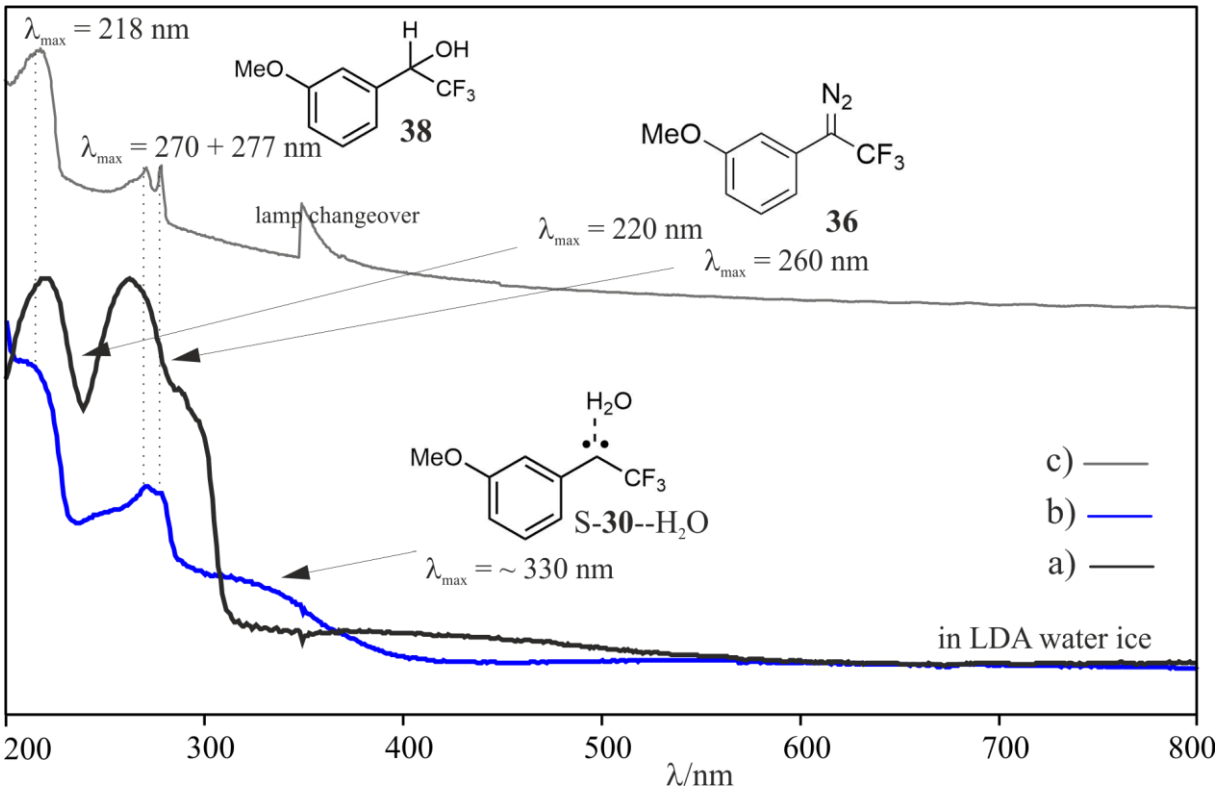

Figure **80:** a) UV-vis spectrum obtained after deposition of **36** with LDA water ice at 9 K and b) after subsequent photolysis. c) UV-vis spectrum of **38** isolated in LDA water ice at 9 K.

To support the findings from the UV-vis experiment of **36** in low density amorphous water ice, the experiment was conducted similarly and observed with IR spectroscopy. The IR spectra obtained after deposition of **36**, and subsequent photolysis are shown in Figure 81. The IR signals of **36** are very similar to the one in argon, except of the usual broadening of the signals in LDA ices. After irradiation of **36** new signals appeared for example at 1604, 1255 and a very broad one at 1150 cm^{-1}. A comparison to an IR spectrum of insertion product **38** in argon at 3 K shows a good agreement. During secondary photolysis and annealing no changes in the IR spectra were observed.

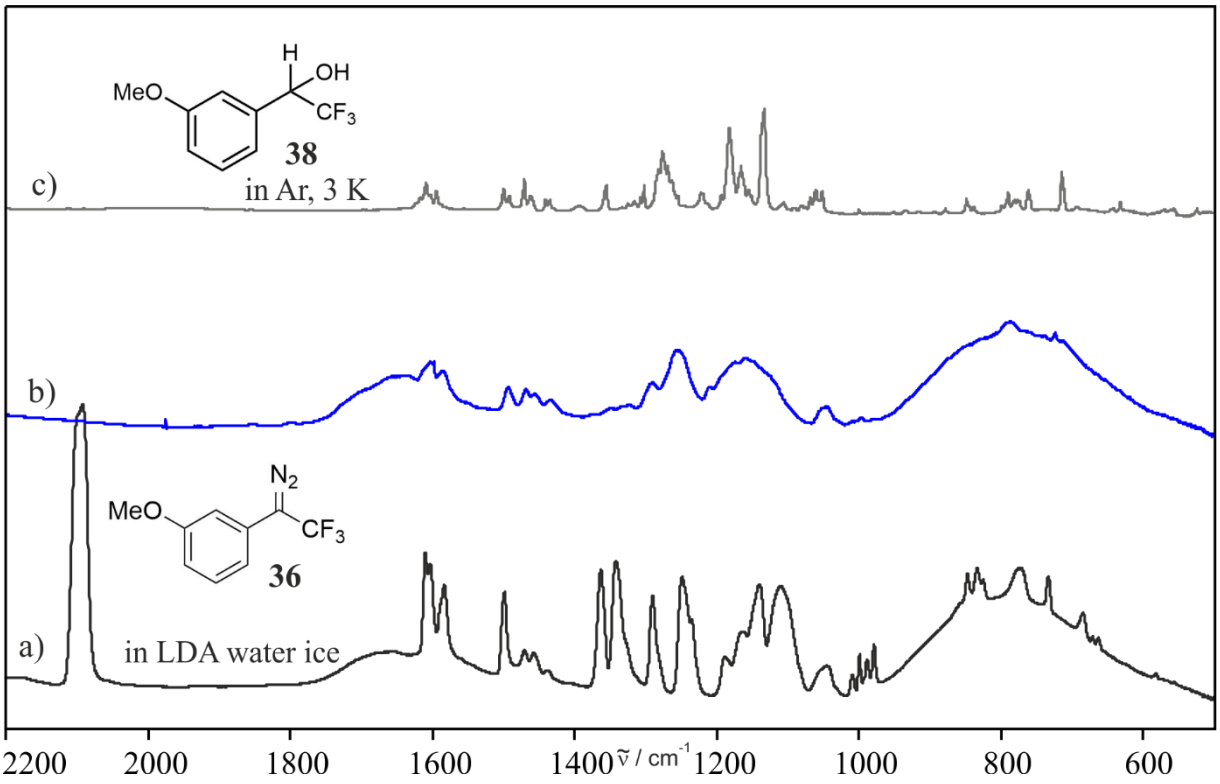

Figure **81:** a) IR spectrum obtained after deposition of **36** in LDA water ice at 9 K and b) obtained after subsequent 450 nm photolysis overnight. c) IR spectrum of **38** in argon at 3 K.

2.5.3.3. Conclusions

In this Chapter the direct reaction of carbene **30** with H_2O was investigated. The results obtained from UV-vis and IR experiments of **36** in low density amorphous water ice are summarized in Scheme 40 a). The photolysis of **36** in water ice did not result in IR or UV-vis signals assignable to T-**30**, but in a directly formed OH insertion product **38**. Alcohol **38** was assigned by comparison to the IR spectrum of an independently synthesized reference. The direct formation of the insertion product is similar to previous experiments of **56** in LDA water ice Scheme 40 b). Traces of singlet S-**30** e.g. S-**30**--H_2O were detected via UV-vis spectroscopy. The singlet carbene formation may be reasoned by a spin switching from the triplet state to singlet as demonstrated in the previous experiments in H_2O-doped argon matrices (Chapter 2.5.2.). Another explanation would be a reaction of the transient hot singlet state, which is initially formed after photolysis of the precursor and reacts directly with the water molecules nearby. Overall, the results are consistent with the expectation that a pull-pull substitution accompanied with a low PA, as calculated for carbene **30**, does not produce observable cations in amorphous water ices.

2.5. m-Methoxyphenyl-1-(trifluoromethyl)carbene

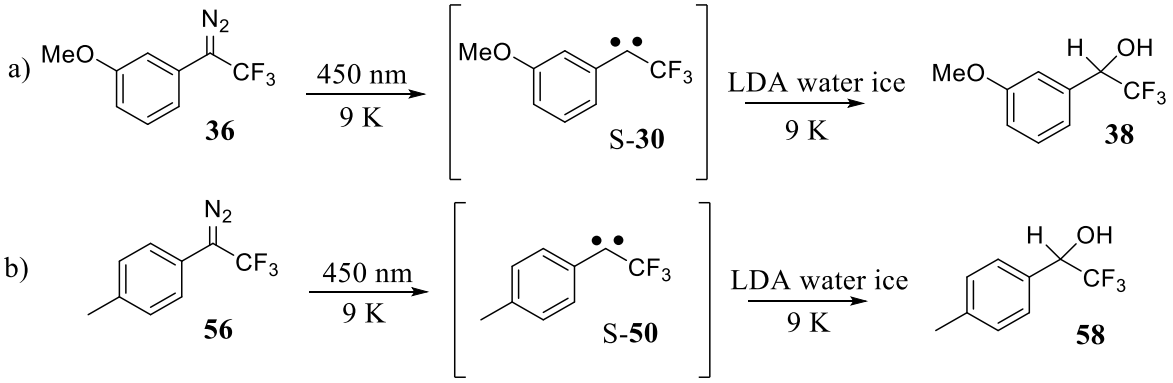

Scheme **40:** Photolysis of a) **36** in LDA water ice and b) of **56** in LDA water ice.[28]

By comparing the experimental results of trifluoromethyl carbene **30** to the results of related carbenes **1** and **20**, it may be assumed that the destabilization of α-fluorinated cations can be overcome by the use of resonance stabilizing groups such as *para*-methoxyphenyl or *para*-dimethylaminophenyl. In this work, matrix isolation experiments demonstrate that, with a push substitution counteracting the pull effect of CF_3, observable cations can be stabilized and observed in LDA water ice matrices or in argon matrices.

3. Experimental part

3.1. Instrumentation

3.1.1. Matrix Isolation

Matrix isolation experiments were performed according to the standard techniques as described in literature.[21] To achieve temperatures from 10 K to 4 K, Air Products Diplex close-cycle helium refrigerator systems (10 K) or Sumitomo Heavy Industries closed-cycle helium refrigerator systems (4 K) were used. High vacuum (10^{-5} to 10^{-7} mbar) was achieved with rotary vane pumps in combination with diffusion pumps or turbomolecular pumps. Matrices were deposited on a cooled cesium iodide disk (IR), a sapphire disk (UV-vis) or a copper rod (EPR). Gas used for matrix isolation was argon (Air Liquide, 99.999 %). For trapping experiments H_2O, D_2O, MeOH, NH_3 (1 % in argon (Airgas)) and ND_3 (Sigma Aldrich, 99%) were used. Liquids like H_2O, D_2O and MeOH were degassed multiple times before use. For the deposition of **6** and **36**, the corresponding sodium salts **5** or **35** were thermolyzed with a sublimation oven or a water bath at 45 °C, to generate **6** or **36**, respectively. The diazo compounds were subsequently deposited on a cold matrix window together with the host gas. Deposition times varied between 15 min for UV-vis and EPR experiments up to 60 min for IR spectroscopy. **26** was directly deposited together with the matrix host on the cold window. As **26** was extremely volatile, the sample had to be cooled with nitrogen before deposition (see Picture **1**). For purification and drying of **26**, multiple degassing cycles were performed directly at the matrix apparatus. **26** was deposited for 20 minutes (UV-vis) up to 50 minutes (IR) at 18 °C. Insertion products **8**, **8a** as well as **28a** and **38** were deposited at room temperature for 30 minutes for the experiment in an argon matrix and LDA ice and for 15 minutes for the UV-vis and the EPR experiment. The temperature of the cold window was for argon matrices during deposition at 20 K and for doped matrices at the coldest possible temperature (3 K for IR and 8 K for UV-vis). To generate a transparent LDA water ice matrix the temperature during deposition was set to 50 K and cooled to the coldest achievable temperature afterwards. The gas flow was controlled by a MKS mass flow controller.

3.1.2. Light sources

Light sources used in this work were LEDs with different wavelengths (650 – 365 nm) and a cold cathode low pressure mercury lamp (PenRay) with 254 nm for UV irradiation.

3.1.3. IR, UV-vis, and EPR Spectroscopy

Matrix-isolation IR spectra were recorded with a Bruker IFS66, a Bruker IFS66s and a Bruker Vertex V70 FTIR spectrometer (resolution of 0.5 cm^{-1}). Matrix-isolation UV/vis spectra were taken with a Varian Cary 5000 spectrometer with a resolution of 0.2 nm. The EPR spectra were recorded with a Bruker ELEXSYS 500 X-band spectrometer. To measure and to evaluate the IR and UV-vis spectra the software OPUS by Bruker Company was used.

3.1.4. Nuclear magnetic resonance spectroscopy (NMR) and mass spectrometry (MS)

^{1}H and ^{13}C spectra were recorded on a Bruker DPX-200 spectrometer. NMR shifts are reported in parts per million (ppm) and referenced with respect to the solvent signal ($CDCl_3$ or DMSO-d_6). Signal multiplicities are reported as singlet (s), doublet (d), doublet of doublets (dd), triplet (t) or multiplet (m). The analysis was performed with MestreNova by Mestrelab Research S.L. Mass spectrometric analysis was recorded on Varian MAT-CH5 spectrometer at 70eV EI.

3.2. Calculations

The calculations were performed using Becke's three-parameter hybrid functional[136] and the correlation functional of Lee, Yang and Parr (B3LYP).[137] For geometry optimizations and for energy estimations, the Pople basis set 6-311+G(d,p)[138] or Karlsruhe basis set Def2-TZVP[139] were used. For the calculation of the IR vibrations the Minnesota functional M06-2x[140] was used without geometry optimizations with the structures obtained with B3LYP/Def2-TZVP as an input, as explained in Chapter 2.2.. The preliminary structures were drawn with *Gaussian View 5.0 for Windows*[141] and the geometries (bond lengths and angles) are shown using the software Diamond.[142] Grimme 3 (D3) optimization was used for all calculations,[143] and the zero point energies were included. The calculations were carried out using a cluster running on Linux software.

3.3. Synthesis

All starting materials and reagents were purchased from commercial supplies and used without further purification. The solvents were purified by standard procedures.

3.3.1. *p*-methoxyphenyl-1-trifluoromethyldiazomethane 6

was synthesized in a 4-step synthesis starting with *p*-(methoxy)bromobenzene.

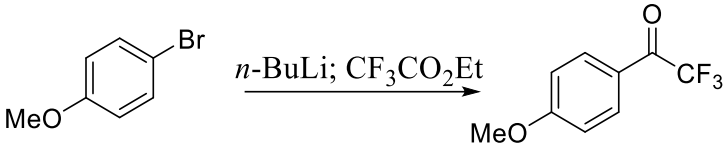

***p*-methoxy-2,2,2-trifluoroacetophenone** was either synthesized according to a literature procedure[144] or purchased from commercial suppliers. Exhibited spectral data identical to a previous report. **Yield:** 38 % as a colorless, aromatically smelling oil. **Molecular Weight:** 204.15 g/mol. **^{1}H-NMR** (200 MHz, $CDCl_3$): δ 8.06 (d, *J* = 8.6 Hz, 2H, arom-C**H**), 7.00 (d, *J* = 8.9 Hz, 2H arom-C**H**), 3.91 (s, 3H, C**H**$_3$). **MS** (EI): (m/z) 204.03 [M+].

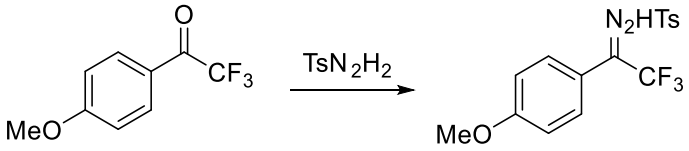

***p*-methoxy-2,2,2-trifluoroacetophenone-*p*-tosylhydrazone** was synthesized according to a literature procedure.[144] Exhibited spectral data identical to a previous report. **Yield:** 69 % as yellow crystals. **Molecular Weight:** 372.36 g/mol. **^{1}H-NMR** (200 MHz, $CDCl_3$): δ 8.01 (d, 2H, arom-C**H**), 7.02 (d, 2H arom-C**H**), 3.91 (s, 3H, C**H**$_3$). **^{13}C-NMR** (50 MHz, $CDCl_3$): δ 161.96, 145.03, 138.83, 135.67, 129.97, 129.21, 128.16, 124.88, 120.26, 115.57, 55.64, 21.84.

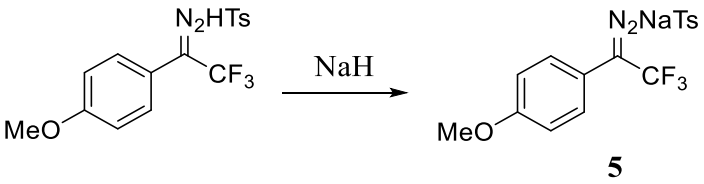

5

Sodium *p*-methoxy-2,2,2-trifluoroacetophenone-*p*-tosylhydrazonide 5 was prepared by deprotonation of the corresponding tosylhydrazone (1 eq) with sodium hydride (NaH) (1.5 eq). NaH was purchased as a dispersion in 60 % mineral oil. To remove the mineral oil, NaH was washed three times with dry pentane. Then *p*-methoxy-2,2,2-trifluoroacetophenone-*p*-tosylhydrazone in 40 ml of dry DCM was added and stirred for three hours at room temperature.

The solvent was removed in vacuo and the crude product **5** was used for the next step without further purification. **Yield:** 82 % of a yellow-orange salt. **Molecular Weight:** 394.34 g/mol. **^{1}H-NMR** (200 MHz, DMSO-d_6) δ 7.62 (d, *J* = 8.7 Hz, 4H, arom-C**H**), 7.55 (d, *J* = 8.1 Hz, 2H, arom-C**H**), 7.19 (d, *J* = 8.1 Hz, 2H, arom-C**H**), 6.90 (d, *J* = 8.9 Hz, 3H, C**H**$_3$). **^{13}C-NMR** (50 MHz, DMSO-d_6)**:** δ 158.02, 151.92, 146.80, 142.60, 139.09, 129.84, 128.32, 126.59, 123.73, 112.97, 55.02, 20.84.

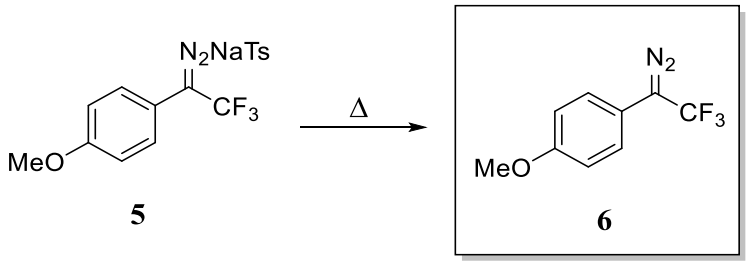

5 **6**

***p*-methoxyphenyl-1-trifluoromethyldiazomethane** **6** was synthesized by thermal decomposition (50 °C) of **5** under reduced pressure and directly used for matrix isolation experiments. The red oil was characterized by ^{1}H-NMR-spectroscopy and matrix isolation IR and UV spectroscopy. Exhibited spectral data identical to a previous report.[145] **Yield:** 23 % of a red volatile oil. **Molecular Weight:** 216.16 g/mol. **^{1}H-NMR** (200 MHz, $CDCl_3$): δ 6.99 (d, *J* = 8.9 Hz, 2H, arom-C**H**), 6.89 (d, *J* = 8.7 Hz, 2H, arom-C**H**), 3.75 (s, 3H, C**H**$_3$). **^{13}C-NMR** (50 MHz, $CDCl_3$): δ 158.45, 132.45, 124.60, 115.33, 114.89, 114.17, 55.54. **IR** (Ar, 3 K): cm^{-1} 2960, 2943, 2918, 2843, 2085 (N=N), 1619, 1520, 1469, 1440, 1358, 1347, 1316, 1294, 1256, 1176, 1150, 1125, 1048, 1013, 963, 960, 823, 799, 735, 640, 621, 609, 521. **UV-vis** (Ar, 3 K): nm 205, 266, 311.

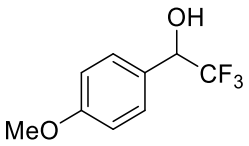

8

3.3.2. 2,2,2-Trifluoro-1-(4-methoxyphenyl)ethanol 8 was obtained as a side product in the synthesis of *p*-methoxy-2,2,2-trifluoroacetophenone and purified by column chromatography (petrolether:EtOAc (1:1.5)). Exhibited spectral data identical to a previous report.[145] **Yield:** 18 % of a colorless oil. **Molecular Weight:** 206.16 g/mol. **^{1}H-NMR** (200 MHz, $CDCl_3$): δ 7.38 (s, 2H, arom-C**H**), 6.93 (d, *J* = 8.9 Hz, 2H, arom-C**H**), 5.07 – 4.86 (qd, *J* = 6.7, 4.4 Hz, 1H, C**H**), 3.82 (s, 3H, C**H**$_3$). **^{13}C-NMR** (50 MHz, $CDCl_3$): δ 160.63, 128.91, 127.19, 126.20, 114.19, 72.51, 55.46. **IR** (Ar, 3 K): cm^{-1} 2919, 2901, 2842, 1626, 1520, 1471, 1356, 1326, 1309, 1280, 1258 (m), 1219, 1174 (i), 1131 (m), 1083, 1042, 866, 853, 819, 804, 778, 694, 590, 576, 529. **UV-vis** (Ar, 3 K): nm 223, 270, 278, 296.

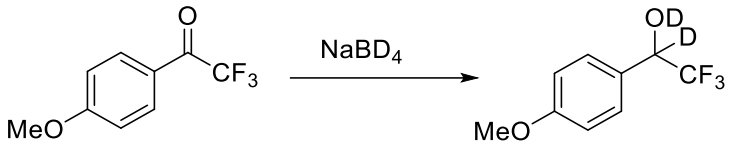

d-**8**

3.3.3. 2,2,2-trifluoro-1-(*p*-methoxyphenyl)ethanol-d2 d-**8** was synthesized as follows: *p*-methoxy-2,2,2-trifluoroacetophenone (0.337 g) was dissolved in 7 ml THF and sodium borodeuteride ($NaBD_4$) (0.069 g) was added at 0 °C. After 15 minutes at 0°, the mixture was stirred for 1.5 hours at room temperature. Then D_2O was added, followed by extraction, filtration and evaporation of the ether. **Yield:** 77 % as a colorless oil. **Molecular Weight:** 219.2 g/mol. **^{1}H-NMR** (200 MHz, $CDCl_3$): δ 7.37 (d, *J* = 8.5 Hz, 2H, arom-C**H**), 6.90 (d, *J* = 8.9 Hz, 2H, arom-C**H**), 3.79 (s, 3H, C**H**$_3$). **^{13}C-NMR** (50 MHz, $CDCl_3$): δ 160.38, 128.89, 126.58, 121.79, 114.05, 71.75, 55.31. **IR** (Ar, 3 K): cm^{-1} 2963, 2911, 2842, 2683, 1621, 1594, 1515, 1469, 1460, 1312, 1289, 1257 (m), 1213 (m), 1167 (i), 1125, 1100, 1061, 1046, 997, 840, 805, 684, 567, 528.

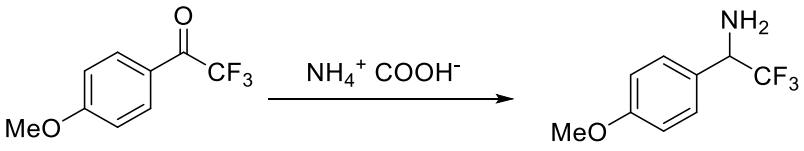

8b

3.3.4. *p*-methoxyphenyl(trifluoromethyl)methanamine 8b was synthesized according to a literature procedure.[146] *p*-methoxy-2,2,2-trifluoroacetophenone (2.4 mmol) and ammonium formiate (12.3 mmol) were stirred for 1.5 hours at 120 °C and three hours at 180 °C. Exhibited spectral data identical to the previous report. **Yield:** 55 % as a colorless oil. **Molecular Weight:** 205.2 g/mol. **^{1}H-NMR** (200 MHz, $CDCl_3$): δ 7.40 (d, *J* = 8.7 Hz, 2H, arom-C**H**), 6.93 (dd, *J* = 9.2, 2.5 Hz, 2H, arom-C**H**), 4.96 (q, *J* = 6.7 Hz, 1H, C**H**), 3.82 (s, 3H, C**H**$_3$). **^{13}C-NMR** (50 MHz, $CDCl_3$): δ 160.64, 128.93, 127.34, 126.42, 114.21, 72.91, 55.46.

3.3.5. *p*-dimethylaminophenyl-1-trifluoromethyldiazomethane 26

was synthesized in a 4-step synthesis starting with *p*-(dimethylamino)bromobenzene.

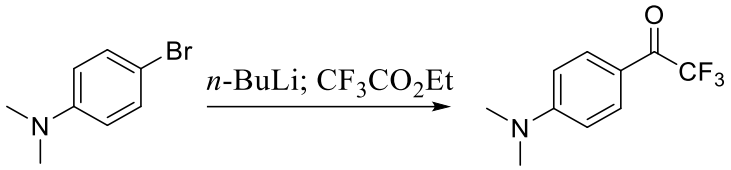

***p*-dimethylamino-2,2,2-trifluoroacetophenone** was either synthesized according to a literature procedure.[147] or purchased from commercial suppliers. Exhibited spectral data identical to the previous report. **Yield:** 43 % as yellow crystals. **Molecular Weight:** 217.2 g/mol. **^{1}H-NMR** (200 MHz, $CDCl_3$): δ 8.06 (d, *J* = 8.6 Hz, 2H, arom-C**H**), 7.00 (d, *J* = 8.9 Hz, 2H, arom-C**H**), 3.91 (s, 3H, C**H**$_3$). **MS** (EI): (m/z) 204.03 [M+].

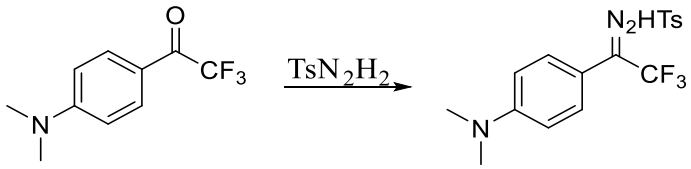

***p*-dimethylamino-2,2,2-trifluoroacetophenone-*p*-tosylhydrazone** was synthesized as follows: A mixture of *p*-toluenesulfone hydrazine (1.2 eq.) and 10 ml of dry ethanol, under argon, was heated up until it was completely solved. After cooling down to room temperature 1-(4-(dimethylamino)phenyl)-2,2,2-trifluoroethan-1-one (1.00 eq) was added and the mixture was heated up to 69 °C and stirred overnight. The solvent was evaporated and the received solid was recrystallized in ethanol. The crystals were washed with cold ethanol and dried. **Yield**: 46% as white crystals. **Molecular Weight:** 385.4 g/mol. **^{1}H-NMR** (200 MHz, DMSO-d_6) δ 8.02 (s, 1H, N**H**), 7.81 (d, *J* = 8.3 Hz, 2H, arom-C**H**), 7.33 (d, *J* = 8.0 Hz, 2H, arom-C**H**), 7.14 (d, *J* = 8.8 Hz, 2H, arom-C**H**), 6.73 (d, *J* = 8.9 Hz, 2H, arom-C**H**), 3.03 (s, 6H, C**H**$_3$), 2.45 (s, 3H, C**H**$_3$). **^{13}C-NMR** (50 MHz, $CDCl_3$): δ 151.99, 144.79, 143.07, 134.90, 129.87, 129.40, 128.14, 117.67, 112.37, 111.22, 40.14, 21.79.

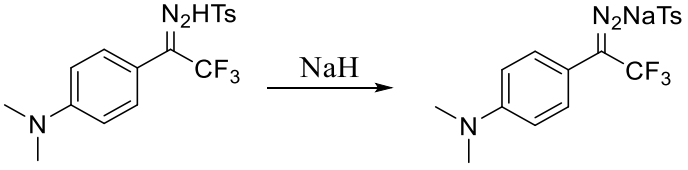

Sodium *p*-dimethylamino-2,2,2-trifluoroacetophenone-*p*-tosylhydrazonide was synthesized by deprotonation of the corresponding tosylhydrazone (1 eq) with sodium hydride (NaH) (1.5 eq.). NaH was purchased as a dispersion in 60 % mineral oil. To remove the mineral

oil, NaH was washed three times with dry pentane. Then *p*-dimethylamino-2,2,2-trifluoroacetophenone-*p*-tosylhydrazone in 40 ml of dry DCM was added and stirred for two hours at room temperature. The solvent was removed in vacuo and the crude product was used for the next step without further purification. **Yield:** 82 % of a yellow salt. **Molecular Weight:** 394.34 g/mol. **^{1}H-NMR** (200 MHz, DMSO-d_6) δ 8.31 (t, *J* = 7.9 Hz, 4H, arom-C**H**), 7.91 (d, *J* = 7.9 Hz, 2H, arom-C**H**), 7.41 (d, *J* = 9.1 Hz, 2H, arom-C**H**), 3.64 (s, 6H, C**H**$_3$), 3.04 (s, 3H, C**H**$_3$).

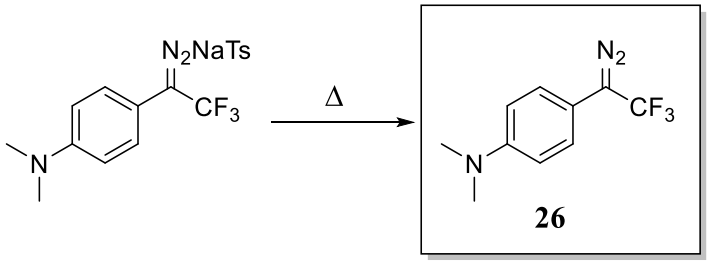

***p*-dimethylaminophenyl-1-trifluoromethyldiazomethane 26** was synthesized by thermal decomposition (70 °C) of sodium *p*-dimethylamino-2,2,2-trifluoroacetophenone-*p*-tosylhydrazonide under reduced pressure. **26** is very volatile and decomposes at room temperature. It was directly used for matrix isolation experiments. **Yield:** 20 % as a volatile red oil. **Molecular Weight:** 229.21 g/mol. **^{1}H-NMR** (200 MHz, DMSO-d_6): δ 7.34 (d, *J* = 7.8 Hz, 2H, arom-C**H**), 7.10 (d, *J* = 7.8 Hz, 2H, arom-C**H**), 2.91 (d, *J* = 1.7 Hz, 6H, C**H**$_3$). **UV-vis** (Ar, 3 K): nm 257, 290. **IR** (Ar, 3 K): cm^{-1} 2084 (i, N=N), 1624, 1533, 1491, 1452, 1443, 1364, 1351, 1339, 1296, 1243, 1233, 1182, 1171, 1155, 1138, 1124, 1066, 1011, 965, 948, 939, 808, 728, 605.

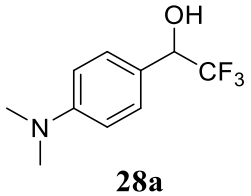

28a

3.3.6. 2,2,2-trifluoro-1-(*p*-dimethylaminophenyl)ethanol 28a was synthesized according to a literature procedure.[148] **Yield:** 89 % of a white powder. **Molecular Weight:** 219.2 g/mol. **^{1}H-NMR** (200 MHz, DMSO-d_6): δ 7.26 (d, *J* = 8.6 Hz, 2H, arom-C**H**), 6.71 (d, *J* = 8.8 Hz, 2H, arom-C**H**), 4.94 (q, *J* = 7.5 Hz, 1H, C**H**), 2.88 (s, 6H, C**H**$_3$). **^{13}C-NMR** (50 MHz, DMSO-d_6): δ 150.62, 128.23, 122.87, 122.44, 111.66, 70.40, 39.92. **^{19}F-NMR**: -78 ppm (without standard). **IR** (Ar, 3 K): cm^{-1} 3636, 2897, 2823, 1624 (m), 1574, 1533 (m), 1491, 1452, 1368, 1353, 1334, 1284, 1252, 1211, 1176 (i), 1169 (i), 1135 (m), 1125, 1081, 1065, 952, 864, 846, 808, 799, 749, 691, 574, 524.

3.3.7. *m*-methoxyphenyl-1-trifluoromethyldiazomethane 36

was synthesized in a 3-step synthesis starting with the ketone.

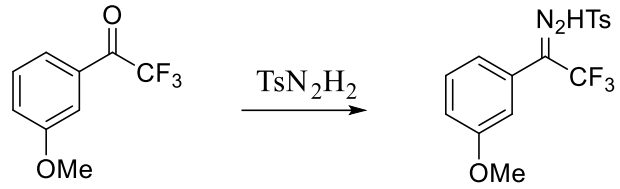

***m*-methoxy-2,2,2-trifluoroacetophenone-*p*-tosylhydrazone** was synthesized according to a literature procedure.[149] Exhibited spectral data identical to a previous report. **Yield:** 69 % as a white solid. **Molecular Weight:** 372.36 g/mol. **^{1}H-NMR** (200 MHz, DMSO-*d6*): δ 11.63 (s, 1H, N**H**), 7.72 (d, *J* = 8,2 Hz, 2H, arom-C**H**), 7.43 (m, J = 8,4 Hz, 3H, arom-C**H**), 7.14 (d, *J* = 8,0 Hz, 1H, arom-C**H**), 6.89 (d, 2H, arom-C**H**), 3.78 (s, 3H, C**H**$_3$) 2.40 (s, 3H, C**H**$_3$). **^{13}C-NMR** (50 MHz, DMSO-d_6): δ 159.52, 144.07, 139.52, 135.37, 130.62, 129.75, 127.71, 127.44, 120.39, 116.46, 115.77, 114.02, 55.36, 21.07.

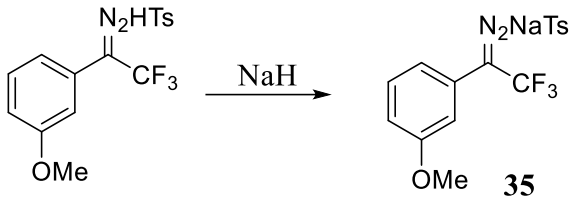

Sodium *m*-methoxy-2,2,2-trifluoroacetophenone-*p*-tosylhydrazonide 35 was prepared by deprotonation of the corresponding tosylhydrazone (1 eq.) with sodium hydride (NaH) (1.5 eq.). NaH was purchased as a dispersion in 60 % mineral oil. To remove the mineral oil, NaH was washed three times with dry pentane. Then *m*-methoxy-2,2,2-trifluoroacetophenone-*p*-tosylhydrazone in 40 ml of dry DCM was added and stirred for three hours at room temperature. The solvent was removed in vacuo and the crude product was used for the next step without further purification. **Yield:** 86 % of a yellow-orange salt. **Molecular Weight:** 394.34 g/mol. **^{1}H-NMR** (200 MHz, DMSO-d_6) δ 7.54 (d, *J* = 8.1 Hz, 2H, arom-C**H**), 7.34 – 7.01 (m, 5H, arom-C**H**), 6.84 (dd, J = 8.0, 2.5 Hz, 1H, arom-C**H**), 3.72 (s, 3H, C**H**$_3$), 2.31 (s, 3H, C**H**$_3$).

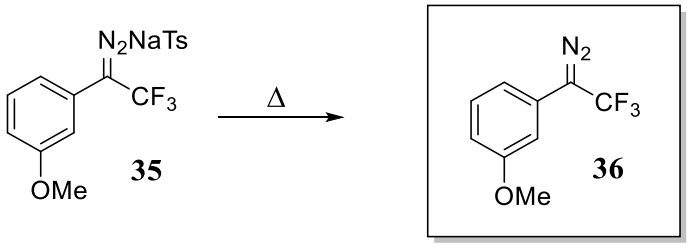

***m*-methoxyphenyl-1-trifluoromethyldiazomethane 36** was synthesized by thermal decomposition of **35** directly at the matrix apparatus. **Molecular Weight:** 229.21 g/mol. **UV-vis** (Ar, 3 K): nm 216, 260. **IR** (Ar, 3 K): cm^{-1} 2965, 2846, 2094, 1611, 1604, 1591, 1586, 1504, 1500, 1470, 1460, 1361, 1344, 1340, 1328, 1290, 1252, 1235, 1190, 1184, 1153, 1147, 1129, 1059, 1051, 1001, 981, 859, 849, 836, 829, 774, 765, 737, 684, 582.

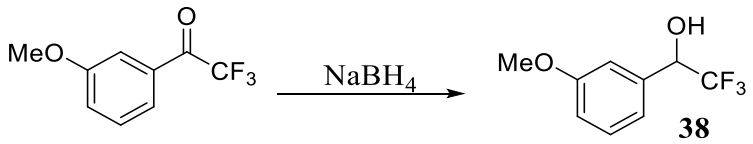

38

3.3.8. 2,2,2-trifluoro-1-(*m*-methoxyphenyl)ethanol 38 was synthesized as follows: *m*-methoxy-2,2,2-trifluoroacetophenone (1 eq) was dissolved in 7 ml MeOH and sodium borohydride ($NaBH_4$) (1 eq) was added at 0 °C. After 15 minutes at 0°, the mixture was stirred for 30 minutes at room temperature. Then H_2O was added, followed by extraction with DCM, filtration and evaporation of the solvent. **Yield:** 89 % of a yellow oil. **Molecular Weight:** 206.16 g/mol. **^{1}H-NMR** (200 MHz, $CDCl_3$) δ 7.32 (t, *J* = 8.2 Hz, 1H, arom-C**H**), 7.13 – 6.86 (m, 3H, arom-C**H**), 4.97 (q, *J* = 6.7 Hz, 1H, C**H**), 3.82 (s, 3H, C**H**$_3$). **^{13}C-NMR** (50 MHz, $CDCl_3$): δ 159.86, 135.67, 129.81, 127.74, 119.94, 115.26, 113.17, 73.19, 55.44. **UV-vis** (Ar, 3 K): nm 218, 270, 278.

4. Appendix

4.1. Additional Figures Tables and Charts

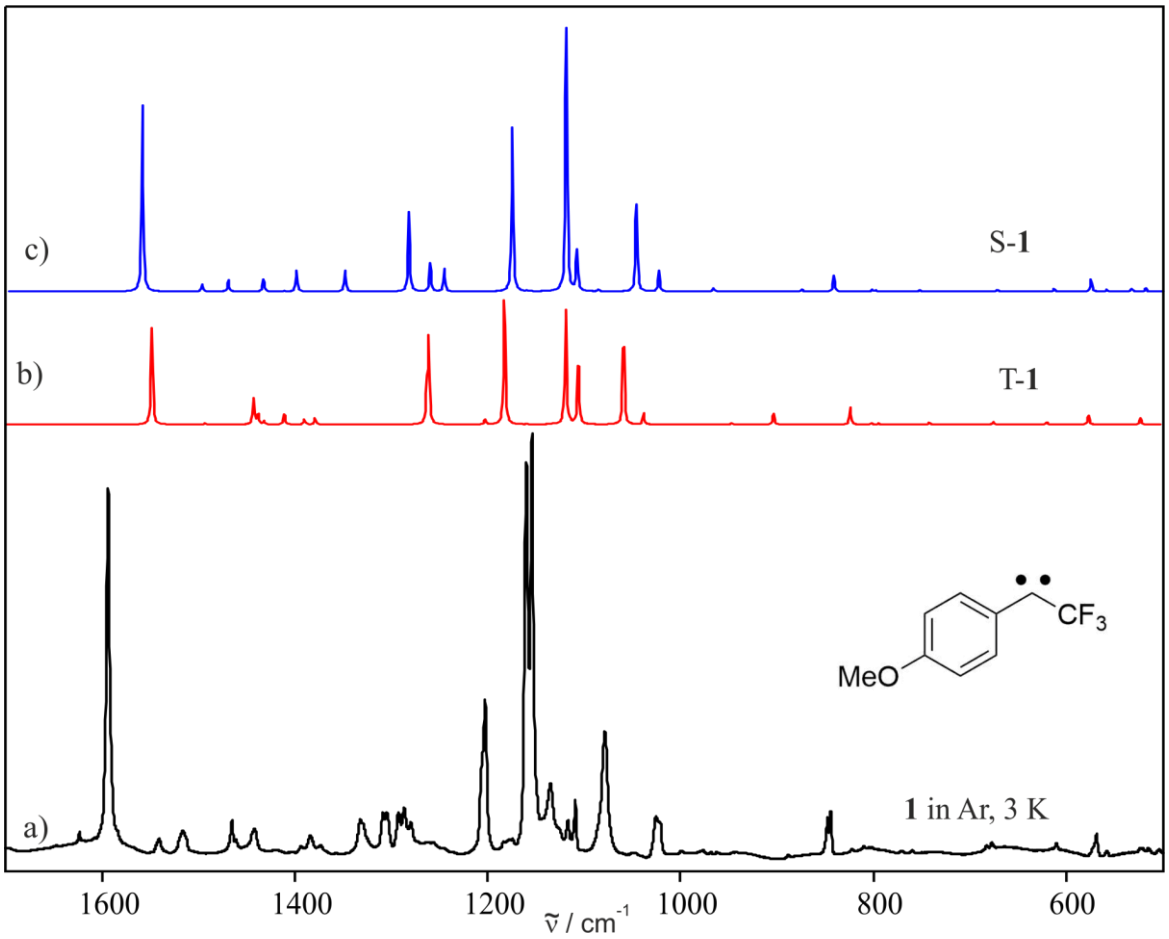

Figure **82:** Comparison of IR spectrum of carbene **1** obtained after photolysis of **6** to the calculation frequencies of S-**1**u and T-**1**u (M062x/Def2-TZVP//B3LYP/Def2-TZVP).

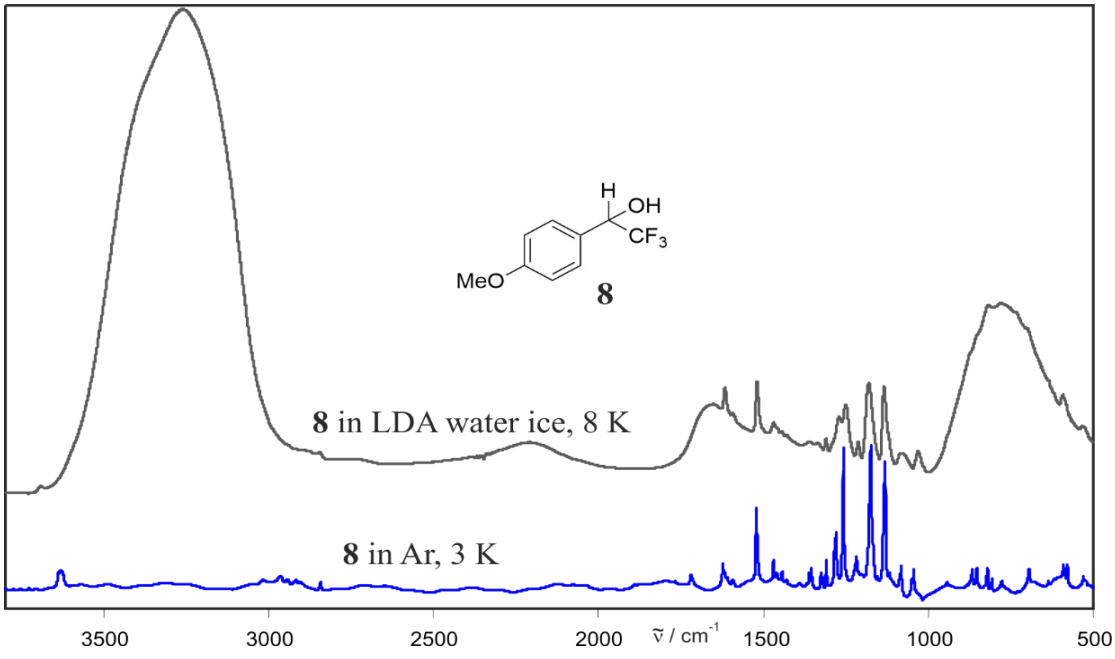

Figure **83:** Insertion product **8** in a) argon and b) in LDA water ice at 9 K.

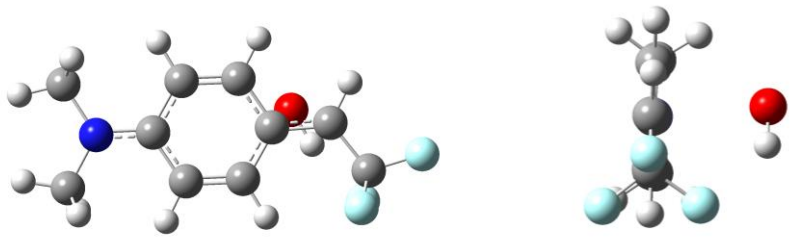

Chart **29:** Calculated structure of radical pair **24 OH** (B3LYP/Def2-TZVP).

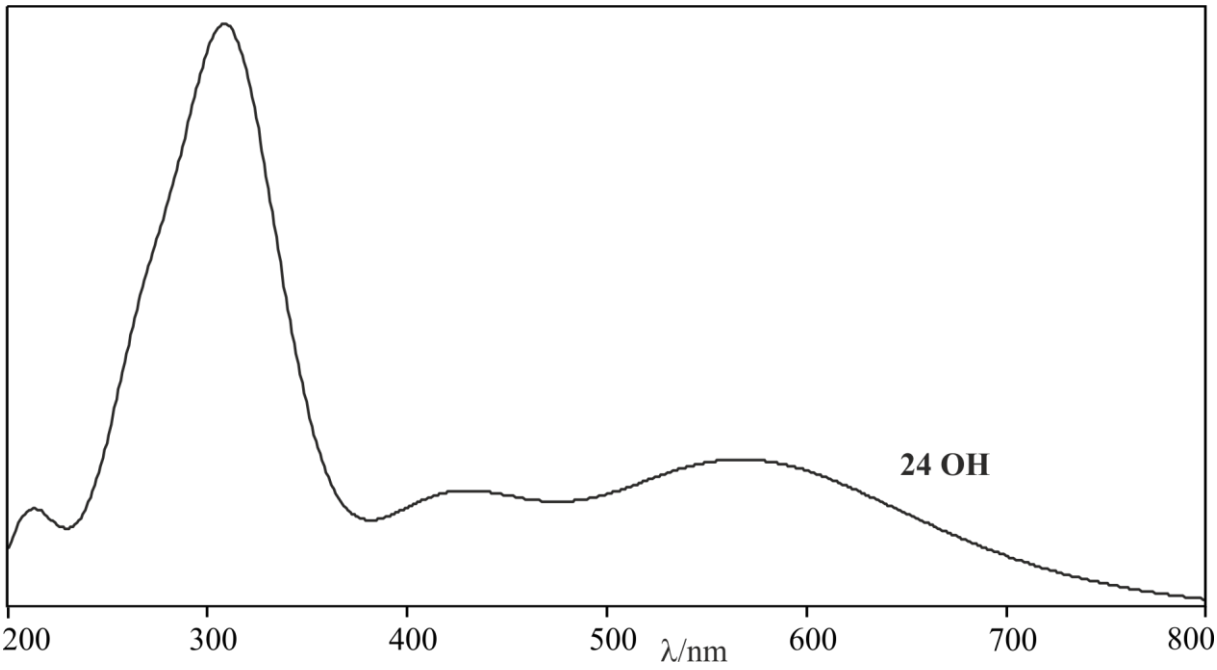

Figure **84:** UV experiment of **26** in argon doped with 1 % water compared to the calculated (TD-B3LYP/Def2-TZVP) spectrum of radical pair **24 OH**.

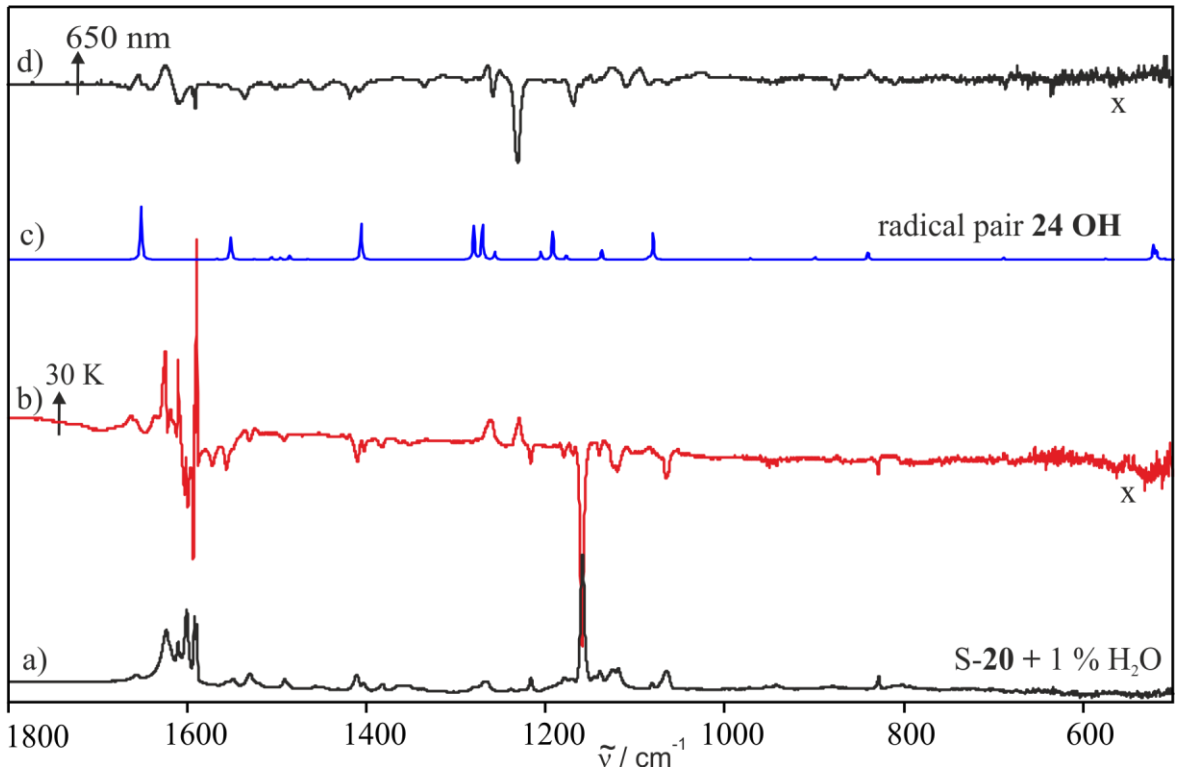

Figure **85:** IR difference spectra obtained by stepwise annealing. a) S-**20** in argon doped with 1 % water at 3 K. b) difference obtained after annealing to 30 K, c) calculated spectrum of radical pair **24 OH** (M062x/Def2-TZVP//B3LYP/Def2-TZVP), d) IR difference obtained after 650 nm irradiation. Bands pointing upwards increase in intensity. Bands pointing downwards decrease in intensity.

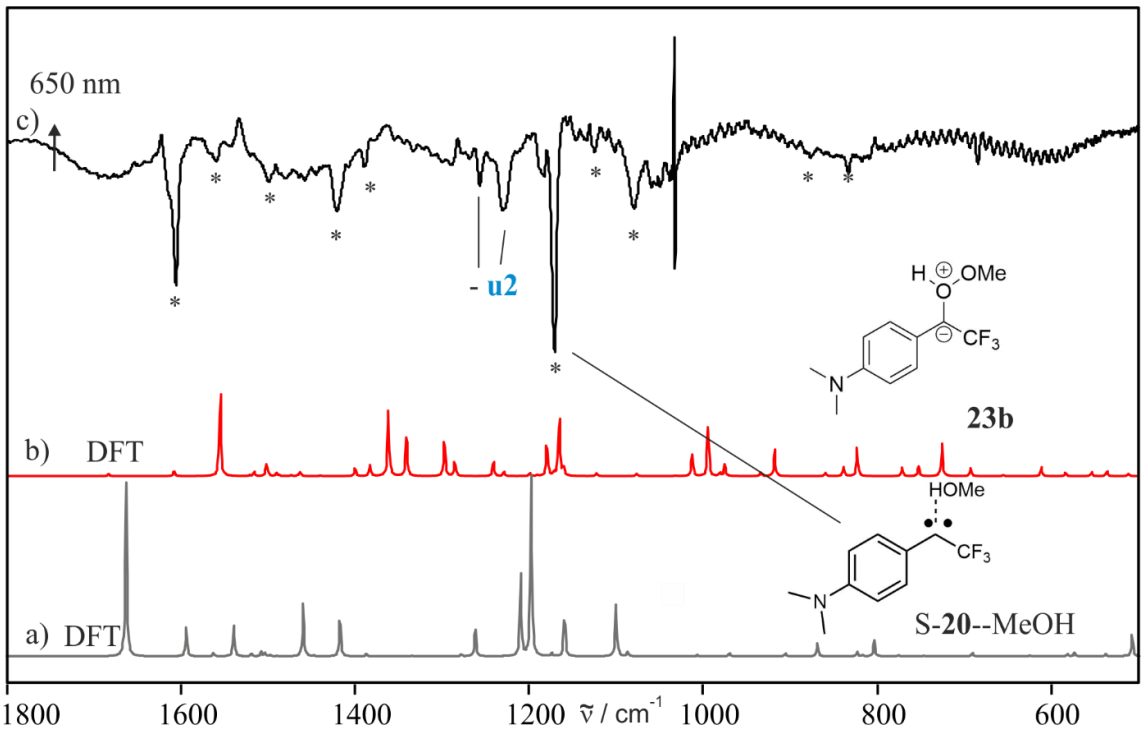

Figure **86** :Comparison of the experimental IR spectrum after 650 nm irradiation in a matrix doped with 1 % methanol at 3 K to the calculated spectra. Calculated IR spectra of a) S-**20**--MeOH and of b) of ylide **23b** (M06-2x/def2-TZVP//B3LYP/def2-TZVP). c) IR difference spectrum obtained after 650 nm photolysis of **u2** and S-**20**--MeOH. Bands pointing upwards increase in intensity. Bands pointing downwards decrease in intensity. * The marked signals are caused by S-**20**--MeOH.

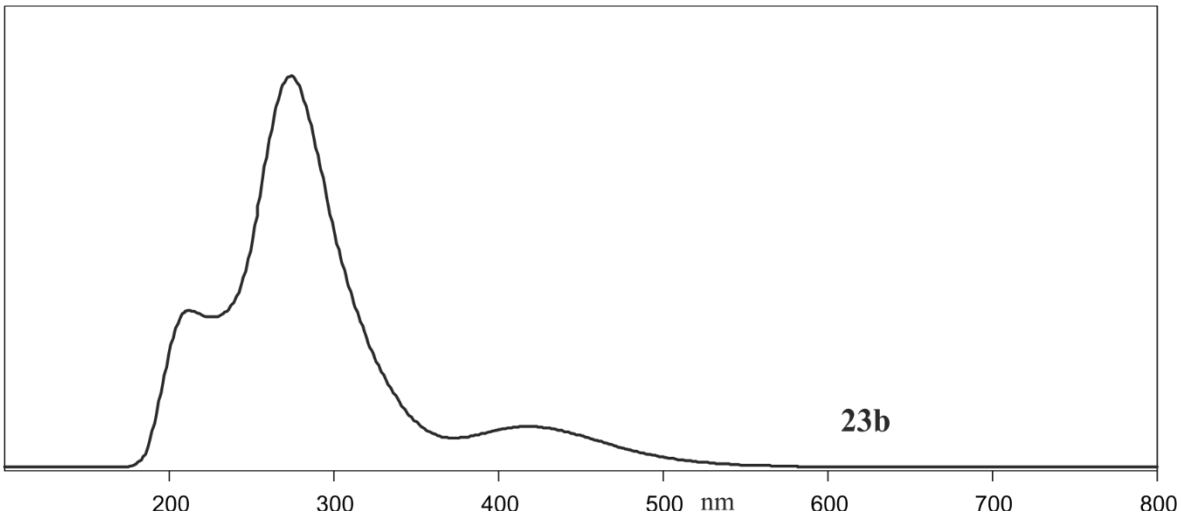

Figure **87:** Calculated (TD-B3LYP/Def2-TZVP) UV-vis spectrum of **23b**.

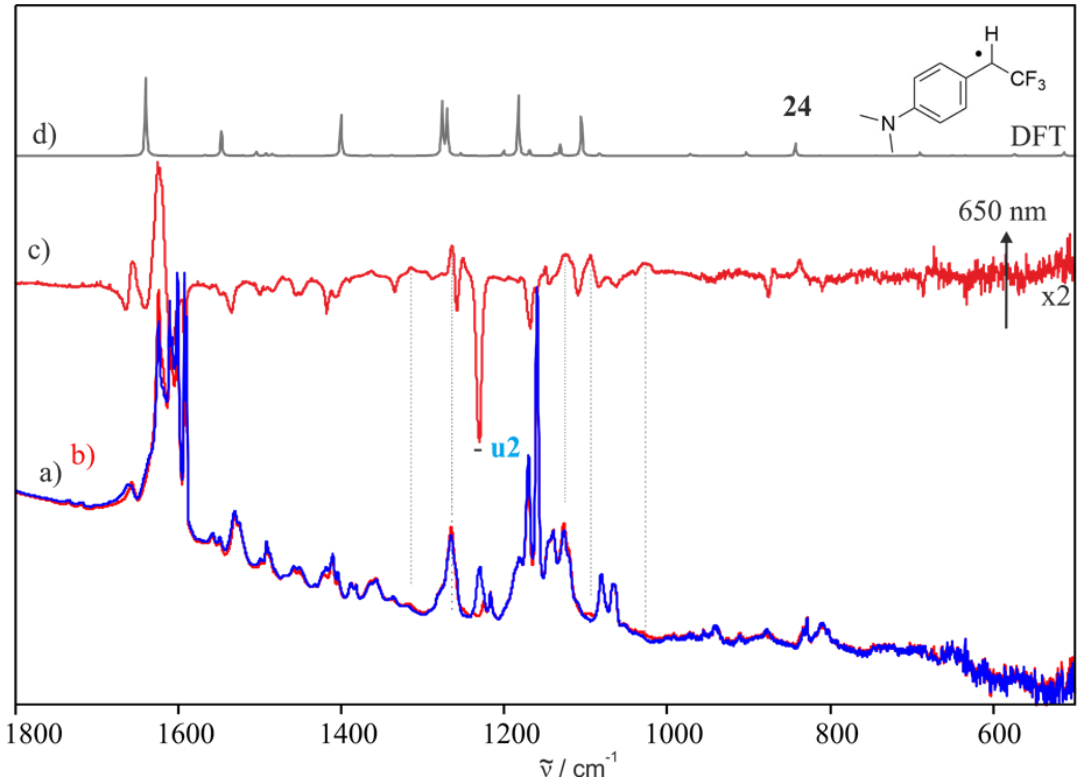

Figure **88:** IR spectra showing the 650 nm photolysis of **u2** in an argon matrix doped with 1 % of water at 3 K and calculated spectra of radical **24**. IR spectrum obtained a) before and b) after 650 nm photolysis. c) Corresponding IR difference spectrum. Bands pointing upwards increase in intensity and are assigned to **u3**. Bands pointing downwards decrease in intensity and are assigned to **u2**. d) Calculated IR spectrum of **24** (M06-2x/Def2-TZVP//B3LYP/Def2-TZVP). ^{x} represents a magnified difference spectrum.

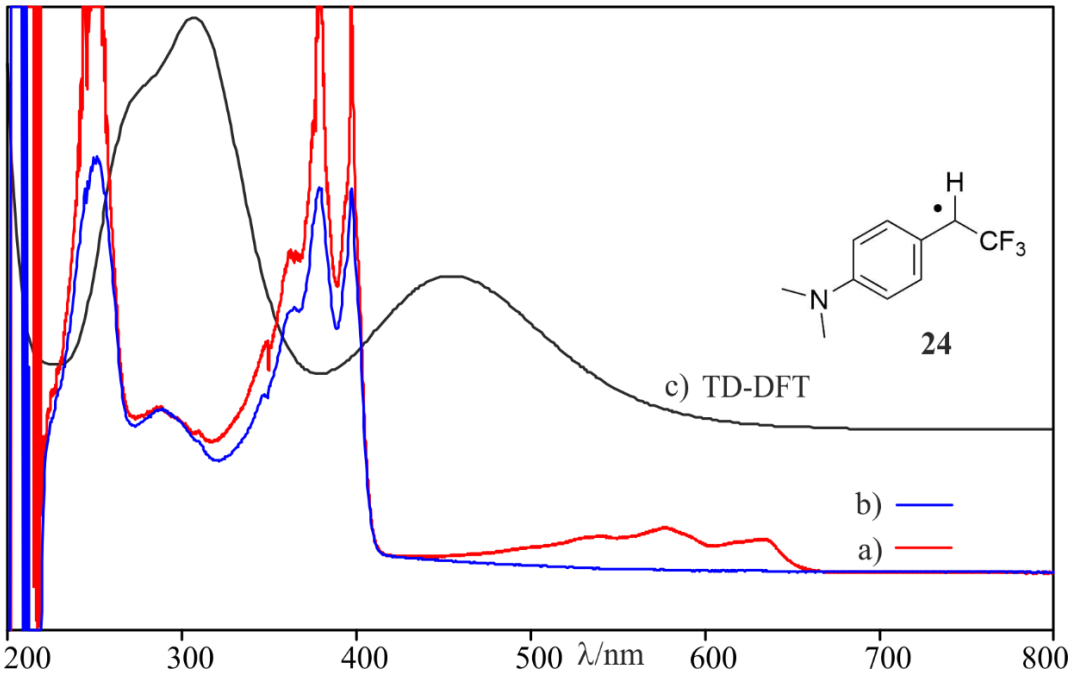

Figure **89:** UV-vis spectra obtained a) before and b) after 650 nm photolysis. c) Calculated (TD-B3LYP/Def2-TZVP) UV-vis spectrum of radical **24**.

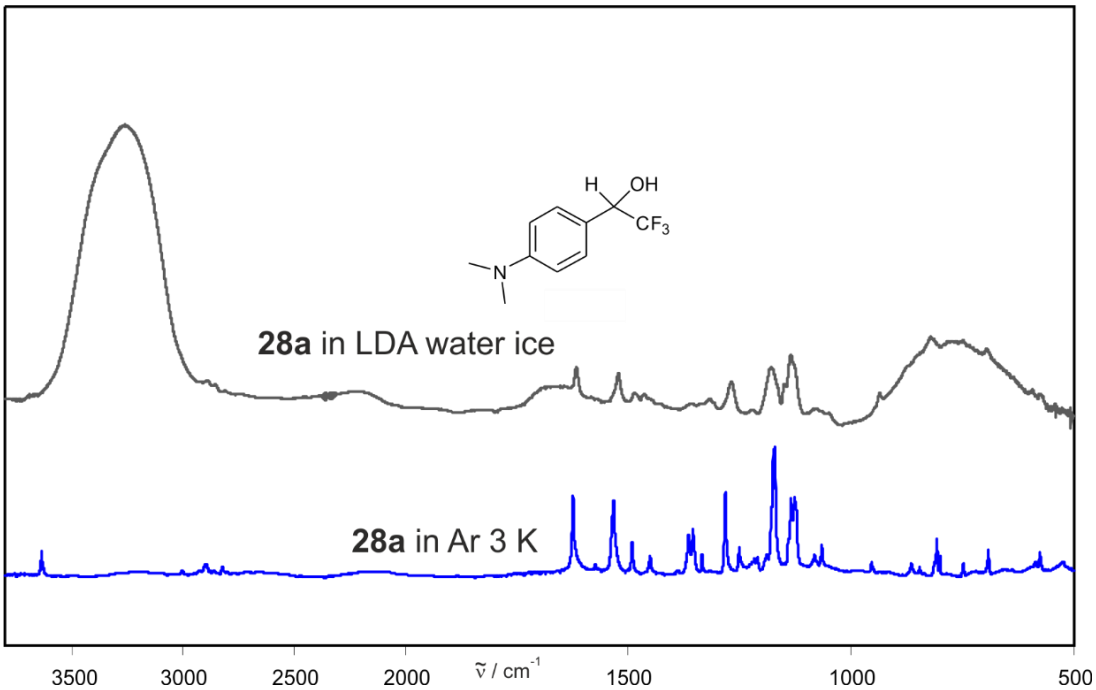

Figure **90:** Insertion product **28a** in a) argon at 3 K and b) in LDA water ice at 9 K.

Table **16:** Experimental IR frequencies of **28a** in argon and LDA water ice.

28a [a]	**28a** [b]	Shift	Assignment
1626	1617	- 9	C=C str.
1533	1522	- 11	C-N str.
1283	1269	- 14	C-F str.
1176	1180	+ 8	C-F str.

Values in cm^{-1}. [a] in argon at 3 K. [b] in LDA water ice at 9 K.

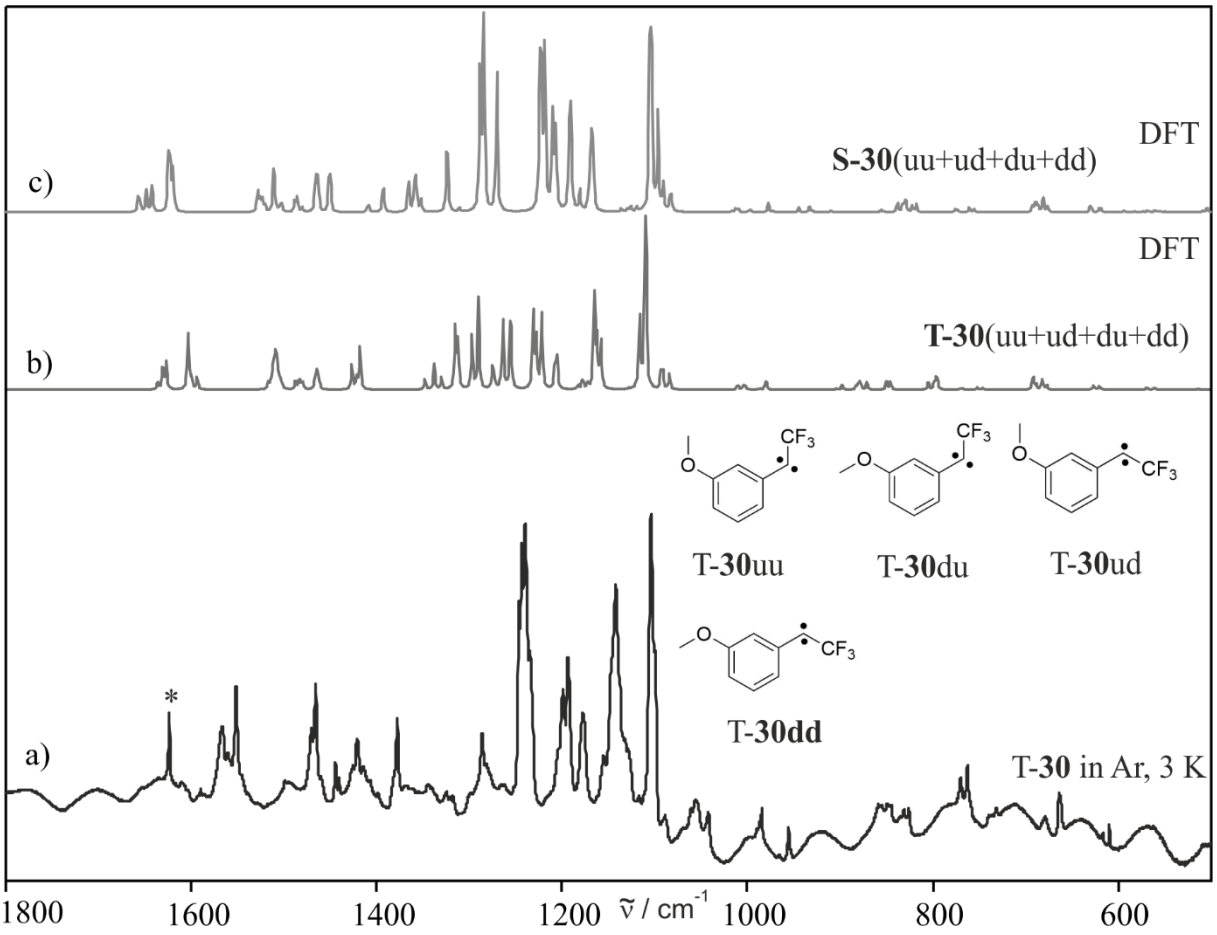

Figure **91:** a) IR spectrum of carbene **30** obtained after photolysis of **36** in argon at 3 K. Calculated IR spectra of b) T-**30** (uu+ud+du+dd) and c) S-**30** (uu+ud+du+dd) at M06-2x/Def2-TZVP//B3LYP/Def2-TZVP level of theory. * The signal marked by an asterisk is caused by H_2O.

Table **17:** Experimental and calculated vibrational frequencies of **8**.

Exp.[b]		Calc.[a]		Assignment [c]
		8		
$\tilde{\nu}$	$I_{rel.}$	$\tilde{\nu}$	$I_{rel.}$	
2919	2	3108.1	11	C-H str. (CH_3)
2901	1	3059.9	7	C-H str.
2842	3	3041.6	17	C-H str. (CH_3)
1626	15	1686.0	33	C=C str.
1520	39	1564.0	53	C-H bend. ring
1471	8	1515.3	12	C-H bend. (CH_3)
1356	12	1387.8	16	C-H bend.
1326	4	1347.8	32	C-H bend.
1309	7	1332.1	34	C-H bend.
1280	27	1314.8	40	C-H bend.
1258	50	1290.9	94	C-O str.
1219	12	1246.2	12	C-H bend.
1174	100	1204.7	98	C-F str.
1131	64	1148.9	100	C-F str.
1083	13	1120.2	22	C-O str.
1042	22	1090.1	18	C-O str
866	6	885.8	7	C-H bend. out of plane
853	5	875.3	13	Ring def.
819	9	846.9	16	C-H bend. out of plane
804	4	829.5	9	C-H bend. out of plane
778	2	792.5	4	Ring def.
694	5	707.5	11	C-F bend.
590	6	599.0	14	Ring def.
576	3	593.0	4	C-H bend. out of plane
529	2	539.5	3	C-H bend. out of plane

[a] Calculated at M06-2x/Def2-TZVP//B3LYP/Def2-TZVP level of theory. [b] In argon doped with 1 % of water at 3 K. [c] Tentative assignment.

Table **18:** Experimental and calculated vibrational frequencies of d-**8**.

Exp.[b]		Calc.[a] d-**8**		Assignment [c]
$\tilde{\nu}$	$I_{rel.}$	$\tilde{\nu}$	$I_{rel.}$	
2963	3	3162.6	4	C-H str. (CH_3)
2911	3	3108.1	8	C-H str. (CH_3)
2842	3	3041.6	13	C-H str. (CH_3)
2683	4	2797.5	15	O-D str.
1621	13	1685.8	25	C=C str.
1594	3	1646.9	6	C=C str.
1515	24	1563.3	40	C-H bend. ring
1469	5	1515.3	9	C-H bend. (CH_3)
1460	2	1502.9	3	C-H bend. (CH_3)
1312	3	1347.5	23	C-C str.
1289	9	1335.9	27	C-H bend.
		1331.6	21	C-H bend.
1257	42	1289.5	62	C-O str.
1213	48	1242.7	56	C-F str.
1167	100	1189.4	100	C-F str.
1125	3	1148.5	10	C-H bend.
1100	17	1129.9	19	C-H bend.
1061	5	1092.1	15	C-O str.
1046	11	1079.0	22	O-D bend.
997	5	999.9	5	C-H bend. out of plane
		992.4	5	C-H bend. out of plane
840	6	867.7	8	C-H bend. out of plane
805	6	816.0	6	C-H bend. out of plane
684	5	694.8	6	Ring def.
567	3	587.8	8	Ring def.
528	2	538.9	3	Ring def. out of plane
		525.9	1	C-F bend.

[a] Calculated at M06-2x/Def2-TZVP//B3LYP/Def2-TZVP level of theory. [b] In argon doped with 1 % of D_2O at 3 K. [c] Tentative assignment.

Table **19:** Experimental and calculated vibrational frequencies of **28a**.

Exp.[b]		Calc.[a] **28a**		Assignment [c]
$\tilde{\nu}$	$I_{rel.}$	$\tilde{\nu}$	$I_{rel.}$	
3636	20	3847.1	28	O-H str.
2897	8	3085.9	10	C-H str. (CH_3)
2823	5	3005.8	25	C-H str. (CH_3)
1624	45	1686.2	60	C=C str.
1574	6	1626.7	5	C=C str.
1533	55	1571.2	85	C-N str.
1491	11	1433.1	7	C-H bend.
1452	8	1391.3	24	C-N str.
1368, 1353	41	1387.9	68	C-H bend.
		1358.7	6	C-H bend.
1334	3	1348.4	10	C-H bend.
1284	35	1310.5	55	C-F str.
1252	9	1272.9	23	C-H bend.
1211	8	1233.1	31	C-H bend.
1176, 1169	100	1203.9	81	C-F str.
1135, 1125	86	1142.2	100	C-F str.
1081	7	1118.0	20	C-O str.
1065	6	1087.1	8	C-H bend. (CH_3)
952	3	976.4	6	N-C str.
864	5	878.4	9	C-H bend. out of plane
846	2	865.8	3	C-H bend. out of plane
808, 799	19	832.7	24	C-H bend. out of plane
749	3	765.6	3	Ring def. out of plane
691	7	703.2	12	Ring def. out of plane
574	2	585.8	7	Ring def.
524	4	527.1	3	C-F bend.

[a] Calculated at M06-2x/Def2-TZVP//B3LYP/Def2-TZVP level of theory. [b] In argon doped with 1 % of water at 3 K. [c] Tentative assignment.

Table **20:** Experimental and calculated vibrational frequencies of **38**.

Exp.[b]		Calc.[a] **38**		Assignment [c]
$\tilde{\nu}$	$I_{rel.}$	$\tilde{\nu}$	$I_{rel.}$	
3639	33	3847.1	38	O-H str.
2968	3	3097.5	12	C-H str. (CH_3)
2843	2	3032.8	19	C-H str. (CH_3)
1610. 1596	43	1686.0	26	C=C str.
		1653.5	28	C=C str.
1499	15	1539.5	32	C=C str.
1471	20	1504.8	35	C-H bend.
1436	7	1478.3	10	C-H bend. (CH_3)
1395	6	1422.5	3	C-H bend.
1355	14	1388.9	18	C-H bend.
1302	7	1345.2	24	C-H bend.
1275	100	1331.0	64	C-H bend.
		1316.6	35	C-H bend.
		1300.8	81	C-F str.
1220	15	1231.2	61	O-H bend.
1182	60	1218.8	18	C-H bend. (CH_3)
1164	22	1210.8	66	C-F str.
		1196.8	20	C-H bend.
		1186.5	15	C-H bend.
1131	78	1149.5	100	C-H bend.
1105	5	1137.4	11	C-O str.
1058	22	1125.7	13	C-H bend.
847	9	1097.9	42	C-O str. (CH_3)
787. 779	22	859.4	9	C-H bend. out of plane
758	9	814.8	19	C-H bend. out of plane
712	18	794.4	27	Ring def.
629	2	726.7	19	C-H bend. out of plane

[a] Calculated at M06-2x/Def2-TZVP//B3LYP/Def2-TZVP level of theory. [b] In argon doped with 1 % of water at 3 K. The IR signals derive from a mixture of conformers and were exemplarily assigned to one conformer. [c] Tentative assignment.

4.2. Computational data

Cartesian coordinates of the optimized structures calculated at the B3LYP-D3/Def2-TZVP level of theory.

E_{ZPE} = - 831.571528

6d

0 1			
C	2.07354300	1.48923600	-0.00001400
C	0.60863800	-0.86301800	0.00001600
C	-0.07160900	0.35692500	0.00000300
C	0.69445600	1.53420900	-0.00001200
H	0.06230500	-1.79495100	0.00002800
H	0.20980100	2.50253600	-0.00002300
C	-2.42175700	-0.79801500	-0.00000600
F	-2.21209600	-1.58637500	-1.07991000
F	-2.21211600	-1.58637800	1.07990200
F	-3.72283500	-0.45433300	-0.00001600
H	2.65808300	2.39951700	-0.00002600
C	2.74324100	0.26293700	-0.00000200
C	1.99834200	-0.91423900	0.00001300
H	2.48155500	-1.87997500	0.00002400
O	4.10125300	0.32560300	-0.00000600
C	-1.53696800	0.40659700	0.00000300
N	-2.15414000	1.55243900	0.00001200
N	-2.64436800	2.57041000	0.00001900
C	4.83760400	-0.88766900	0.00000400
H	5.88668500	-0.60115400	-0.00000400
H	4.62579400	-1.48436100	0.89279600
H	4.62578600	-1.48438000	-0.89277500

E_{ZPE} = -831.571415

6u

0 1			
C	-2.24695100	0.99332400	0.00000200
C	-0.44008900	-1.11892200	-0.00001500
C	0.05058700	0.19680100	-0.00000200
C	-0.87925000	1.23921700	0.00000700
H	0.24196100	-1.95627700	-0.00002200
H	-0.54629000	2.26971000	0.00001800
C	2.54232500	-0.60682700	0.00001000
F	2.44825900	-1.41734200	1.07976800
F	2.44828000	-1.41733700	-1.07975500
F	3.78034500	-0.07928300	0.00002200
H	-2.92745400	1.83169900	0.00000900
C	-2.71813600	-0.31857700	-0.00001100
C	-1.79813600	-1.36906200	-0.00001900
H	-2.17162300	-2.38438000	-0.00002900
O	-4.03041500	-0.67361800	-0.00001600
C	1.49361500	0.45868700	0.00000300
N	1.93766900	1.68168900	0.00000200
N	2.27012600	2.76160000	0.00000400
C	-5.01273800	0.35037500	-0.00000700
H	-5.97445100	-0.15732700	-0.00001300
H	-4.93634900	0.97901900	0.89282200
H	-4.93634600	0.97903700	-0.89282400

E_{ZPE} = -798.527872	0 1			
	C	-1.70621300	1.28624900	0.52810100
	C	-0.64083500	-0.81370100	-0.92718800
	C	0.19067400	0.21809300	-0.51472900
	C	-0.36000600	1.27169700	0.21972400
	H	-0.23280000	-1.63813900	-1.49986800
	H	0.27611200	2.08541400	0.53870800
	C	2.47608900	-0.41714400	0.33113800
8	F	2.32080600	0.24467500	1.48521900
	F	2.14685900	-1.70379300	0.53902200
	F	3.80154800	-0.38601400	0.02901700
	H	-2.14290600	2.09954700	1.09224500
	C	-2.53662300	0.23976200	0.11424300
	C	-1.99835000	-0.81659400	-0.61900000
	H	-2.61580500	-1.63477800	-0.95810600
	O	-3.84424000	0.34670100	0.46880100
	C	-4.74225300	-0.68209400	0.08253900
	H	-4.80023100	-0.77514700	-1.00645900
	H	-4.45577600	-1.64662400	0.51322900
	H	-5.71566000	-0.39064900	0.47025400
	C	1.66314600	0.18399900	-0.82655500
	H	1.84335200	-0.48926400	-1.67381400
	O	2.12777600	1.49233400	-1.09737800
	H	3.07874400	1.46193500	-1.25653900

E_{ZPE} = -721.973096	0 1			
	C	-2.02020800	1.10522500	0.00000100
	C	-0.01759500	-0.86657000	-0.00000200
	C	0.36384200	0.51505700	-0.00000100
	C	-0.69215100	1.46717100	-0.00000100
	H	0.74691200	-1.62941600	-0.00000400
S-**1**u	H	-0.40622900	2.51060100	0.00000000
	C	1.66255300	1.05308200	-0.00000300
	C	2.78271500	0.05791500	0.00000100
	F	2.75957600	-0.75036000	1.10156000
	F	2.75958500	-0.75034900	-1.10156600
	F	3.99812400	0.63774400	0.00001000
	H	-2.78968600	1.86244000	0.00000300
	C	-2.34780000	-0.26000800	0.00000000
	C	-1.33217400	-1.24014500	-0.00000200
	H	-1.63063500	-2.28008900	-0.00000300
	O	-3.59702600	-0.73381400	0.00000100
	C	-4.70269400	0.17267800	0.00000100
	H	-4.69351300	0.79948000	-0.89428700
	H	-5.59161500	-0.45173400	-0.00000100
	H	-4.69351500	0.79947700	0.89429200

E_{ZPE} = -721.972771

S-**1**d

0 1

C	-1.88135100	1.56500400	-0.00000100
C	-0.15796600	-0.63899400	0.00000100
C	0.39969800	0.67499800	0.00000000
C	-0.52597200	1.76145400	0.00000000
H	0.50229600	-1.49350700	0.00000100
H	-0.10913800	2.75966200	-0.00000100
C	1.76120400	1.02441100	0.00000100
C	2.73281300	-0.11659900	0.00000000
F	2.59921800	-0.91593900	1.10134800
F	2.59921700	-0.91594200	-1.10134600
F	4.01639500	0.28950600	-0.00000200
H	-2.58247900	2.38847700	-0.00000100
C	-2.38974500	0.25396400	0.00000000
C	-1.51486600	-0.85080000	0.00000000
H	-1.90161900	-1.85898400	0.00000100
O	-3.72200500	0.15153500	-0.00000100
C	-4.34251900	-1.13661800	-0.00000100
H	-4.07127900	-1.70160400	-0.89437600
H	-4.07128000	-1.70160300	0.89437500
H	-5.41170500	-0.94426800	-0.00000100

E_{ZPE} = -721.972409

T-**1**u

0 3

C	-2.06709800	1.08494700	0.00000000
C	-0.12426700	-0.92785700	0.00000100
C	0.28896900	0.43978400	0.00000100
C	-0.72866000	1.42683800	0.00000000
H	0.62543900	-1.70697700	0.00000200
H	-0.44330600	2.47043900	0.00000000
C	1.63013500	0.78693300	0.00000100
C	2.89678700	0.05544600	0.00000000
F	3.02925400	-0.75707900	1.08490600
F	3.02925400	-0.75707500	-1.08490900
F	3.95282200	0.89035500	0.00000100
H	-2.81017200	1.86876100	0.00000000
C	-2.44449300	-0.26325100	0.00000000
C	-1.45504700	-1.26007100	0.00000000
H	-1.76980400	-2.29538500	0.00000000
O	-3.72334600	-0.70601100	0.00000000
C	-4.78205600	0.24310000	0.00000000
H	-4.75077100	0.87365600	-0.89325800
H	-5.70144600	-0.33708900	0.00000400
H	-4.75076700	0.87366000	0.89325400

E_{ZPE} = -721.972523

T-**1**d

0 3

C	1.92678500	1.53743900	0.00000000
C	0.27323800	-0.70598000	0.00000500
C	-0.31562000	0.58855500	0.00000300
C	0.56596500	1.70730900	0.00000300
H	-0.36609000	-1.57826700	0.00000700
H	0.14498300	2.70384600	0.00000400
C	-1.68976100	0.76181700	0.00000300
C	-2.86023100	-0.11431100	0.00000000
F	-2.89663100	-0.93648100	-1.08515100
F	-2.89663500	-0.93648500	1.08514600
F	-4.00730800	0.59061400	-0.00000100
H	2.59604400	2.38753500	0.00000000
C	2.48664300	0.24898800	-0.00000200
C	1.64507400	-0.86960600	0.00000200
H	2.05195300	-1.87016700	0.00000300
O	3.83887000	0.19646000	-0.00000500
C	4.48040100	-1.07255000	0.00000000
H	4.22230000	-1.64875700	0.89323400
H	4.22230100	-1.64876300	-0.89323100
H	5.54774100	-0.86590900	0.00000000

E_{ZPE} = -798.430613

S-**1**u--H_2O

0 1

C	2.08231200	0.94324300	0.03714600
C	0.72893400	1.18635200	0.04491500
C	-0.23253500	0.13151200	0.01659500
C	0.27673900	-1.21004400	-0.02215500
C	1.61796200	-1.45868400	-0.03383900
C	2.53695000	-0.38501200	-0.00371900
C	-1.57424400	0.52215800	0.02386000
H	2.77784000	1.76843500	0.06065800
H	0.35798000	2.20345500	0.07630700
H	2.01338000	-2.46508700	-0.06576800
H	-0.41420900	-2.03949100	-0.04591000
O	-1.58725500	3.43711600	-0.09232500
H	-1.80250100	2.47288200	-0.04779100
H	-2.32600700	3.89018600	0.32437200
C	-2.60200400	-0.56808100	0.00846700
F	-3.86050400	-0.09033400	0.05007200
F	-2.48981500	-1.41092400	1.07581200
F	-2.52525100	-1.32794000	-1.12041500
O	3.82192200	-0.73916400	-0.01724400
C	4.84267200	0.26426700	0.00886300
H	4.77902200	0.86017700	0.92143100
H	5.78336300	-0.27840700	-0.01011800
H	4.77321600	0.91275400	-0.86664700

E_{ZPE} = -798.429841

S-**1**d--H_2O

0 1

C	-1.88931100	1.47053100	-0.04000000
C	-0.52104100	1.48886800	-0.04324600
C	0.24765300	0.28026600	-0.01800600
C	-0.48236700	-0.94951100	0.01154600
C	-1.85274900	-0.97550900	0.01805000
C	-2.56989100	0.24005500	-0.00862500
C	1.63761600	0.42568000	-0.01884700
H	-2.47354500	2.38042000	-0.05961100
H	0.01806100	2.42778800	-0.06809200
H	-2.37373100	-1.92089400	0.04361700
H	0.05609700	-1.88557300	0.03266800
O	2.17692800	3.29227600	0.09487200
H	2.21168200	2.30544700	0.05122400
H	2.98194900	3.60202500	-0.33016100
C	2.45868100	-0.82699500	-0.00492000
F	3.78154200	-0.57679200	-0.02939100
F	2.21222100	-1.62607600	-1.08366400
F	2.23910100	-1.57433000	1.11427700
O	-3.90096400	0.31746400	-0.00624600
C	-4.69402900	-0.87338900	0.02367000
H	-4.50058800	-1.44798400	0.93168600
H	-5.72597800	-0.53443400	0.01825900
H	-4.50481600	-1.48991000	-0.85731700

E_{ZPE} = -798.420298

T-**1**u--H_2O

0 3

C	2.15184700	0.94077200	-0.00000200
C	0.78638500	1.14554100	-0.00000100
C	-0.12153700	0.05479600	0.00000100
C	0.42889300	-1.26356000	0.00000500
C	1.78684800	-1.45629700	0.00000500
C	2.66712600	-0.36145800	0.00000000
C	-1.48967600	0.26777100	-0.00000100
H	2.80955800	1.79737500	-0.00000400
H	0.38277700	2.14951800	-0.00000400
H	2.20757000	-2.45322700	0.00000800
H	-0.23616600	-2.11650100	0.00000800
O	-1.84023100	3.29650700	0.00000400
H	-2.23223300	2.85192700	0.76038600
H	-2.23224400	2.85193600	-0.76037800
C	-2.69145600	-0.55986400	-0.00000200
F	-3.80700500	0.20753200	0.00000000
F	-2.77499600	-1.37648500	1.08468900
F	-2.77499700	-1.37648200	-1.08469400
O	3.98437800	-0.66991100	-0.00000100
C	4.94082300	0.38270900	-0.00000300
H	4.84525800	1.00675500	0.89312600
H	5.91451300	-0.10084100	0.00000000
H	4.84525900	1.00675000	-0.89313500

E_{ZPE} = -722.392067

2u

1 1			
C	-2.38481400	-0.26459200	0.00000000
C	-2.04453700	1.12147800	0.00000000
C	-0.73602500	1.47531500	-0.00000700
C	0.31797100	0.48406500	-0.00000800
C	-0.06233000	-0.91418800	-0.00001000
C	-1.36614900	-1.26874400	-0.00000500
C	2.81728600	-0.00693100	0.00000400
F	2.81128400	-0.79531100	-1.08744700
F	3.93602300	0.71266100	0.00003000
F	2.81125800	-0.79534600	1.08742800
C	1.60597100	0.90689000	-0.00000200
H	1.84222700	1.96448200	-0.00000600
H	-0.45995300	2.52240900	-0.00001000
H	-2.81713600	1.87532300	0.00000300
H	-1.68055200	-2.30344800	-0.00000500
H	0.70477300	-1.67513800	-0.00001500
O	-3.60137300	-0.71461300	0.00000100
C	-4.76014800	0.16409500	0.00000900
H	-4.75757700	0.77778100	-0.89992200
H	-5.61365500	-0.50465000	0.00001700
H	-4.75756400	0.77778500	0.89993700

E_{ZPE} = -778.640152

8a

0 1			
C	1.87486200	0.93347700	0.15931300
C	0.50811500	1.01754200	-0.08457200
C	-0.20386400	-0.07062100	-0.57852300
C	0.48513200	-1.26004400	-0.82284000
C	1.84353100	-1.36110900	-0.58321700
C	2.55000600	-0.26232900	-0.08845000
H	2.39556200	1.79845700	0.54272200
H	-0.01358700	1.94405000	0.11260700
H	2.38091900	-2.28048000	-0.77362900
H	-0.05011200	-2.12129800	-1.20475300
C	-2.48767500	-0.16170500	0.47100500
F	-3.81898800	-0.06254800	0.22701500
F	-2.19018700	0.74495600	1.41206500
F	-2.27454400	-1.38349000	0.99735800
O	3.88091900	-0.45425600	0.11281400
C	4.65498000	0.62115900	0.62115400
H	4.30486200	0.93438600	1.60960900
H	5.67229000	0.24527200	0.70258200
H	4.64020700	1.48053900	-0.05647000
N	-2.06638800	1.30399300	-1.40503500
H	-1.51050600	1.48977700	-2.22965600
H	-3.04550000	1.32259300	-1.66189400
C	-1.69338200	0.01828800	-0.82711400
H	-1.99352300	-0.84541900	-1.43686400

E_{ZPE} = -778.533664

S-**1**--HNH_2u

0 1			
C	2.06451700	0.90295500	0.00000700
C	0.70985200	1.14800100	0.00000300
C	-0.25223900	0.09501100	-0.00000100
C	0.25671500	-1.24706300	0.00000000
C	1.59837900	-1.49757400	0.00000500
C	2.51814900	-0.42501800	0.00000800
C	-1.59625500	0.49087000	-0.00000600
H	2.76012600	1.72866000	0.00001000
H	0.33901200	2.16735100	0.00000200
H	1.99247700	-2.50511100	0.00000600
H	-0.43403500	-2.07696600	-0.00000300
C	-2.61589200	-0.60668000	-0.00001000
F	-3.88073700	-0.14021600	-0.00001500
F	-2.51904200	-1.40963500	1.10032000
F	-2.51903400	-1.40963600	-1.10033700
O	3.80476300	-0.78165800	0.00001300
C	4.82383500	0.22207300	0.00001800
H	4.75743600	0.84532300	0.89415200
H	5.76551600	-0.31951600	0.00002300
H	4.75744500	0.84532400	-0.89411500
N	-1.40276500	3.77017500	-0.00000300
H	-1.77204100	4.24757600	0.81504000
H	-1.78569400	2.82175500	-0.00000500
H	-1.77203600	4.24757800	-0.81504600

E_{ZPE} = -778.532904

S-**1**--HNH_2d

0 1			
C	1.86018600	1.45119400	0.00009000
C	0.49038200	1.45335000	0.00010800
C	-0.26379000	0.23659800	0.00005400
C	0.48168600	-0.98386800	-0.00001300
C	1.85317600	-0.99365600	-0.00003400
C	2.55558400	0.23002300	0.00001700
C	-1.65874800	0.36936700	0.00005300
H	2.43264700	2.36895100	0.00012900
H	-0.06115300	2.38716900	0.00016300
H	2.38520100	-1.93333400	-0.00009100
H	-0.04429500	-1.92723000	-0.00005300
C	-2.45516200	-0.89877300	0.00001000
F	-3.78478200	-0.67720300	0.00004600
F	-2.21032700	-1.66991500	1.10062300
F	-2.21036000	-1.66978400	-1.10070600
N	-2.09314500	3.62809200	-0.00008700
H	-2.28729200	2.62421500	-0.00004400
H	-2.54592600	4.02659400	-0.81533600
H	-2.54600200	4.02667700	0.81507900
O	3.88786800	0.32289300	-0.00000600
C	4.69181400	-0.85972500	-0.00005900
H	5.72082400	-0.51145900	-0.00005900
H	4.50677500	-1.45818500	0.89439400
H	4.50675500	-1.45812000	-0.89455100

0 3

E_{ZPE} = -778.529121

T-**1**--HNH_2u

C	2.12951600	0.90140700	-0.00002100
C	0.76320500	1.10320300	-0.00002600
C	-0.13946200	0.00797000	-0.00000900
C	0.41490400	-1.30851700	0.00001200
C	1.77393500	-1.49664800	0.00001700
C	2.64954300	-0.39865100	0.00000100
C	-1.50834300	0.21649700	-0.00001400
H	2.78457500	1.76023300	-0.00003500
H	0.35216400	2.10536600	-0.00004200
H	2.19818900	-2.49213100	0.00003300
H	-0.24727900	-2.16376800	0.00002400
C	-2.70948400	-0.61135500	-0.00000300
F	-3.82719200	0.15001400	-0.00001500
F	-2.79014200	-1.43008700	1.08476600
F	-2.79014000	-1.43011600	-1.08475200
O	3.96954600	-0.70253000	0.00000800
C	4.92009300	0.35420700	0.00000100
H	4.82177700	0.97841900	0.89291800
H	5.89657400	-0.12400700	0.00001600
H	4.82179200	0.97839300	-0.89293700
N	-1.64270000	3.59799700	0.00001700
H	-2.31736200	2.84006300	-0.00002600
H	-1.83205200	4.16741800	-0.81720300
H	-1.83202000	4.16729200	0.81733200

E_{ZPE} = -722.395323

d-**2**u

1 1			
C	-2.38481400	-0.26459200	0.00000000
C	-2.04453700	1.12147800	0.00000000
C	-0.73602500	1.47531500	-0.00000700
C	0.31797100	0.48406500	-0.00000800
C	-0.06233000	-0.91418800	-0.00001000
C	-1.36614900	-1.26874400	-0.00000500
C	2.81728600	-0.00693100	0.00000400
F	2.81128400	-0.79531100	-1.08744700
F	3.93602300	0.71266100	0.00003000
F	2.81125800	-0.79534600	1.08742800
C	1.60597100	0.90689000	-0.00000200
D	1.84222700	1.96448200	-0.00000600
H	-0.45995300	2.52240900	-0.00001000
H	-2.81713600	1.87532300	0.00000300
H	-1.68055200	-2.30344800	-0.00000500
H	0.70477300	-1.67513800	-0.00001500
O	-3.60137300	-0.71461300	0.00000100
C	-4.76014800	0.16409500	0.00000900
H	-4.75757700	0.77778100	-0.89992200
H	-5.61365500	-0.50465000	0.00001700
H	-4.75756400	0.77778500	0.89993700

E_{ZPE} = -850.982876

26

0 1			
C	-2.43207300	0.00958700	0.07348500
C	-1.57588600	-1.10828900	0.05664000
C	-0.19945200	-0.96818800	0.03703200
C	0.40624400	0.29339300	0.02284400
C	-0.44002000	1.40804100	0.02393100
C	-1.81640400	1.27673000	0.04390100
H	-1.98054800	-2.10886100	0.05937600
H	0.40498500	-1.86377400	0.02785500
H	-0.02506600	2.40852000	0.00327100
H	-2.41220500	2.17668900	0.03606600
N	-3.80690900	-0.12854200	0.12461300
C	-4.64577200	1.03548300	-0.08271500
H	-4.50517900	1.48814600	-1.07378900
H	-5.68952700	0.74597600	0.01485100
H	-4.44765800	1.80184500	0.67021600
C	-4.39624400	-1.43738700	-0.08118400
H	-4.05695400	-2.14552800	0.67836800
H	-5.47761900	-1.36022500	0.00543600
H	-4.15833200	-1.85712800	-1.06790400
C	1.86488900	0.43697300	-0.00062700
C	2.82155600	-0.71048500	-0.01311200
F	4.09987700	-0.28879300	-0.03529100
F	2.64388900	-1.51455000	-1.08801200
F	2.67949000	-1.50882100	1.07122200
N	2.40910900	1.61831800	-0.01233300
N	2.82891000	2.66860600	-0.02173600

E_{ZPE} = -741.391464

S-**20**

0 1			
C	-0.23906400	1.65881500	-0.00000100
C	0.75190300	0.63184200	0.00000200
C	0.25167800	-0.71073700	0.00000700
C	-1.08481100	-0.98951800	0.00000400
C	-2.05376800	0.05756100	0.00000400
C	-1.58184900	1.39923600	0.00000000
H	0.12062000	2.67950600	-0.00000700
H	0.95146000	-1.53347900	0.00001300
H	-1.40333800	-2.02079100	0.00000600
H	-2.27837300	2.22328300	-0.00000800
C	2.08533700	1.05236600	-0.00001300
C	3.11374300	-0.03400900	-0.00000200
N	-3.37796700	-0.22022000	0.00000600
F	3.02859300	-0.84402400	-1.10094800
F	3.02859000	-0.84400000	1.10096200
F	4.37772800	0.43767800	-0.00000800
C	-3.85109800	-1.59969800	-0.00000700
H	-4.93700100	-1.60320400	-0.00000600
H	-3.50883200	-2.13830400	-0.88699800
H	-3.50882900	-2.13832300	0.88697100
C	-4.36209100	0.85546400	-0.00000200
H	-5.35952700	0.42604100	0.00003300
H	-4.26222600	1.48602100	0.88694900
H	-4.26226400	1.48597600	-0.88699000

E_{ZPE} = -741.386156

T-**20**

0 3			
C	-0.26911900	1.60007000	0.00662100
C	0.67773200	0.54009600	0.00661500
C	0.14822800	-0.78379500	0.01120500
C	-1.20533600	-1.01676500	0.01779300
C	-2.14184600	0.04576600	0.02332200
C	-1.62179000	1.36338400	0.01304600
H	0.09236800	2.62005600	-0.00054000
H	0.82996800	-1.62361700	0.00733600
H	-1.54492400	-2.04169000	0.01742500
H	-2.28897300	2.21203400	0.00953400
C	2.03830500	0.78267300	-0.00025700
C	3.24734900	-0.03340600	-0.00548100
N	-3.49326400	-0.19081200	0.03978400
F	3.32597600	-0.85506300	-1.09191700
F	3.33276800	-0.85880600	1.07754800
F	4.36133900	0.72578800	-0.00777000
C	-3.99787500	-1.55003100	-0.01971200
H	-5.08371300	-1.53133200	0.02244600
H	-3.70167400	-2.05786300	-0.94451300
H	-3.64098300	-2.14654000	0.82483000
C	-4.42972900	0.91511700	-0.03180800
H	-5.44467600	0.52833300	0.00690600
H	-4.30217600	1.60310700	0.80907600
H	-4.31862900	1.48727500	-0.95980600

E_{ZPE} = -741.829865

22

1 1			
C	-1.60785100	1.40618600	-0.00000400
C	-0.28383300	1.66243800	-0.00000900
C	0.70087000	0.60124800	-0.00001300
C	0.20194400	-0.75879500	-0.00001300
C	-1.12086900	-1.02108200	-0.00000900
C	-2.09427000	0.04675700	-0.00000400
H	-2.30412600	2.22947200	-0.00000300
H	0.06409100	2.68778600	-0.00000900
H	-1.44994000	-2.04797800	-0.00000800
H	0.90577900	-1.57850200	-0.00001500
C	3.14017500	-0.10033900	0.00000600
F	4.32122800	0.51674200	0.00001800
F	3.07391400	-0.89282700	-1.08627400
F	3.07388600	-0.89281700	1.08629100
N	-3.39178200	-0.21427000	0.00000200
C	-4.39051300	0.86876300	0.00001200
H	-4.28410800	1.48771300	-0.89092600
H	-5.38243700	0.43193500	0.00003200
H	-4.28407800	1.48772300	0.89094000
C	-3.89493600	-1.59932900	-0.00000400
H	-3.55786300	-2.12923900	0.89083100
H	-4.97855100	-1.57890900	-0.00000800
H	-3.55785800	-2.12923400	-0.89084000
C	2.01707500	0.91308800	-0.00001500
H	2.34356800	1.94563000	-0.00000800

E_{ZPE} = -817.849792

S-**20**--H_2O

0 1

C	2.26359500	-0.02688900	-0.00686200
C	1.41895400	-1.17942300	0.01269400
C	0.06226000	-1.05299100	0.00490200
C	-0.58517000	0.22786700	-0.01981000
C	0.28242700	1.36763300	-0.04113500
C	1.64334800	1.25395000	-0.03650400
H	1.85215700	-2.16763300	0.03464500
H	-0.54225100	-1.94816500	0.02134800
H	-0.18019200	2.34677400	-0.06413900
H	2.24352500	2.15038800	-0.05338300
N	3.60773200	-0.15295900	0.00299900
C	4.46448100	1.02857000	-0.01638100
H	4.28781700	1.65999300	0.85723900
H	5.50383100	0.71497100	-0.00506100
H	4.29664700	1.62429100	-0.91641300
C	4.23660300	-1.46943800	0.03599400
H	3.96670700	-2.06124200	-0.84174700
H	5.31549000	-1.34792200	0.04377200
H	3.94997000	-2.02428200	0.93230300
C	-2.86279700	-0.70955400	-0.00550100
F	-4.16649900	-0.36338700	-0.02405400
F	-2.70128600	-1.48290400	1.10868200
F	-2.68505500	-1.52589100	-1.08780000
C	-1.95285300	0.47680400	-0.01837600
O	-2.29380000	3.36208200	0.10366600
H	-2.37529000	2.37439800	0.06296600
H	-3.07167500	3.70295200	-0.34742200

E_{ZPE} = -857.135557

S-**20**--MeOH

0 1

C	1.82151300	-1.18682300	0.09298800
C	0.46124100	-1.25770700	0.05759800
C	-0.36006600	-0.08795200	-0.07629400
C	0.33726600	1.16019900	-0.16578000
C	1.69956900	1.24461700	-0.12910700
C	2.49437100	0.07076400	0.00032500
H	2.39069400	-2.09819800	0.19348300
H	-0.01007300	-2.22714500	0.13045800
H	2.16666500	2.21440200	-0.20281800
H	-0.26258000	2.05729700	-0.26507700
C	-2.48708400	-1.33088400	-0.03213800
F	-3.82451000	-1.16991200	-0.08365800
F	-2.24021500	-1.98800600	1.14084500
F	-2.17750300	-2.19212400	-1.04594900
C	-1.74768300	-0.03540400	-0.13392800
H	-2.43244600	1.74803600	-0.42242400
C	4.52270000	1.42769200	-0.05112500
H	4.30141600	1.93146400	-0.99491600
H	4.23067700	2.08487000	0.77103200
H	5.59510800	1.26815500	0.00612000
O	-2.53907000	2.73085800	-0.50176800
N	3.84200000	0.13934700	0.03445300
C	4.65156400	-1.06891800	0.15688900
H	5.70213000	-0.79531300	0.14444100
H	4.44658000	-1.59235700	1.09371200
H	4.46869000	-1.75440400	-0.67350200
C	-3.40494000	3.16332800	0.52592000
H	-4.42219600	2.76733900	0.40721200
H	-3.04629500	2.87706500	1.52466400
H	-3.46046800	4.25339300	0.48735100

E_{ZPE} = -817.502030

S-**20**--D_2O

0 1

C	2.26359500	-0.02688900	-0.00686200
C	1.41895400	-1.17942300	0.01269400
C	0.06226000	-1.05299100	0.00490200
C	-0.58517000	0.22786700	-0.01981000
C	0.28242700	1.36763300	-0.04113500
C	1.64334800	1.25395000	-0.03650400
H	1.85215700	-2.16763300	0.03464500
H	-0.54225100	-1.94816500	0.02134800
H	-0.18019200	2.34677400	-0.06413900
H	2.24352500	2.15038800	-0.05338300
N	3.60773200	-0.15295900	0.00299900
C	4.46448100	1.02857000	-0.01638100
H	4.28781700	1.65999300	0.85723900
H	5.50383100	0.71497100	-0.00506100
H	4.29664700	1.62429100	-0.91641300
C	4.23660300	-1.46943800	0.03599400
H	3.96670700	-2.06124200	-0.84174700
H	5.31549000	-1.34792200	0.04377200
H	3.94997000	-2.02428200	0.93230300
C	-2.86279700	-0.70955400	-0.00550100
F	-4.16649900	-0.36338700	-0.02405400
F	-2.70128600	-1.48290400	1.10868200
F	-2.68505500	-1.52589100	-1.08780000
C	-1.95285300	0.47680400	-0.01837600
O	-2.29380000	3.36208200	0.10366600
D	-2.37529000	2.37439800	0.06296600
D	-3.07167500	3.70295200	-0.34742200

E_{ZPE} = -817.939067

28a

0 1

C	2.24078500	0.01633700	0.01524700
C	1.46580100	-1.15612600	-0.10908300
C	0.10827400	-1.14946500	0.15793000
C	-0.54039900	0.01048600	0.57575600
C	0.21908600	1.16640300	0.72228200
C	1.57797100	1.18033300	0.45327400
H	1.92302600	-2.08412100	-0.41696600
H	-0.45819700	-2.06496000	0.05510400
H	-0.25452500	2.08203700	1.05751000
H	2.12037300	2.10275000	0.59282500
N	3.58995400	0.02297000	-0.28078400
C	4.38831700	1.18680500	0.04942000
H	4.40090000	1.39865400	1.12704300
H	5.41264600	1.02257000	-0.27702700
H	4.01902000	2.07709600	-0.46540300
C	4.27515500	-1.23127000	-0.52455900
H	3.84261000	-1.75717200	-1.37897300
H	5.31778500	-1.02948700	-0.75920400
H	4.24205100	-1.90552300	0.34160300
C	-2.83045400	0.22878200	-0.44995900
F	-4.16242200	0.19054900	-0.17118200
F	-2.59890000	-0.70977500	-1.37757400
F	-2.57662600	1.42966900	-0.99805600
C	-2.02024900	0.02274500	0.83956700
H	-2.27387700	0.88611000	1.46755400
O	-2.41428200	-1.19314700	1.44925100
H	-3.37143500	-1.18773600	1.56947100

E_{ZPE} = -817.887436

29a2

0 1

C	1.61152700	1.49742300	0.02760600
C	0.30164600	1.76322500	0.13479900
C	-0.68746100	0.70455800	0.08560400
C	-0.18525700	-0.72427600	0.25663500
C	1.26497000	-0.90184300	-0.06578200
C	2.12432200	0.13269300	-0.13247400
H	2.31281400	2.31932900	-0.01151700
H	-0.04457600	2.78828700	0.19507400
H	1.59703700	-1.92616300	-0.13865500
H	-0.78291900	-1.39297600	-0.36989000
C	-3.09314700	0.01988400	-0.24108100
F	-4.28155200	0.64636800	-0.32564800
F	-3.18770500	-0.85267400	0.80551200
F	-2.97275500	-0.75123100	-1.34798800
N	3.48766800	0.01105400	-0.44446100
C	4.43743900	0.67188000	0.44544200
H	4.57733700	0.11130300	1.38145300
H	5.40337700	0.75472100	-0.05451600
H	4.10758900	1.67457900	0.70470600
C	3.94881300	-1.29908200	-0.86173100
H	3.31969400	-1.67579700	-1.66811700
H	4.97050700	-1.21109200	-1.23231400
H	3.94540200	-2.03614600	-0.04408700
C	-1.98440600	1.00738900	-0.08584600
H	-2.31082800	2.03770600	-0.14273200
O	-0.33519800	-1.11840400	1.63777400
H	-1.28009000	-1.18715800	1.82371000

E_{ZPE} = -817.887108

29a4

0 1

C	-1.42446200	1.46434500	0.11477000
C	-0.12075100	1.69158000	-0.04276900
C	0.87441400	0.62704200	0.04063000
C	0.37952000	-0.68064300	0.45985300
C	-0.92267300	-0.92009000	0.61991800
H	-2.12485100	2.28726000	0.09365600
H	0.23702200	2.69820300	-0.22646400
H	-1.25158000	-1.88368100	0.98321800
H	1.09772300	-1.46305400	0.66233300
C	3.27369300	-0.10895400	-0.15649300
F	4.43831000	0.44428000	-0.55114100
F	3.06116800	-1.19092800	-0.94314000
F	3.47086400	-0.59050000	1.09721300
N	-2.88080300	-0.31251200	-0.70130600
C	-3.94269100	0.63795800	-1.03449900
H	-3.52735600	1.59744600	-1.33519300
H	-4.49469000	0.24810100	-1.88947000
H	-4.64903600	0.79976300	-0.20993500
C	-3.41924800	-1.66794000	-0.57984100
H	-4.03662900	-1.80552400	0.31743500
H	-4.03572400	-1.87047700	-1.45527600
H	-2.61987700	-2.40599600	-0.57628300
C	2.16694900	0.89234900	-0.22437200
H	2.48403400	1.88554400	-0.51139600
C	-2.01202900	0.09923800	0.38432200
O	-2.81531200	0.18478600	1.60129800
H	-2.24033300	0.44673400	2.33063400

E_{ZPE} = -857.113574

23b

0 1			
C	-1.82622400	1.12383800	0.28798300
C	-0.44227500	1.18690000	0.13771700
C	0.31114400	0.08639300	-0.28484400
C	-0.41377300	-1.09240900	-0.55380400
C	-1.78034900	-1.16291900	-0.37760000
C	-2.53361200	-0.05536100	0.04764700
C	1.75874500	0.12764300	-0.52002100
H	-2.34263500	2.02129300	0.59682400
H	0.03994300	2.13467600	0.33611400
H	0.10784600	-1.97048600	-0.90605500
H	-2.27316200	-2.10757600	-0.56481800
C	2.62436100	-0.81311200	0.20938200
F	2.67335900	-0.58131300	1.60188500
F	3.94340700	-0.70665700	-0.14275200
F	2.26526900	-2.08852000	0.06268600
O	2.28006100	1.48917300	-0.05767400
C	3.26797300	2.13736900	-0.91340200
H	4.17128500	1.53565700	-0.94733000
H	2.80295000	2.19424900	-1.89077600
H	3.44748400	3.12658300	-0.49365000
H	2.52481800	1.50996800	0.89016000
N	-3.92631800	-0.17135900	0.24804100
C	-4.60677300	0.95991100	0.84269800
H	-4.65612800	1.84004700	0.17964000
H	-5.62953800	0.66890000	1.08546800
H	-4.11320000	1.25522500	1.76883900
C	-4.69866100	-0.78067200	-0.82619700
H	-4.22931900	-1.69539400	-1.17796600
H	-5.69232200	-1.03920400	-0.45634600
H	-4.81592500	-0.10488500	-1.68870500

E_{ZPE} = -1482.984573

25

0 1

C	4.70378900	-0.05037300	0.21525600
C	4.17385300	-0.59250300	-0.97546300
C	2.81158300	-0.74266700	-1.14918400
C	1.90164600	-0.35540100	-0.16278700
C	2.42149900	0.16919200	1.02167400
C	3.78347000	0.31287800	1.21865000
H	4.82884500	-0.90018500	-1.77612300
H	2.44740800	-1.15810700	-2.07884000
H	1.74355600	0.47070300	1.80916700
H	4.12572700	0.71199100	2.16116200
N	6.06092500	0.11908900	0.38515600
C	6.57762700	0.53367000	1.67445200
H	6.35189200	-0.18896900	2.46939200
H	7.65778200	0.64131400	1.60986200
H	6.16679500	1.50193400	1.97175200
C	6.98341100	-0.42608400	-0.59133900
H	6.81566500	0.00730000	-1.58086700
H	8.00152800	-0.18392800	-0.29599900
H	6.90275400	-1.51703500	-0.68080600
C	0.43404200	-0.48682100	-0.32996800
C	-0.07043900	-1.92539500	-0.38949500
F	0.81842000	-2.73389400	-1.00403400
F	-1.23066300	-2.08357600	-1.04650900
F	-0.24229900	-2.42810400	0.85901300
C	-0.43955300	0.53776100	-0.31520900
C	0.06476700	1.97730900	-0.35070000
F	1.21915400	2.14827700	-1.01449900
F	-0.82953200	2.79718000	-0.94178600
F	0.24734800	2.45525300	0.90583800
C	-1.90566600	0.40452300	-0.13605200
C	-2.82426600	0.80776100	-1.10778200
C	-2.41453900	-0.14904400	1.03993400
C	-4.18499600	0.65362900	-0.92487700
H	-2.46796500	1.23197000	-2.03657200
C	-3.77465500	-0.29779800	1.24550600
H	-1.72933100	-0.47704300	1.81030200
C	-4.70497900	0.10598300	0.26741000
H	-4.84613400	0.96191000	-1.72017800
H	-4.10806500	-0.73273500	2.17527700
N	-6.06373500	-0.02243300	0.46786500
C	-6.54919400	-0.77578700	1.60793800
H	-7.63658800	-0.76122100	1.60984000
H	-6.21882100	-1.82253400	1.59054200
H	-6.21270200	-0.33050700	2.54741400
C	-6.97816200	0.22781600	-0.62927100
H	-8.00013200	0.10923300	-0.27671900
H	-6.87612900	1.24978800	-1.00185600
H	-6.82369700	-0.45859100	-1.47226000

E_{ZPE} = -857.134730

22b

0 1

C	1.04423300	1.47710700	0.22246400
C	-0.27849300	1.64654500	0.43200900
C	-1.25235400	0.62799700	0.10681000
C	-0.72009500	-0.59625300	-0.45110600
C	0.60362900	-0.76909500	-0.65911100
C	1.56486200	0.26292600	-0.35699300
H	1.72081900	2.27341900	0.48917500
H	-0.63421100	2.57296700	0.86562700
H	0.94316600	-1.70473600	-1.07457500
H	-1.40075200	-1.39716200	-0.70053800
C	-3.65557100	-0.13061900	0.04005300
F	-4.86168500	0.37556700	0.36525800
F	-3.51983900	-1.29893600	0.72060000
F	-3.71310100	-0.47798100	-1.27316900
N	2.85871800	0.13353600	-0.66982200
C	3.76181200	1.28672700	-0.61653700
H	3.69982300	1.77020600	0.35140600
H	4.77741500	0.92740900	-0.72697500
H	3.51817700	1.99390700	-1.41544400
C	3.32470100	-0.99230700	-1.48403400
H	2.97653200	-0.88216800	-2.51579000
H	4.40689200	-1.01022500	-1.44966200
H	2.97768100	-1.92990900	-1.06531200
C	-2.57459900	0.84784600	0.33693100
H	-2.91709700	1.78057900	0.76162200
O	3.97836000	-0.74074800	1.08650700
C	3.00972100	-0.95589200	1.99303700
H	3.12494000	-0.37984200	2.93225500
H	2.00331600	-0.62005100	1.59718100
H	2.84993400	-2.02089800	2.25240000

E_{ZPE} = -817.829739

22a

0 1			
C	1.26166800	1.44035200	-0.10498600
C	-0.06562600	1.68155300	-0.01883700
C	-1.04699200	0.62028700	-0.02794100
C	-0.51952100	-0.72281200	-0.12419100
C	0.80936800	-0.96232800	-0.20923700
C	1.77255800	0.10284500	-0.22042600
H	1.94328100	2.27577600	-0.08411000
H	-0.41779000	2.70252300	0.06139400
H	1.14227700	-1.98611800	-0.27762000
H	-1.20714300	-1.55597000	-0.13066400
C	-3.46054000	-0.10404600	0.05564300
F	-4.66774500	0.48598100	0.15998400
F	-3.36209900	-0.98992800	1.08152600
F	-3.48513100	-0.85782100	-1.07573500
N	3.09045200	-0.14229200	-0.25834500
C	4.02762600	0.94972500	-0.56350200
H	3.90959800	1.75058600	0.15523200
H	5.03522500	0.56906700	-0.45654900
H	3.85411100	1.30561500	-1.58312400
C	3.57778600	-1.47862300	-0.63412300
H	3.32203900	-1.68179500	-1.67853400
H	4.64940200	-1.49969500	-0.48710900
H	3.14934900	-2.23139600	0.01592700
C	-2.37368800	0.91222200	0.05498400
H	-2.71439000	1.93520300	0.12608400
O	4.02741300	-0.31175700	1.65607100
H	3.22049700	-0.47282500	2.16264700

E_{ZPE} = -817.830235

24 OH

0 3

C	-1.70741900	1.20646200	0.57951900
C	-0.36194400	1.42848600	0.68849700
C	0.60128600	0.42726300	0.37668100
C	0.08512800	-0.83095200	-0.04281300
C	-1.26197900	-1.05680000	-0.15550500
C	-2.21103400	-0.04755900	0.14734000
H	-2.38427400	2.01248000	0.81922900
H	-0.01022300	2.40287800	1.00259400
H	-1.59170800	-2.02997600	-0.48652200
H	0.76905200	-1.63216700	-0.28420800
C	3.04768000	-0.26374000	0.22209700
F	4.26386800	0.25970400	0.46516700
F	3.05309300	-0.65926500	-1.09583400
F	2.96585500	-1.42421400	0.92785500
N	-3.55506000	-0.27339400	0.02669200
C	-4.50582800	0.78776600	0.30828400
H	-4.35930600	1.64777400	-0.35285100
H	-5.51493900	0.41420100	0.15758000
H	-4.42527800	1.13376500	1.34291300
C	-4.04534300	-1.55442400	-0.45120700
H	-3.73423400	-2.37286800	0.20455400
H	-5.13154300	-1.53688100	-0.47262000
H	-3.68861200	-1.77211100	-1.46293300
C	1.97332400	0.69923700	0.53305000
H	2.30749100	1.67718900	0.84212900
O	1.08923400	1.59185800	-1.90878100
H	1.70654500	0.87415400	-2.13680500

E_{ZPE} = -722.395323

d-**22**

1 1

C	-2.38481400	-0.26459200	0.00000000
C	-2.04453700	1.12147800	0.00000000
C	-0.73602500	1.47531500	-0.00000700
C	0.31797100	0.48406500	-0.00000800
C	-0.06233000	-0.91418800	-0.00001000
C	-1.36614900	-1.26874400	-0.00000500
C	2.81728600	-0.00693100	0.00000400
F	2.81128400	-0.79531100	-1.08744700
F	3.93602300	0.71266100	0.00003000
F	2.81125800	-0.79534600	1.08742800
C	1.60597100	0.90689000	-0.00000200
D	1.84222700	1.96448200	-0.00000600
H	-0.45995300	2.52240900	-0.00001000
H	-2.81713600	1.87532300	0.00000300
H	-1.68055200	-2.30344800	-0.00000500
H	0.70477300	-1.67513800	-0.00001500
O	-3.60137300	-0.71461300	0.00000100
C	-4.76014800	0.16409500	0.00000900
H	-4.75757700	0.77778100	-0.89992200
H	-5.61365500	-0.50465000	0.00001700
H	-4.75756400	0.77778500	0.89993700

E_{ZPE} = -831.572565

36uu

0 1

C	1.78776600	2.43860400	-0.00019000
C	2.38404400	0.11475000	-0.00029800
C	1.03639000	-0.23461600	-0.00014200
C	0.05153000	0.76496700	-0.00000600
C	0.43773800	2.10859000	-0.00003300
H	0.74890200	-1.27260800	-0.00012400
H	-0.30141300	2.89846600	0.00007000
C	-1.87729500	-1.01489900	0.00023800
F	-1.45605500	-1.71377100	-1.07966300
F	-1.45576200	-1.71376200	1.08003000
F	-3.22230000	-1.04864500	0.00042000
H	2.07868500	3.48137200	-0.00020800
C	2.76445600	1.45892600	-0.00032200
H	3.81751600	1.70424600	-0.00044400
O	3.39995100	-0.78724100	-0.00043600
C	3.08933200	-2.17310600	-0.00041800
H	4.04491000	-2.69217400	-0.00054600
H	2.52371000	-2.45660900	0.89243500
H	2.52348500	-2.45658200	-0.89313600
C	-1.36584900	0.39007300	0.00016500
N	-2.28334100	1.31534500	0.00027100
N	-3.04194900	2.15003900	0.00035800

E_{ZPE} = -721.964816

S-**30**uu

0 1

C	1.96457400	2.24897600	-0.00000100
C	0.60332600	-0.20589900	0.00000200
C	-0.13564900	1.01475400	-0.00000700
C	0.57859600	2.23715200	-0.00000900
H	0.07125700	-1.14239200	0.00000400
H	0.00172200	3.15107600	-0.00001700
C	-1.54735700	1.15604100	-0.00001400
C	-2.33684700	-0.12062900	0.00000300
F	-2.07987000	-0.88402800	-1.10228600
F	-2.07987000	-0.88400800	1.10230000
F	-3.66508400	0.08796200	0.00000000
H	2.50797800	3.18449700	-0.00000100
C	1.98491300	-0.18344800	0.00000600
C	2.65996400	1.05105700	0.00000500
H	3.74276000	1.03395200	0.00000900
O	2.78618300	-1.27646400	0.00001300
C	2.17678300	-2.56355700	-0.00001300
H	2.99502600	-3.27896000	-0.00002300
H	1.56269600	-2.71125700	0.89288200
H	1.56270200	-2.71122300	-0.89291700

E_{ZPE} = -721.971338

T-**30**uu

0 3

C	-1.99944700	2.25330000	0.00000300
C	-2.08940300	-0.16484300	0.00000100
C	-0.70773200	-0.22787500	-0.00000400
C	0.05864400	0.97500900	-0.00000500
C	-0.61638600	2.22120700	-0.00000100
H	-0.18965600	-1.17378300	-0.00000900
H	-0.03898100	3.13514900	-0.00000200
C	1.44483800	0.92486500	-0.00000800
C	2.45290000	-0.13851600	-0.00000100
F	2.34570300	-0.95256900	1.08518400
F	2.34560000	-0.95267700	-1.08509400
F	3.70148500	0.36097200	-0.00008400
H	-2.51312600	3.20613400	0.00000600
C	-2.74166300	1.07993700	0.00000500
H	-3.82304000	1.09482000	0.00000800
O	-2.90740500	-1.24785600	0.00000200
C	-2.32368700	-2.54391300	-0.00000200
H	-3.15485000	-3.24481900	0.00000000
H	-1.71228900	-2.70560200	-0.89280600
H	-1.71228300	-2.70560500	0.89279700

E_{ZPE} = -798.420852

S-**30**--H_2Ouu

0 1

C	1.34286000	2.54330500	-0.05803500
C	0.97036600	-0.24001800	0.00012000
C	-0.16270000	0.63085100	-0.02601000
C	0.05371200	2.03439200	-0.05330200
H	0.81391800	-1.30538100	0.02243200
H	-0.80966000	2.68637100	-0.07272500
C	-1.51615000	0.23486300	-0.02283100
C	-1.79868800	-1.23913700	-0.01958100
F	-1.25367100	-1.87927500	-1.09260500
F	-1.32163900	-1.83860100	1.10608400
F	-3.11545200	-1.50943500	-0.05950400
H	1.50947400	3.61191500	-0.08021600
C	2.24711200	0.28273400	0.00098800
O	-3.13439300	2.67439200	0.14705900
H	-4.01165700	2.65496700	-0.24624300
H	-2.78869000	1.75329400	0.08277800
C	2.42514400	1.67978500	-0.02985200
H	3.44031300	2.05721600	-0.02970100
O	3.39173600	-0.44083600	0.02848100
C	3.29417300	-1.86140600	0.06201900
H	4.31692700	-2.22848900	0.08076800
H	2.76769600	-2.20057800	0.95863400
H	2.78483400	-2.24418400	-0.82692100

E_{ZPE} = -798.418888

T-**30**--H_2Ouu

0 3

C	1.58256400	2.46937300	-0.00000700
C	1.08038200	-0.28371200	-0.00000400
C	-0.00501900	0.64217500	-0.00000600
C	0.26935100	2.03384700	-0.00000800
H	0.86419800	-1.34046300	0.00000000
H	-0.56070900	2.72670000	-0.00000700
C	-1.31534800	0.18992700	-0.00001000
C	-1.98579800	-1.10909800	-0.00000600
F	-1.67191800	-1.86550700	-1.08494400
F	-1.67186100	-1.86552400	1.08491000
F	-3.33041600	-0.95914400	0.00003100
H	1.79321900	3.53119900	-0.00000800
C	2.38150100	0.18397700	-0.00000400
O	-3.08102600	2.65171800	0.00002200
H	-3.24288000	2.08288400	-0.76116100
H	-3.24283600	2.08282900	0.76117200
C	2.63729200	1.56626900	-0.00000500
H	3.66661100	1.89842100	-0.00000500
O	3.48367400	-0.60914800	0.00000600
C	3.30803400	-2.01914900	0.00001200
H	4.30873500	-2.44434700	0.00002100
H	2.77123300	-2.35392400	0.89278400
H	2.77124600	-2.35393300	-0.89276500

E_{ZPE} = -798.527181

38

0 1

C	-1.40459800	2.27507600	-0.45871300
C	-2.32171600	0.09172000	-0.03403200
C	-1.07264300	-0.34170500	0.40467200
C	0.01055600	0.53925300	0.40184100
C	-0.14985200	1.84863500	-0.03008600
H	-0.92847100	-1.35654200	0.74581100
H	0.69207300	2.52480600	-0.02175500
C	2.14442600	-0.58641300	-0.32561500
F	1.52156600	-1.67915800	-0.80189500
F	2.33627200	0.26124200	-1.34245600
F	3.37259200	-0.98146500	0.10368000
H	-1.53835200	3.29611400	-0.79290100
C	-2.48457700	1.41021500	-0.46599200
H	-3.46408300	1.72958300	-0.79620000
O	-3.43657900	-0.68765200	-0.07047800
C	-3.33537000	-2.04221200	0.33843400
H	-4.32872300	-2.46733100	0.21443000
H	-2.62482000	-2.59652500	-0.28279100
H	-3.03748300	-2.12322900	1.38879300
C	1.36364200	0.03536900	0.84436300
H	1.23300200	-0.78498600	1.56130300
O	2.11571600	1.09146300	1.40294800
H	2.99068600	0.76243100	1.64036500

5. References

1. Keeffe, J. R.; O'Ferrall, R. A. M., The protonation of carbenes and structural effects on the α-proton acidity of carbocations. *ARKIVOC (Gainesville, FL, U. S.)* **2008,** (10), 183-204.
2. Belt, S. T.; Bohne, C.; Charette, G.; Sugamori, S. E.; Scaiano, J. C., Carbocation Formation Via Carbene Protonation Studied by the Technique of Stopped-Flow Laser-Flash Photolysis. *Journal of the American Chemical Society* **1993,** *115* (6), 2200-2205.
3. Costa, P.; Fernandez-Oliva, M.; Sanchez-Garcia, E.; Sander, W., The highly reactive benzhydryl cation isolated and stabilized in water ice. *J Am Chem Soc* **2014,** *136* (44), 15625-30.
4. Costa, P.; Trosien, I.; Fernandez-Oliva, M.; Sanchez-Garcia, E.; Sander, W., The Fluorenyl Cation. *Angew. Chem. Int. Ed.* **2015,** *54* (9), 2656-2660.
5. Richter, G.; Mendez-Vega, E.; Sander, W., Singlet Halophenylcarbenes as Strong Hydrogen-Bond Acceptors. *The Journal of Physical Chemistry A* **2016,** *120* (20), 3524-3532.
6. Creary, X., Electronegatively substituted carbocations. *Chemical Reviews* **1991,** *91* (8), 1625-1678.
7. Tidwell, T. T., Destabilized carbocations. *Angew. Chem.* **1984,** *96* (1), 16-28.
8. McClelland, R. A.; Cozens, F. L.; Steenken, S.; Amyes, T. L.; Richard, J. P., Direct observation of β-fluoro-substituted 4-methoxyphenethyl cations by laser flash photolysis. *Journal of the Chemical Society, Perkin Transactions 2* **1993,** (10), 1717-1722.
9. Richard, J. P.; Amyes, T. L.; Vontor, T., Reactions of ring-substituted 1-phenyl-2,2,2-trifluoroethyl carbocations with nucleophilic reagents: a bridge between carbocations which follow the reactivity-selectivity principle and the N+ scale. *Journal of the American Chemical Society* **1992,** *114* (14), 5626-5634.
10. Guthrie, J. P.; Pitchko, V., Reactions of carbocations with water and azide ion: calculation of rate constants from equilibrium constants and distortion energies using No Barrier Theory. *Journal of Physical Organic Chemistry* **2004,** *17* (6-7), 548-559.
11. Richard, J., A consideration of the barrier for carbocation-nucleophile combination reactions. *Tetrahedron* **1995,** *51*, 1535-73.
12. Raut, A. H.; Costa, P.; Sander, W., Reactions of Arylcarbenes with Lewis Acids. *Chemistry – A European Journal* **2018,** *24* (68), 18043-18051.
13. Costa, P.; Sander, W., Hydrogen Bonding Switches the Spin State of Diphenylcarbene from Triplet to Singlet. *Angew. Chem., Int. Ed.* **2014,** *53* (20), 5122-5125.
14. Eisenthal, K. B.; Moss, R. A.; Turro, N. J., Divalent carbon intermediates: laser photolysis and spectroscopy. *Science* **1984,** *225* (4669), 1439-45.
15. Zewail, A. H., Femtochemistry. Past, present, and future. *Pure and Applied Chemistry* **2000,** *72* (12), 2219-2231.
16. Eigen, M., Die „unmeßbar" schnellen Reaktionen (Nobel-Vortrag). *Angewandte Chemie* **1968,** *80* (21), 892-906.
17. Norrish, R. G. W., Untersuchungen einiger schneller Reaktionen in Gasen durch Blitzlichtphotolyse und kinetische Spektroskopie (Nobel-Vortrag). *Angewandte Chemie* **1968,** *80* (21), 868-881.
18. Porter, G., Die Blitzlichtphotolyse und einige ihrer Anwendungen (Nobel-Vortrag). *Angewandte Chemie* **1968,** *80* (21), 882-891.
19. Becker, E. D.; Pimentel, G. C., Spectroscopic Studies of Reactive Molecules by the Matrix Isolation Method. *The Journal of Chemical Physics* **1956,** *25* (2), 224-228.
20. Norman, I.; Porter, G., Trapped Atoms and Radicals in a Glass 'Cage'. *Nature* **1954,** *174* (4428), 508-509.

21. Dunkin, I. R., The matrix isolation technique and its application to organic chemistry. *Chemical Society Reviews* **1980,** *9* (1), 1.
22. Bally, T., Matrix isolation. Wiley Online Library: 2004; p 820.
23. Van Thiel, M.; Becker, E. D.; Pimentel, G. C., Infrared Studies of Hydrogen Bonding of Water by the Matrix Isolation Technique. *The Journal of Chemical Physics* **1957,** *27* (2), 486-490.
24. Henkel, S.; Costa, P.; Klute, L.; Sokkar, P.; Fernandez-Oliva, M.; Thiel, W.; Sanchez-Garcia, E.; Sander, W., Switching the Spin State of Diphenylcarbene via Halogen Bonding. *Journal of the American Chemical Society* **2016,** *138* (5), 1689-1697.
25. Romano, R. M.; Downs, A. J., Matrix-Isolated van der Waals Complexes Formed between CO and Dihalogen Molecules, XY with X, Y = Cl, Br, or I. *The Journal of Physical Chemistry A* **2003,** *107* (27), 5298-5305.
26. Gudipati, M. S., Matrix-isolation in cryogenic water-ices: Facile generation, storage, and optical spectroscopy of aromatic radical cations. *Journal of Physical Chemistry A* **2004,** *108* (20), 4412-4419.
27. Bahou, M.; Das, P.; Lee, Y.-F.; Wu, Y.-J.; Lee, Y.-P., Infrared spectra of free radicals and protonated species produced in para-hydrogen matrices. *Physical Chemistry Chemical Physics* **2014,** *16* (6), 2200.
28. Tsegaw, Y. A. Chemistry in cryogenic matrices. 2018.
29. Zins, E. L.; Krim, L., Formation and characterization of VUV photolytically-induced (NH2)(NH3)n aggregates, $0 \leq n \leq 3$. *RSC Advances* **2013,** *3* (26), 10285.
30. Fausto, R.; Khriachtchev, L.; Hamm, P., Conformational Changes in Cryogenic Matrices. 2019; pp 51-84.
31. Moss, R. A.; Sauers, R. R.; Sheridan, R. S.; Tian, J.; Zuev, P. S., Carbon tunneling in the ring expansion of noradamantylchlorocarbene. *J Am Chem Soc* **2004,** *126* (33), 10196-7.
32. Gudipati, M. S.; Jacovi, R.; Couturier-Tamburelli, I.; Lignell, A.; Allen, M., Photochemical activity of Titan's low-altitude condensed haze. *Nature Communications* **2013,** *4*.
33. Buchner, E.; Curtius, T., Ueber die Einwirkung von Diazoessigäther auf aromatische Kohlenwasserstoffe. *Berichte der deutschen chemischen Gesellschaft* **1885,** *18* (2), 2377-2379.
34. Staudinger, H.; Kupfer, O., Über Reaktionen des Methylens. III. Diazomethan. *Berichte der deutschen chemischen Gesellschaft* **1912,** *45* (1), 501-509.
35. Kirmse, W., Carbene. *Chemie in unserer Zeit* **1969,** *3* (6), 184-191.
36. Bertrand, G., *Carbene chemistry : from fleeting intermediates to powerful reagents*. Marcel Dekker ; FontisMedia: New York Lausanne, Switzerland, 2002; p xv, 301.

37. Hermann, M., Ueber die bei der technischen Gewinnung des Broms beobachtete flüchtige Bromverbindung. *Annalen der Chemie und Pharmacie* **1855,** *95* (2), 211-225.
38. Moritani, I.; Murahashi, S. I.; Nishino, M.; Kimura, K.; Tsubomura, H., Electronic Absorption Spectra of the Products formed by the photolysis of diazo compounds at 77K, possibly identified as carbenes. *Tetrahedron Lett.* **1966,** *4*, 373-378.
39. Piquet, V.; Baceiredo, A.; Gornitzka, H.; Dahan, F.; Bertrand, G., The Stable (Phosphino)(Silyl)Carbene As A Useful Building Block: Synthesis And Reactivity of 2-Phosphorus-Substituted 2H-Azirines. *Chemistry – A European Journal* **1997,** *3* (11), 1757-1764.
40. Arduengo, A. J.; Harlow, R. L.; Kline, M., A stable crystalline carbene. *Journal of the American Chemical Society* **1991,** *113* (1), 361-363.
41. Trosien, I. Matrix isolation study of aryl and cyclopentadienyl carbenes. 2019.

42. Chen, B.; Rogachev, A. Y.; Hrovat, D. A.; Hoffmann, R.; Borden, W. T., How to Make the σ0π2 Singlet the Ground State of Carbenes. *Journal of the American Chemical Society* **2013,** *135* (37), 13954-13964.
43. Bourissou, D.; Guerret, O.; Gabbaï, F. P.; Bertrand, G., Stable Carbenes. *Chemical Reviews* **2000,** *100* (1), 39-92.
44. Eisenthal, K. B.; Turro, N. J.; Sitzmann, E. V.; Gould, I. R.; Hefferon, G.; Langan, J.; Cha, Y., Singlet-Triplet Interconversion of Diphenylmethylene - Energetics, Dynamics and Reactivities of Different Spin States. *Tetrahedron* **1985,** *41* (8), 1543-1554.
45. Sander, W.; Bucher, G.; Wierlacher, S., Carbenes in Matrices - Spectroscopy, Structure, and Reactivity. *Chem. Rev.* **1993,** *93* (4), 1583-1621.
46. Kirmse, W., *Carbene Chemistry*. Academic Press: New York, London, 1971.
47. Kirmse, W., Stable Singlet Carbenes—Plentiful and Versatile. *Angewandte Chemie International Edition* **2004,** *43* (14), 1767-1769.
48. Song, M.-G.; Sheridan, R. S., Regiochemical Substituent Switching of Spin States in Aryl(trifluoromethyl)carbenes. *J. Am. Chem. Soc.* **2011,** *133* (Copyright (C) 2012 American Chemical Society (ACS). All Rights Reserved.), 19688-19690.
49. Lide, D. R., *CRC handbook of chemistry and physics: a ready-reference book of chemical and physical data*. CRC press: 1995.
50. Kirmse, W., Carbenes and the O-H bond. In *Advances in carbene chemistry*, Brinker, U. H., Ed. Jai Press: Greenwich, Conn., 1994; Vol. 1, pp 1 - 57.
51. Brahms, D. L. S.; Dailey, W. P., Fluorinated Carbenes. *Chem. Rev.* **1996,** *96* (5), 1585-1932.
52. Song, M.-G.; Sheridan, R. S., Effects of CF3 groups and charged substituents on singlet carbene stabilities-a density functional theory study. *J. Phys. Org. Chem.* **2011,** *24* (Copyright (C) 2013 American Chemical Society (ACS). All Rights Reserved.), 889-893.
53. Pauling, L., The structure of singlet carbene molecules. *J. Chem. Soc., Chem. Commun.* **1980**, 688-689.
54. Bertrand, G., Stable singlet carbenes. *Reactive Intermediate Chemistry* **2004**, 329-373.
55. Buron, C., Stable Versions of Transient Push-Pull Carbenes: Extending Lifetimes from Nanoseconds to Weeks. *Science* **2000,** *288* (5467), 834-836.
56. Moss, R. A.; Zdrojewski, T.; Krogh-Jespersen, K.; Wlostowski, M.; Matro, A., Push-pull carbenes: alkoxy cyano carbenes. *Tetrahedron Lett.* **1991,** *32*, 1925-1928.
57. Moss, R. A.; Zdrojewski, T.; Ho, G. J., Push-pull carbenes: methoxytrifluoromethylcarbene. *J. Chem. Soc., Chem. Commun.* **1991**, 946-947.
58. Moss, G. P.; Smith, P. A. S.; Tavernier, D., Glossary of class names of organic compounds and reactivity intermediates based on structure (IUPAC Recommendations 1995). *Pure and Applied Chemistry* **1995,** *67* (8-9), 1307-1375.
59. McClelland, R. A., Carbocations. *Reactive Intermediate Chemistry* **2004**, 3-40.
60. Aue, D. H., Carbocations. *Wiley Interdiscip. Rev.: Comput. Mol. Sci.* **2011,** *1* (4), 487-508.
61. Olah, G. A., Stable carbocations. CXVIII. General concept and structure of carbocations based on differentiation of trivalent (classical) carbenium ions from three-center bound penta- of tetracoordinated (nonclassical) carbonium ions. Role of carbocations in electrophilic reactions. *Journal of the American Chemical Society* **1972,** *94* (3), 808-820.
62. Olah, G. A., My Search for Carbocations and Their Role in Chemistry (Nobel Lecture). *Angewandte Chemie International Edition in English* **1995,** *34* (13-14), 1393-1405.
63. Meerwein, H.; van Emster, K., Über die Gleichgewichts-Isomerie zwischen Bornylchlorid, Isobornylchlorid und Camphen-chlorhydrat. *Berichte der deutschen chemischen Gesellschaft (A and B Series)* **1922,** *55* (8), 2500-2528.

64. Rzepa, H. S.; Allan, C. S. M., Racemization of Isobornyl Chloride via Carbocations: A Nonclassical Look at a Classic Mechanism. *Journal of Chemical Education* **2010,** *87* (2), 221-228.
65. Allen, A. D.; Tidwell, T. T. In *Antiaromaticity effects in cyclopentadienyl carbocations and free radicals*, John Wiley & Sons, Inc.: 2004; pp 103-123.
66. Amyes, T. L.; Richard, J. P.; Novak, M., Experiments and calculations for determination of the stabilities of benzyl, benzhydryl, and fluorenyl carbocations: antiaromaticity revisited. *J. Am. Chem. Soc.* **1992,** *114* (21), 8032-41.
67. Von E.Doering, W.; Knox, L. H., The Cycloheptatrienylium (Tropylium) Ion. *Journal of the American Chemical Society* **1954,** *76* (12), 3203-3206.
68. Vancik, H., Matrix isolation and vibrational spectroscopy of carbocations. *Pure Appl. Chem.* **1995,** *67* (5), 761-767.
69. Kirsch, P., *Modern fluoroorganic chemistry: synthesis, reactivity, applications*. John Wiley & Sons: 2013.
70. Olah, G. A.; Prakash, G. K. S.; Sommer, J., Superacids. *Science* **1979,** *206* (4414), 13-20.
71. Mcclelland, R. A., Flash photolysis generation and reactivities of carbenium ions and nitrenium ions. *Tetrahedron* **1996,** *52* (20), 6823-6858.
72. Das, P. K., Transient carbocations and carbanions generated by laser flash photolysis and pulse radiolysis. *Chemical Reviews* **1993,** *93* (1), 119-144.
73. Kirmse, W., Nucleophiles Verhalten des Diphenylcarbens. *Angewandte Chemie* **1963,** *75* (14), 678-678.
74. Kirmse, W.; Kilian, J.; Steenken, S., Carbenes and the oxygen-hydrogen bond: spectroscopic evidence for protonation of diarylcarbenes to give diarylcarbenium ions. *J. Am. Chem. Soc.* **1990,** *112* (17), 6399-400.
75. Xu, J.; Mieres-Perez, J.; Sanchez-Garcia, E.; Lee, J. K., Gas-Phase Deprotonation of Benzhydryl Cations: Carbene Basicity, Multiplicity, and Rearrangements. *The Journal of Organic Chemistry* **2019,** *84* (12), 7685-7693.
76. Mayer, R. J.; Hampel, N.; Mayer, P.; Ofial, A. R.; Mayr, H., Synthesis, Structure, and Properties of Amino-Substituted Benzhydrylium Ions - A Link between Ordinary Carbocations and Neutral Electrophiles. *European Journal of Organic Chemistry* **2019,** *2019* (2-3), 412-421.
77. A. Fleming, S., Chemical reagents in photoaffinity labeling. *Tetrahedron* **1995,** *51* (46), 12479-12520.
78. Blencowe, A.; Hayes, W., Development and application of diazirines in biological and synthetic macromolecular systems. *Soft Matter* **2005,** *1* (3), 178-205.
79. Hashimoto, M.; Hatanaka, Y., Recent Progress in Diazirine-Based Photoaffinity Labeling. *European Journal of Organic Chemistry* **2008,** *2008* (15), 2513-2523.
80. Brunner, J.; Senn, H.; Richards, F. M., 3-Trifluoromethyl-3-phenyldiazirine. A new carbene generating group for photolabeling reagents. *J Biol Chem* **1980,** *255* (8), 3313-8.
81. Smith, E.; Collins, I., Photoaffinity labeling in target- and binding-site identification. *Future Medicinal Chemistry* **2015,** *7* (2), 159-183.
82. Dubinsky, L.; Krom, B. P.; Meijler, M. M., Diazirine based photoaffinity labeling. *Bioorg Med Chem* **2012,** *20* (2), 554-70.
83. Dankbar, D. M.; Gauglitz, G., A study on photolinkers used for biomolecule attachment to polymer surfaces. *Analytical and Bioanalytical Chemistry* **2006,** *386* (7), 1967-1974.
84. Blencowe, A.; Blencowe, C.; Cosstick, K.; Hayes, W., A carbene insertion approach to functionalised poly(ethylene oxide)-based gels. *Reactive and Functional Polymers* **2008,** *68*, 868-875.
85. Raut, A. H. Reactivity of carbenes with Lewis acids. 2019.

86. Richter, G. Matrixisolationsstudien von Arylhalogencarbenen und 1,3-Di-\(\it tert\)-butylimidazol-2-yliden. 2016.
87. Hopkinson, A. C.; Lien, M. H., Substituent effects in carbocations CX+, CHX+., and CH2X+, and in singlet and triplet carbenes CHX. Proton affinities of singlet carbenes. *Can. J. Chem.* **1985,** *63*, 3582-3586.
88. Radhakrishnan, S. Matrix isolation and solvation studies of reactive intermediates. 2018.
89. Courtney, M. C.; MacCormack, A. C.; O'Ferrall, R. A. M., Comparison of pKR values of fluorenyl and anthracenyl cations. *J. Phys. Org. Chem.* **2002,** *15* (8), 529-539.
90. Hohenberg, P.; Kohn, W., Density functional theory (DFT). *Phys. Rev* **1964,** *136*, B864.
91. Kreienborg, N. M.; Merten, C., How to treat C–F stretching vibrations? A vibrational CD study on chiral fluorinated molecules. *Physical Chemistry Chemical Physics* **2019,** *21* (7), 3506-3511.
92. Tsegaw, Y. A.; Kadam, P. E.; Tötsch, N.; Sanchez-Garcia, E.; Sander, W., Is Magnetic Bistability of Carbenes a General Phenomenon? Isolation of Simple Aryl(trifluoromethyl)carbenes in Both Their Singlet and Triplet States. *Journal of the American Chemical Society* **2017,** *139* (35), 12310-12316.
93. Trosien, I.; Mendez-Vega, E.; Thomanek, T.; Sander, W., Conformational Spin Switching and Spin-Selective Hydrogenation of a Magnetically Bistable Carbene. *Angewandte Chemie International Edition* **2019,** *58* (42), 14855-14859.
94. Woodcock, H. L.; Moran, D.; Brooks, B. R.; Schleyer, P. v. R.; Schaefer, H. F., Carbene Stabilization by Aryl Substituents. Is Bigger Better? *Journal of the American Chemical Society* **2007,** *129* (12), 3763-3770.
95. Sheridan, R. S., Exploring matrix isolated carbenes and bis-carbenes with electronic spectroscopy as a guide. *Journal of Physical Organic Chemistry* **2010**, n/a-n/a.
96. Lopes Jesus, A. J.; Reva, I.; Araujo-Andrade, C.; Fausto, R., Conformational changes in matrix-isolated 6-methoxyindole: Effects of the thermal and infrared light excitations. *The Journal of Chemical Physics* **2016,** *144* (12), 124306.
97. Kuş, N.; Sharma, A.; Reva, I.; Lapinski, L.; Fausto, R., Thermal and Photoinduced Control of Relative Populations of 4-Methoxybenzaldehyde (p-Anisaldehyde) Conformers. *The Journal of Physical Chemistry A* **2010,** *114* (29), 7716-7724.
98. Bentwood, R. M.; Barnes, A. J.; Orville-Thomas, W. J., Studies of intermolecular interactions by matrix isolation vibrational spectroscopy. *Journal of Molecular Spectroscopy* **1980,** *84* (2), 391-404.
99. Arunan, E.; Desiraju, G. R.; Klein, R. A.; Sadlej, J.; Scheiner, S.; Alkorta, I.; Clary, D. C.; Crabtree, R. H.; Dannenberg, J. J.; Hobza, P.; Kjaergaard, H. G.; Legon, A. C.; Mennucci, B.; Nesbitt, D. J., Definition of the hydrogen bond (IUPAC Recommendations 2011). *Pure and Applied Chemistry* **2011,** *83* (8), 1637-1641.
100. Grabowski, S., *Hydrogen Bonding—New Insights*. 2006; Vol. 3.
101. Kirmse, W., Carbene Protonation. In *Advances in Carbene Chemistry*, Brinker, U. H., Ed. Elsevier Science B.V.: 2001; Vol. 3, pp 1-51.
102. Barnes, A. J., Studies of intermolecular interactions by matrix isolation vibrational spectroscopy: self-association of ammonia. *Journal of Molecular Structure* **1990,** *237*, 19-32.
103. Allodi, M. A.; Baragiola, R. A.; Baratta, G. A.; Barucci, M. A.; Blake, G. A.; Boduch, P.; Brucato, J. R.; Contreras, C.; Cuylle, S. H.; Fulvio, D.; Gudipati, M. S.; Ioppolo, S.; Kanuchova, Z.; Lignell, A.; Linnartz, H.; Palumbo, M. E.; Raut, U.; Rothard, H.; Salama, F.; Savchenko, E. V.; Sciamma-O'Brien, E.; Strazzulla, G., Complementary and Emerging Techniques for Astrophysical Ices Processed in the Laboratory. *Space Science Reviews* **2013,** *180* (1-4), 101-175.

104. Mcclelland, R. A.; Cozens, F. L.; Steenken, S.; Amyes, T. L.; Richard, J. P., Direct observation of β-fluoro-substituted 4-methoxyphenethyl cations by laser flash photolysis. *J. Chem. Soc., Perkin Trans. 2* **1993,** (10), 1717-1722.
105. Radhakrishnan, S.; Mieres-Perez, J.; Gudipati, M. S.; Sander, W., Photoinduced Reversible Electron Transfer Between the Benzhydryl Radical and Benzhydryl Cation in Amorphous Water–Ice. *The Journal of Physical Chemistry A* **2017,** *121* (34), 6405-6412.
106. Jones, W. M., Carbene-carbene rearrangements in solution. *Accounts of Chemical Research* **1977,** *10* (10), 353-359.
107. Wentrup, C., Carbenes and Nitrenes: Recent Developments in Fundamental Chemistry. *Angewandte Chemie International Edition* **2018,** *57* (36), 11508-11521.
108. Pollok, C. H.; Merten, C., Conformational distortion of α-phenylethyl amine in cryogenic matrices – a matrix isolation VCD study. *Physical Chemistry Chemical Physics* **2016,** *18* (19), 13496-13502.
109. Barnes, A. J., Matrix isolation vibrational spectroscopy as a tool for studying conformational isomerism. *Journal of Molecular Structure* **1984,** *113*, 161-174.
110. Richard, J. P., Aromatic substitution reactions of amines with ring-substituted 1-phenyl-2, 2, 2-trifluoroethyl carbocations. *Journal of the American Chemical Society* **1989,** *111* (17), 6735-6744.
111. Ta-Shma, R.; Jencks, W. P., How does a reaction change its mechanism? General base catalysis of the addition of alcohols to 1-phenylethyl carbocations. *Journal of the American Chemical Society* **1986,** *108* (25), 8040-8050.
112. Jagannadham, V.; Amyes, T. L.; Richard, J. P., How delocalised are resonance-stabilised 1-[4-(N-methyl-N-alkylamino)phenyl]-2,2,2-trifluoroethyl carbocations? *Journal of the Chemical Society, Perkin Transactions 2* **1993,** (2), 171.
113. Moss, R. A.; Wang, L.; Weintraub, E.; Krogh-Jespersen, K., The Solvation of Carbenes: π and O-Ylidic Complexes of p-Nitrophenylchlorocarbene. *The Journal of Physical Chemistry A* **2008,** *112* (20), 4651-4659.
114. Hoijemberg, P. A.; Moss, R. A.; Krogh-Jespersen, K., Reversible O-Ylide Formation in Carbene/Ether Reactions. *J. Phys. Chem. A* **2012,** *116* (1), 358-363.
115. Wentrup, C., Nitrenes, Carbenes, Diradicals, and Ylides. Interconversions of Reactive Intermediates. *Acc. Chem. Res.* **2011,** *44* (Copyright (C) 2012 American Chemical Society (ACS). All Rights Reserved.), 393-404.
116. Dreuw, A.; Head-Gordon, M., Failure of time-dependent density functional theory for long-range charge-transfer excited states: the zincbacteriochlorin− bacteriochlorin and bacteriochlorophyll− spheroidene complexes. *Journal of the American Chemical Society* **2004,** *126* (12), 4007-4016.
117. Adamo, C.; Jacquemin, D., The calculations of excited-state properties with Time-Dependent Density Functional Theory. *Chemical Society Reviews* **2013,** *42* (3), 845-856.
118. Richard, J. P.; Amyes, T. L.; Bei, L.; Stubblefield, V., Effect of .beta.-fluorine substituents on the rate and equilibrium constants for the reactions of .alpha.-substituted 4-methoxybenzyl carbocations and on the reactivity of a simple quinone methide. *Journal of the American Chemical Society* **1990,** *112* (26), 9513-9519.
119. Knorr, J.; Sokkar, P.; Schott, S.; Costa, P.; Thiel, W.; Sander, W.; Sanchez-Garcia, E.; Nuernberger, P., Competitive solvent-molecule interactions govern primary processes of diphenylcarbene in solvent mixtures. *Nature Communications* **2016,** *7*, 12968.
120. Richard, J. P., A consideration of the barrier for carbocation-nucleophile combination reactions. *Tetrahedron* **1995,** *51* (6), 1535-1573.
121. Mieres-Perez, J.; Costa, P.; Mendez-Vega, E.; Crespo-Otero, R.; Sander, W., Switching the Spin State of Pentafluorophenylnitrene: Isolation of a Singlet Arylnitrene Complex. *Journal of the American Chemical Society* **2018,** *140* (49), 17271-17277.

122. Kruk, N. N.; Parkhots, O. P.; Ivashin, N. V., Spectral Manifestations of Anion-Cation Interactions of Water-Soluble Porphyrins. *Journal of Applied Spectroscopy* **2001,** *68* (6), 924-929.
123. Vatsadze, S. Z.; Loginova, Y. D.; dos Passos Gomes, G.; Alabugin, I. V., Stereoelectronic Chameleons: The Donor–Acceptor Dichotomy of Functional Groups. *Chemistry – A European Journal* **2017,** *23* (14), 3225-3245.
124. Aoki, S.; Kagata, D.; Shiro, M.; Takeda, K.; Kimura, E., Metal Chelation-Controlled Twisted Intramolecular Charge Transfer and Its Application to Fluorescent Sensing of Metal Ions and Anions. *Journal of the American Chemical Society* **2004,** *126* (41), 13377-13390.
125. Fujimoto, H.; Denno, S.; Jinbu, Y., Theoretical study of stable carbocations and their interactions with anions. *J. Phys. Chem.* **1991,** *95*, 1612-1618.
126. Moreno, A.; Pregosin, P. S.; Veiros, L. F.; Albinati, A.; Rizzato, S., Ion Pairing and Salt Structure in Organic Salts through Diffusion, Overhauser, DFT and X-ray Methods. *Chemistry - A European Journal* **2009,** *15* (28), 6848-6862.
127. Abe, M., Diradicals. *Chemical Reviews* **2013,** *113* (9), 7011-7088.
128. Stuyver, T.; Chen, B.; Zeng, T.; Geerlings, P.; De Proft, F.; Hoffmann, R., Do Diradicals Behave Like Radicals? *Chemical Reviews* **2019,** *119* (21), 11291-11351.
129. Wenthold, P. G.; Winter, A. H., Nucleophilic Addition to Singlet Diradicals: Homosymmetric Diradicals. *The Journal of Organic Chemistry* **2018,** *83* (20), 12390-12396.
130. Abe, M.; Ye, J.; Mishima, M., The chemistry of localized singlet 1,3-diradicals (biradicals): from putative intermediates to persistent species and unusual molecules with a π-single bonded character. *Chemical Society Reviews* **2012,** *41* (10), 3808.
131. Grabowski, Z. R.; Rotkiewicz, K.; Rettig, W., Structural Changes Accompanying Intramolecular Electron Transfer: Focus on Twisted Intramolecular Charge-Transfer States and Structures. *Chemical Reviews* **2003,** *103* (10), 3899-4032.
132. Dar, A. H.; Gowri, V.; Gopal, A.; Muthukrishnan, A.; Bajaj, A.; Sartaliya, S.; Selim, A.; Ali, M. E.; Jayamurugan, G., Designing of Push–Pull Chromophores with Tunable Electronic and Luminescent Properties Using Urea as the Electron Donor. *The Journal of Organic Chemistry* **2019,** *84* (14), 8941-8947.
133. Mayr, H.; Bug, T.; Gotta, M. F.; Hering, N.; Irrgang, B.; Janker, B.; Kempf, B.; Loos, R.; Ofial, A. R.; Remennikov, G.; Schimmel, H., Reference Scales for the Characterization of Cationic Electrophiles and Neutral Nucleophiles. *Journal of the American Chemical Society* **2001,** *123* (39), 9500-9512.
134. Reichardt, C., Solvatochromic dyes as solvent polarity indicators. *Chemical reviews* **1994,** *94* (8), 2319-2358.
135. Song, M.-G.; Sheridan, R. S., Regiochemical Substituent Switching of Spin States in Aryl(trifluoromethyl)carbenes. *Journal of the American Chemical Society* **2011,** *133* (49), 19688-19690.
136. Becke, A. D., Density-functional thermochemistry. III. The role of exact exchange. *The Journal of Chemical Physics* **1993,** *98* (7), 5648-5652.
137. Lee, C.; Yang, W.; Parr, R. G., Development of the Colle-Salvetti correlation-energy formula into a functional of the electron density. *Physical Review B* **1988,** *37* (2), 785-789.
138. Francl, M. M.; Pietro, W. J.; Hehre, W. J.; Binkley, J. S.; Gordon, M. S.; DeFrees, D. J.; Pople, J. A., Self-consistent molecular orbital methods. XXIII. A polarization-type basis set for second-row elements. *The Journal of Chemical Physics* **1982,** *77* (7), 3654-3665.
139. Weigend, F.; Ahlrichs, R., Balanced basis sets of split valence, triple zeta valence and quadruple zeta valence quality for H to Rn: Design and assessment of accuracy. *Physical Chemistry Chemical Physics* **2005,** *7* (18), 3297.
140. Zhao, Y.; Truhlar, D. G., Density Functionals with Broad Applicability in Chemistry. *Accounts of Chemical Research* **2008,** *41* (2), 157-167.

141. Frisch, M.; Trucks, G.; Schlegel, H.; Scuseria, G.; Robb, M.; Cheeseman, J.; Scalmani, G.; Barone, V.; Mennucci, B.; Petersson, G.; Nakatsuji, H.; Caricato, M.; Li, X.; Hratchian, H.; Izmaylov, A.; Bloino, J.; Zheng, G.; Sonnenberg, J.; Hada, M.; Fox, D., Gaussian 09 (Revision A02). *Gaussian Inc. Wallingford CT* **2009**.
142. Pennington, W. T., DIAMOND–visual crystal structure information system. *Journal of Applied Crystallography* **1999,** *32* (5), 1028-1029.
143. Grimme, S.; Antony, J.; Ehrlich, S.; Krieg, H., A consistent and accurate ab initio parametrization of density functional dispersion correction (DFT-D) for the 94 elements H-Pu. *The Journal of Chemical Physics* **2010,** *132* (15), 154104.
144. Emer, E.; Twilton, J.; Tredwell, M.; Calderwood, S.; Collier, T. L.; Liégault, B.; Taillefer, M.; Gouverneur, V., Diversity-Oriented Approach to CF3CHF-, CF3CFBr-, CF3CF2-, (CF3)2CH-, and CF3(SCF3)CH-Substituted Arenes from 1-(Diazo-2,2,2-trifluoroethyl)arenes. *Organic Letters* **2014,** *16* (22), 6004-6007.
145. Raimer, B.; Lindel, T., Photoactivation of (p-Methoxyphenyl)(trifluoromethyl)diazirine in the Presence of Phenolic Reaction Partners. *Chemistry – A European Journal* **2013,** *19* (21), 6551-6555.
146. Kato, K.; Gong, Y.; Saito, T.; Yokogawa, Y., Enzymatic resolution of 2,2,2-trifluoro-1-arylethylamine derivatives by Pseudomonas fluorescens lipase in organic solvents. *Journal of Molecular Catalysis B: Enzymatic* **2004,** *30* (2), 61-68.
147. Creary, X., Reaction of organometallic reagents with ethyl trifluoroacetate and diethyl oxalate. Formation of trifluoromethyl ketones and .alpha.-keto esters via stable tetrahedral adducts. *The Journal of Organic Chemistry* **1987,** *52* (22), 5026-5030.
148. Stewart, R.; Teo, K. C., The reduction of aryl trifluoromethyl ketones by sodium borohydride. The hydride transfer process. *Canadian Journal of Chemistry* **1980,** *58* (23), 2491-2496.
149. Liang, X.; Guo, P.; Yang, W.; Li, M.; Jiang, C.; Sun, W.; Loh, T.-P.; Jiang, Y., Stereoselective synthesis of trifluoromethyl-substituted 2H-furan-amines from enaminones. *Chemical Communications* **2020,** *56* (13), 2043-2046.

6. Acknowledgments

Zuallererst möchte ich mich bei Prof. Dr. Wolfram Sander für die Möglichkeit zur Durchführung dieser Arbeit bedanken. Ich bedanke mich für die Vergabe dieses spannenden und interessanten Forschungsthemas, sowie für die Diskussionsbereitschaft und hilfreiche Unterstützung während der gesamten Promotion.

Zudem möchte ich mich bei Prof. Dr. P. B. Petersen dafür bedanken, daß er bereit war mein Zweitprüfer zu sein.

Ich möchte mich bei allen aktuellen und ehemaligen Mitgliedern im AK Sander für die gute Arbeitsatmosphäre, den stetigen Wissensaustausch und die allgegenwertige Hilfsbereitschaft bedanken. Außerdem möchte ich mich bei allen für all die interessanten und auch die lustigen Diskussionen bedanken. Im einzelnen: Nadja, Andre, Fee, Sandra, Melanie, Geneviève, Iris, Paolo, Stefan, Tim, Adam, Arun, Akshay, Enrique, Pritam, Soumya, Bishnu, Sujan, Yetsedaw, Nesli, Gizem, Mohamed, Tobias, Mika, Adrián, Julien, Ginny, Ankit, Alexander, Kseniya, Melania, Joel, Corina, Christian, Tino, Kevin, Nora, Luisa.

Außerdem Danken möchte ich meinen Bachelor- und Masterstudenten Kseniya, Dennis, Elisa und Negar, für ihren Beitrag zu dieser Arbeit.

Einen großen Dank an Heidi, Catharina, Klaus, Elric, Torsten, Robin, Sabine, Jacinta, Annika, Hannah und Dirk für die stetige freundliche Hilfsbereitschaft bei technischen oder administrativen Fragen.

Ich bedanke mich bei Enrique, Iris, Stefan, Tim, Adrián, Mika, Tobi, Julien und Cihad für das Korrekturlesen einzelner Kapitel dieser Arbeit und die aufbauenden Worte.

Zudem bedanke ich mich bei Jana für ihre Unterstützung während des gesamten Studiums.

Einen großen Dank möchte ich an meine Eltern geben, dafür daß sie mir das alles erst ermöglicht haben und mich stets unterstützt und ermuntert haben. Einen großen Dank auch an Dina für die mentale Unterstützung. Zudem möchte ich mich bei Cihad bedanken, dafür daß er immer für mich da war, mir geholfen und mich immer wieder aufgebaut hat.